Utilization of Instrument Response of SuperPave™ Mixes at the Virginia Smart Road to Calibrate Laboratory Developed Fatigue Equations

Walid M. Nassar
The Via Department of Civil and Environmental Engineering
Virginia Polytechnic Institute and State University
Blacksburg, VA 24061

Dissertation submitted to the Faculty of the
Virginia Polytechnic Institute and State University
in partial fulfillment of the requirements for the degree of

Doctor of Philosophy
in
Civil Engineering

Imad L. Al-Qadi, Chair
Gerardo W. Flintsch
Kenneth L. Reifsnider
Antonio A. Trani
John C. Duke

July 2001
Blacksburg, Virginia

Keywords: Hot Mix Asphalt, Fatigue, Pavement Stress and Strain, Pavement Instrumentation, And Resilient Modulus

Utilization of Instrument Response of SuperPave™ Mixes at the Virginia Smart Road to Calibrate Laboratory Developed Fatigue Equations

Walid M. Nassar
The Via Department of Civil and Environmental Engineering
Virginia Polytechnic Institute and State University
Blacksburg, VA 24060, 2001

ABSTRACT

In the current mechanistic-empirical (M-E) design procedures for flexible pavements, the primary transfer functions are those that relate (a) maximum tensile strain in the hot-mix asphalt (HMA) surface layer to fatigue cracking and (b) compressive strain at the top of the subgrade layer to rutting at the surface. These functions, called fatigue and rutting equations, are usually derived from statistically based correlations of pavement condition with observed laboratory specimen performance, full-scale road test experiments or by both methods. Hot-mix asphalt fatigue behavior is an important component of a M-E design procedure; unfortunately, most of the existing models do not reflect field fatigue behavior. This is manifested in the fact that HMA fatigue failure is achieved much faster under a laboratory setting than in a field environment. This difference has been typically accounted for by the use of a single shift factor based mainly on engineering experience.

The flexible pavement portion of the Virginia Smart Road includes 12 different flexible pavement designs. Each section is approximately 100m long. The sections are instrumented with pressure cells, strain gages, time-domain reflectometry probes,

thermocouples, and frost probes. The instruments were embedded as layers were built. Laboratory fatigue tests of field cores and field-mixed laboratory-compacted specimens along with measured response from the instrumented pavement sections at the Virginia Smart Road were used to quantify the differences between laboratory and field environments.

Four shift factors were identified to correlate field and lab fatigue behavior: stress-state, material difference, traffic wander, and healing. Field-measured critical strains and strain energy exerted during truck loading were both used to determine the stress state shift factor. Strain measurements of truck loading distribution (wander) were used to determine the wander shift factor. Finally, results from laboratory fatigue tests on cores and laboratory compacted specimens were used to evaluated a shift factor to account for the difference in compaction procedures. While the derived shift factors utilize the measured stresses and strains at the Virginia Smart Road, calculated strains and stresses, based on appropriate pavement and loading modeling, may also be used.

Acknowledgements

I would like to express my deepest gratitude to my friend and advisor, Dr. Imad L. Al-Qadi, who has provided me with numerous opportunities to perform research in the area of pavement design and instrumentation. I am greatly indebted to him for the challenges he has placed upon me as well as his invaluable guidance throughout this research. I would also like to express my appreciation to my committee members, Dr. Gerardo Flintsch, Dr. Kenneth L. Reifsnider, Dr. Antonio A Trani and Dr. John Duke, for their suggestions and advice throughout this research. Their suggestions and guidance helped me enhance the quality of this research. I would also like to thank my parents for their support and care provided to me throughout my education. Their support has been invaluable.

I finally would like to thank my friends and research associates who assisted in this research over the past four years: Mostafa El-Seifi, Amara Loulizi, and Samer Lahouar and Kenneth Taylor and Kevin of Virginia Department of Transportation (VDOT).

Special thanks go William Hobbs (Big Dog) the asphalt technician at the Civil Engineering department in Virginia Tech.

Table of Contents

List of Tables

List of Figures

CHAPTER 1: INTRODUCTION

This chapter serves as an introduction to the research performed at the Virginia Smart Road pavement instrumentation project. Pavement research in general, which includes current problems and future research focus, is discussed in Section 1.1. Section 1.2 presents a brief background needed to address the problem statement in Section 1.3. Section 1.4 presents the objectives of the research. Finally, Section 1.5 describes the scope and the limitations of the research and outlines the rest of the document.

1.1 Introduction

Hot mix asphalt, HMA, is used as surface or base layers in a pavement structure to distribute stresses caused by traffic loading. To adequately address this function over the pavement design life, the HMA must also withstand the effects of environment and resist rutting and cracking caused by either loading (fatigue) or by the environment (low temperature). In addition, HMA must provide a smooth surface for the users. Many factors affect the ability of an HMA to meet these structural and functional requirements. Mixture design, construction practices, properties of the different component materials (aggregates and binder), and the use of additives all play important roles in the resulting pavement characteristics. It is also important to recognize the interaction between mixture design and pavement design to arrive at cost-effective solutions. Although great efforts have been made to better understand the behavior of HMA, through research and implementation of new asphalt paving technologies, and the factors that affect their performance, much work remains. The following list provides a summary of some of the principal issues associated with the design and production of HMA that can meet the increasing needs of modern pavements:

- Changes in the properties of the materials, primarily in the availability of modifiers and manufacturing processes, but also in the availability of different sources of the two main components—asphalt binder and aggregate;
- Changes in the current state of knowledge and accordingly material characterization tests, whether laboratory or insitu.

- Increased loading conditions under which HMA is expected to perform, greater tire contact stresses, loads, and load repetitions.
- Increased need to reduce the environmental impacts of paving operations and to increase the recycling of HMA.

Fundamental engineering research on the properties of HMA and their effects on specific distress mechanisms have significantly contributed to the development of materials that are expected to perform better under specific environmental and traffic conditions. Much of this development has been possible through reductions in computing costs and improvements in laboratory testing technology. It is hoped that the implementation of improved technology and the availability of new materials would meet the increase in performance requirements for HMA and flexible pavement structures due to changes in traffic.

To perform satisfactorily in pavement systems, HMA should exhibit (a) the ability to distribute stresses; (b) the ability to resist permanent deformation; (c) resistance to cracking; and (d) resistance to freeze-thaw and moisture damage. Numerous factors and associated properties affect the ability of HMA to meet these structural requirements:

- Factors:
  - Binder characteristics;
  - Aggregate characteristics;
  - Additives;
  - Temperature;
  - Moisture;
  - Loading history (e.g., loading and rest times, loading rate, load level);
  - Aging characteristics;
  - Stress state; and
  - Compaction method.
- Properties:
  - Stiffness,
  - Binder and HMA rheological properties,
  - Permanent deformation properties, and
  - Cracking properties.

Although studying the variations associated with the flexible pavement properties and design models through mechanistic approaches has been found to give many

desirable results (Finn, 1987), these variations are sometimes large enough that a global assessment of the total variability is needed. For example, instead of studying the variability associated with aggregate and asphalt binder properties separately, a study of the total mix might be simpler and more beneficial. The relationship between mixture and binder properties in laboratory testing has been the focus of research for many years; for example, in 1954, the ZACA-Wigmore test project was developed where a relation between binder film and fatigue cracking was investigated (Zube, 1969; Santucci, 1969). Unfortunately, these efforts have not yet yielded a strong relationship between the asphalt binder and the asphalt mix, which further emphasizes the importance of a global assessment of the pavement structure. Furthermore, to relate the fatigue life obtained from laboratory results to fatigue life obtained in the field, one overall shift factor has been used. On the other hand, with reference to the HMA only, analyzing the differences between laboratory and field environments and deriving shift factors that account separately for these differences might provide a more accurate value for the shift factors. Also, the global assessment of the pavement structure through deflection testing, for example, has been successful through the use of the Falling Weight Deflectometer, FWD (SHRP, 1991).

1.2 Background

An examination of the history of pavement design reveals an evolutionary process that began with rule-of-thumb procedures and gradually evolved into empirical design equations based on experience and road test pavement performance studies. Through the years, much of the development has been hampered by the complexity of the pavement structural system both in terms of its indeterminate nature and in terms of the changing and variable conditions to which it is subjected. Accordingly, research efforts have been directed towards further evolution of the pavement design methods from empirical methods to more mechanistic methods. In the mechanistic design concept, the pavement system is analyzed on the basis of the structural response (stress, strain, and deflection) of the system to moving vehicle loads. Pavement layer thickness and strength are selected to resist the detrimental effects of the predicted response for some desired number of load

repetitions. The number of load repetitions found under laboratory conditions has been significantly different that its counter part obtained in the field. In this respect, this background will start with a brief overview of the issues related to understanding the differences between laboratory and field settings.

1.2.1 Stiffness

Hot- mix asphalt stiffness is required to evaluate both the load-induced and thermal stress and strain distribution in flexible pavements. Stiffness has also been used as an indicator of mixture strength and to evaluate damage and age-hardening trends of HMA. However, a practical and reliable method to determine HMA stiffness remains a challenge. In addition, the proper use of stiffness in the evaluation and design of HMA and pavements is still under development. Furthermore, there are numerous definitions of stiffness, including uniaxial elastic modulus, dynamic modulus, resilient modulus, bulk modulus, shear modulus, and creep compliance, which all depend on temperature, time or frequency of loading, stress state, and test method. Much work remains to evaluate the relevance of stiffness as a measure of mixture quality and its relation to pavement performance. Higher stiffness mixtures reduce load-induced stresses to underlying layers, but increase both load-induced and thermal stresses in the HMA. Higher stiffness can be achieved by changing any of the following: aggregate gradation, asphalt content, HMA compaction, filler content, and binder type, including additives.

1.2.2 Resistance to Cracking

Cracking of the HMA layer in pavement structures can be classified into four categories according to cause of the cracking: fatigue cracking, thermal cracking, reflection cracking in overlays, and construction-related cracking. The first three are significantly influenced by the characteristics of the HMA paving mixture and are discussed in the following sections.

1.2.2.1 Fatigue Cracking

Fatigue is a phenomenon by which a material fails when subjected to repetitive stresses lower than its quasi-static strength. These stresses could be a mixture of compressive, tensile, and shear stresses. Preexisting defects in the pavement, such as surface and internal flaws and micro-cracks, may result in the formation of small cracks under service loading. These cracks grow gradually by the fatigue mechanism until they reach a size at which fracture occurs under regular service stresses. A reliable structural model must account for the effects of temperature, loading rate and time, rest periods, aging, and multilevel loads. The complex interaction of these variables calls for utilizing advanced mechanics theories such as viscoelasticity, damage mechanics, and fracture mechanics in understanding the failure mechanisms. Once mechanisms of failure are more adequately defined, a significant amount of work will be required to quantify the effects of different factors on fatigue performance, (Terrel, 1971).

1.2.2.2 Reflection Cracking

Reflection cracks result from vertical and horizontal movement of discontinuities in underlying layers caused by wheel loads and by thermal expansion and contraction. Reflection cracking is common in overlaid pavements, where an HMA course is placed over an existing, usually heavily deteriorated, pavement. The existing pavement may be either an asphalt pavement or PCC pavement. Reflection cracking stems from the movement of the underlying pavement structure, causing stresses to develop in the overlay. The movement may be due to traffic- or environmentally-induced forces, and includes differential vertical movements, thermal expansions and contractions, moisture-induced expansion, or curling of the underlying layers or slabs. If the stresses generated from these movements are of sufficient magnitude, the overlay will crack. Even if the stresses are less than the yield strength of the overlay, cracking may eventually occur as a product of fatigue due to cyclic loading. Because of complex stress and strain fields caused by both vertical and horizontal movements in the supporting layer, laboratory characterization of reflection cracking resistance is difficult.

Reflection cracking is a major source of pavement distress; it causes spalling of the pavement, allows surface water infiltration, and produces a general reduction in the layer stiffness. Several methods have been developed to address the mitigation of reflection cracking. These include cushions, stress-absorbing membrane layers, geotextiles, and the use of thicker overlays (Roberts, 1996).

1.2.2.3 Low Temperature Cracking

Low temperature cracking, or thermal cracking, is caused by the brittle behavior of asphalt pavements at low temperatures. There are several proposed mechanisms by which low temperature cracking occurs. In general, it can be attributed to the shrinkage of the pavement at low temperatures, which causes tensile stresses to build until failure of the pavement (cracks) is reached. Another method that has been proposed is thermal susceptibility. Unstabilized granular bases have been found to contract at temperatures below freezing due to the reorientation of clay-sized material. This reorientation is due to a drying effect resulting from the freezing of water in larger voids (Carpenter and Lytton, 1977). The contraction results in tensile stresses along the bottom of the HMA layer along the length of the pavement. Due to the inhomogeneity of the base material, variations will be present, causing stress concentrations and initiating cracking in the pavement (Carpenter and Lytton, 1978).

1.2.3 Laboratory Tests to Evaluate HMA

The development of reliable and practical approaches to evaluate the ability of HMA to meet structural requirements remains a major challenge. A variety of tools are needed to evaluate the HMA during design, production, quality control, and performance related specifications. Each of these stages requires a different level of sophistication. Design tests should be very comprehensive and should consider pavement structure including unstabilized aggregate and subgrade layers, traffic loading forecast, environmental effects that include seasonal variations, construction issues, and life-cycle cost analysis. Production tests should include simple and effective tests for mixture

optimization and even simpler, process-oriented tests for quality control during production. More sophisticated tests are then needed to determine fundamental properties to ensure that mixtures will meet a minimum standard of performance when used in a pavement system.

Countless laboratory testing protocols have been proposed to evaluate a mixture's resistance to the different distresses discussed above, but none have been generally accepted or even verified to work for the variety of aggregates, binders, mixture types, environments, and loading conditions encountered in the HMA industry. In addition, each testing system has advantages and disadvantages in applicability, cost, and level of complexity. Simple strength tests include Marshall and Hveem stability, shear strength from the gyratory testing machine, confined or unconfined compressive strength, and indirect tensile strength. More sophisticated tests are found at accelerated pavement testing facilities where a full-scale pavement is continuously loaded. These tests are gaining more popularity due to the higher reliability of information obtained from these tests. Other forms of full-scale testing are those related to pavement instrumentation, where the response of the full-scale pavement is measured under a variety of loading conditions. Rapid developments in instrumentation and computer capabilities continue to make these measurements more viable for pavement response evaluation. However, identification and verification of the most appropriate constitutive models for HMA is a major challenge. Hot-mix asphalt behavior is highly complex: its response to stress can be elastic, viscous, plastic, or dilatant, and may also include micro-damage and fracture.

1.2.4 Pavement Instrumentation

During the past three decades, attempts were made to enhance pavement analysis and design by measuring the stresses and strain at critical locations inside a pavement system, and compare them to calculated strain levels at critical locations in the pavement system for determining failure strains (Battiato *et al*. 1977; Ku *et al*. 1967).

As technological capability advances, so does the entire supporting infrastructure. Thus, pavement instrumentation today is experiencing a technological revolution to withstand the demands on the infrastructure by understanding the material performance in the field as well as pavement system response to loading and environment. This revolution is directed towards developing sensors to measure pavement response parameters. Parameters that need to be measured in the field include strains, stresses, deflections, moisture, and temperature. Measuring these parameters in the field allows for the assessment of the major differences in the behavior of HMA between laboratory and field conditions.

With different accelerated pavement testing projects being constructed today, different sensor manufacturers are finding a new practice of marketing their products. Before implementing any of these products, one has to verify their applicability and usefulness in pavement applications.

According to NCHRP Synthesis 235 (Metcalf, 1996), on Full-scale Accelerated Pavement Testing, the limitations of test roads are the following: limited scope for acceleration of loading, no climate control, limited control of traffic speed and loading, and fixed location.

To address these issues, a recent test road/track was built in Southwest Virginia, the Virginia Smart Road. It is a unique, state-of-the-art, full-scale research facility for pavement research and evaluation of Intelligent Transportation Systems (ITS) concepts, technologies, and products. The Virginia Smart Road is the first facility of its kind to be built from the ground up with its infrastructure incorporated into the roadway. The Virginia Smart Road will be a 9.6-km connector highway between Blacksburg and I-81 in Southwest Virginia, with the first 3.2 km designated as a controlled test facility. This facility allows for testing under realistic conditions on an actual roadway. Climatic test chambers exist that are large enough to test vehicles on a limited scale, but no open-air facilities like this, with controlled climate, exist anywhere in the world.

It must be noted here that the benefits of full-scale testing are several but it is still a novel field and there is much to be learned. The benefits are large but there are many problems yet to be solved, such as the sensor-pavement interactions and the robustness of the installation procedures.

1.3 Problem Statement

Traditionally, the performance of HMA has been studied through the application of the remaining life concept given by Miner's Law. Performance measures may include roughness, rutting, and percent cracking, among others. These measures, functional and structural, are based on distress surveys of in-service pavements. Such models are only valid for the pavements with the same structure and that are subjected to similar loading.

In addition, the main focus of HMA research so far has been on obtaining the number of cycles to failure. Little has been done to evaluate the fatigue performance of HMA. Furthermore, research on HMA fatigue lacks a meaningful relationship between laboratory performance and field performance. This is mainly because the tests conducted to evaluate specific distresses use different measures than what are used in performance prediction models. Also, the shift factor used in relating field and laboratory performance incorporates a large variety of factors that cannot be quantified with just one value.

1.4 Objectives

To address the aforementioned problem, it is the main objective of this study to develop fatigue models for different types of currently used HMA based on fatigue testing. To achieve this, the following need to be accomplished:

1. Study the variations associated with the fatigue tests and field behavior. Model HMA fatigue under laboratory tests to arrive at laboratory-performance curves. These curves should address the difference in results between the two main test methods: Indirect Tensile Fatigue Test and Third-Point Bending Test (ITFT and TPBT). In

addition, the specimen preparation effect needs to be considered. Therefore, in this study two types of specimens were evaluated: field cores, and field mixed laboratory-compacted samples.

2. Utilization of pavement instrumentation to obtain realistic shift factors between laboratory setting and field environment. This is required to develop shift factors that may account for the difference in state of stress, traffic wander, and material difference.

CHAPTER 2: PRESENT STATE OF KNOWLEDGE

Currently, the primary concern of highway officials is the cost-effective preservation of highway networks. This can be achieved through the implementation of a sound Pavement Management System, PMS. Pavement performance prediction is the most essential part of a PMS and is defined as the change of pavement condition with time. Due to traffic and environment loading, the pavement's initial level of serviceability is reduced. When the pavement's serviceability reaches an unacceptable condition, it is considered the end of its service life. Many performance prediction models have been developed over the past two decades to illustrate pavement condition over time and provide a method of extrapolating the future performance of pavements for planning purposes. Various techniques have been used to develop these models, such as regression equations and probability functions. However, there is currently no mechanistic pavement performance model that is used by US DOT agencies.

Pavement performance modeling requires functional and structural evaluation. The methods used to evaluate pavement performance depend upon the importance of the project. They may range from subjective estimates of general pavement quality and appearance to detailed procedures involving structural capacity evaluation and quantification of distress severity. Although methods of evaluating pavement performance are vast, there is no consistency between the evaluated parameters. For example, some research uses number of loading cycles to failure; while others use percent cracking, rut depth or several other parameters. It is absolutely essential to establish standards for performance evaluation that account for different pavement distresses.

While these distresses have been thoroughly identified, their mechanisms are not yet modeled. For example, fatigue cracking has been identified as a major distress in pavements; however, its mechanism and the damage evolution are still researched. One

method to better understand fatigue cracking is to monitor its development in the field. This may be achieved through pavement instrumentation.

2.1 Pavement Instrumentation

Pavement instrumentation is not an objective, but rather a tool to achieve specific goals. It is a process to monitor the behavior of a specific pavement system. It comprises identification of critical locations in the pavement, selection of sensors, calibration of the sensors, identification of possible errors, installation, and finally data collection.

Once proper planning is accomplished, collected data can be used to serve two main purposes. The first purpose is to validate existing or novel design approaches. This is accomplished by verifying that field-measured parameters coincide with analytically evaluated parameters. The second purpose is to monitor trends in measured parameters that may identify the proper theory to be used in analyzing these parameters. For example, measuring stresses and strains in the field and then comparing them to their calculated counterpart in a pavement structural model may serve the first purpose. On the other hand, monitoring moisture contents at different locations in the pavement may yield information on how the water moves through the pavement and accordingly assist in the second purpose.

The critical problems that face pavement researchers are the rapid and continuously growing demands to design and build better performing pavements. The objectives of pavement studies should be well planned so that by the time these objectives are to be implemented, the updates in traffic, material, and construction requirements, discussed in chapter one, are fully met. Focusing the research on pavement design methodologies and mechanistic pavement performance procedures rather than evaluating new materials or new pavement configurations may allow for extrapolation to new updates in traffic, material, and construction requirements. On the other hand, focusing research on the evaluation of new materials, such as SuperPave^{TM}, may assist in

validating or modifying existing design procedures, as far as the understanding of the needs in pavement, materials, and construction practices are considered.

The primary requirement of any pavement instrumentation project is that it should be part of a lucid pavement research program to obtain maximum benefits. A few published reports were found on the variability associated with pavement instrumentation. The process itself is complex, with a lot of variability associated with the installation, sensor-pavement interactions, data acquisition, and interpretations. Studying pavement performance through the use of instrumentation without proper assessment of the sensor performance may lead to unreliable results.

Without a doubt, the benefits from pavement instrumentation projects are significant and a lot of information can be learned. This part of the literature review discusses the instrumentation facilities found to date, while a review of the different sensors used and the typical responses obtained from these instrumentation projects are presented in the second part.

2.1.1 Penn State Test Track

In the late 1980s, under part of a research project sponsored by the FHWA, Penn State undertook a project to evaluate different pavement instrumentation (Sebealy *et al.*, 1991). The Pennsylvania research program was divided into two phases. In the first phase, an extensive literature search was conducted to identify the existing pavement instrumentation and to select the most promising types of gauges for a field-testing program. Two sections of flexible pavements, 152- and 254-mm-thick HMA, were constructed and instrumented with selected gauges. The response of the gauges to dynamic loading applied by a tractor-semi-trailer at different levels of axle loading, tire pressure, and speed were investigated. In the second phase, new concepts in pavement instrumentation were investigated. Table 2-1 shows the type of instrument used for measurement of a specific variable. Table 2-2 shows the number of instruments, their location and orientation in the test section.

Table 2-1 Sensor type for the Penn State project (after Sebealy *et al.*, 1991).

Pavement Response	Sensor Type
Stress	• Nottingham diaphragm-type pressure cell
Deflection	• Geophones • Single-layer deflectometer • Multi-depth deflectometer
Strain	• Dynatest H-gauge and Kyowa H-gauge • Alberta Research Council (ARC) HMA carrier block gauge • Core gauge
Temperature	• Thermocouples • Solid state sensors
Moisture	• Nuclear dual tube • Moisture/suction-AGWATRONIX
Trigger	• Ultrasonic sensor

Table 2-2 Summary of gauges for field tests (after Sebealy *et al.*, 1991).

Gauge Type	Number of Gauges/Section	Orientation	Location
Nottingham pressure cells	2 / thin	Vertical	At the top of base course
Geophones	3 / thin and thick	Vertical	At the pavement surface
Geophones	3 / thin and thick	Vertical	At the top of base course
Geophones	3 / thin and thick	Vertical	At the top of subgrade
Single layer deflectometer	1 / thick	Vertical	At the top of base course
Single layer deflectometer	1 / thick	Vertical	At the top of subgrade
Multi-depth deflectometer	1 / thin and thick	Vertical	Throughout the depth of pavement
Dynatest strain gauge (H-Type)	2 / thin and thick	Longitudinal	At the bottom of HMA
Kyowa strain gauge (H-Type)	4 / thin and thick	Longitudinal	At the bottom of HMA
HMA block gauge (ARC)	1 / thin and thick	Longitudinal	At the bottom of HMA
Core gauge	4 / thin and thick	Longitudinal	At the bottom of HMA
Core gauge	2 / thin and thick	Vertical	At the lower one-third of HMA
Core gauge	2 / thin and thick	Transverse	At the bottom of HMA
Thermocouples	8 / thin and thick	N/A	Throughout the pavement depth
Solid state temperature sensors	8 / thin and thick	N/A	Throughout the pavement depth

Prototype gauges were built and evaluated first in the laboratory and then in the field. The pavement response data collected in the field-testing program was used to evaluate methods for backcalculating pavement material properties.

It was demonstrated that the backcalculated moduli were much more accurate if data from multiple sensors placed throughout the pavement structure were used in the analysis as compared to a single sensor.

In summary, the Penn State study contribution was to evaluate various types of pavement instruments, to examine several methods to measure strain, stress, and deflection in flexible pavements, and to evaluate procedures that use this data to determine layer moduli and to validate strains computed by mechanistic techniques.

2.1.2 MnRoad

Recently, a pavement research facility was constructed in the state of Minnesota: Minnesota/Road (MnRoad). It consists of approximately 40-160m of pavement test sections. Twenty-three of these test sections have been loaded with freeway traffic, and the remainder sections have been loaded with calibrated trucks. Freeway traffic loading began in June 1994. Embedded in the roadway are 4572 electronic sensors, 1151 of which are used to measure pavement response to dynamic axle loading. The specific brands and models of each type of sensor were selected based on Minnesota Department of Transportation (MnDOT's) recommendations derived from four research contracts for evaluation of pavement sensors, and by consultation with other government agencies and instrumentation experts worldwide. The main purpose of this facility is to verify and improve existing pavement design models, learn more about the factors that affect pavement response and performance, and develop new pavement models that will allow building and maintaining more economical roadways.

One report from a series of reports published by the MnROad research team discusses the sensor survivability (Baker, 1994). The report presents the percentage of sensors that have failed during construction and those that failed later with reference to the time to failure.

2.1.3 Ohio Test Track

As part of the Long Term Pavement Performance (LTPP) Specific Pavement Studies (SPS), a project was started in Athens Ohio, the Ohio Test Track. All the test sections were constructed as part of one project where the climate, soil, and topography are uniform throughout. Since the basic instrumentation plan proposed by the Strategic Highway Research Program (SHRP) was limited, the Ohio Department of Transportation (ODOT) opted to develop a more comprehensive plan for the test track. The four independent parts of the Ohio project are divided into the following categories in accordance with the LTPP:

SPS-1 (Strategic Study of Structural Factors for Flexible Pavements): Variables studied in this project include HMA thickness, base type and thickness, and the presence or absence of drainage conditions.

SPS-2 (Strategic Study of Structural Factors for Rigid Pavements): Variables in this study include Portland cement concrete thickness, base type and thickness, concrete strength, pavement width, and the presence or absence of drainage conditions.

SPS-8 (Study of Environmental Effects in the Absence of Heavy Traffic-Asphalt and Concrete): This project includes two instrumented sections, one of HMA and the other of Portland cement concrete. These sections are subjected to low volume and lightweight traffic.

SPS-9 (Asphalt Program Field Verification Studies): The objective of the project is to verify the SHRP asphalt specifications.

The main objective of the Ohio Test Track was to encompass a long-term study of structural factors, maintenance effectiveness, rehabilitation, and environmental factors on

the mechanistic response of various pavement sections. Of particular interest is the interaction of load response to environmental parameters.

2.1.4 Denver Airport

In 1992, the Federal Aviation Administration (FAA) initiated a major research effort to study the in-situ response and performance of Portland cement concrete pavements. FAA, in cooperation with the U.S. Army Corps of Engineers and Waterways Experiment Station (CEWES), instrumented several pavement slabs in the take-off area of Runway 34R at the Denver International Airport (DIA), which was under construction at that time. With the support of the DIA airport authority, the City and County of Denver, and the FAA Denver Airport District Office, a total of 460 sensors were installed in the various layers of the pavement structure. A comprehensive data acquisition system was also installed for remote access. Video cameras were installed next to the instrumented pavement section to provide live images of the aircraft landing, and a record of time- based surface deterioration. Since the opening of the airport, the FAA has completed a series of tests to debug the entire system. Data collected in this project include real-time pavement responses to actual aircraft traffic, environmental parameters, and weather conditions. The focus of the test section is to determine the effect of aircraft loading on pavement design and service life, as well as monitor deterioration development due to environmental loading.

2.1.5 WesTrack

The WesTrack is a 2.9-km oval loop built in western Nevada. The construction and the two-year truck loading of the track are being funded by the FHWA as part of a significant study of HMA paving materials and construction. Construction of the first pavement test sections on WesTrack was completed in October 1995, and truck loading was initiated in March 1996. The main focus of this project is not on pavement design development, but rather on HMA performance evaluation. The WesTrack program therefore has two major objectives: continued development of performance-related

specifications (PRS) for HMA pavement construction by emphasizing how materials and construction variability affect the eventual pavement performance and service life, and to provide an evaluation of SHRP SuperPave^{TM}. The Project was completed in 2000.

2.1.6 Bedford Project

The main focus of this project was to study the effectiveness of the use of geosynthetic in flexible pavements and how it can be factored in the design procedure. Nine instrumented secondary road test sections were constructed as part of the realignment of Routes 757 and 616 located in Bedford County, Virginia. Each test section was 15 m long. Three test sections were constructed using a geogrid, three with a geotextile, and three were non-stabilized. The constructed base course thicknesses were 100, 150, and 200mm. The HMA thickness averaged 8.9mm. The pavement test sections were instrumented with earth pressure cells, HMA and soil strain gauges, soil moisture sensors, and thermocouples. The geotextiles and geogrids were also instrumented with strain gauges. The majority of the instruments were placed in the right wheel path of the inside lane of the test sections. All instrumentation, cabling, and data acquisition facilities were located underground. The data acquisition system was triggered by truck traffic passing over piezoelectric sensors, and was operated remotely. Once the system was triggered, the instrumentation was continuously sampled at a frequency of 200 Hz for a period of either 12 or 10 seconds depending on the triggering location (Al-Qadi, 1999). The corresponding data were transferred to Virginia Tech via a modem for processing.

All instruments were placed during construction of each corresponding layer. Instruments located in the subgrade were Kulite earth pressure cells, Carlson earth pressure cells, soil strain gauges, thermocouples, and gypsum blocks. Pressure cells, gypsum blocks, and thermocouples were installed below the compacted surface of the base course and backfill each sensor to avoid instrument damage from large angular aggregate.

The HMA strain gauges and thermocouples were also placed prior to the chip seal and the two 38-mm class SM-2A HMA layers. The gauges were coated with an emulsion mixture to protect them during paving. Four piezoelectric traffic sensors were installed in the HMA wearing surface along the length of the pavement test sections. Two sensors acted as triggers for the data acquisition system, and the other two were used as weigh-in-motion sensors. The data were collected for three years from the sensors, while the FWD and rutting data were collected for six years.

2.1.7 Saskatchewan Highways and Transportation

In 1978, testing in a 6-m-radius circular track at the Central Laboratory of Saskatchewan Highways and Transportation was initiated (Metcalf, 1996). Testing was performed at loads up to 60kN and speeds up to 29km/h with both single and dual wheel loads. The track is instrumented with strain gauges, pressure cells, and temperature measurements at the surface/base, base/subbase, and subbase/subgrade interfaces. This track is not running any more.

2.1.8 Canterbury Accelerated Pavement Testing Indoor Facility

In 1987, a 4.6-m-radius circular track at the Canterbury Accelerated Pavement Testing Indoor Facility was commissioned in New Zealand (Pidwerbesky, 1994). Testing was performed at loads up to 60kN and speeds up to 50km/h. The track is instrumented with strain gauges at the surface/base, base/subbase, and subbase/subgrade interfaces. Pressures were measured only on top of the subgrade. Tire pressures from 0.56 to 0.84 MPa were evaluated.

2.1.9 Laboratoire Central des Ponts et Chausees

The 20-m-radius circular track in France at the Laboratoire Central des Ponts et Chausees (LCPC) is probably the largest controlled track found to date (Hines, 1998). Testing started in 1978 with loads up to 75kN and speeds up to 105km/h. The track is

instrumented with strain gauges at the surface/base, base/subbase, and subbase/subgrade interfaces. Pressures were measured between the base and subbase and between the subbase and subgrade. Tire pressures from 0.61 to 1.00MPa were evaluated. This track is being continuously updated with new pavements and new test setups.

2.1.10 Washington State Track

One of the oldest circular tracks found is the Washington State University track established in 1965 (Krukar, 1971). Speeds of up to 24km/h and loads up to 45kN were evaluated. The pavements were instrumented with strain gauges only. This track is not running any more.

2.1.11 FHWA-ATF

The first Federal Highway Administration (FHWA) pavement instrumentation project was installed in 1986, and the second in 1995 (Metcalf, 1996). Only wearing surface layers were instrumented with strain gauges. Speeds up to 20km/h and loads up to 100kN were tested. Tire pressures of 0.54 to 0.99 MPa were evaluated. This track is being continuously updated with new pavements and new test setups.

2.1.12 Louisiana

In 1994, the Louisiana Transportation Research Center Pavement Research Facility was opened (Metcalf, 1996). All layers were instrumented with strain gauges, pressure cells, and a Multi-Depth-Deflection device (MDD). Speeds up to 20km/h and loads up to 100 kN were tested. Tire pressures of 0.90 to 0.95MPa were evaluated.

2.1.13 Denmark

In 1973, the Danish Road Testing Machine was built (Metcalf, 1996). All layers were instrumented with strain gauges, pressure cells, and a Linear Variable Differential Transformer (LVDT). Speeds up to 30km/h and loads up to 65kN were tested.

2.1.14 LINTRACK

In 1991, the Road and Railroads Research Laboratory of Delft University of Technology in the Netherlands started testing using single, dual- and super single-wheel tire assemblies (Metcalf, 1996). Surface and base layers were instrumented with strain gauges, and the subgrade was instrumented with pressure cells. Speeds up to 20km/h and loads up to 100kN were tested. Tire pressures of 0.50 to 1.10MPa were evaluated.

2.1.15 TxMLS

Texas commissioned the Texas Mobile Load Simulator in 1995. All layers were instrumented with strain gauges, pressure cells, and a Multi-Depth-Deflection device (Hugo, 1991). Speeds up to 20km/h and loads up to 190kN were tested. Tire pressures of around 0.64MPa were evaluated.

2.2 Response Monitoring

Measurement or calculation of traffic-induced pavement strains at specific locations is important to predict the failure mechanisms and understand material performance in the field. Calculating response has been of interest since Burmister solved the multi-layer elastic system using the theory of elasticity in 1945 (Huang, 1993). Numerous computer programs were developed since then to understand the pavement system behavior and obtain values for response parameters. Although these programs have aided engineers in designing more cost effective pavements, the assumptions associated with the solution incorporated in these programs may sometimes lead to inaccurate pavement response. Accordingly, pavement instrumentation is crucial to understanding material performance in the field, as well as pavement system response to loading and environment. Parameters that need to be measured in the field include strains, stresses, deflections, moisture, and temperature. Measuring these parameters in the field allows for the development of an accurate performance model and the

calibration of potential mechanistic pavement design. The following sections detail current instrumentation used to measure pavement system response to loads and environment, and the response shapes and types obtained from previous instrumentation projects.

2.2.1 Strain Gauges

It has been documented that mechanical loading may cause strain-based failures at the bottom of HMA (fatigue), or at the top of the subgrade (rutting). The viscoelastic nature of HMA may also cause plastic flow rutting in the HMA layers. As the critical locations in any pavement system can be identified, it becomes possible to choose appropriate instrumentation to measure the relative strains at these locations. Different strain gauges have been tested over the years. The Denver Airport used H-bar strain gauges, which operate in a dynamic mode, to measure strains induced at the top and bottom of concrete layers. The Penn State Test Track, MnRoad, WesTrack, Ohio SPS, and the researchers at Virginia Tech also used H-Type strain gauges. This type of embedment gauge consists of an electrical resistance strain gauge embedded within a strip of glass-fiber-reinforced epoxy, which is surrounded by several protective layers of various materials. These strain gauges have been installed in the longitudinal and the transverse directions of traffic. The performance of some of these gauges has been very successful in the field. The major manufacturers of this type of gauge are Dynatest, Tokyo Sokki, and Kyowa.

Researchers from Alberta Research Council in Canada (ARC) embedded strain gauges in thin sheets of asphalt (50 mm x 150 mm x 13 mm) to measure the longitudinal strain at the bottom of HMA. The procedure allows asphalt on the surface of the carrier block (which will soften when it comes in contact with the HMA) to bond monolithically with the HMA layer. This type of gauge is used in MnRoad and WesTrack. In addition, there is another type of gauge called the foil strain gauge. These gauges are attached to full-depth cores extracted from an actual pavement, and the instrumented core is replaced into the pavement section. The main concern with this approach is whether effective

bonding is achieved between the instrumented core and the surrounding pavement. If the epoxy-bonding agent is too stiff compared to the surrounding pavement, then stress concentrations will occur and inaccurate measurements of strain will be recorded. Field experience with this approach has shown that there are some epoxies commercially available that work well, but high failure rates are still normally encountered.

Strain gauges are also used in concrete slabs to measure strains induced by slab deflection, dynamic mechanical impact on joints, and curl and warp conditions. MnRoad and Ohio SPS used Dynatest Past-II-PCC embedment strain gauges which consist of electrical resistance strain gauges embedded within strips of glass-fiber-reinforced epoxy, with transverse steel anchors at each end to form an H-shape. Tokyo Sokki TML-60 strain gauges were also used in both projects; TML KM-100B was used in Ohio. These standard wire gauges are designed for the measurement of internal strains in concrete under dynamic loading. The gauge is coated with coarse grit to help bond the gauge to the concrete. Measurement Group LWK-06-W250B-350 and Geokon VCE 4200 Vibrating Wire strain gauges are also used in the field to measure static compression and tension in dowel bars, and to measure warp and curl in concrete slab. A thermistor is built into the vibrating wire gauge so that accompanying temperature measurements can be made. Carlson A-8 strain meters were used in the Ohio SPS sections to measure strains resulting from thermal variations. These gauges are elastic wire strain meters containing two coils of highly elastic steel wire, one of which increases in length and electrical resistance with change in strain. Soil Strains were measured in the Penn State Test Track using Transportation and Road Research Laboratory (TRRL) soil strain gauges and Carlson strain gauges. The gauges used at Penn State were placed after the construction of the base course by excavating to the subgrade and backfilling. It is important to monitor this type of gauge performance during backfilling and compaction.

Regardless of the type of strain gauge used to measure strain in HMA layers, the reported response found in the literature is identical. Four types of response could be found: tensile peak value, compressive peak value, tensile peak value with compressive

strain preceding the tensile strain, and tensile peak with compressive strain before and after the tensile peak, Figure 2-1 (Ullidtz, 1987).

In a study to investigate the effects of truck speed and tire pressure on pavement response, strain was measured at the bottom of the HMA layer (Chatti, 1995). The test section consisted of a 137-mm average surface layer over a 330-mm crushed stone base layer and the subgrade was sandy clay. A foil-type gauge was used to measure the various strain responses. Longitudinal strain responses were similar to those in Figure 2-1 (d). Transverse strain responses were similar to those in Figure 2-1 (a). The response was measured under a single and a tandem axle configuration, and only the peak tensile strain response was used in the data analysis. It was concluded that the effect of speed on the response of HMA pavements was significant. Increasing speed from 2.7km/h to 64km/h reduced the longitudinal strain by around 35%. The effect of speed on the transverse strain showed more variability and was less pronounced. Also, it was found that although the tire pressure did not have a significant effect on the strain at highway operating speeds (64km/h), the effect of the tire pressure increased with decreasing speed.

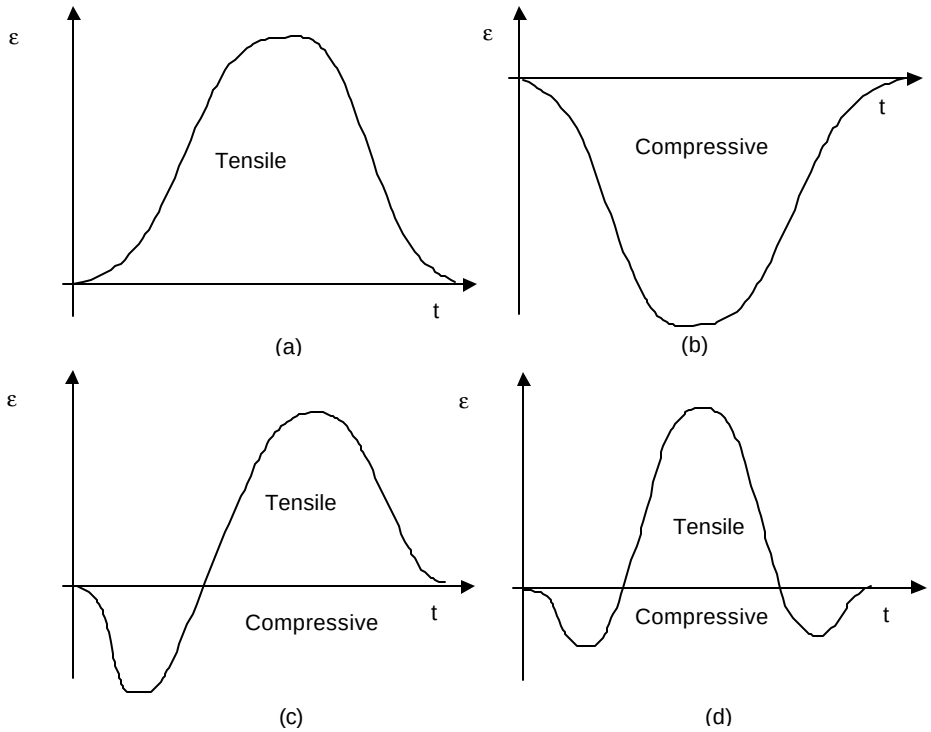

Figure 2.1. Typical Strain Responses from Pavement Instrumentation Projects

Huhtala *et al*. (1989) also studied the effect of tires and tire pressures on pavement response using strain gauges at the bottom of the wearing surface. The strain gauges were glued to 152-mm core samples that were fit back into the pavement and glued to the HMA pavement with tolerance of 1-mm. The gauges were placed in the longitudinal and transverse directions. Longitudinal strain gauges were used to compare the effects of the different axles or tires. Typical signals obtained from those gauges were similar to that in Figure 2-1 (d). Only the peak tensile values of the longitudinal strain were used in the comparisons. Temperature variations were measured hourly and accordingly, the time and date of the minimum variation were chosen for testing and measurements. They reported that 30 passes are usually needed to obtain a well-defined shape of the strain versus transverse position. This required about 1600 vehicle passes. The results, based on fatigue performance, showed that wide-base tires are 2.3 to 4 times more aggressive than twin tires. The results were discussed based on strain response only, and other factors such as pressure distribution, rolling resistance, and safety were not considered. Furthermore, the effect of retrofitting and the effect of sensor installation procedures were not discussed.

In another study to compare backcalculated moduli from FWD and truck loading, two pavement sections were instrumented (Sebaaly *et al.*, 1992). The first consisted of 152-mm of HMA over a 203-mm crushed aggregate and a 308-mm subbase. The second consisted of 254-mm of HMA over a 254-mm crushed aggregate and a 308-mm subbase. Three types of strain gauges were used: Kyowa, Dynatest, and instrumented core gauges. The strain response was identical to that shown in Figure 2-1 (d). Only the maximum tensile peak value for the strain was used in the study. The strain was measured using the strain gauges, and calculated, using a procedure developed by Uzan, at distances away from the load (Uzan, 1988). Similar technique for matching the measured and calculated deflections employed in the backcalculation procedure was used to match the measured and the calculated strains at different distances away from the load. It was found that it is almost impossible to produce one set of moduli for the different layers that satisfies pavement response from strain gauges. When combining the strain response with the

deflections at different depths, measured by a Multiple-Depth-Deflectometer, MDD, the backcalculated moduli are more accurate than utilizing measured strain only. However, those moduli did not satisfy the FWD and surface deflection data.

Siddharthan and Sebaaly (1998) later published results comparing the strain response between the two pavements discussed above. The results were obtained for dual wide-base tires traveling at 72km/h at a temperature of 40^0C, Figure 2-2. It can be seen that a compressive strain is found before and after the tensile peak for both the thick and thin pavements, but with a lower value for the thick pavements. These results suggest that the compressive strain, although its ratio to the tensile strain value may be comparable for both thicknesses, is dependent on pavement layer configuration.

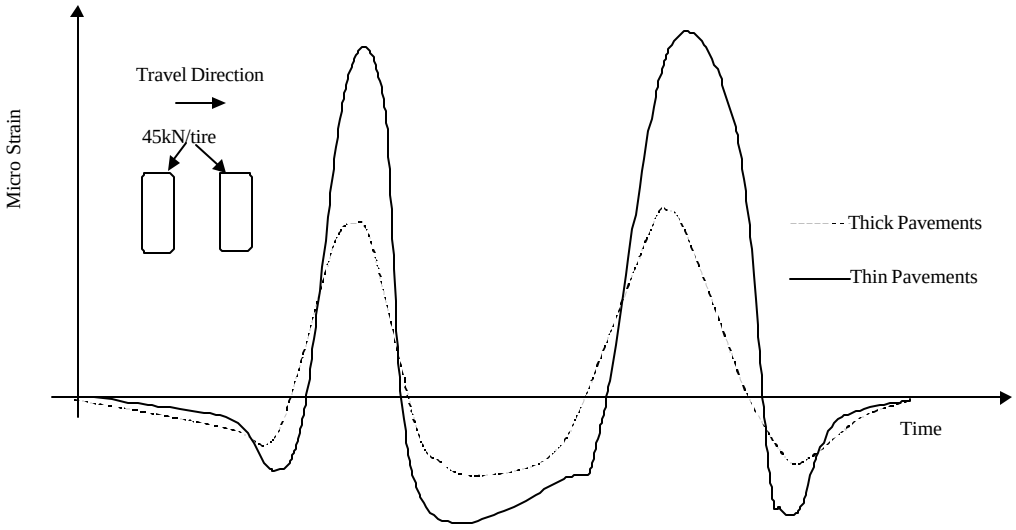

Figure 2.2. Strain Responses from a Dual Wide-Base Tire (after Siddharthan and Sebaaly, 1998)

In a small-scale wheel tracking study performed by the SHRP at the Nottingham Slab Testing Facility (STF), responses from strain gauges were similar to the aforementioned calculated ones (Rowe, 1997). A moving wheel applied the load to instrumented slabs, and strain gauges at the underside of the slab measured the strain response. The loading was applied by means of twin beams acting as a lever on the moving carriage. The slabs, contained within the sidewalls, were placed upside down on

a rubber mat to allow attachment of strain gauges with epoxy resin. The undersides of most slabs were instrumented with eight, 60-mm, 120-ohm foil gauges and the slabs were subsequently treated with a white emulsion paint to facilitate better observations of cracking. The instrumented slab was then carefully placed on a rubber mat within the STF. One gauge was used to monitor large residual/delayed elastic-visco-plastic transverse strain. The load was measured and adjusted to produce the required strain for testing, typically between 100 and 500 micro-strains.

The response measured from these gauges was identical to that shown in Figure 2-1 (d). The response obtained from the transverse strain gauges is shown in Figure 2-3, and was found to be completely tensile and not completely recovered after the load application.

The initial tensile strain magnitude was similar in both directions, however, the transverse strain was composed of two parts: elastic strain (resilient strain) and delayed (residual) visco-elasto-plastic strain. The latter was partly recoverable if the test was stopped for a short period of time. The effect of this part of the strain on the fatigue performance is considerable and has been studied by many researchers (Kim *et al.*, 1998; Brunton, 1989; Bonnaure *et al.*, 1982). The investigators also studied the effect of the installation procedure on the strain gauge response. Figure 2.4 shows how the improper installation could affect the strain response.

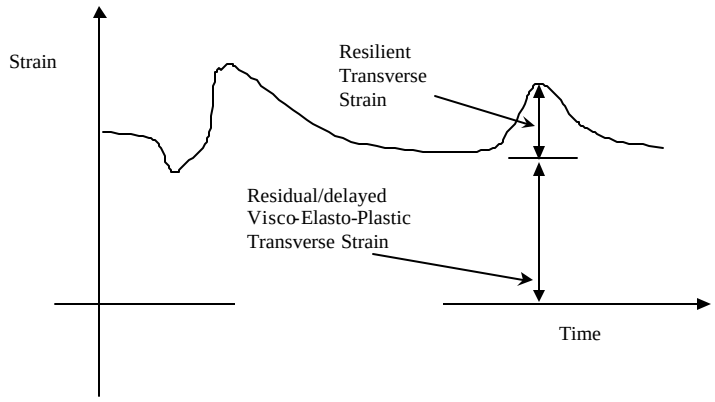

Figure 2.3. Transverse Strain Responses (after Siddharthan and Sebaaly, 1998)

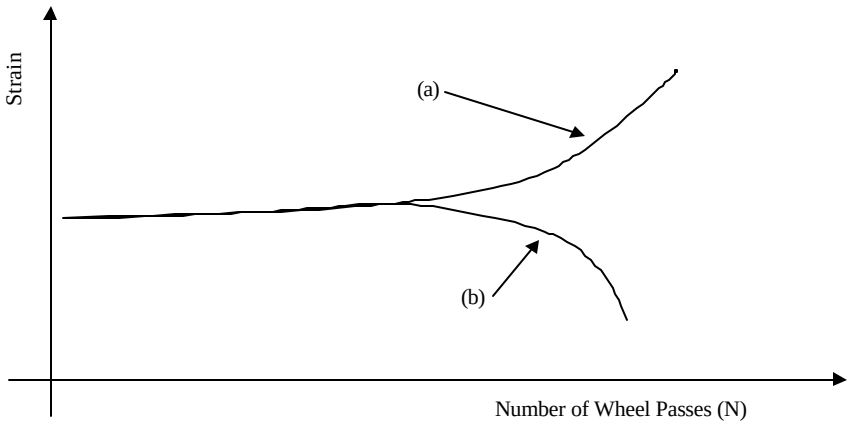

Figure 2.4 Influence of Installation Procedure on Strain Response with Number of Passes (after Rowe, 1997).

Curve (a) shows the strain response, versus number of wheel passes, as the cracks develop within the gauge length, resulting in an increasing strain and eventually gauge failure. Curve (b) shows the strain response as cracks form around the gauge due to superior strength of the epoxy, resulting in a strain decrease with number of passes.

Strain gauges were used to measure top and bottom strain in PCC slabs midway between the joints and close to the joints at the Ohio test. The response obtained was a combination of those shown in Figure 2-1. It should also be noticed that the response from the gauges placed at the bottom of the slab and those placed at the top are highly symmetric, Figure 2-5. Although this research was performed on PCC slabs only, general sensor installation guidelines are very helpful, and have been proven to be robust, and can be used for flexible pavements (Sargand and Hazen, 1996).

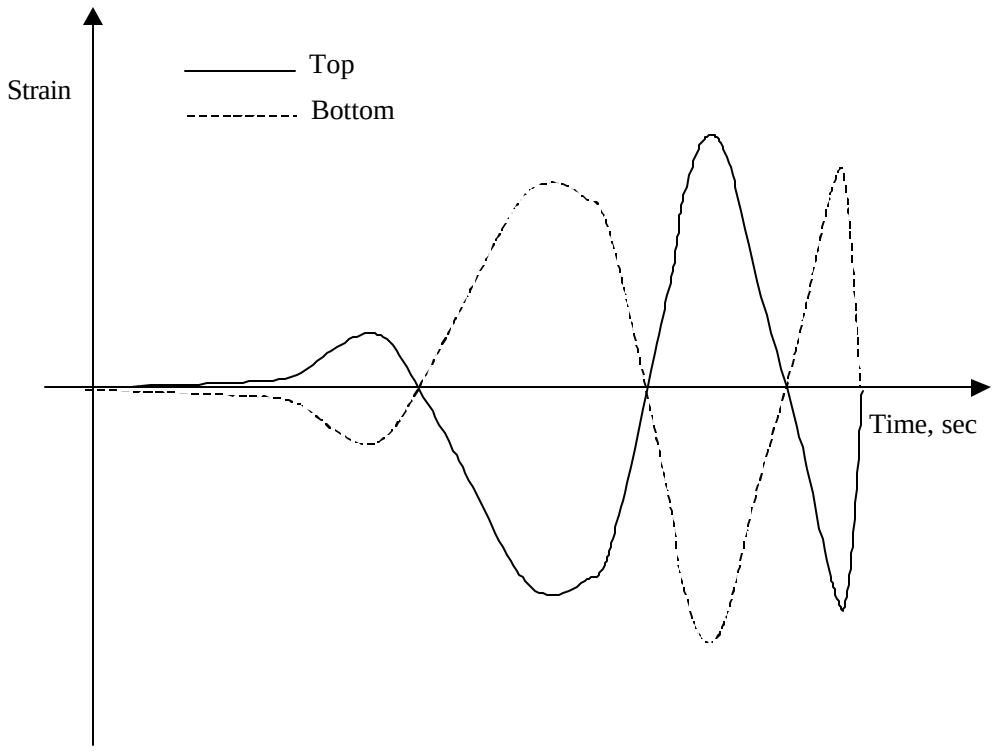

Figure 2.5. Longitudinal Strain Response from Strain Gauges at the top and at the bottom of PCC Slabs (after Sargand and Hazen, 1996).

Based on strain response measurements obtained from the FHWA pavement testing facility and discussed in section 2.1.11, doubling the tire pressure has no significant effect on the measured strain value. On the other hand, doubling the load increased the measured strain by 200 to 400 percent. However, as with other pavement instrumentation projects, these comparisons were based on the maximum tensile peak in the longitudinal strain response and the compressive strain preceding the tensile peak.

The shape of the strain response, whether in the longitudinal or the transverse direction, has been very consistent between all the instrumentation projects. The compression-tension behavior has been observed in most of the instrumented projects. However, explanation of this behavior has not been as detailed and the effect of the compressive strain on the performance of the HMA pavements has been ignored. Furthermore, very few pavement structural models show longitudinal strain response comparable to the measured response.

Sebaaly and Mamlouk (1987) developed a pavement structural model that takes into account the inertial forces of the pavement elements to calculate the stresses and strains in the pavement. The solution is based on a numerical solution for a set of orthogonal differential equations that describe a dynamic harmonic loading. They showed that the vertical acceleration of a point within the pavement changes from positive to negative as the loading axle passes over it. This means that the acceleration of a point within the pavement changes direction as the load passes, from an upward acceleration to a downward acceleration. Although this is not a conclusion from their research, it can be a cause of the compressive strain found in the longitudinal strain signal.

In 1993, Siddharthan calculated pavement strain from a moving dynamic load in a layered soil using a continuum-based finite-layer approach, which showed the compression tension behavior of the longitudinal strains (Siddarthan, 1993). The solution is achieved by first assuming the normal stress, σ_{zz}, and the shear stress components, τ_{xz} and τ_{yz}, which characterize a contact surface pressure moving at a velocity, V, in the longitudinal direction in the following form:

$$\sigma_{zz} = \sum_{n=1}^{N}\sum_{m=1}^{M} B_{mn} e^{i l_n (x - Vt)} e^{i m_m y} \tag{2.1}$$

$$\tau_{xz} = \sum_{n=1}^{N}\sum_{m=1}^{M} C_{mn} e^{i l_n (x - Vt)} e^{i m_m y} \tag{2.2}$$

$$\tau_{yz} = \sum_{n=1}^{N}\sum_{m=1}^{M} D_{mn} e^{i l_n (x - Vt)} e^{i m_m y} \tag{2.3}$$

where B_{mn}, C_{mn}, and D_{mn} are Fourier coefficients; and λ_n and μ_m are corresponding wavelengths of the harmonics. The response for a linear or viscoelastic system at any point is then given by the algebraic sum of the harmonics:

$$u = u(x - Vt) = \sum_{n=1}^{N} \sum_{m=1}^{M} U_{mn}(z) e^{i l_n (x - Vt)} e^{i m_m y} \tag{2.4}$$

in which $U_{mn}(z)$ reflects the variation in displacement of u with z only for the nth and mth harmonics. The major advantage of writing the response in this form is the ease of computing the derivatives with respect to x, y, and t.

Knowing that the response will be in the form given above, steps similar to those followed by Siddharthan *et al.* (1993) and Zafir *et al.* (1994) will lead to a sixth-order ordinary differential equation shown below, which can easily be solved to arrive at the final solution for U and, accordingly, the displacements:

$$D_1 \frac{d^6 U_{nm}}{dz^6} + D_2 \frac{d^4 U_{nm}}{dz^4} + D_3 \frac{d^2 U_{nm}}{dz^2} + D_4 U_{nm} = 0 \tag{2.5}$$

where D_1, D_2, D_3, and D_4 are constants that depend on the layer material properties and velocity of the vehicle, λ_n and μ_m, respectively.

In summary, proper understanding of the compression-tension behavior of the strain in the longitudinal direction is still under development, and the effects of the different loading parameters on the measured response still need to be evaluated further.

2.2.2 Stress/Pressure Cells

Although measurement of strain is clearly important in determining certain major failure modes, the relative importance of stress/pressure measurement cannot be overlooked. Stresses can be calculated from measured strains if material properties, loading, and layer thicknesses are known. However, because some of these parameters are not known (in the field), stress measurements will be essential to back-calculate material properties under field "construction" conditions. In addition, there are certain

factors in the field that are practically impossible to simulate accurately numerically (e.g. geosynthetics and drainage effect). Attempts have been made to model these conditions numerically, but the absence of meaningful data from field tests has made stress measurement a necessity.

The primary function of pressure cells is to monitor the change in the stress-state of the overlying layers and to measure the increase in vertical pressure due to dynamic traffic loading. This section details the pressure cells that have been used in the field in various projects, the advantages/disadvantages of these instruments, and their working principles. The Kulite type 0234 earth pressure cells are designed to operate within a vertical pressure range of 0 to 690kPa, and are 54mm in diameter, with a thickness of 14.3mm. It comprises a diaphragm that excites a strain gauge upon diaphragm deformation. The Carlson-type TP-101 has a stainless steel pressure head that is 114mm in diameter and 6.4-mm-thick, and is welded to a 16-mm outside diameter stainless steel tube that is attached to a silicon strain gauge transducer. It is designed to operate within a pressure range of 0 to 690kPa. Geokon 3500 is a large diameter soil stress cell consisting of two circular steel plates welded together around their rims to create a composite assembly 13-mm-thick with a diameter of 150mm. The space between the plates is filled with liquid. A steel tube connects the liquid to an electrical pressure transducer mounted several centimeters from the cell. The pressure transducer responds to changes in total stress applied to the cell. Geokon 3410S is a pore water pressure cell normally used in subsurface applications. It is similar in operation to the Geokon 3500, but is specifically designed to operate under intense static load conditions. MnRoad and Ohio SPS used Geokon 3500 pressure cells. Kulite 0234 has been used successfully in MnRoad. Penn State Test Track used Nottingham pressure cells at the interface of the base course and Virginia Tech used Kulite 0234 and Carlson-J1 (RST) in the Bedford project.

At the Virttaa test field in Finland, two types of pressure measurements were reported. The first is the traditional diaphragm-type pressure cell manufactured by the Road and Traffic Laboratory of the Technical Research Center of Finland, VTT. These

were installed at five different depths (Huhtala *et al.*, 1989). The second was used to measure the contact pressure between the truck tire and the pavement in the laboratory. The tire rolled slowly over a measuring point and the force was measured. Axle loads and tire pressures were varied and the results show that for truck tires, the maximum contact pressure is measured at the center of the wheel. However, when passenger cars were tested, the maximum response was seen at the edges of the tires. These results contradict the common assumption that the contact pressure distribution is the same for both trucks and passenger cars.

The primary use of the pressure cells mentioned above was in measuring the subgrade pressure (Metcalf, 1998; Sargand *et al.*, 1997; Selig *et al.*, 1997). This is because, as mentioned in chapter one, one of the main objectives of a pavement-layered system is to reduce the traffic load on the subgrade. Although the transducers used in measuring the subgrade pressure are several, measuring stresses in base material suffers from a large range of dispersion. This could be a result of disturbance of the base layer in which the pressure cells were incorporated.

Another explanation for the disturbance in the results can be drawn from the work done at MnRoad. Large diameter hydraulic pressure cells manufactured by Geokon Inc. were used for installation in granular base layers. During pre-installation sensor testing, it was discovered that about 40% of these sensors exhibited a damped oscillation when subjected to dynamic loads, but no oscillations in the response were found with the static loading (Beer *et al.*, 1997). Nearly all the pressure cells that have been tested show a linear response with the FWD load level. However, comparison of maximum pressures measured during FWD tests with values predicted from backcalculation parameters show that the measured values are typically less than those predicted from backcalculation models.

Vertical pressure on top of the subgrade was measured using the Kulite pressure cell at MnRoad (Dai and Van Deusen, 1998) for different truck speeds. The loads were

53,400N for the steering axle and ranged from 69,420N to 81,880N for tractor tandem axles. Speeds from about 32km/h to 75km/h were used on a pavement section that has a 127-mm HMA layer and a 305-mm dense graded gravel base. Testing was done at an average pavement temperature of 18^0C. It was found that the pressure on the subgrade did not significantly change with speed. It was also noticed that pressures were small, less than 10kPa. The same tests were repeated for an average pavement temperature of 9^0C. The measured pressures were reduced to about 50% of the values obtained at 18^0C, but still the effect of speed was insignificant. However, the effect of speed was significant at Bedford project (Al-Qadi, 1999). One has to note that the HMA thickness was 89mm and the base layer varies from 100-200 mm.

One of the main objectives of pavement instrumentation is to compare the measured values with existing pavement structural models. Accordingly, the difference between measured pressure values and pressures calculated using FWD results and the independency of the pressure measurements from speed, mentioned above, identifies two major problems with current mechanistic design procedures. First, the pavement is a dynamically loaded system and accordingly, any structural model should address the dynamics of the loading. Furthermore, pressure cells manufactured for pavement applications should be capable of measuring the dynamic response of the pavement. This can be seen from the dependency of the strain measurements on the speed, discussed in section 2.2.1, and the opposite for the measured pressures.

Second, while pavement materials are anisotropic in nature (properties in tension are different than the properties in compression), they are assumed isotropic. This means that vertical stress compatibility in pavement structural models is based on the same modulus as the horizontal stress compatibility, which may cause substantial errors. Accordingly, a sound structural model should take into account the difference in material properties in the three directions. This may cause the reported discrepancy between FWD calculations and pressure measurements.

Furthermore, the effect of temperature was found to be highly significant and accordingly, environmental measurements are essential in any pavement instrumentation project.

2.2.3 Environmental Measurements

The two most important environmental factors that influence the service life of pavements are temperature and moisture. Excessive temperature changes may cause flow and contraction in HMA, and curl and warp in concrete. Although low temperature is one of the most important failure modes in pavements, until recently, it has not been included in any design procedure. Moisture also causes major problems ranging from pumping to subgrade weakness. Therefore, temperature and moisture monitoring is important to develop a database that will be used to calibrate any pavement design models. Instruments used to measure temperature are thermocouples and thermistors. For moisture measurements, gypsum blocks, Time Domain Reflectometry probes (TDRs), and frequency-domain probes were used to predict moisture contents. Good experience was obtained with using measurements from Gypsum block, however, installation of these blocks in pavements is a major drawback (Al-Qadi and Bhutta, 1999; Brandon *et al.*, 1996). A comparison of the TDR probes and frequency-domain probes was performed in the Seasonal Monitoring Program (SMP) by the Federal Highway Administration's (FHWA) Long-Term Pavement Performance (LTPP) studies. Based on their findings, the TDR probes were selected over the frequency-domain probes because: (1) they provided more reasonable and reliable moisture contents, and due to (2) concerns about the effects of salinity on the frequency-domain probes (Rada, 1994).

Denver Airport uses thermistors to measure hourly temperature profiles in the concrete slabs. In Ohio SPS sections, thermistors are also used to monitor the temperature profiles in the HMA, base course, and subgrade. WesTrack uses thermocouples because of their excellent performance history and relatively low cost. Moisture measurements were taken in the past using gypsum blocks that provided a

qualitative measurement. However, Time Domain Reflectometry (TDR) is a highly efficient technique and performs well under adverse conditions. The precision of the measurements performed by TDR is very close to actual moisture levels inside a pavement section, if accurate dielectric properties of the soil can be determined. Projects like MnRoad and Ohio SPS use TDR. The Long Term Pavement Performance Program also recommends TDR as a standard moisture measurement device.

The main problem associated with TDR probe measurements is converting the change in dielectric constant to moisture content. This requires calibration of the probes using the same material used with in the field. Other factors, such as clay content, affect the dielectric constant. Topp *et al*. (1994) developed a universal equation for use with any soil. In a surprising number of instances, Topp's equation has been shown to be quite broadly applicable, even for gravelly soil. This led to the use of the term "universal" for this equation with the appropriate caveat that in organic soils or heavy clay soils, problems arise that may require specific calibrations. The successful use of the TDR depends on ensuring that the calibration equation used is appropriate for the soil and the application. For example, Australian Road Research Board's experience in their Accelerated Loading Facility show that this equation is unsuitable for high density crushed rock pavement material and a modified calibration relationship had to be determined. Topp's equation and comparable calibration equations are more readily applicable where changes in water content are desired rather than determination of absolute values.

Three fundamental questions exist concerning the calibration of TDR: (1) what volume of the porous material is measured by the TDR probe, (2) at what density was the calibration done, and (3) what spatial weighting of the water content does the probe use. The first question was answered by Knight *et al*. (Knight, 1994). He presented an equation for the proportion of the energy in the intended measurement region, and further recommended that this portion of energy should be no more than 5%.

$$P(\rho,\beta) = 1 - \frac{\ln[(\rho^2 + 1 - \beta^2)/(\rho^2 - 1 + \beta^2)]}{2\ln[\beta^{-1} + \sqrt{\beta^{-2} - 1}]}, \Rightarrow \rho \geq 1 + \beta \quad (2.6)$$

where,
ρ = r/d,
β = b/d,
r = radius of total energy measurement (r > b + d),
b= radius of the probe wires,
2d = distance between probe wires.

This equation can be used to backcalculate the correct container size for calibration. To eliminate the effect of density on the calibration, first one should try to reach the density obtained in the field, and second, include the density in the calibration equation. To avoid problems caused by undue weighting given to possible air gaps for regions of soil compacted around the wires, Knight recommended that the ratio of wire diameter to wire spacing should be less than about 0.1.

In addition to moisture and temperature measurements, other sensors have been manufactured to measure specific pavement environmental parameters. For example, soil suction was measured using a tensionmetric-type sensor in Saskatchewan (Fredlund, 1997). Another example is measuring the depth of the frost in cold seasons and whether it reaches the subgrade; this has been of concern at MnRoad and the Ohio SPS pavement testing sections. The Cold Regions Research and Enginering Laboratory (CRREL) Resistivity Probe developed a frost penetration measurement probe that is simply a series of thermistors at 25mm spacing. As the water freezes, its electrical conductivity increases rapidly and accordingly, the frost depth can be measured to an accuracy of 25mm (the thermistor spacing).

2.3 Fatigue

A rational approach to determining a material's response to given loading environments should consist of two stages: first, development of the physical

understanding of the operative mechanisms that govern the response, and second, incorporation of this understanding in a mathematical model that could provide relationships between the response characteristics and the variables characterizing the underlying mechanisms. In the previous section, the first step was addressed with relation to field behavior of flexible pavements. In this section, laboratory testing performed to understand the fatigue mechanisms will first be addressed, then the developed mathematical models will be reviewed.

Fatigue damage of pavements is a very complex process affected by pavement structural capacity, vehicle characteristics, mix properties, climatic effects, and time. Pavement structural capacity and the vehicle's characteristics affect the stress level at the bottom of the HMA layer and accordingly affect the fatigue life of the pavement (Pell and Copper, 1975; Eduardo and Manuel, 1981; Chatti *et al.*, 1995; Kong *et al.*, 1997; Simmons and Seaman, 2000).

Fatigue cracking is directly related to the strain development in the HMA layer and it starts when the tensile strains exceed a threshold value of the HMA. Attempts to quantify this threshold have been made but were unsuccessful due to the large number of parameters that affect the variability in HMA (Epps and Monismith, 1970; Ruth *et al.*, 1982). The location of the maximum tensile strains in the HMA layer has been argued to be either directly under the load or at the bottom of the layer. Recent research at the FHWA on instrumented pavement test section under simulated traffic and environmental loading shows that for thick pavements, cracks start at the bottom of the layer, while for thin pavements, cracks start at the top (Romero, 1999). Whether cracks start at the bottom or at the top, fatigue cracking starts as micro cracks that further become macro cracks. The macro cracks in HMA grow in a disjointed manner that depends on the aggregate size and surface texture (Yeou-Shang, 1991).

Crack growth measurements in HMA were conducted in laboratory tests using crack foil gauges at the outside of the specimens. The tests showed that the fracture

process consisted of three parallel occurring processes: cohesive crack growth through the binder, adhesive crack growth separating the aggregate from the binder, and a crack retardant process (Jacobs *et al.*, 1996). The crack retardant process is a temporary decrease in crack growth speed caused by a change in crack growth direction due to aggregates or air voids. The difference in crack growth characteristics between different mixes is due to different contributions of each parallel process to the overall behavior. This highlights some concerns with the application of fracture mechanics concepts since the crack growth is dependent on the configuration of the binder-aggregate structure which is different from one mix to another and from one point to another within the same mix.

Crack growth modeling has been studied through the principles of fracture mechanics. Although it provides some theoretical modeling to the fatigue phenomenon, its disadvantages are several. First, it is too complex for the practitioners. Secondly, it requires parameters that may be either very difficult to obtain or accurately assumed.

Another problem associated with fatigue studies, in general, is that they posse difficulties in relating the strains produced in test specimens in the laboratory to comparable strains in pavement systems. In the laboratory, the maximum strains in the test specimens are in essentially a one-dimensional (flexural beam tests) or two-dimensional (diametrical tests) state of strain (Tayebali *et al.*, 1995). In the pavement, however, the HMA is in a three-dimensional state of strain (Siddharthan *et al.*, 1998).

Under certain conditions, where the stresses normal to the bottom surface of the HMA are high, the strains parallel to the bottom of the surface layer may greatly be influenced by the Poisson's ratio of the HMA. The resultant tensile strain at the bottom interface is affected by the HMA Poisson's ratio when a compressive stress is applied at the top surface (Ullidtz, 1987). A serious question arises whether under such conditions the calculated strains in flexible pavement can be related to the fatigue response in laboratory specimens in which all tensile strains are produced by tensile stresses (beam

fatigue tests). However, in the case of indirect tensile test, the resultant tensile strain is mainly due to both compressive and tensile stresses. One way to solve the problem is by visual assessment of the in-service pavements and monitoring their performance. The Federal Highway Administration realized this fact and started a nationwide effort to collect performance data of in service pavement for more than 2000 newly-constructed and rehabilitated sites for 20 years starting in the late 1980's. The data are complied and are continuously updated in the Long-Term Pavement Performance (LTPP) database.

Although the LTPP data have been available for some time, very few attempts were successful in interpreting the data. In one of these attempts, a group of models were fitted to LTPP data to construct a continuous function between fatigue cracking damage ratio and observed fatigue cracking (Ali *et al.*, 1998). Different statistical models were developed to fit the data. It should be noted that there were only a few points that had considerable damage, using percent cracking as a criteria for damage evolution. Consequently, the models were unable to accurately define the failure point and the models may not be extrapolated to other conditions.

Similar work has been done in Louisiana using data from the Louisiana Accelerated Loading Facility (Djakfar and Roberts, 2000). In that study, different distresses were used in developing performance prediction curves. While the results showed good agreement between the predicted and measured distresses, cracking was found to reduce the accuracy of the prediction models. This may result from the inability to accurately assess the damage through visual observations of the percent area cracked. Therefore, a parameter that more accurately describes the deterioration of the HMA is needed. One alternative is the use of the stiffness modulus, which is related to the mix design and its resistance to deformation (Safwat, 1996; Kong *et al.*, 1997; Von Quintus *et al.*, 1982).

Mix properties can be separated into the stiffness of the binder, grading of the aggregate, and compaction of the mix. A further study of these variables can be

simplified by determining the value of the mix factor only, which may reduce superfluous laboratory effort significantly (Heukelom, 1966). The recently introduced SuperPave™ mixes have been reported to be less susceptible to fatigue damage presumably due to better aggregate structure and higher binder content than the traditional HMA (Wu *et al.*, 2000).

The influence of load level, mix properties, and environment must be considered simultaneously in any fatigue testing. A thorough comparison between many methods is presented in the SHRP A-404 "Fatigue Response of Asphalt Aggregate Mixes" (SHRP A-404, 1994). Fatigue testing is usually conducted using cylindrical or beam specimens. The indirect tensile fatigue test, ITFT, has a biaxial state of stress that is more representative of field conditions than the uniaxial stress state. Recent work by Read and Collop (1997) promoted the use of the ITFT for fatigue characterization due to the fewer number of specimens needed for fatigue characterization. They also listed the advantages and disadvantages of the ITFT:

ITFT advantages:

- Simple.
- Equipment applicable for other tests.
- Failure in a region with relatively uniform tensile stress
- Biaxial state of stress more representative of field conditions than uniaxial.
- Test can be performed on either cores or laboratory molded specimens.
- Discriminates between mixtures with different binder types based on stiffness and cycles to failure.
- Better repeatability than beam flexure.
- May be performed at different temperatures.

ITFT disadvantages:

- It is impossible to vary the ratio of vertical to horizontal stress.

- The method significantly underestimates fatigue life if the principal tensile stress is used as the damage determinant.
- The absence of stress reversal is of concern.

The Third Point Bending Test (TPBT) is very attractive because of its uniaxial state of stress (SHRP A-404, 1994), but specimen preparation required special equipment. Usually the binder and the aggregate are mixed in the lab, and then compacted using the Rolling Wheel Compactor (Ghuzlan and Carpenter, 2000; Harvey et al., 1993; La Roche et al., 1994) or the Kneading Compactor (Wu et al., 2000; Simons and Seaman, 2000). A more rational approach is to saw-cut samples from in-service pavements (Wu et al., 2000; Raad et al., 1992). Although this approach reduces the differences between field and laboratory compaction methods, cutting beams from pavements is not an easy task.

Other methods such as the Trapezoidal (Rowe, 1993; Smith and Hesp, 2000), Three Point Flexural Test (Read et al., 2000; Judycki, 1996), and uniaxial compression (Harvey et al., 1993; La Roche et al., 1994) were also researched.

Using these tests, many models were developed to characterize the fatigue of flexible pavements. Some of these models were developed to best suit specific characteristics of a particular institute, and some were just the output of an extensive laboratory testing.

2.3.1 The Asphalt Institute Fatigue Model

The laboratory model developed by Monismith et al. (1966) has been used by various agencies as the base case fatigue model, which has been calibrated by means of shift factors to correlate with their field conditions:

$$N_f = 0.00432\ \varepsilon_t^{-3.291}\ E_1^{-0.854} \qquad (2.7)$$

where,
N_f = number of cycles to failure;
E_1 = Dynamic Modulus; and
ε_t = tensile strain.

Finn et al. (1990) modified the above model by applying a shift factor of 18.4 to provide an indication of approximately 20% or greater fatigue cracking (based on total area) in sections of the AASHO Road Test.

The Asphalt Institute adopted the Finn model and modified it to reflect the effect of both percent air volume, Va, and percent asphalt volume, Vb, (AI, 1982). The final form of the equation used by the Asphalt Institute is the following:

$$N_f = 10^{M}(18.4)(0.00432)\,\varepsilon_t^{-3.291}\,E_1^{-0.854} \qquad (2.8)$$

where,
$M = 4.84\,\{V_b / (V_b+V_a) - 0.69\}$.

This model is adopted by the Idaho Department of Transportation, IDT (Bayomy, 1996). Note that for a standard mix with an asphalt volume, Vb, of 11% and an air void volume of 5%, M = 0. The shift factor used by IDT is 18.4 for new pavements, and that factor is incorporated in the following model:

$$N_f = 0.0796\,\varepsilon_t^{-3.291}\,E_1^{-0.854} \qquad (2.9)$$

2.3.2 The Illinois Fatigue Model

A condition survey is used to determine pavement sections that are candidates for overlay and should receive nondestructive testing. The testing is conducted using a Road Rater Model 2008 with a 35,600N load or a falling weight deflectometer with a 40,000N load. Pavement temperatures are recorded to allow temperature adjustments. Equations and nomographs have been developed for determining the remaining life and designing overlays for conventional flexible pavements and full-depth HMA; however, only

pavements on fine grain subgrades are addressed. The following fatigue equation was developed:

$$N_f = 5.0 \times 10^{-6} \varepsilon_t^{3.0} \quad (2.10)$$

A relationship between the deflection and strain at the bottom of the HMA surface layer, developed by the Strategic Highway Research Program, is used with a fatigue relation to determine the total number of loads, which can be carried in the spring and in the summer-fall periods (SHRP, 1991).

2.3.3 Arizona DOT Model

The fatigue model developed by the Arizona Department of Transportation, ADOT, is based on data obtained from 20 selected sites and the fatigue models previously developed by other researchers (Mamlouk, 1990):

$$N_f = 9.33 \times 10^{-7} \varepsilon_t^{-3.84} \quad (2.11)$$

The value of 3.84 for the strain power was chosen as the average of all strain power values of existing fatigue functions. To use this model, a multi-layer elastic program such as Chevron can be used to compute the tensile strain at the bottom of the HMA layer caused by a 40,000N dual-tire load. The layer moduli can be obtained from the FWD backcalculation. The HMA layer modulus is adjusted to a standard temperature of 21oC based on the AASHTO guide.

2.3.4 Shell Model

In this procedure the pavement is modeled as a three-layer linear elastic system consisting of an HMA concrete surface layer, an unbound or cemented base layer, and a subgrade with infinite thickness. The materials are assumed to be homogeneous and

isotropic, which allows them to be characterized by a modulus of elasticity and Poison's ratio. With this information, the stress and strains can be calculated for the pavement section. Relationships for HMA tensile strain fatigue and subgrade compressive strain for traffic loading have both been developed for use in predicting performance. The following relationship is used for fatigue:

$$N_f = 0.0685\ \varepsilon_t^{-5.671}\ E_1^{-2.363} \quad \text{(for a temperature of } 21^oC) \qquad (2.12)$$

The Shell method uses results from an NDT evaluation conducted with a falling weight deflectometer (FWD) to establish the effective thickness of the surface layer and the elastic modulus of the underlying subgrade. The surface modulus is determined by using the surface type and the surface temperature during FWD testing in a stiffness modulus chart developed for FWD loading conditions. The base layer thickness is assumed, taken from construction records, or measured from cores. Poison's ratio for all layers is assumed or measured in lab tests. The elastic modulus of cemented base material can be calculated using the following relationship:

$$E_2 = k\ E_3 \qquad (2.13)$$

where:
$k = 0.206(h_2)^{0.45}$;
h_2 = base thickness (mm);
E_2 = base modulus (MPa); and
E_3 = subgrade modulus (MPa).

This relationship was developed using the BISAR elastic-layers program. Equation 2.12 is typically used for overlay design. The required overlay thickness is selected as the most conservative value determined from subgrade strain or HMA strain fatigue. The future fatigue is adjusted for the decrease in strain at the bottom of the HMA layer due to overlay. If the pavement is extensively cracked, the existing pavement is analyzed as a granular layer and the overlay is selected on that basis. The temperature of

the pavement used in the design is the mean annual air temperature, weighted to account for daily and monthly temperature gradients in the HMA layer (Bayomy *et al.*, 1995).

2.3.5 Federal Highway Administration Model

The FHWA model uses an elastic-layered analysis (ELSYM5) of the pavement to determine the stress or strain created in the pavement by loading. An empirical relationship for the pavement life was developed based on AASHO Road test data:

$$N_f = 9.73 \times 10^{-15} \varepsilon_t^{5.16} \quad (2.14)$$

The Non-Destructive Evaluation (NDT) evaluation allows use of different deflection equipment such as the Dynaflect, Road Rater, Benkelman Beam, and the Deflectograph.

The modulus of elasticity for each of the pavement layers above the subgrade is determined from laboratory testing of pavement layer materials. The subgrade modulus is determined using a combination of laboratory test data and deflection matching procedure based on elastic-layer analyses. The ELSYM5 program is used to determine relationships between the resilient modulus and deflection and between resilient modulus and deviator stress. The laboratory curve of resilient modulus versus deviator stress is then adjusted to reflect the relationship found above, and the existing resilient modulus is then selected from this adjusted curve at the design load.

A detailed condition survey is conducted to determine the remaining fatigue life classification of the existing pavement. The type of overlay to be placed, the type of existing surface material, and remaining fatigue life is used to select a subsystem for overlay design and the appropriate fatigue model. A total of 18 different design subsystems are available for use for flexible and rigid pavements combined (Majidzadeh, 1983).

2.3.6 NCHRP

Background for the NCHRP investigation to develop a series of models designed to predict physical distress in HMA pavements (Finn *et al., 1987*) was developed under previous NCHRP projects, specifically NCHRP project 1-10 and NCHRP project 9-4, along with a number of sources in the United States, Canada, and Europe.

Three types of materials were considered in that investigation: HMA, asphalt emulsion mixes, and cement-treated bases. It was desirable to obtain a single damage hypothesis for the three materials. A computer program was developed through the investigation and is referred to as PDMAP (Probabilistic Distress Models for HMA Pavements).

The procedure used to develop a prediction model was the following: (1) select a set of laboratory curves as a base case for crack initiation; and (2) calibrate the laboratory curves by means of a shift factor to correlate with different levels of cracking based on field observations.

The base case fatigue curves selected were reported by Monismith *et al*. (1990). Initial efforts to calibrate the PDMAP prediction models for HMA were based on observations of cracking and rutting at the AASHO Road Tests.

A regression equation to model the maximum tensile strain at the bottom of the HMA layer as a function of the layer thickness, layer moduli, and the applied load was developed. The damage for 12-hr periods was then calculated using the following relationship:

$$D_i = n_i / N_i \qquad (2.15)$$

where
D_i = damage during period i,

n_i = number of load applications during period i, and
N_i = total allowable load applications for strain value calculated during period i.

The accumulated damage calculated by this model is then compared to the actual observed damage in 17 sections, in Florida and Utah, and the corresponding shift factor is calculated. Based on Mitchell and Monismith studies, a fatigue cracking model proposed for used with PDMAP is as follows:

$$N_f = 9.73 \times 10^{-15} \varepsilon_t^{5.16} \quad (2.16)$$

In calibrating the predictions models in PDMAP, it was found that PDMAP under-predicted the load cycles to initial fatigue cracking at one of the sites.

2.3.7 Washington State Department of Transportation Model

The Washington State Department of Transportation (WSDOT) fatigue equation is somewhat similar to those used elsewhere. This is because they also used the Monismith and Epps model that was later modified by Finn to account for field conditions (using a shift factor of 13.4).

In the development of the overlay procedure for Washington State, 16 test sites were selected. Washington State Department of Transportation collected pavement surface deflection measurements with the FWD. These measurements were collected in the outer wheel path nearly every season from 1985 to 1988. The following is the equation used to perform the temperature adjustment of HMA material:

$$\log E_{AC} = 6.4721 - 0.000147362 (T)^2 \quad (2.17)$$

and for unstabilized materials:

$$E_{BS} = 8{,}500\, \theta^{0.375} \quad (2.18)$$

where,
T = Pavement temperature ^{o}F, and
θ = Bulk stress (psi).

EVERCALC was used to backcalculate the moduli. This program is based on the multi-layered program CHEVRON. When six test sites were tested to investigate the shift factor, it ranged from 0.1 to 6 depending on the HMA layer thickness. High shift factors were associated with low thickness and vice versa. It must be noted that six test sites is not very reliable. Further studies of the shift factors at the WSDOT used a shift factor of 10 for relatively thin HMA layers.

Several studies in Washington State have examined the various aspects of seasonal pavement material changes. The results of the observation that indicated that the base course changes the most came as no surprise. This change is probably due to the greater layer moisture change in the base course layer, compared with those of subgrade.

2.3.8 Other models

Many other agencies have developed their own models. The equations developed by these agencies are presented below (Bayomy, 1995).

a) Transport and Road Research Laboratory, U.S.

$$N_f = 1.66 \times 10^{-10} \varepsilon_t^{4.32} \quad (2.19)$$

b) U.S. Army Corps of Engineering

$$N_f = 497.156 (\varepsilon_t)^5 (E_1)^{2.665} \quad (2.20)$$

c) Belgian Road Research

$$N_f = 4.92 \times 10^{-14} \varepsilon_t^{4.76} \quad (2.21)$$

Regardless of the test type and configuration, there is a common problem in all models, which is failure definition. Fatigue life obtained using constant stress testing is faster than the fatigue life resulting from the constant strain testing for the same initial conditions. This would be expected as the same stress is used during the constant stress test while it decreases during constant strain testing. Some studies show that the fatigue life obtained from constant strain testing is two to three times the fatigue life obtained from the constant stress testing for the same initial strain in the first cycles (Bazin and Sauier, 1967). Monismith and Epps (1973) recommended the use of constant strain testing for thin pavements (less than 50 mm), and constant stress for thick pavement (greater than 150 mm).

Kim et al. (1997) proposed the 50th percent reduction in initial stiffness as failure criteria in fatigue testing to be dependent on mode of loading. They use the pseudo strain concept, needed for the correspondence principle, to simplify the task of separating the viscoelastic behavior and the damage growth of HMA. It was recommended to use constant stress testing in HMA because of the difficulties in calculating pseudo strain values in constant stress. This indicates that further work is still required before this procedure can be universally applied (Ghuzlan and Carpenter, 2000).

Himeno et al. (1997) defined failure in fatigue of HMA when the stress level changes suddenly. It is obvious that this definition depends on constant strain testing, and it cannot be used in constant stress testing. The use of dissipated energy to define damage accumulation and hence, failure was used by Ghuzlan and Carpenter (2000). They defined an energy ratio term equal to the change in dissipated energy between two cycles divided by the total dissipated energy. Then the failure is defined as the number of load cycles at which the change in this energy ratio begins to increase rapidly.

The validity of a unique performance model, based on correlating the accumulated traffic to distress survey data for in-service pavements, is debatable. Therefore, fatigue concepts that consider the effect of loading cycles to be additive are

considered to be inadequate in most cases for pavement life predictions (Ruth et al., 1982). Perhaps the only method for validating any criterion is the direct measurement of failure in in-service pavements. The most accurate technique to measure in-service failure is through proper pavement instrumentation. This will also allow the monitoring of the pavement as it gets damaged and consequently fails.

CHAPTER 3: Research Approach

The approach taken in the assessment of fatigue life prediction for the Virginia Smart Road mixes entailed several steps. First, the strains in the field must be measured accurately. This entails proper calibration and installation. Once the strains are measured, different analytical methods would be evaluated for their applicability in defining the critical pavement strains. These critical strains are then used in laboratory tests to measure the fatigue life. The fatigue life obtained in the laboratory may be converted to fatigue life in the field through the application of several shift factors. The shift factors are calculated using stress and strain measurements in the field and in the lab.

3.1 Pavement Response Measurements

As technological capability advances, so does the entire supporting infrastructure. Thus pavement instrumentation today is experiencing a technological revolution to withstand the demands on the infrastructure by understanding the material performance in the field as well as pavement system response to loading and environment. This revolution is directed towards developing sensors to measure pavement response parameters. Parameters that need to be measured in the field include strains, stresses, deflections, moisture, and temperature. Measuring these parameters in the field allows for accurate performance model development and mechanistic pavement design calibration.

With different accelerated pavement testing projects being constructed today, different sensor manufacturers are finding a new practice of marketing their products. Before implementing any of these products, one has to make sure of their applicability and usefulness in pavement applications. With that said, what does usefulness and applicability mean? Ask this of different people and there are likely to be as many

answers as there are people asked. The user or agency providing funds for research demands to know everything. The researcher wants to keep it all within capability whereas the manufacturer wants to keep things as inexpensive as possible.

This section presents the steps taken to ensure the usefulness and applicability of the instrumentation in the Virginia Smart Road project. In section 3.1.1, the typical pavement sections used in Virginia are identified and incorporated into the design of the 12 different flexible pavements at the Virginia Smart Road. Section 3.1.2 discusses the sensors selected to measure these parameters. Calibration of these sensors is presented in section 3.1.3. Finally, the procedures that are needed for proper installation of the sensors are presented in section 3.1.4.

3.1.1 Flexible pavement sections

The Virginia Smart Road is being built in stages, with the first two miles of the west–bound lanes being constructed first to allow researchers to utilize a portion of the roadway as a controlled testing facility for several focus areas. Until the east-bound lanes are paved, a portion of the east-bound lanes will be paved to allow conventional traffic to bypass the original test-bed. When this occurs, researchers will be able to route conventional traffic around the test-bed with the use of a gated detour.

The flexible pavement portion of the Virginia Smart Road includes 12 different flexible pavement designs, Figures 3.2 through 3.4. Each section is approximately 100m long. Seven of the 12 sections are located on a fill, while the remaining five sections are located in a cut. All 12 sections are closely observed through a complex array of sensors located beneath the roadway and embedded during construction. Diagrams for the location of these sensors are shown in Appendix A. The experimental pavement section partially overlaps the all-weather-testing section so that weathering effects can be

measured. The weather-generation capability helps accelerate pavement service life in those sections.

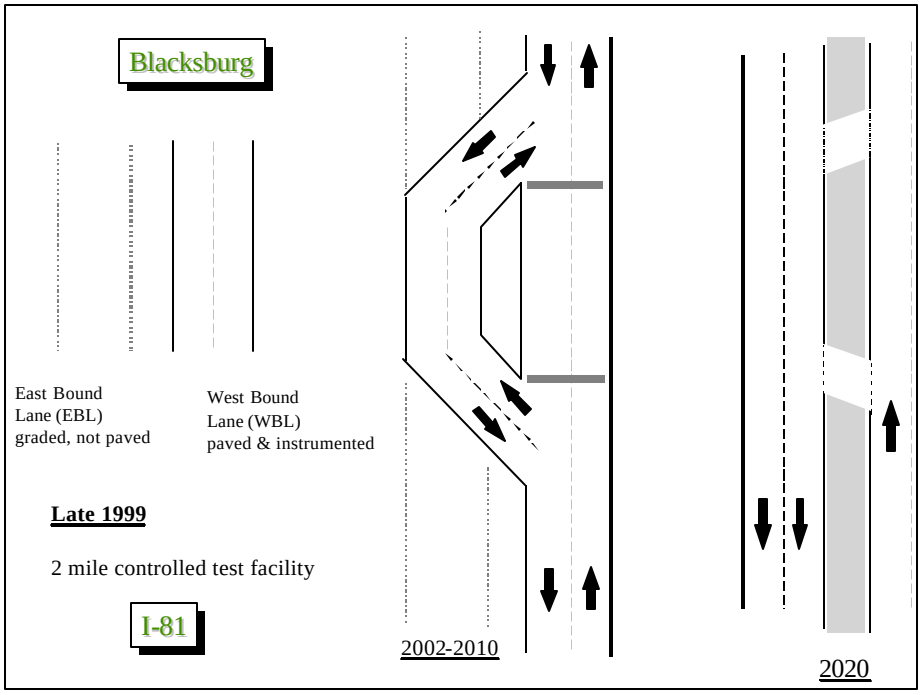

Figure 3.1. Virginia Smart Road Layout

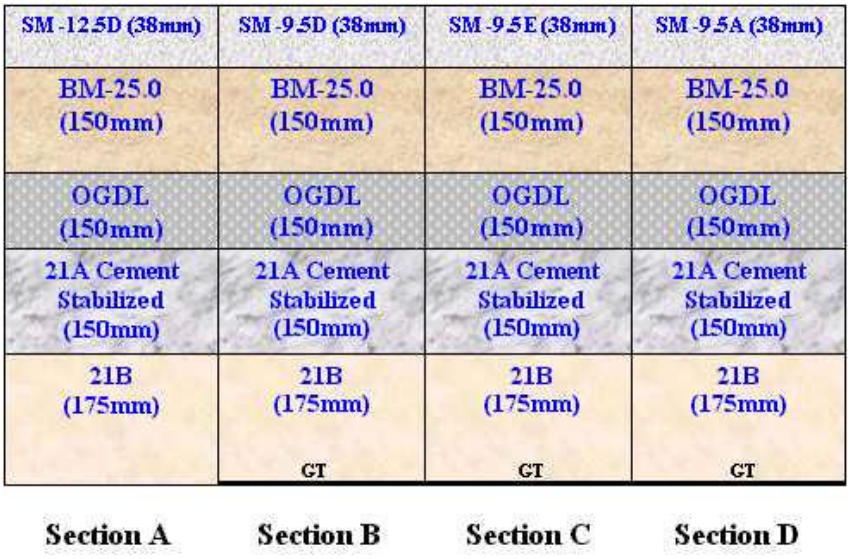

Figure 3.2. Pavement Design- Sections A-D

Instruments from every two adjacent sections are connected to one bunker station where the computer for the data acquisition is located. To precisely position instrumentation in each section, a coordinate system was established. Since all the wiring from the instruments is going to the bunker station, the coordinate system will start at the bunker. For that reason, all the sensor locations are referenced to their relative bunker station. The instruments are located within 10m of each section. The beginning of the instrumentation for each section is located ten meters away from its relative bunker station.

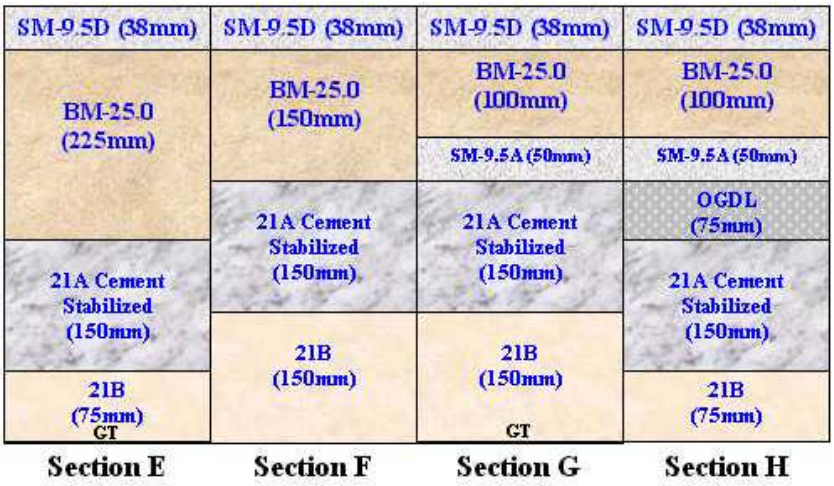

Figure 3.3. Pavement Design- Sections E-H

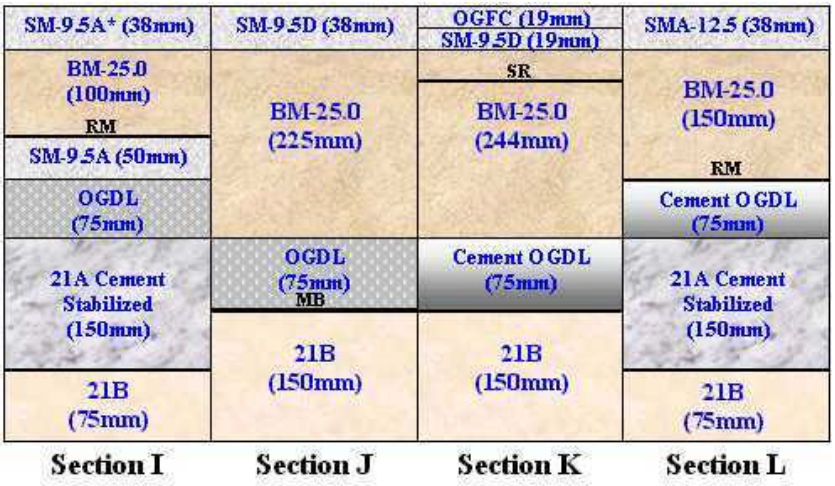

Figure 3.4. Pavement Design- Sections I-L

3.1.2 Instrument Selection

The two prime requirements in instrument selection are sensitivity sufficient to produce the necessary information, and reliability to ensure that dependable data can be obtained throughout the period for which the data is needed. Nevertheless, simple instruments are sometimes inappropriate and more complex instrumentation must be used. For example, a thermocouple is more than enough to measure the temperature, while measuring strains in the HMA layers requires a special HMA strain gauge to withstand large strain and the high HMA placement temperature.

Based on the literature review, Dynatest gauges have good performance in most of the test tracks and test roads. Accordingly, they are used for the major HMA strain measurements in the Virginia Smart Road, Figure 3.5. A few Kyowa gauges are also used for evaluation, Figure 3.6.

Strains in the base/subbase interface or in the subbase/subgrade interface have not been measured in any of the test roads, but have been measured in many of the test tracks and scaled down pavement facilities. Therefore, a sensor that would withstand the heavy construction operations is needed. Accordingly, the sensor that was chosen for this purpose in the Virginia Smart Road is a modified Geokon model 3900. The gauge that was manufactured for the first time for this project comprises a full bridge, bonded strain transducer mounted in housing with electrical cable leading to the readout location, Figure 3.7. The full-scale range of the gauge is 3.2mm.

Figure 3.5. Dynatest Strain Gauge

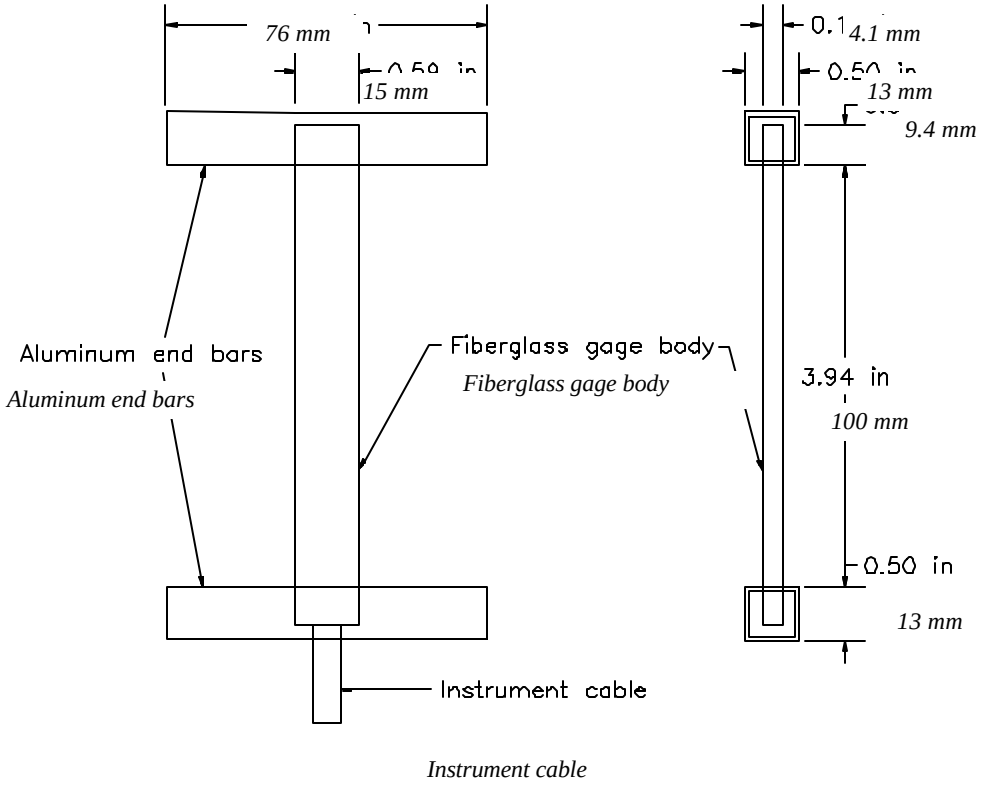

Figure 3.6. A Schematic of the Kyowa Type Embedded HMA Strain Gauge.

Soil horizontal strains may be measured using Carlson J-1 and Geokon-VCE-4200 vibrating wire strain gauges. Although Geokon-VCE-4200 is used primarily to evaluate the effects of curling and warping caused by temperature and moisture effects in concrete slabs, it can successfully be used in soils to measure static strain. The Geokon model VCE-4200 Vibrating Wire Strain Gauge was selected for this project, Figure 3.8. It was used in the Minnesota Road research project for static measurement of the horizontal strains in concrete. It is 152-mm-long and is widely used for strain measurements in different civil engineering applications.

Figure 3.7. Aggregate Strain Gauge

Geokon 3500 (690 kPa and 345 kPa) pressure cells have been chosen for this project due to their imprint size, accuracy, price, and survivability. The larger diameter cell (345 kPa) is used in the lower layers of the pavement, below the OGDL, while the smaller diameter (690 kPa) is used in the HMA layers. The larger diameter cells are used in the lower layers to capture as much of the stress that is laterally distributed as the pavement depth increases. In addition, all the pressure cells used in the HMA had a special heat-resistant wire to withstand the high HMA lay-down temperature. These pressure cells were modified from their original design to suit the pavement application at

the Virginia Smart Road, Figure 3.9. The modification was mainly in the connecting tube between the transducer casing and the load-sensing element. The connecting tube was bent at a 45^0 angle to allow the transducer casing to be buried in the underlying layer to protect it from the heavy construction equipment.

Figure 3.8. Vibrating Wire Strain Gauge

Figure 3.9. Pressure Cell

For temperature measurements, T-type thermocouples are used for their excellent service life, field installation, and price. In-house manufactured gauges were used, Figure 3.10. The CS615 and the CS610 time domain reflectometery (TDR) probes were chosen for moisture measurements, Figure 3.11 and 3.12, respectively. The CS615 is used as the main measuring probe, and the CS610 provides a backup in case of CS615 failure. This decision was made based on accuracy and the survivability of the CS610 in pavements. Finally, resistivity gauges are used to estimate the depth of frost in the wintertime as well as the depths of the thaw lines in the spring, Figure 3.13. Table 3.1 shows a summary of the number of instruments used in each section.

Figure 3.10. T-type Thermocouple

Figure 3.11. TDR CS615

Figure 3.12. TDR CS610

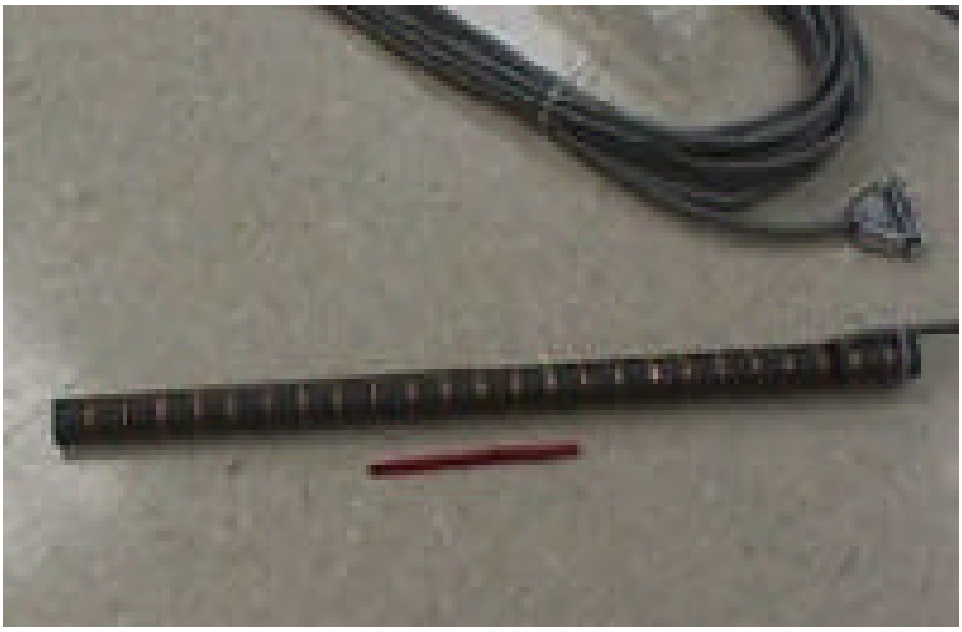

Figure 3.13. Resistivity Probes

Table 3.1. Instrument Summary

	A	B	C	D	E	F	G	H	I	J	K	L	Total
Aggregate Strain Gauge	6	3	0	3	0	3	3	0	6	3	6	3	36
Dynatest	11	21	3	3	3	3	9	9	17	6	12	7	104
Kyowa	3	0	2	0	0	0	0	0	0	0	0	6	11
Vibrating Wire	6	0	0	0	0	0	3	0	3	0	3	3	18
Pressure Cell	12	12	6	6	3	6	12	9	15	9	12	15	117
TDR CS615	4	10	0	2	4	4	4	4	4	4	4	4	48
TDR CS610	2	5	0	0	2	2	5	2	4	3	3	3	31
Thermocouple	17	6	6	6	8	8	14	8	14	10	6	12	115
Resistivity	1	1	0	0	1	1	0	0	1	1	1	1	8

3.1.3 Instrument Calibration

A typical dictionary definition for calibration is to "ascertain the caliber of; to test the accuracy of an instrument against standard." The British Calibration Service defines calibration as: "A calibration, whether it be of an instrument or work piece, provides a set of authenticated measurements by means of which the measurement capability of the instrument or the correctness of the work piece to a specification can be judged." All of the sensors used in pavement evaluation studies today have no standard, but their performance has to be identified and formulated in order to be able to evaluate the performance of the pavement. It follows from this discussion that calibration, then, is to subject a transducer to a selected environment generally similar to that to be experienced in use but in a controlled and measurable way. Again, it is not always possible to model the field environment, especially since the environment is sometimes unknown; such is the case in pavement applications. Therefore, the goal of the calibration in this study was to subject the sensors to a repeatable and close-to-field environment.

3.1.3.1 Identification of Errors

Most instrument manufacturers supply information on the various error sources that they think are important. Unfortunately, because the pavement instrumentation is under development, not all sources of errors are identified. This results in little chance of correcting for a particular error and poses a difficulty in comparison between similar products. Errors can be grouped into five basic errors:

1. Intrusive error. This is where the inclusion of the transducer may well change the performance of the caliber or the environment it is to be placed in. These effects are due to the transducer modifying the performance of the test facility.
2. Combination error. The combination of the caliper and the transducer may well provide repeatable but erroneous results. Cases where this can arise are often due to the ability of transducers to respond to input other than their designed input. As an example, the error that occurs in load cells where they are often bending sensitive.
3. Dynamic error. In pavement applications, almost all that needs to be measured is dynamic in nature, but most calibrations are static, i.e. subject to a constant input. Examples of these are hysteresis effects, where loading response is different from the unloading response.
4. Signal conditioning errors. While great attention is paid to the performance of the transducer, signal conditioning is often forgotten. This will be addressed in the data acquisition section later.
5. Repeatability. It is accepted by convention that three tests are sufficient. If there is a systematic change from test to test, then three tests may not be sufficient to measure the maximum possible error. This suggests that calibration results must be examined with care before being used.

Some sensors must have zero output for zero input. However, most devices do provide a signal output as a datum level when no input is applied. The monitoring of this zero value serves three purposes: it is a measure of the long-term stability of the device; it allows a check to be made on the system noise level; and it is the only value available to the user that does not require a calibrated input.

Therefore, the zero reading must form part of any calibration. For that purpose, a caliper has been manufactured in-house to simulate the expected range of strain that might be required to measure from the strain gauge. Most of the calipers available in the market are provided for specified dimensions of gauges and are unable to apply bi-directional force on the gauge. This caliper is capable of applying uniform static or dynamic tension and compression force to the gauge by means of a screw shaft that moves in both directions without applying torsion to the gauge or bending it. A sensitive micrometer head ($2x10^{-4}$ mm) was connected to the system to measure the exact amount of applied displacement to the gauge. By changing the fixing apparatus, this caliper was suitable for any type of strain gauge, Figure 3.14. It was used for the three main types of strain gauges used in this project.

3.1.3.2 Hot-Mix Asphalt Strain Gauges

The PAST transducer has a resistance of 120ohms, and a gage factor of 2.0. It can be incorporated into a full bridge setup with up to 12V excitation voltage. The average modulus of the cell body is as low as 2.200MPa due to the special properties of the cell materials. A cross-section area of only $5000mm^2$ results in an extremely low "strain force" of 0.11N/microstrain. This takes into consideration any intrusive errors.

It must be emphasized that data from this type of gauge are the average strain in the area between the anchors. Under special load conditions, such as a high tire pressure,

a gauge having a relatively short distance between the anchors would record higher strain values than its longer counterpart.

The gauge factor has higher accuracy than what would be obtained by a workshop calibration. Consequently, no efforts were made to reassess the instrument. Krarup (1991) had arrived at the same conclusion and suggested that lower accuracy would resulted if an in-house gauge factor were to be used over the manufacturer's factor.

3.1.3.3 Aggregate Strain Gauges

To check the value and calibration curves provided by Geokon, the above-mentioned caliper was used to determine the zero value of the gauges. The manufacturer provided calibration curves for each gauge. These calibrations were done by comparison with standards traceable to the NIST, in compliance with ANSI Z540-1. The caliper developed at Virginia Tech was used to check the calibration curves from the manufacturer with special emphasis on the zero value of the gauge. Readings from the caliper were directly comparable to those provided by the manufacturer.

3.1.3.4 Soil Strain Gauges

The VCE-4200 offers a range of frequency between 400 and 1000 Hz, with a mid-range frequency (equilibrium position) ranging between 830 and 915 Hz. This high mid-range frequency offers a wide range of measurements in compression, but a very small range in tension. The induced tension was very low and a solution needed to be found.

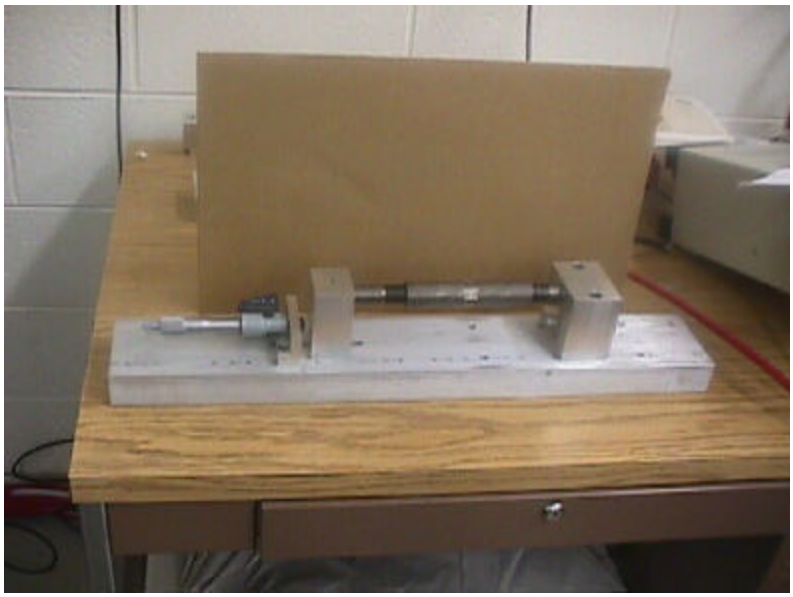

Figure 3.14 Strain Gauge Caliper

In order to solve this very small range of tension, the ability of the data acquisition software to detect frequency was increased to 1500 Hz. Also, after contacting the manufacturing company, it became apparent that the upper range of frequency might be increased up to 1250 Hz without any risk on the gauge performance.

Before installing the equipment, a check of all the vibrating wires, as well as a record of the mid-range frequency, was performed.

It appeared during the first day of installation that recording this equilibrium frequency was very useful. By knowing this frequency, it is possible to monitor the behavior of the strain gauge directly after installation and after the installation of each layer. It appeared that a slight compression force was induced in the strain gauge just after installation. This was mainly attributed to the increasing load due to compaction and layer placement.

3.1.3.5 Time Domain Reflectometry

Topp *et al*. (1980) presented several equations that could be used to describe the dielectric properties of soil as a function of moisture content. It was assumed that the electric loss associated with soils was negligible; therefore, the apparent dielectric constant of soil could be approximated by its real component. They also presented a relationship described as "universal" in yielding the volumetric water content, θ_v, in terms of the apparent dielectric constant. This equation is considered independent of soil density, texture, and salt content. Topp *et al*. in 1980 and Rada *et al*. in 1994 recommend that for more accurate determination of moisture content, a series of calibration measurements should be performed.

A wooden calibration box (0.84m x 0.85m x 0.45m) was constructed, using no metallic fasteners, to be used in the calibration process. The calibration box allows four probes to be tested simultaneously without adversely affecting the measurements. To evenly mix water with soil, a 0.4-m^3 concrete mixer was used to mix approximately 40 kg of soil per batch. The procedure was repeated until enough soil was mixed with the desired amount of water to fill the calibration box. Soil was placed in the calibration box in three layers. Each layer, approximately 150mm thick, was placed and then compacted before the following layer was placed. The probes were placed within the second layer, separated by at least 150mm, before this layer was compacted. After TDR measurements were taken, a sample of soil (approximately 3kg) was removed from the middle layer and placed in an oven at 110 °C so that the gravimetric moisture content could be determined.

3.1.3.6 Pressure Cells

Pressure is a mechanical concept that is referred to in the field of mechanics as compressive stress. No definition of pressure is really useful to the engineer until it is translated into measurable characteristics. A pressure transducer can convert the

mechanical input, pressure, into an electrical output, voltage. Selecting the right transducer requires knowledge of both its application and the characteristics of transducers that make the measurements. Power supplies, amplifiers, signal conditioners, and the data acquisition system dictated the transducer output levels and input excitation.

The RST pressure cell was selected for this project. It is a complete system, accepting an input pressure at one end and providing an electrical output. It consists of two circular steel plates welded together around their rims to create a cell approximately 150mm or 225mm in diameter and 12.5mm thick. The space between the plates is liquid-filled. The fluid has a boiling point of 197^0C. This boiling point was chosen as such to be higher than the lay-down temperature of the HMA to prevent expansion of the cell diaphragm. A steel tube connects the liquid to an electrical pressure transducer mounted several centimeters from the cell. The pressure transducer responds to changes in total stress applied to the material in which the cell is embedded.

The transducer is enclosed in a heavy protective 316 stainless pipe to prevent damage from the aggregate and to prevent problems with over pressure. The transducer consists of two basic elements, one mechanical and the other electrical. The mechanical, or force-summing element, converts the applied pressure into a deflection or displacement that is proportional to the pressure. The mechanical displacement is transmitted to the strain-sensing element, thus changing the electrical resistance of the sensing element. The sensitive side of the load-sensing element is made of nominal 12-gauge stainless steel. The load averages over the total area of the cell and point loads are largely compensated for. Side loading should have little effect, as the surface is quite small. The dimensions of the cell were chosen to minimize the effects of side and point loads that may affect the response.

This pressure transducer is a strain-gauge type. The strain gauge in the transducer is bonded to a diaphragm that flexes with pressure. A pair of gauges (one on each side) is

mounted at the center of the diaphragm, and two are mounted in the comparatively unstressed area at the edge of the diaphragm as shown in Figure 3.15.

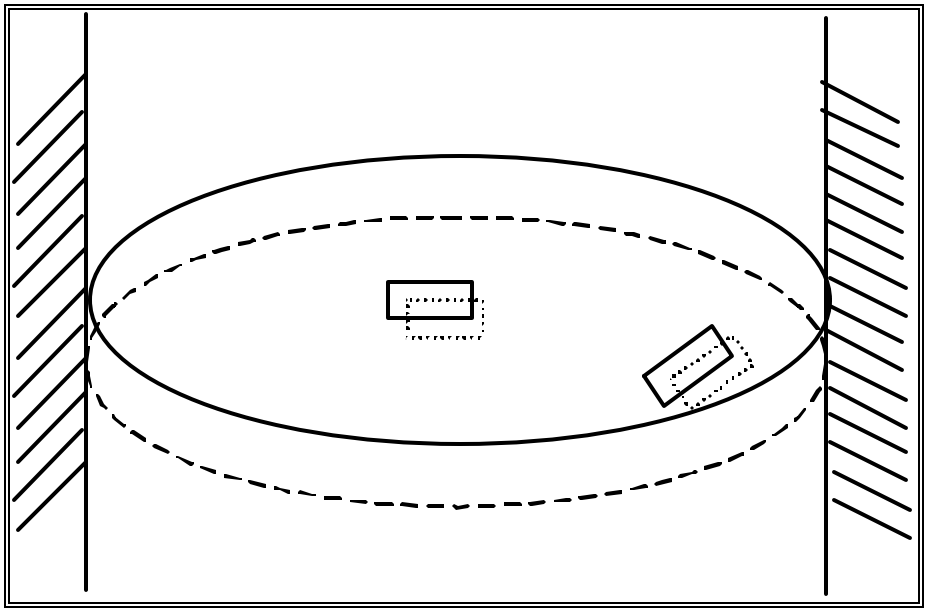

Figure 3.15. Diaphragm inside the Pressure Cell Transducer

The unstressed gauges are known as dummy gauges, and are included in the bridge circuit to provide automatic temperature compensation. The gauges at the center of the diaphragm give an output, which is proportional to pressure. The pressure represents the force applied over the area of the steel sensing-element. The transducer measures fluid pressure.

The first pressure cell selected has a diameter of 150mm and can measure up to 690kPa. These pressure cells were placed in the upper layers of the pavement structure, i.e. HMA layers. They have been specially designed to withstand high temperatures during placement. The second pressure cell, placed in aggregate layers and subgrade, has a 225-mm diameter and can measure up to 345kPa. These pressure cells are designed for base layers and subgrade where the stress is lower than the surface and the influence area is greater.

Calibration curves were developed by the manufacturer to convert the measured voltage from the cell to pressure. Each cell was placed between two rigid plates, which had inflatable rubber membranes. The pressure in these membranes was gradually increased and held constant for a specific time, and then the voltage was measured. This process was repeated until the full range of the pressure cell was covered. A typical calibration curve as provided by the manufacturer is shown in Figure 3.16.

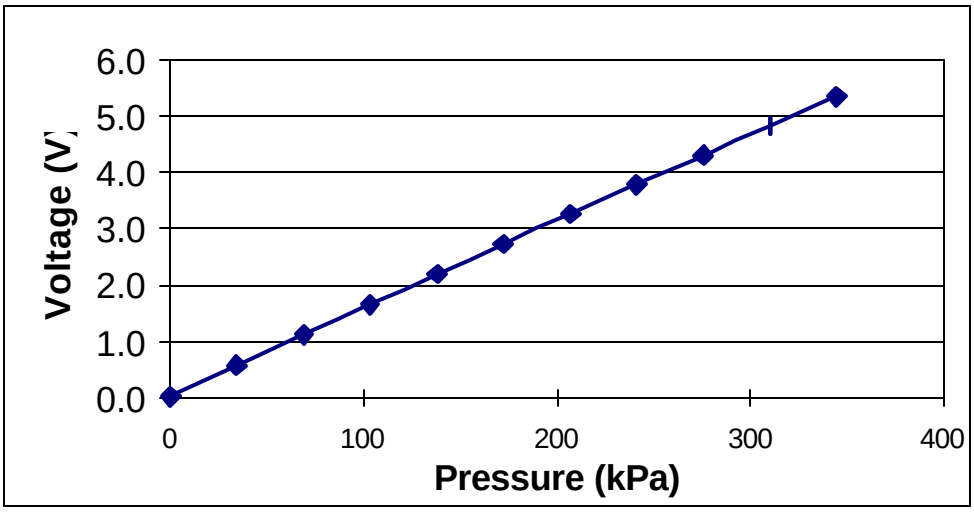

Figure 3.16. Calibration Curve for Pressure Cell Labeled 9p2-1 by the Manufacturer.

This calibration does not consider the rate of loading and material properties where the cell will be embedded. Thus, such effects may affect the calibration curves. The assumptions associated with using the manufacturer's calibration curves are the following:

- Load in the field is dynamic in nature.
- The material surrounding the cell in the field is not a liquid. If the cell is to be used in the HMA layers, time-dependent properties need to be carefully considered.

- If the cell is to be used in the lower layers of the pavement, the behavior of this cell to particulate material surrounding it is assumed to be of no significant effect.
- The dependency of the cell to rate of loading is ignored.

To evaluate the aforementioned effects, testing of some pressure cells in a Gyratory compactor and in an Instron machine was conducted.

Pressure Cell Calibration Using Gyratory Equipment

The pressure cells were placed in the Gyratory compactor to apply a static load, and the output voltage was measured. A solid steel spacer cylinder was placed in the Gyratory. A 150-mm cell was placed on top of the spacer. The cell was then loaded using the 150-mm puck that comes with the Gyratory. The cell was connected to the data acquisition system to measure the voltage output and the Gyratory was set to apply a load of 200kPa on the cell and the voltage reading was noted. This was repeated at different pressure levels, and the curve of voltage vs. pressure was plotted, Figure 3.17.

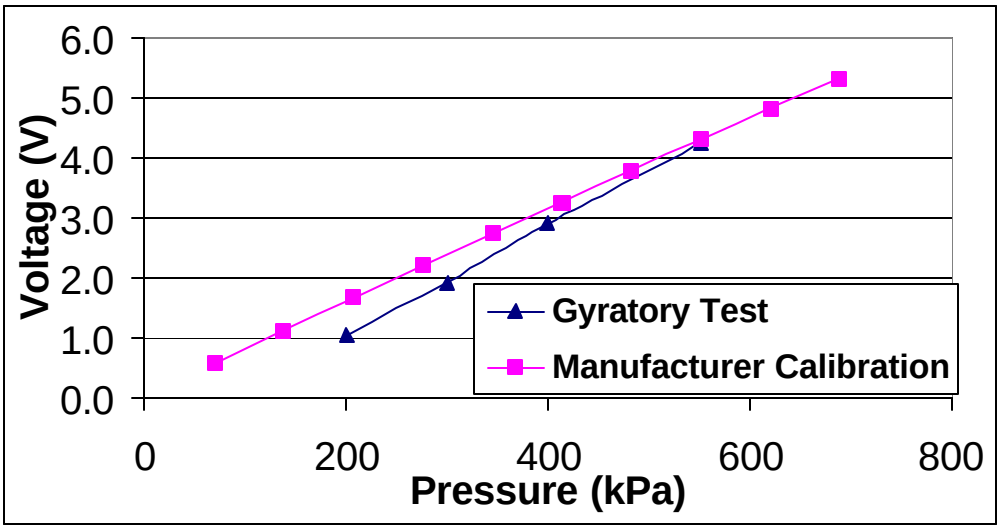

Figure 3.17. Typical Curves using the Gyratory Compactor and the Manufacturer Calibration.

To assess the difference between the manufacturer calibration curve and the curve obtained from using the Gyratory compactor, they were plotted on the same graph, Figure 3.17. The difference between the two calibrations is diminishing at high values. At low pressure, the difference is considered significant due to the edge effect and contact areas between the puck and the pressure cell.

The two curves are close because both are using static loading conditions where a load is applied and held constant while the voltage is measured. This is not the case in the field; as the truck approaches the cell location, the cell is exposed to a constant loading. It increases rapidly until it reaches a maximum right on top of the cell, then decreases as the truck travels away from the cell. Therefore, testing is needed with a machine that can apply a monotonically increasing load on the cell until it reaches a specific value, and then apply a monotonically decreasing load. The Instron Material Testing System can provide these parameters.

Pressure Cell Caibration Using Instron Machine Equipment

This machine can apply a constant rate of loading and unloading. Unfortunately, the machine cannot be set to reach a specific maximum desired load. Thus, the machine needed to be stopped manually when the desired load was reached. That posed some risk in damaging the cell being tested, especially at high rates of loading where the whole loading and unloading takes a few seconds. The highest loading rate used was the equivalent to loading and unloading the cell in 1.6 sec.

The pressure cell was placed on top of the bottom loading head, and the platform head was lowered using a constant rate of 0.25 and 0.025 mm/min. From Figure 3.18, it can be seen that the curves obtained from loading and unloading at a constant rate are different from the manufacturer's calibration (static). The slope of the curve is less in the constant rate case because the cell and the transducer have less time to react to any

change in pressure. It was also noticed that since both the cell and the loading plates have a 150-mm diameter, the effect of alignment is considerable. Therefore, 284mm by 284mm plates were added to the setup. These were used on top and beneath the cell. In additon, rubber sheets were placed between the plates and the cell. That was done to remove the effect of any irregularities in the plates that might cause concentrated loading at a point, and to simulate the compression that occurs in the pavement layers above the cell. To evaluate the effect of loading rate, a few cells were tested at different loading rates.

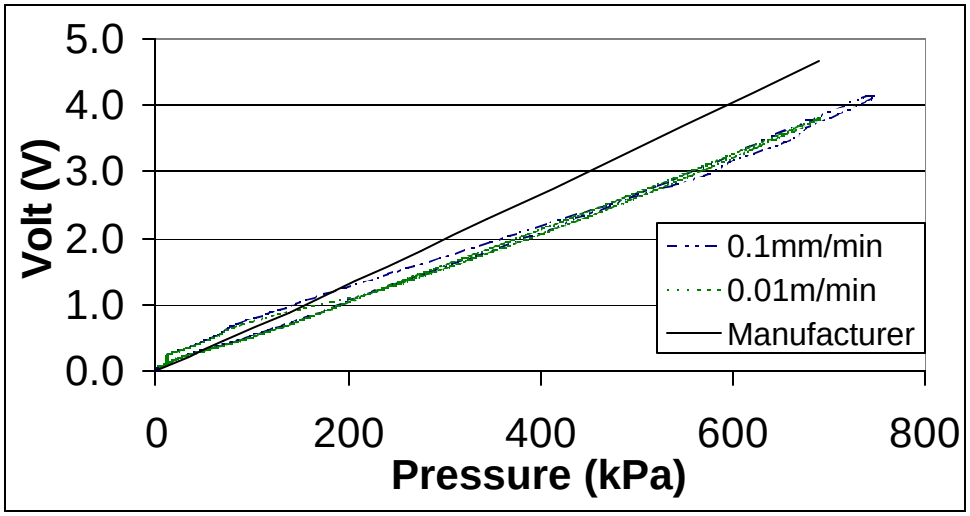

Figure 3.18. Calibration Using the Instron Machine

3.1.4 Instrument Installation

Low sensor survivability is the chief cause of failed roadway performance experiments relying on electronic sensors for data. This is largely due to harsh environmental conditions after placement. To avoid splicing in the field, all pressure cells arrived with the exact wire length to connect it then to the data acquisition system.

The general installation procedure for the sensors follows. These instructions were adapted from the previous experience of the Virginia Tech group at the Bedford Project and information available by the manufacturers.

3.1.4.1 Dynatest PAST-2AC

To ensure good results, the following installation procedures were performed:

1. Trenches for the wire were dug to the location of the sensor. They were then filled with a thin layer of sand.
2. A small piece of geosynthetic was placed on the finished base layer. The geosynthetic was cut to the smallest size possible. This was done to protect the sensor form and sharp aggregates that might act as a lever point of bending to the gauge.
3. A thin layer of asphalt emulsion was applied to the area where the transducer is to be placed. It was left to cure.
4. A thin layer of 3-4 mm slurry seal was applied on the cured asphalt emulsion. The anchor bars of the transducer were pressed by hand into the slurry seal.
5. The wire was run through the trenches and covered with a mastic geosynthetic, previously cut to the right size.
6. Hot Mix Asphalt was taken from the paver. Large size aggregates were removed, and a 20-30-mm-thick layer was placed on top of the transducer to cover it.
7. The material was compacted first by applying a static pressure, followed by compaction using a hand roller. The compaction was performed perpendicular to the strain gauge direction.
8. The HMA layer was placed and compacted.

3.1.4.2 Aggregate and Subgrade Strain Gauge Installation

To evaluate the compaction effort that can be applied to the vibrating wire strain gauges in the field, a lab compaction test was performed. Sand was used below and on the top of the strain gauge to create a resting bed between the soil and the gauge. A 127-mm thickness of 21B was compacted before installing the gauge. Then, 25mm of 21B

was installed on top of the gauge. The compaction effort was gradually increased by increasing the number of blows up to five blows. In addition, the height of the compacting hammer was increased from 20 to 120mm. The results showed that the compaction process does not significantly affect the gauge, and a hand compaction with a height not exceeding 70 to 80 mm seems acceptable. Neither tension nor compression was actually detected in the gauge after the process of compaction. The following is a description of the aggregate strain gauge and vibrating wire strain gauge installation:

1. Trenches for the wire were dug to the location of the sensor. They were then filled with a thin layer of sand.
2. For each gauge, the smallest possible hole was dug, just enough to fit the gauge, in the finished subgrade/aggregate layer. During excavation, extra care was taken to minimize disturbance of the soil/aggregate and keep the size of the hole to a minimum.
3. For the vibrating wire gauge, the gauge was placed on a very thin layer of sand and then back-filled with the excavated material in small layers, and hand compacted carefully. No sand was used for the aggregate strain gauges.
4. The wire was run through the trenches and covered with a thin layer of geosynthetic, previously cut to the right size.

3.1.4.3 Pressure Cell Installation

1. Trenches for the wire were dug to the location of the sensor. They were then filled with a thin layer of sand.
2. Using a small shovel, a shallow 38.1-mm (1.5in) circular hole was excavated at the proposed location of the cell. The diameter of the excavation was roughly the same diameter as a cell load-sensing element. Additionally, a trench approximately 75mm-

wide by 381mm-long and 127mm-deep was excavated to accommodate the transducer housing.

3. Any particles greater than 6.35mm in diameter were removed from the hole.
4. A smooth surface at the bottom of the excavation was prepared by tamping the soils with the tamper.
5. A thin layer (nominal 2.5mm-thick, 100% passing No. 10 sieve) of sand was placed and compacted. In the case of the OGDL layer, a geosynthetic was placed underneath the pressure cell.
6. The sand layer was smoothed and the cell was placed on top. Good contact between the cell sensitive face and the sand layer was ensured. The diaphragm tube and housing were checked for firm support and good contact with the soil. The orientation of the fluid tube transducer housing assembly was placed parallel to the wheel path to reduce effect on adjacent cells. The leveling was checked using a small bubble level and the location was surveyed.
7. A trench was excavated to get the protected wires to the bunker.
8. The pressure cells were checked using tampers and/or small trucks.

3.1.4.4 Time Domain Reflectometery Probes Installation

The following lists the procedure for placing the TDR probes at the Virginia Smart Road. Once locations to place TDR instruments had been chosen, the following procedures were used to install TDRs. Additionally, the probes must be handled carefully so that the metallic waveguides are not bent.

1. A hole that allows the placement of the TDR horizontally was prepared.
2. The top of the TDR was placed at 150mm and 600mm depths from the subgrade surface.
3. Sand was placed in areas where large aggregates were present.

4. Two instruments were placed at each location: one in the direction of the traffic, and the other perpendicular to the direction of traffic; both 500mm from the road centerline.
5. After placing the TDR, the subgrade/aggregate was carefully compacted around and over the probe.
6. The TDR was checked after installation after compaction was complete.
7. All cables were protected by geotextile all the way until it reached the conduit using Ottawa sand or soil passing sieve number 50.
8. Cables were extended to the edge of the lane (transverse to traffic direction) and then parallel to the traffic direction.
9. As for all instruments wires, a snake was used to pull the cables through the conduit entrance to the bunker.

3.2 Laboratory Testing

Laboratory tests are divided into two main groups. First, resilient modulus tests to evaluate the anisotropic behavior of the pavement. Second, fatigue tests to evaluate the performance of the different mixes used at the Virginia Smart Road. Fatigue tests were performed using the Indirect Tensile Test and the Third Point Bending Test. Originally, it was proposed to conduct fatigue testing on five SuperPave^{TM} mixes used at the Virginia Smart Road. The S-N curves were to be obtained for field cores (Type I), field-mixed laboratory-compacted specimens (Type II), and laboratory-mixed laboratory compacted specimens (Type III). Six specimens were to be tested at three different stresses, two at each stress and accordingly develop the S-N curves. These S-N curves were to be obtained for at least two temperatures in both the Indirect Tensile Test and the Third Point Bending Test. However, due to time restrictions, only the testing presented in section 3.2.3 were conducted.

3.2.1 Resilient Modulus

To assess the material isotropic behavior of HMA, the modulus of resilience (M_r) has been identified as a material property indicative of the strength of the HMA. The resilient modulus is defined as the ratio of the applied stress to the recoverable strain when a dynamic load is applied. The resilient modulus is calculated using the applied load, specimen dimensions, and measured Poisson's ratio and horizontal deformations. The repeated load indirect tension resilient modulus test of HMA cores is conducted through repetitive applications of compressive loads in a haversine waveform. The compressive load is applied along the vertical diametric plane of a cylindrical core of HMA. The repeated cyclic stress of fixed magnitude has a loading duration of 0.1sec and a total cycle duration of 1.0sec. The load level was determined to keep the specimen within the linear visco-elastic range. This is accomplished by targeting 150 to 500 micro-strains. During testing, the specimen is subjected to a dynamic cyclic stress (90 percent of total load) and a constant stress (10 percent of total load).

The deformations are measured using on-sample displacement measurement gauges (OSDM). These OSDM gauges are attached to the center of the specimen.

The equations for the total resilient modulus (AASHTO, 1996a) are as follows:

$$M_{RT} = \frac{P\,(\nu_{Rt} + 0.27)}{t\,\Delta H_t} \tag{3.1}$$

where,

M_{RT} = total resilient modulus of elasticity, MPa;

P = repeated load (applied load – minimum contact load), N;

t = thickness of specimen, mm;

ΔH_t = total recoverable horizontal deformation, mm; and

ν_{Rt} =total resilient Poisson's ratio.

Poisson's ratio may be calculated for the instantaneous and total cases as follows (SHRP A005):

$$\nu_{Rt} = -0.10 + 1.480\left(\frac{\Delta H_t}{\Delta V_t}\right)^2 - 0.778\left(\frac{t}{D}\right)^2\left(\frac{\Delta H_t}{\Delta V_t}\right)^2 \quad (3.2)$$

where,

ν_{Rt} = total Poisson's ratio;

D = sample diameter, mm; and

ΔV_t = total recoverable vertical deformation, mm.

To test for transverse isotropy, the following Analysis Of Variance (ANOVA) experimental program was designed.

ANOVA

Four cores were taken from every mix at the Virginia Smart Road, namely SMA-12.5, SM-9.5A in section H, SM-9.5A in section D, SM-9.5E, BM-25.0, OGFC, and SM-9.5D. The direction parallel to traffic was marked before coring in order to test two in the direction parallel to traffic and two in the direction perpendicular to traffic. The measured resilient modulus will depend on both the material and direction of test. Accordingly, the following model was chosen to isolate the effect of the mixes on the tested hypothesis.

Model:

$$Y = \mu + \alpha_i + \beta_j + \alpha\beta_{ij} + \varepsilon_{ijk} \quad (3.3)$$

where,

Y = resilient modulus observation;

μ = overall mean;

α_I = effect of mix type on resilient modulus;

β_j = effect of test direction on resilient modulus;

$\alpha\beta_{ij}$ = effect of interaction between mix type and test direction on resilient modulus; and

ε_{ijk} = experimental error.

For the ANOVA, the hypothesis is that the resilient modulus in the direction of traffic is equal to the resilient modulus in the direction perpendicular to traffic or $\beta_1 = \beta_2$.

3.2.3 Fatigue Tests

The aforementioned test configuration for resilient modulus tests was used in this research, and the loading waveform was applied until failure. Failure is defined as the cycle at which the change in dissipated energy begins to increase rapidly. Dissipated energy is calculated as follows (Haddad, 1995):

$$\text{Dissipated Energy} = \pi \sigma \varepsilon \sin \delta \tag{3.4}$$

where,

σ = applied stress;

ε = measured strain; and

δ = phase angle.

Two types of test configurations were used: the indirect tensile fatigue test and the third point-bending test, ITFT and TPBT, respectively. Two SuperPave^{TM} mixes used at the Virginia Smart Road were tested, SM-9.5A and SM-9.5E. The S-N curve was obtained for field cores (Type I), and field-mixed laboratory-compacted samples (Type II), while type I was used for TPBT. A total of six samples were used to obtain the S-N curve with the ITFT, and a total of four samples were used to obtain the S-N curve with the TPBT.

3.2.3.1 Developing the Best Correlation Method

The number of cycles to failure, N_f, obtained from both the ITFT and the TPBT are expected to be different. Since the proposed method discussed later depends mainly on M_r values and since these are traditionally obtained from the indirect tensile test, stresses in both tests need to be correlated. This correlation should not be based on the

tensile stress alone, but on all the damaging stresses. The damaging stresses in the beam fatigue test are uniaxial and are in the form:

$$\sigma = \frac{M \times y}{I} \tag{3.5}$$

and,

$$M = \frac{P \times L}{3} \tag{3.6}$$

$$I = \frac{t \times d^3}{12} \tag{3.7}$$

where,

M = bending moment in the middle third of the beam;
I = moment inertia of the beam cross-section;
y = distance of lower most fiber from the neutral axis;
P = applied load;
L = length of the beam;
t = thickness of the beam; and
d = depth of the beam.

Substituting equations (3.6) and (3.7) into (3.5) and calculating the stress in the lowest fiber at y equal to d/2, the final form of the tensile stress in TPBT is given as follows:

$$\sigma = \frac{2 \times P \times L}{t \times d^2} \tag{3.8}$$

The damaging stresses in the ITFT are biaxial. Several researchers solved the stress equations of the circular element subjected to concentrated forces (Mirza, *et al*., 1997). Hondros (1959) took the next step and developed a closed-form solution of stresses along the horizontal and vertical diametrical axis due to strip loading. Stresses along the principal diameters are given by the following equations:

$$\sigma_{yx} = \frac{-2P}{\pi at}\left[\frac{(1-r^2/R^2)\sin 2\alpha}{(1+2r^2/R^2\cos 2\alpha + r^4/R^4)} + \tan^{-1}\frac{(1-r^2/R^2)}{(1+r^2/R^2)}\tan\alpha\right] \quad (3.9)$$

$$\sigma_{xx} = \frac{+2P}{\pi at}\left[\frac{(1-r^2/R^2)\sin 2\alpha}{(1+2r^2/R^2\cos 2\alpha + r^4/R^4)} - \tan^{-1}\frac{(1-r^2/R^2)}{(1+r^2/R^2)}\tan\alpha\right] \quad (3.10)$$

$$\sigma_{xy} = \frac{+2P}{\pi at}\left[\frac{(1-r^2/R^2)\sin 2\alpha}{(1-2r^2/R^2\cos 2\alpha + r^4/R^4)} - \tan^{-1}\frac{(1+r^2/R^2)}{(1-r^2/R^2)}\tan\alpha\right] \quad (3.11)$$

$$\sigma_{yy} = \frac{-2P}{\pi at}\left[\frac{(1-r^2/R^2)\sin 2\alpha}{(1-2r^2/R^2\cos 2\alpha + r^4/R^4)} + \tan^{-1}\frac{(1+r^2/R^2)}{(1-r^2/R^2)}\tan\alpha\right] \quad (3.12)$$

where,

σ_{yx} = stress in the vertical direction along the horizontal axis;

σ_{xx} = stress in the horizontal direction along the horizontal axis;

σ_{xy} = stress in the horizontal direction along the vertical axis;

σ_{yy} = stress in the vertical direction along the vertical axis;

r = distance along the axis at which stresses are calculated;

a = width of the strip loading;

t = thickness of the specimen;

α = angle at the center of the specimen subjected by the strip loading; and

R = radius of the sample.

Consider a point on the S-N curve obtained from the ITFT (S_1, N_1). This means that at S_1 stress, the failure is reached after N_1 cycles in the ITFT. This may be related to (S'_1, N'_1) in the S-N curve obtained from the TPBT. If N'_1 is equated to N_1, a relationship between S_1 and S'_1 may be found.

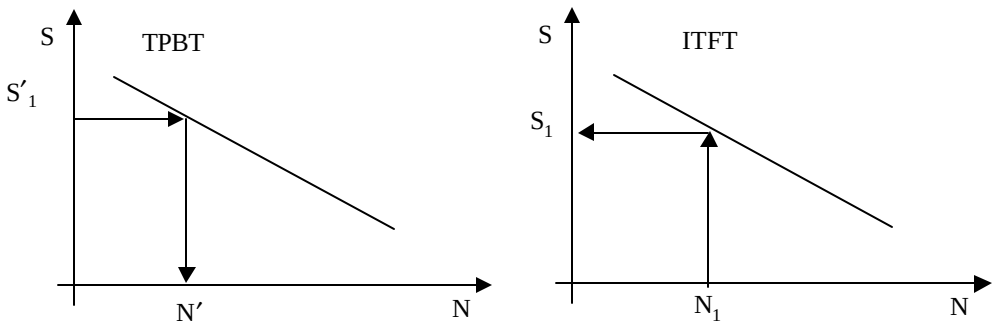

Figure 3.19. Comparison between Failure in ITFT and TPBT.

Since the state of stress in the ITFT is biaxial, the equivalent stress from both the vertical and horizontal stress needs to be compared to the uniaxial stress in the TPBT. This will depend on the method by which the equivalent stress is calculated; therefore, the comparison will be based on a number of equivalent stress criteria. The equivalent stresses can be calculated according to the following five criterias:

1. Equivalent stress based on von Mises theory

$$\sigma_{eq} = \frac{1}{\sqrt{2}}\left[(\sigma_1 - \sigma_2)^2 + (\sigma_2 - \sigma_3)^2 + (\sigma_3 - \sigma_1)^2\right]^{\frac{1}{2}} \tag{3.13}$$

$$\sigma_{TPBT} = \frac{1}{\sqrt{2}}\left[(\sigma_{yx} - \sigma_{xy})^2 + (\sigma_{yx})^2 + (\sigma_{xy})^2\right]^{\frac{1}{2}} \tag{3.14}$$

2. Maximum shear stress (Tresca)

$$\frac{1}{2}\sigma_{eq} = \frac{1}{2}Max\left[|\sigma_1 - \sigma_2|, |\sigma_2 - \sigma_3|, |\sigma_3 - \sigma_1|\right] \tag{3.15}$$

$$\sigma_{TPBT} = Max\left[|\sigma_{yx} - \sigma_{xy}|, \sigma_{yx}, \sigma_{xy}\right] \tag{3.16}$$

3. Strain Energy Density

$$\sigma_{eq} = \left[\sigma_1^{\,2} + \sigma_2^{\,2} + \sigma_3^{\,2} - 2\nu(\sigma_1\sigma_2 + \sigma_1\sigma_3 + \sigma_2\sigma_3)\right]^{\frac{1}{2}} \tag{3.17}$$

$$\sigma_{TPBT} = \left[\sigma_{yx}^{\,2} + \sigma_{xy}^{\,2} - 2\nu\sigma_{yx}\sigma_{xy}\right]^{\frac{1}{2}} \tag{3.18}$$

4. Octahedral Shear Stress

$$\sigma_{eq} = \frac{1}{3}\left[(\sigma_1 - \sigma_2)^2 + (\sigma_2 - \sigma_3)^2 + (\sigma_3 - \sigma_1)^2\right]^{\frac{1}{2}} \tag{3.19}$$

$$\sigma_{TPBT} = \frac{1}{3}\left[(\sigma_{yx} - \sigma_{xy})^2 + (\sigma_{yx})^2 + (\sigma_{xy})^2\right]^{\frac{1}{2}} \quad (3.20)$$

5. Octahedral Shear Stress

$$\sigma_{eq} = \frac{1}{\sqrt{15}}\left[(\sigma_1 - \sigma_2)^2 + (\sigma_2 - \sigma_3)^2 + (\sigma_3 - \sigma_1)^2\right]^{\frac{1}{2}} \quad (3.21)$$

$$\sigma_{TPBT} = \frac{1}{\sqrt{15}}\left[(\sigma_{yx} - \sigma_{xy})^2 + (\sigma_{yx})^2 + (\sigma_{xy})^2\right]^{\frac{1}{2}} \quad (3.22)$$

3.2.3.2 Construction of Remaining Life Curve

The method to be considered in this study is adapted from that given by Reifsnider (1993), who have developed a mechanistic, non-linear life prediction model in which residual strength is assumed to be a damage metric. First, the necessary testing will be discussed, followed by the model formulation.

From each resilient modulus test, four values are identified: M_r at 0%, 50%, 75%, and 85% of the number of cycles to failure. This is shown graphically in Figure 3.20. Note that for the resilient modulus at 0% of N_f, the strain was taken after 200 cycles to allow the seating of the sample as recommended by ASTM.

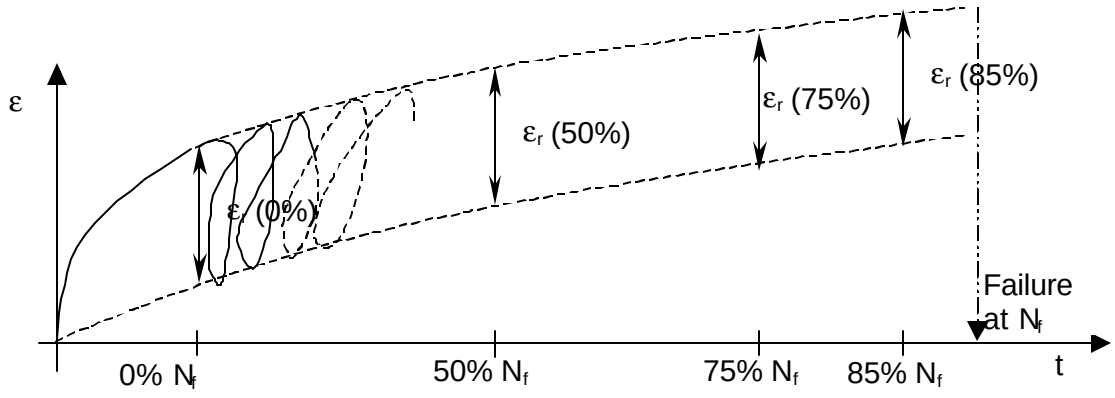

Figure 3.20 Graphical Representation of M_r Calculations.

Therefore, the following equations were used:

$$Mr(0\%) = \frac{\sigma}{\varepsilon_r(0\%)}$$
$$Mr(50\%) = \frac{\sigma}{\varepsilon_r(50\%)}$$
$$Mr(75\%) = \frac{\sigma}{\varepsilon_r(75\%)} \qquad (3.23)$$
$$Mr(85\%) = \frac{\sigma}{\varepsilon_r(85\%)}$$

The model is based on the assumption that damage associated with property degradation is widely distributed within the HMA, and that a Representative Volume Element (RVE) can be chosen such that the state of stress in the RVE is typical of the rest of the material at that critical location which is the bottom of the HMA, Figure 3.21.

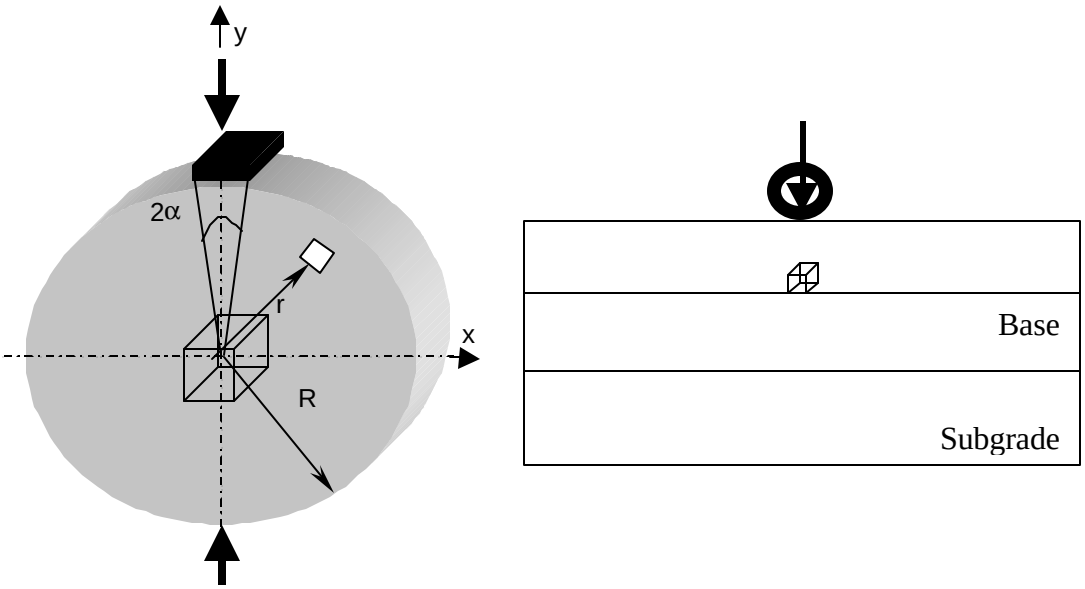

Indirect Tensile Fatigue Test Layered Pavement System

Figure 3.21 Representative Volume Element in Fatigue Test Specimen

Moreover, it is postulated that the RVE is comprised of critical and sub-critical elements, where failure of the critical element, whose state of stress is influenced by the sub-critical elements, leads to failure of the entire RVE and therefore the HMA layer.

The residual strength in the critical element is calculated using a non-linear damage evolution equation. When the residual strength of the critical element equals the applied load, the HMA is said to fail. For a few decades, the resilient modulus has been a measure to indicate the strength of HMA. Therefore, assume a failure criterion in the following form:

$$F_a = \frac{M_{r(50\%,\,75\%,\,85\%)}}{M_{r(0\%)}} \tag{3.24}$$

Further assume a parameter, ψ, which is equal to 1 - F_a, where ψ is called the continuity. Using the following damage evolution law, it is possible to arrive at a remaining strength equation (Reifsnider, 1993).

$$\begin{aligned} &\frac{\partial y}{\partial t} = -yj t^{\,j-1} \\ &y_i - y_0 = -\int_0^{t_i} yj t^{\,j-1} dt \end{aligned} \tag{3.25}$$

where τ is the generalized time given in terms of the ratio between the applied number of cycles, n, to the number of cycles to failure, N_f, and j, a material property. Failure occurs when the remaining life (F_r) is equal to F_a. Hence, the remaining life is equal to 1 minus the change in F_a, ΔF_a, as shown below:

$$\begin{aligned} y_i &= 1 - F_{ai} \\ y_0 &= 1 - F_{ao} \\ y_i - y_0 &= 1 - F_{ai} - (1 - F_{a0}) = \Delta F_{ai} \\ F_r &= 1 - \Delta F_{ai} \end{aligned} \tag{3.26}$$

$$\begin{aligned} -\Delta F_{ai} &= -\int_0^{t_i} (1 - F_a)\, j t^{\,j-1} dt \\ F_r &= 1 - \int_0^{t_i} (1 - F_a)\, j t^{\,j-1} dt \end{aligned} \tag{3.27}$$

Values for F_r will be calculated for the modulus at 50%, 75% and 85% of the number of cycles to failure as discussed above. These will be plotted and equation (3.27) will be fitted to the data. The final form of a typical remaining life prediction model is shown in Figure 3.22. Fitting will yield a j value for each mix, which is the characteristic value of the remaining life curve.

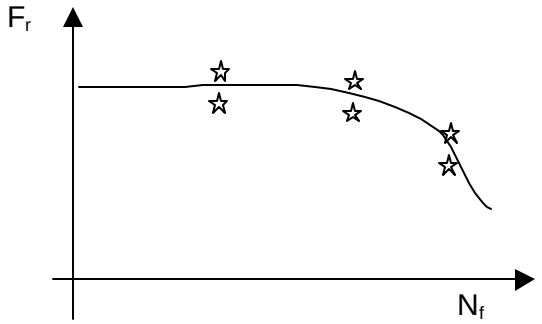

Figure 3.22 A Typical Remaining Life Curve

3.3 Fatigue Testing Shift Factors

The difference between laboratory and field environments is attributed to four major factors: difference in the state of stress, traffic wander in the field, material difference between field core and laboratory prepared specimens, and HMA healing due to rest periods. An overall shift factor may be defined as follows:

$$SHF_{overall}(t) = SHF_{stress\text{-}state}(t) \; x \; SHF_{traffic\text{-}wander}(t) \; x \; SHF_{material\text{-}difference}(t) \; x \; SHF_{healing}(t) \quad (3.28)$$

where,

$SHF_{overall}(t)$ = Overall shift factor;
$SHF_{stress\text{-}state}(t)$ = Shift factor to account for difference in stress state;
$SHF_{traffic\text{-}wander}(t)$ = Shift factor to account for traffic wander;
$SHF_{material\text{-}difference}(t)$ = Shift factor to account for difference in materials used in the lab and that placed in the field; and
$SHF_{healing}(t)$ = Shift factor to account for HMA healing during rest periods.

Although HMA fatigue is usually discussed in terms of apparent surface cracking, HMA fatigue can manifest itself in the form of stiffness reduction. Once the stiffness of the HMA is changed, the number of cycles to failure will change and thus the shift factor.

Therefore, all the components of the overall shift factor are a function of time, i.e., it is dependent on the HMA age and damage.

3.3.1 In-Service Measured Critical Strains

Figure 2.1 shows the different types of strains typically measured in the field. The compressive strain in the longitudinal strain gauge response may be related to the bending and horizontal shearing. The bending effects can be seen in Figure 3.23a. When the load is directly on top of the strain gauge, the measured strain is tensile. However, due to the bending of the HMA layer, at a distance away from the strain gauge, the strain is compressive. So, when the loading point is before or after the position of the strain gauge, the strain gauge measures compressive bending strain and compressive shear at its location. When the loading point is ahead of the strain gauge, compressive bending and tensile shear strains result at the strain gauge location.

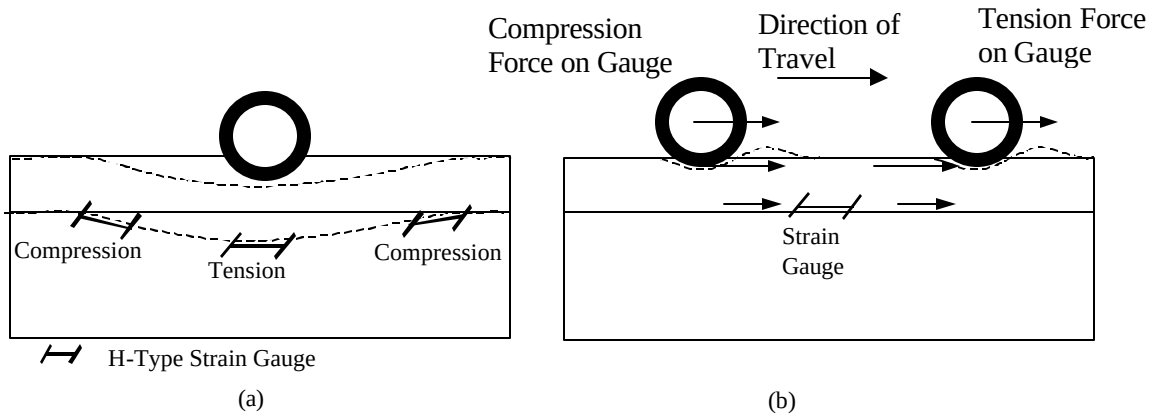

Figure 3.23 Compressive strain explanation

Most of the response obtained from the longitudinal strain gauges placed in the wearing surface at the Virginia Smart Road has compressive strains preceding the tensile strains and none following. This may be explained by the shearing effects (which are high at that depth), as seen in the schematics in Figure 3.23b. As the vehicle travels, the tire imposes horizontal shearing forces on the pavement due to friction between the tire

and the pavement. When the load is moving towards the strain gauge, these shearing forces act to produce compressive strains. However, when the load moves away from the strain gauge, the same forces act to produce tensile strains that may balance the bending compressive strain. These two effects may also explain why the transverse strain relaxes after the application of the load and the longitudinal strain does not. For the same reason, transverse strain gauges register compressive strains when the load is at a lateral distance away from the gauge due to bending effects. Further explanation with measured data is provided in Chapter 4.

All laboratory fatigue equations are dependent on either maximum strain or maximum stress obtained in the field. Due to the difference in transverse and longitudinal strains, a comparison between the two is necessary to determine which direction is more critical for fatigue analysis. Comparison between the two strains due to different loads, speeds, and tire pressures was conducted on the strain response from the wearing surface mixes at the Virginia Smart Road. The comparison was based on four criteria: maximum tensile strain, maximum total strain, average strain, and strain derived from strain rate. The first and second methods were simply comparing maximum values obtained in the two directions. The average strain was calculated as follows:

$$\text{Average Strain} = A / t_r \tag{3.29}$$

where,

A =Total area under the strain-response curve; and

t_r = Total response time.

Since HMA is a viscoelastic material that relaxes over time and dissipates energy when a cyclic load is applied, whether tension or compression, it is assumed that a compressive strain is as damaging as a tensile strain. The representative strain for the fourth criteria, obtained from strain rates, may then be calculated using equation (3.30), where points a, b, c, d, e, and f are shown in Figure 3.24.

$$\varepsilon_{rL} = \int_a^b \left|\frac{\partial \varepsilon}{\partial t}\right| dt + \int_b^c \left|\frac{\partial \varepsilon}{\partial t}\right| dt + \int_c^d \left|\frac{\partial \varepsilon}{\partial t}\right| dt$$
$$\varepsilon_{rT} = \int_a^e \left|\frac{\partial \varepsilon}{\partial t}\right| dt + \int_e^f \left|\frac{\partial \varepsilon}{\partial t}\right| dt \qquad (3.30)$$

where,

ε_{rL} = representative longitudinal strain based on strain rate; and

ε_{rT} = representative transverse strain based on strain rate.

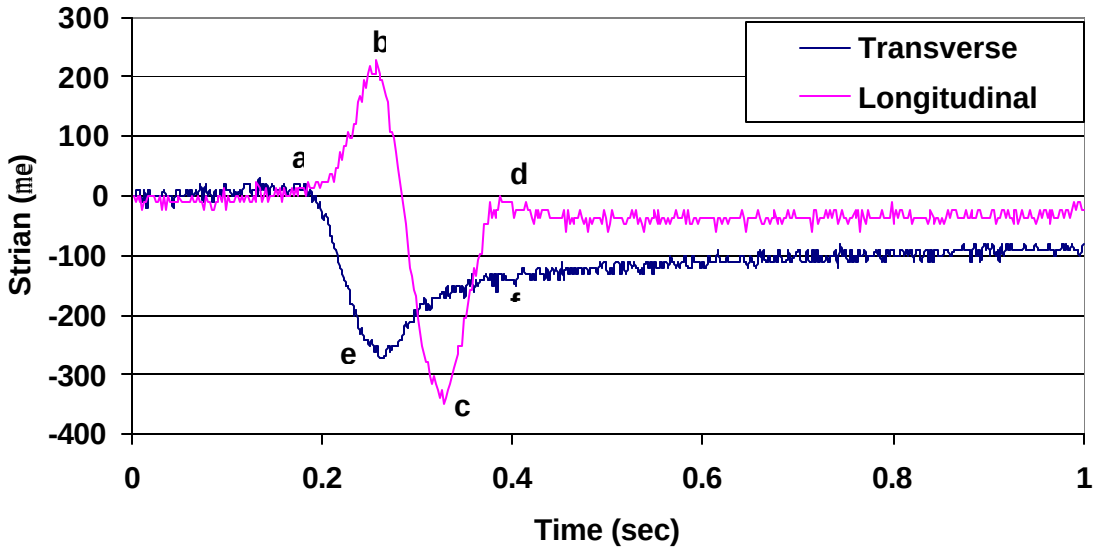

Figure 3.24 Typical Transverse and Longitudinal Strain Response

It is assumed in these calculations that the maximum strain point corresponds to the load directly on top of the strain gauge. This has been verified by the strain distribution obtained from the three embedded strain gauges within a 1-m-wide wheel path. The total response time is taken as twice the time from zero to maximum strain. The area under the strain-response curve is then calculated using numerical integration of the time signal.

3.3.2 Stress State Shift Factor

Fatigue distress accumulates rapidly under moderate to cool temperatures and rapid traffic loading; therefore, the theory of linear elasticity provides a reasonable indication of the response of the pavement, particularly for calculating strain energy. In addition, Read and Collop (1997) suggest that when the test temperature is less than 300C, linear elastic theory is applicable for calculating the stresses and strains in an indirect tensile specimen. To account for the difference in stress state, the total work done by the traffic loading to the pavement should be compared to the total work done by laboratory loading. This comparison can be made using the energy needed to deform the pavement, strain energy:

$$W = 0.5 (\sigma_x \varepsilon_x + \sigma_y \varepsilon_y + \sigma_z \varepsilon_z + \tau_{xy} \gamma_{xy} + \tau_{xz} \gamma_{xz} + \tau_{zy} \gamma_{zy}) \quad (3.31)$$

where,

W = strain energy;

ε_x, ε_y, ε_z = are the strain components in the x, y, and z directions;

σ_x, σ_y, σ_z = are the stress components in the x, y, and z directions;

γ_{xy}, γ_{zy}, γ_{xz} = are the shear strain components in the xy, zy, and xz planes; and

τ_{xy}, τ_{zy}, τ_{xz} = are the shear stress components in the xy, zy, and xz planes.

For load directly on top of the analyzed point, there are no shearing stresses and the strain energy equation is reduced to:

$$W = 0.5 (\sigma_x \varepsilon_x + \sigma_y \varepsilon_y + \sigma_z \varepsilon_z) \quad (3.32)$$

The horizontal strains and the vertical compressive stresses are measured at the Virginia Smart Road using H-Type strain gauges and pressure cells. Therefore, equation 3.32 may be rewritten in terms of the horizontal strains and the vertical stress, where $\sigma=E \varepsilon$:

$$W = 0.5 (E_x \varepsilon_x^2 + E_y \varepsilon_y^2 + \sigma_z^2 / E_z) \quad (3.33)$$

where E_x, E_y, and E_z are the three components of the elastic modulus.

The state of stress in both ITFT and TPBT is different than that in the field. Stresses in the third point bending fatigue test are uniaxial; therefore, only one component of the strain is taken into account in the lab test. Hence, a shift factor based on strain energy that takes into account the state of stress can be postulated as follows:

$$SH_s = W_{uniaxial} / W_{triaxial} = (E_x \varepsilon_x^2) / (E_x \varepsilon_x^2 + E_y \varepsilon_y^2 + \sigma_z^2 / E_z) \quad (3.34)$$

Similarly, stresses in the indirect tensile fatigue test are biaxial with one axis in compression and one in tension; therefore, the corresponding shift factor can be postulated as follows:

$$SH_s = W_{biaxial} / W_{triaxial} = (E_x \varepsilon_x^2 + \sigma_z^2 / E_z) / (E_x \varepsilon_x^2 + E_y \varepsilon_y^2 + \sigma_z^2 / E_z) \quad (3.35)$$

The stiffness of the HMA in compression is different from that in tension and should be accounted for. Based on the data presented by Khanal (1995) for harmonic loading at 25^0C, a value for the modulus of resilience (in compression) may be calculated to be 1.46 times greater than that in tension. Therefore, E_z may be approximated to 1.46 E_x, although it may vary based on the mix and test parameters.

3.3.3 Wander Shift Factor

As indicated earlier, constant load or deformation is applied in every cycle in the laboratory; loads in the field vary in magnitude due to axle load and traffic wander. For example, in an indirect tensile fatigue test, the stress level at the center of the sample is

the same for each cycle. However, depending on the position of the load in the field, the stress level varies. Yet the stress level applied in the laboratory is used to predict failure in the field. To arrive at a shift factor for traffic wander based on traffic data alone is not advantageous since the pavement structure plays an important role in the strain or stress magnitude. The pavement strain response, along with the load location, is essential to obtain a wander shift factor. Therefore, a shift factor may be estimated by measuring the HMA strain distribution in the wander area.

Truck testing performed at known locations away from the strain gauges may provide a typical distribution for the strains and accordingly, an exponential curve can be fitted to the data. Then by assuming that traffic is normally distributed around the wheel path with a mean of zero and standard deviation of σ, accordingly, the probability density function takes the form shown in equation (3.36):

$$f(x) = \frac{1}{\sqrt{2\pi}\,s} e^{-\frac{1}{2}\left[\frac{(x-m)}{s}\right]^2} \tag{3.36}$$

A shift factor to account for the traffic wander can then be calculated as follows:

$$\mathrm{SHF}_{traffic\text{-}wander} = \frac{1}{\int_{-\infty}^{\infty} f(x) \times e_{ratio}(x)\,dx \Big/ \int_{-\infty}^{\infty} e_{ratio}(x)\,dx} \tag{3.37}$$

CHAPTER 4: Data Analysis

This chapter presents the data collected during field and laboratory testing. First, volumetric properties of the HMA mixes tested are presented in section 4.1. Section 4.2 presents sensor calibration data followed by data collected from field testing and data collected in the laboratory tests, sections 4.3 and 4.4, respectively. Finally, a comparison between lab and field environments is made, and shift factors to relate field and lab failures are calculated.

4.1 Mixture Properties

SM9.5A and SM9.5E were placed as the wearing surface in sections D and C, respectively. For these two mixes, two sets of gradation were performed. The first set was done from samples taken from behind the paver at the sensor location. The second set was randomly taken from behind the paver in the same section. Figures 4.1 and 4.2 show the gradations for SM9.5A and SM9.5E, respectively.

From the design prospective, both mixes should have the same gradation; the only difference will be the binder type used. Of course, due to plant batch mixing variability, the gradations shown in Figures 4.1 and 4.2 are not the same. To study the variability between the different samples tested, the coefficient of correlation was calculated for all the samples, Table 4.1.

Table 4.1 Correlation Coefficients Between Samples Tested

	SM9.5E(Sensor)	*SM9.5A(Sensor)*	*SM9.5E(Random)*	*SM9.5A(Random)*
SM9.5E(Sensor)	1.0000			
SM9.5A(Sensor)	0.9997	1.0000		
SM9.5E(Random)	0.9997	0.9994	1.0000	
SM9.5A(Random)	0.9985	0.9984	0.9996	1.0000

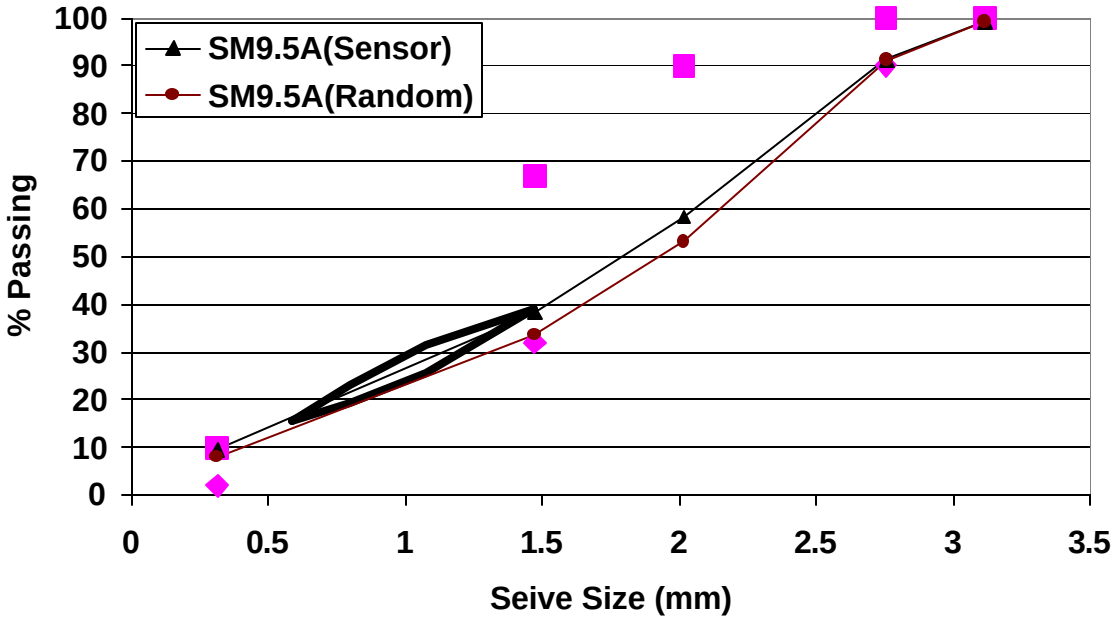

Figure 4.1. Gradations for the SM9.5A

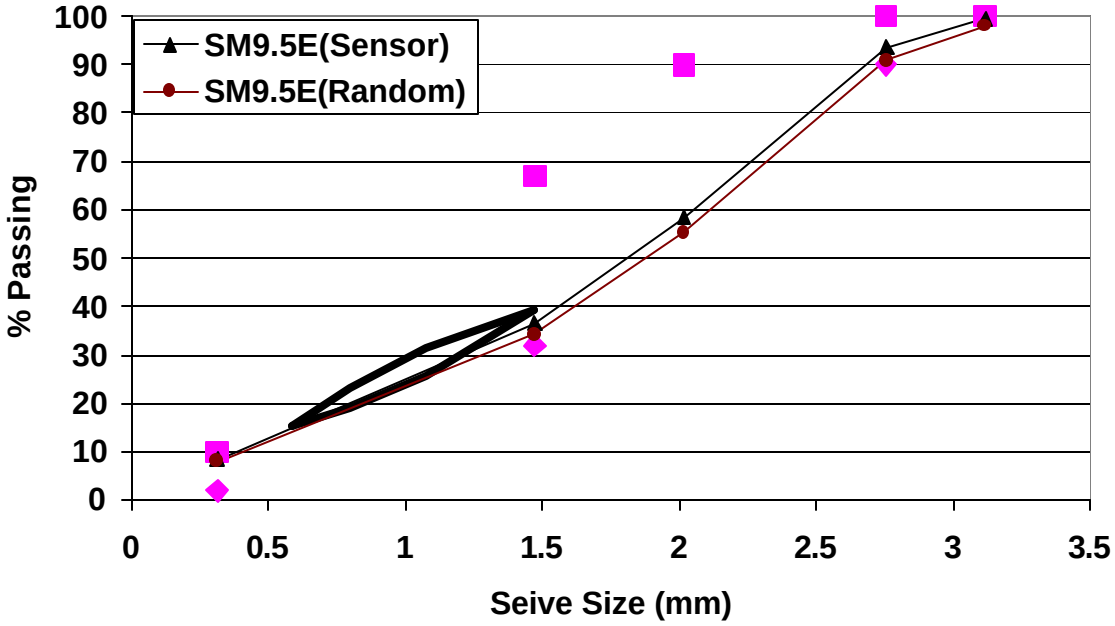

Figure 4.2. Gradations for the SM9.5E

The SM9.5A samples have an average air void of 5.51 and an average bulk specific gravity of 2.393. The SM9.5E samples have an average air void of 8.93 and an average bulk specific gravity of 2.309.

4.2 Calibration Data

The Next Section presents the data collected from the lab and field calibration tests performed on the pressure cells.

4.2.1 Pressure Cells

Three sets of calibration tests were performed: laboratory static tests, laboratory dynamic tests, and field dynamic tests. Laboratory static tests were performed using the Gyratory machine to check the manufacturer's calibration. The laboratory dynamic tests were performed on a screw-type material testing system to evaluate the applicability of the cell for dynamic truck loading measurements. The field dynamic tests were done using Falling Weight Deflectometer to evaluate whether the manufacturer's calibration curves can be used to convert the voltage reading from the pressure cell to pressure values.

4.2.1.1 Static Tests

For the static tests, the cell was placed in the Gyratory compactor to apply a static load, and the output voltage was measured. A 150-mm cell was placed on top of a steel spacer in the Gyratory compactor. The cell was then loaded using the 150-mm puck of the Gyratory. The cell was connected to the data acquisition system to measure the voltage output.

After the above setup was done, the Gyratory was set to apply a load of 200kPa on the cell, and the voltage reading was recorded. The difference between the measured voltage and that obtained from the manufacturer's curves was found to be diminishing at high values, Figure 4.3. At low pressure, the difference is considered significant due to the edge effect and contact areas between the puck and the pressure cell. It must be noted

here that the manufacturer calibration was obtained by inserting the cell into a pressure chamber under adjustable static hydraulic pressure.

The loading in the field, however, is different than the above loading approach. As the truck approaches the cell location, there is an increase in the load cell response until it reaches a maximum value when the truck is right on top of the cell; it then decreases as the truck travels away from the cell. Therefore, a better calibration may be achieved using a machine that can apply a monotonically increasing load on the cell until it reaches a specific value, and then a monotonically decreasing load.

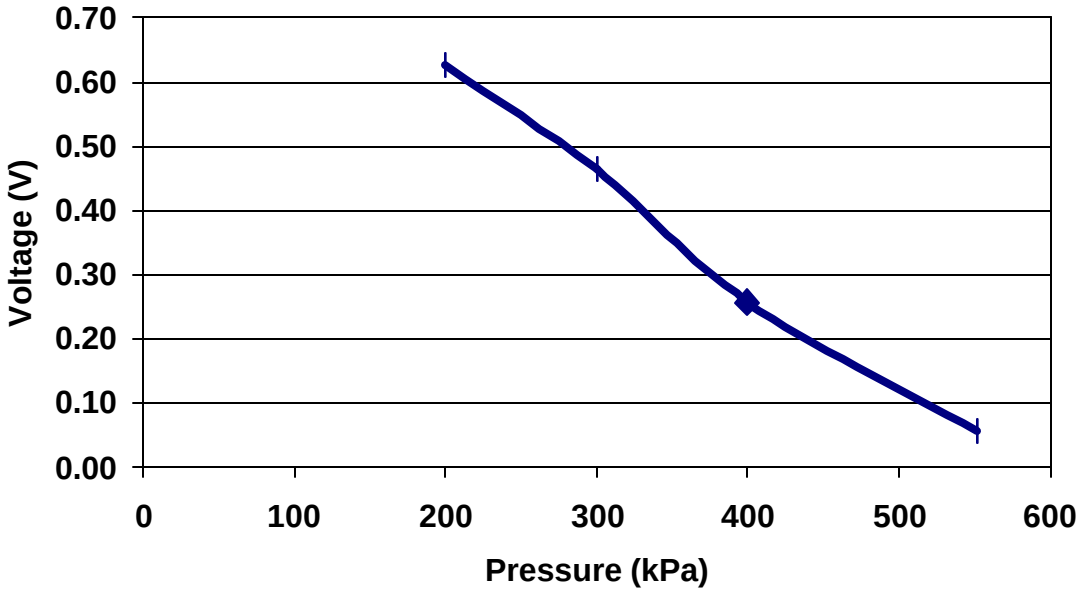

Figure 4.3 Differences in the Voltage Reading and Manufacturer's Calibration

4.2.1.2 Calibration Using Instron Machine

The curves obtained from loading and unloading, at a constant rate, are different from the manufacturer's calibration (RST), Figure 4.4. The slope of the curve is less in

the constant rate case because the cell and the transducer have less time to react to any change in pressure.

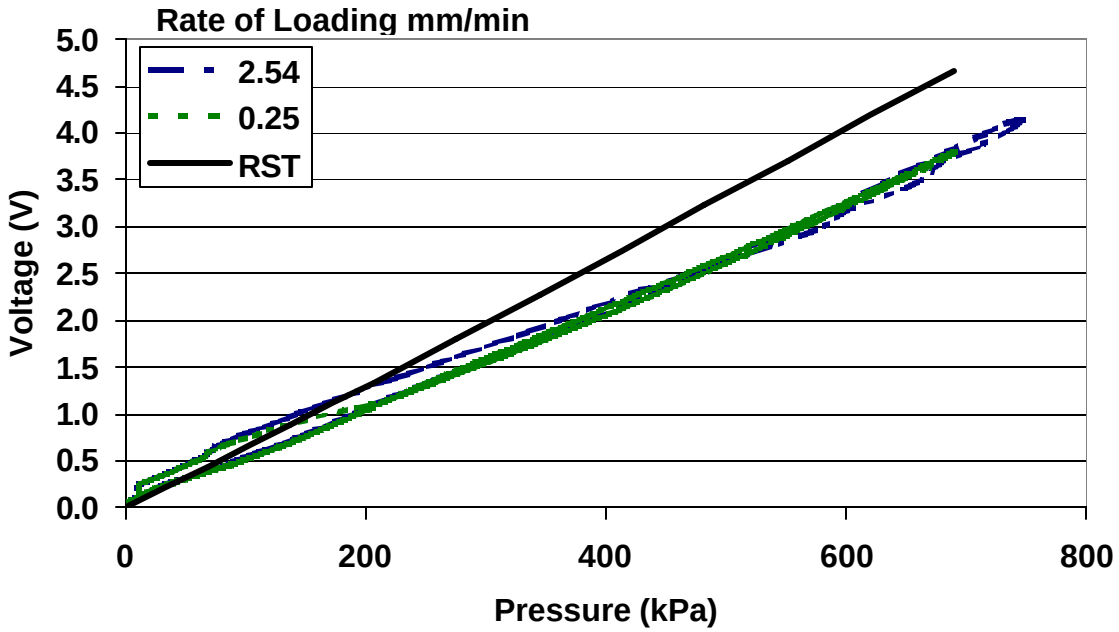

Figure 4.4 Calibration Using the Instron Machine

(a)

(b)

Figure 4.5 (a): Placing Rubber and Plates on Top and Bottom of Cell; b: Cell under Loading

It was also noticed that since both the cell and the loading plates have a 150-mm diameter, the effect of alignment might be significant. Therefore, two 284mm by 284mm plates were added to the setup and were used on top and beneath the cell. Also, rubber sheets were placed between the plates and the cell. This was done to reduce the effect

that might be caused by any possible metal to metal contact, which could result in localized loading. In addition, this arrangement may better simulate the compression that occurs in the pavement layers above the cell. Figure 4.5 shows the final setup that was used to calibrate the cells. Appendix A shows the results obtained from all the cells that were tested.

To evaluate the effect of loading rate, a few cells were tested at different loading rates. The results for one of them are shown in Figures 4.6 and Figure 4.7. It can be clearly seen that the rate of loading does not affect the results from this experimental setup. The difference in slope between the manufacturer's calibration curve and the curves obtained from the Instron Machine is not due to the rate of loading, but could be due to the difference in the test setup.

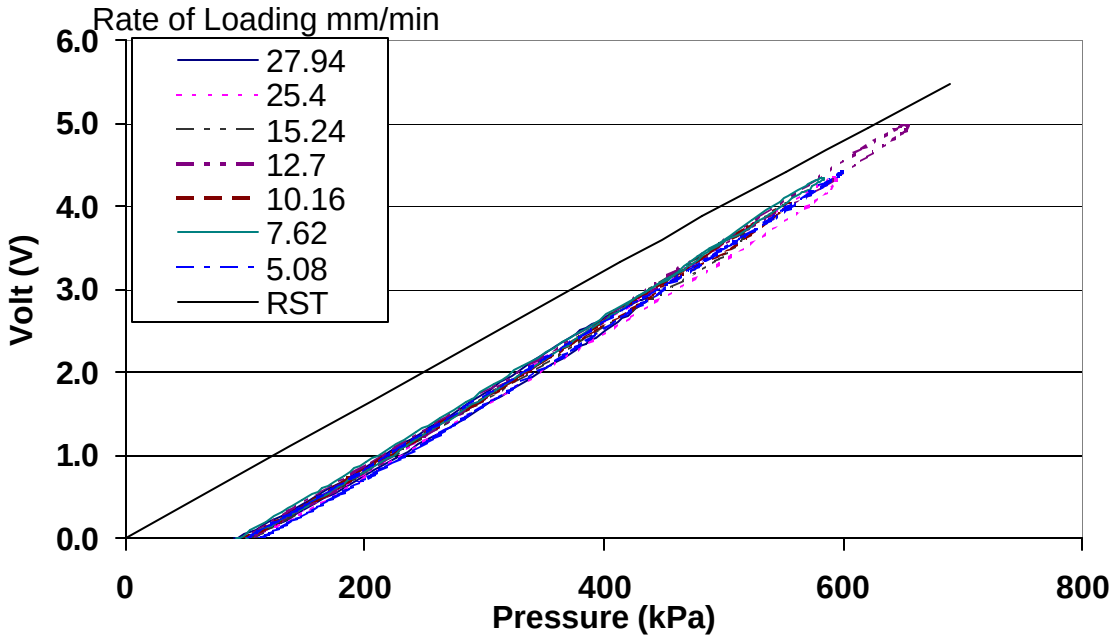

Figure 4.6. Calibration Curves for Rates Ranging from 5.08 to 27.94 mm/min

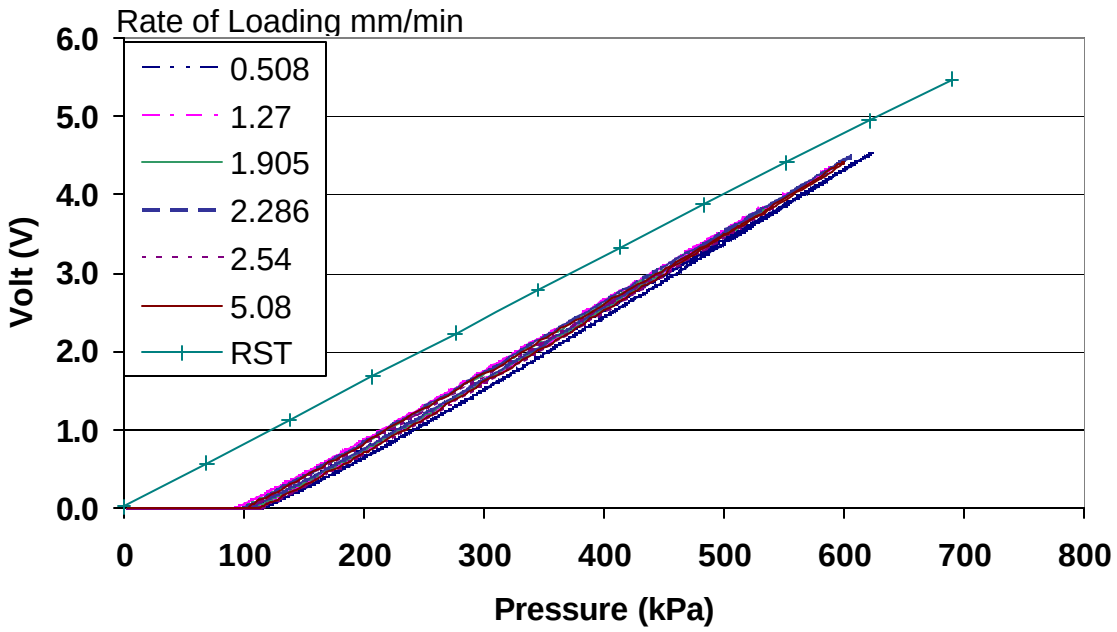

Figure 4.7. Calibration Curves for Rates Ranging from 0.508 to 5.08 mm/min

Figure 4.8 below shows the calibration curves for two different rates of loading, provided by the manufacturer, and a curve using three rubber layers between the cell and the plates (for 2.54mm/min rate of loading). The following can be concluded from the laboratory calibration process:

1. The relationship between measured volts and applied pressure is linear and is independent of the loading rate.
2. For any two different loading rates, it can be seen that the area enclosed between the loading and unloading curves increases with increase in rate of loading. This is probably due to the compliance of the different components of the pressure cell system: hydraulic fluid, stainless steel casing, and the pressure sensing membrane.
3. For the curve using the rubber, the cell at the beginning does not show any response because it takes time for the rubber to compress and then transfer the loads. This is because the pressure is measured by dividing the load applied (measured by the load cell in the top chamber of the Instron machine) by the area of the force-summing element. Accordingly, although there is a force applied, the cell does not give any readings.

4. The slope of the rubber curve is higher than that for the one without rubber.
5. All the calibrations done on the Instron Machine are lower than the RST calibration curves.

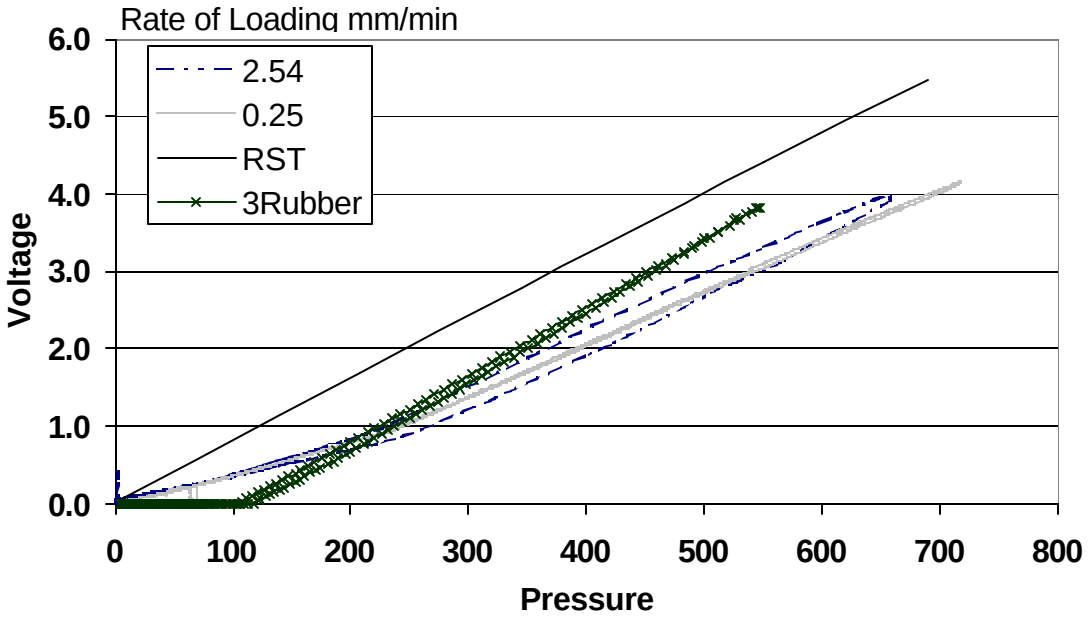

Fi

Figure 4.8. Calibration for Two Different Loading Rates without Plate or Rubber and One with three Sheets of Rubber

To evaluate the loading rate effect, the calibration curves were obtained for different rates of loading. For each rate of loading, the cell was loaded to a safe pressure that would not damage the cell. The pressure was different for each loading rate because it is user dependent. Then the maximum pressure and the corresponding voltage were noted for each loading rate. The maximum pressure was then used to determine the expected voltage for that pressure from the RST calibration curves. The difference between measured and RST voltage is plotted versus loading rate, as shown in Figure 4.9.

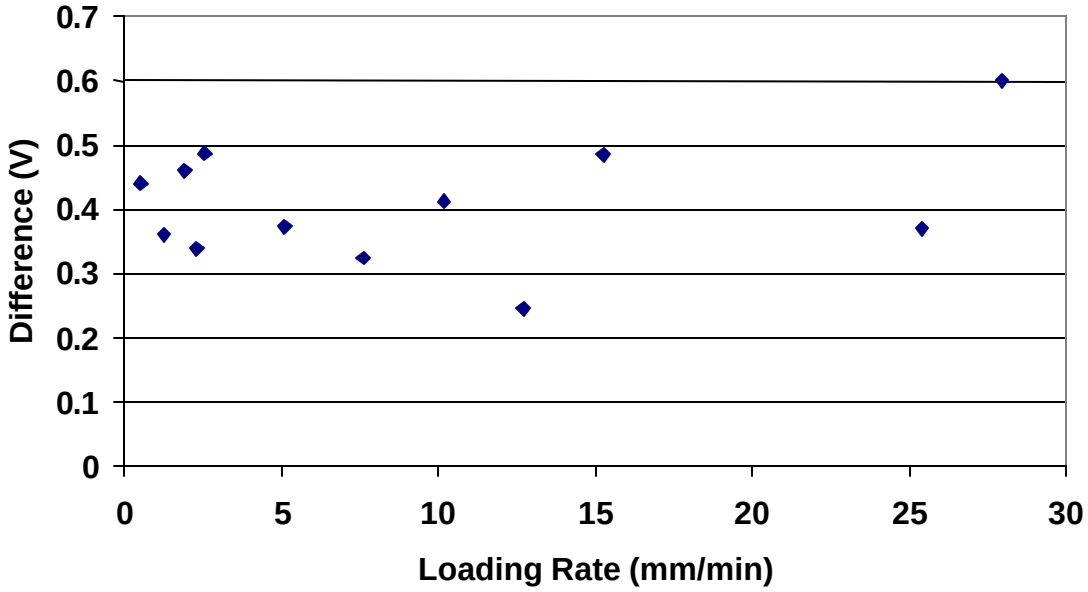

Figure 4.9. Difference between Manufacturer and Instron Calibrations as a Function of Rate of Loading for Maximum Load Applied

The above figure shows that the difference between the manufacturer and the in-house calibrations (for pressure cell labeled 9p2-1) is not loading rate dependent. This is contrary to what is expected; that is, that the difference would increase as the loading rate is increased. The same steps were followed using 206 and 413 kPa pressure, and the same trend was obtained. However, the difference was less when six layers of rubber were used at 206 kPa, Figure 4.10.

One may conclude that the loading material is very important and that a true representation of the field condition is found with the use of the pressure chamber (manufacturer's calibration). However, the use of a pressure chamber allows for static measurements only. Accordingly, in-situ calibration is needed.

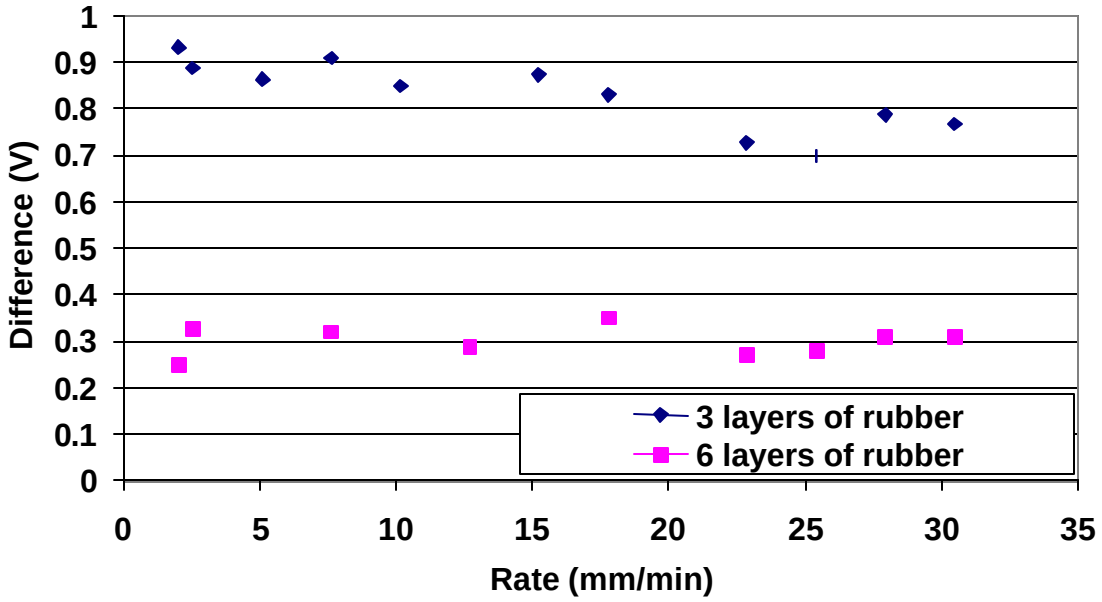

Figure 4.10. Difference between Manufacturer and Instron Calibrations as a function of Rate of Loading for Two Different Rubber Thicknesses

4.2.1.3 Field Dynamic Calibration

Falling weight deflectometer tests were also performed to check the performance of some of the embedded instrumentation using different loads at different distances from the cells. The pressure distribution under the BM-25.0 layer due to five different FWD weights is shown in Figure 4.11.

In addition to verifying the total vertical load, time histories for the pressure cell measurements under FWD loading were recorded. These were compared to loading time histories recorded by the FWD machine. Both load histories were of the same shape and coincided perfectly. To evaluate the effect of HMA thickness, the pressure was measured underneath the BM-25.0 in sections E through G. These three sections have different BM-25.0 HMA thicknesses (225, 150, and 100mm, respectively). The FWD load was dropped at 150-mm increments away from the pressure cell in two directions. Figure 4.12 shows the response of the pressure cells for these sections.

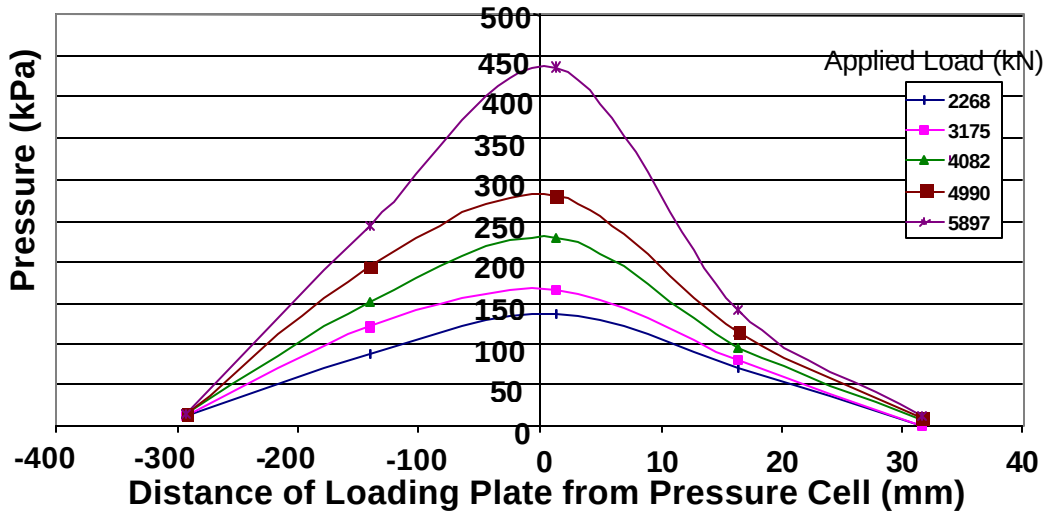

Figure 4.11. Pressure Cell Response under FWD Load.

By integrating the area under the surface of revolution produced by the curves shown in Figure 4.11, the total force acting at the pressure cell level can be calculated, P_p. Then by summing the forces acting in the vertical direction, namely the FWD load P_{FWD} and P_p, the result should be zero. It was found that the difference between P_{FWD} and P_p is within 10% of the applied load. This difference is believed to be directly related to the limited number of load points and the inaccurate pressure measurements at large distances away from the cell.

It can be concluded from these field calibrations that since the manufacturer's calibration curves were used to convert the voltage readings under these FWD tests, it is sufficient to use them for any further testing.

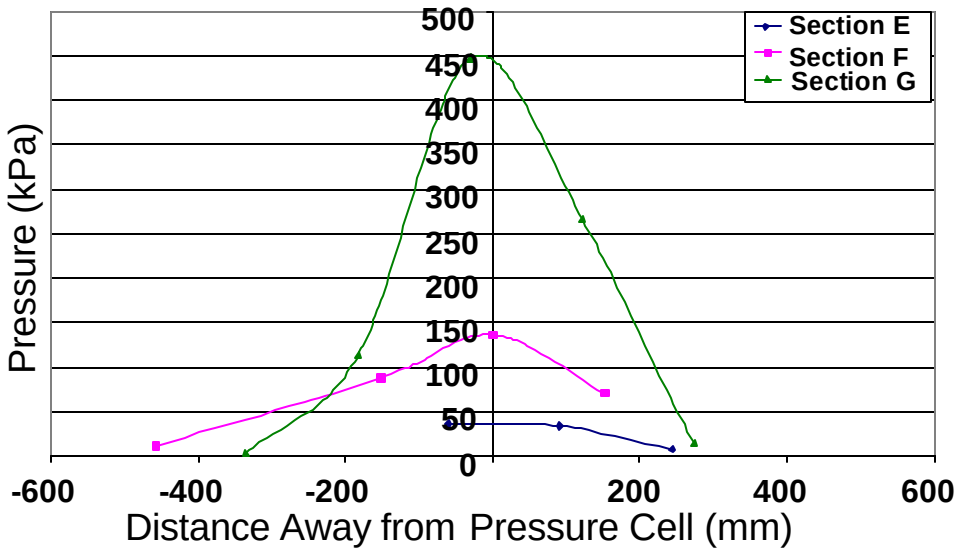

Figure 4.12. Pressure Cell Response under Different Layer Thicknesses

4.3 Field Data

Load response sensors include HMA strain gauges (Dynatest Past-IIAC) and HMA pressure cells (RST TP-6-S). In the previous section, efforts to ensure the quality of the data were presented. In the following sections, the use of the measured response in the fatigue design of HMA is presented. Section 4.3.1 presents an explanation of the different strain responses obtained in the field. A discussion on what strain response value should be used with fatigue design follows. The direction of the principal strain is first investigated, followed by the evaluation of which strain value is more damaging, transverse strain or longitudinal strain.

4.3.1 Response Explanation

Typical response from the strain gauges is shown in Figure 3.24. It can be seen that while the strain in the transverse direction (perpendicular to traffic) is always in tension, the longitudinal strain has a compressive strain preceding the tensile strain.

Research in other instrumented pavement facilities showed similar results. Longitudinal strain response can be classified into three types: completely tensile, compressive strain preceding the tensile strain, and compressive strain before and after the tensile strain. It can also be noticed from Figure 3.24 that the transverse strain has a recovery period after the application of the load, while the longitudinal has much less of a recovery period.

The compressive strain in the longitudinal strain gauge response may be related to the combination of bending stresses and horizontal shear stresses. The bending effects can be seen in Figure 4.13. When the load is directly on top of the strain gauge, the measured strain is tensile. However, due to the bending of the HMA layer, at a distance away from the strain gauge, the strain is compressive. So, when the loading point is before or after the position of the strain gauge, the strain gauge measures compressive bending strain at its location.

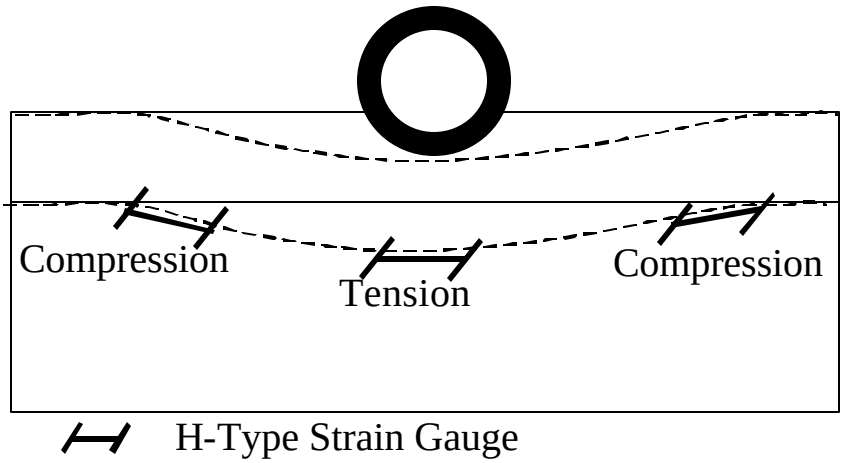

Figure 4.13. Bending Effects to Explain Longitudinal Strain Response

Most of the response obtained from the longitudinal strain gauges placed in the wearing surface at the Virginia Smart Road has compressive strains preceding the tensile strains and none following. The horizontal shearing effects may explain this, which are

highest below the wearing surface. Before the horizontal shearing forces can be explained, a clear distinction between two cases has to be made: the case of no vertical deformation, and the case of vertical deformation.

Case I: No vertical deformation.

As the vehicle travels, the tire imposes horizontal shearing forces on the pavement due to friction between the tire and the pavement. When the load is moving towards the strain gauge, these shearing forces act to produce tensile strains. However, when the load moves away from the strain gauge, the same forces act to produce compressive strains that increase the compressive portion of the response that succeed the maximum tensile strain, Figure 4.14.

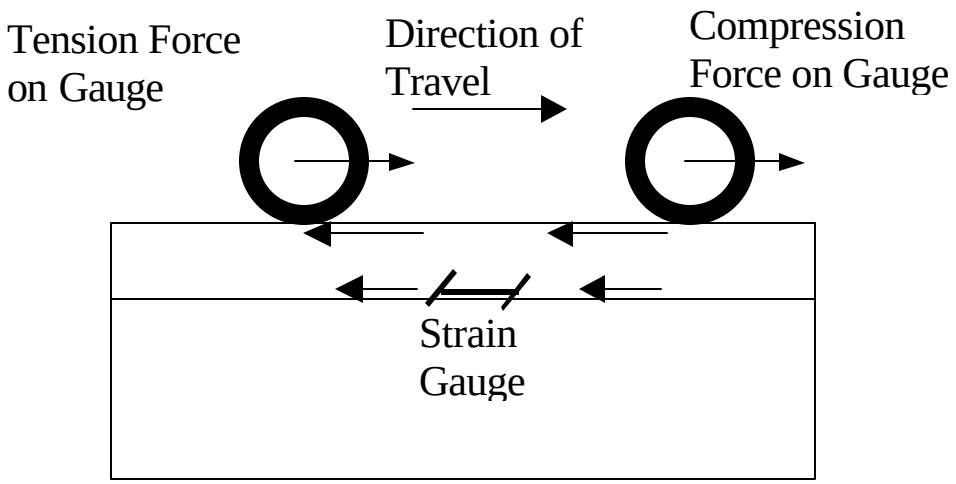

Figure 4.14 Explanation of Case I: No Vertical Deformation

Case II: Vertical deformation.

When a traffic wheel load moves on the road, the pavement surface is subjected to pulses of stress. Using electronic sensors at the pavement surface, the acceleration signals can be recorded and automatically integrated to obtain velocity and deflection signals. This has been performed by Sebaaly and Mamlouk (1987) and the typical results are shown in Figure 4.15. This behavior underneath the loading wheel that was observed by

Sebaaly and Mamlouk is not restricted to the pavement surface. This behavior has been also noted at lower levels in the pavement system. Gunaratne and Sanders also show similar results analytically (Gunaratne and Sanders; 1996), Figure 4.16. Figure 4.17 shows the shape of the vertical and horizontal displacements at the base/subgrade interface.

These curves have been obtained by superimposing the effects of a vertical and a horizontal strip load. In this case, when the load is approaching the strain gauge, the horizontal shearing forces act to produce compressive strains. However, when the load moves away from the strain gauge, the same forces act to produce tensile strains that may balance the bending compressive strain, Figure 4.18. For the same reason, bending effects, transverse strain gauges register compressive strains when the load is at a lateral distance away from the gauge.

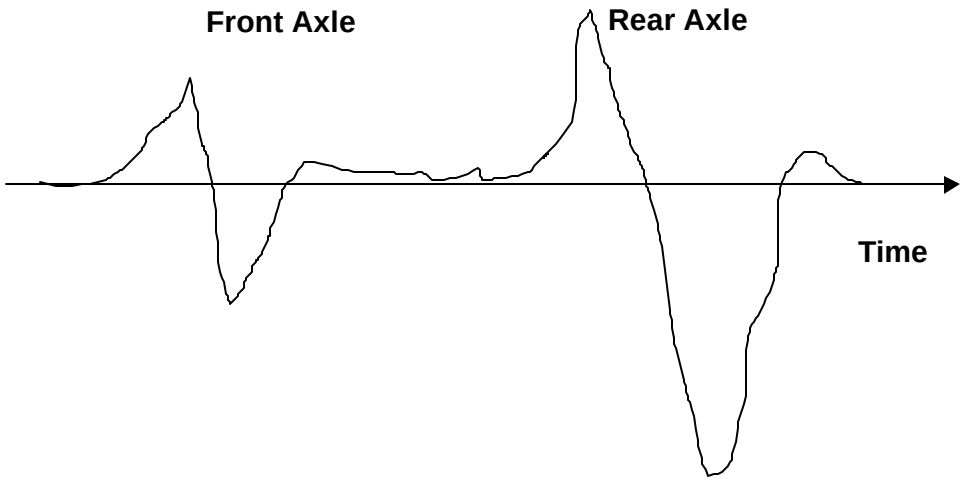

Figure 4.15. Acceleration Signal on the Pavement Surface

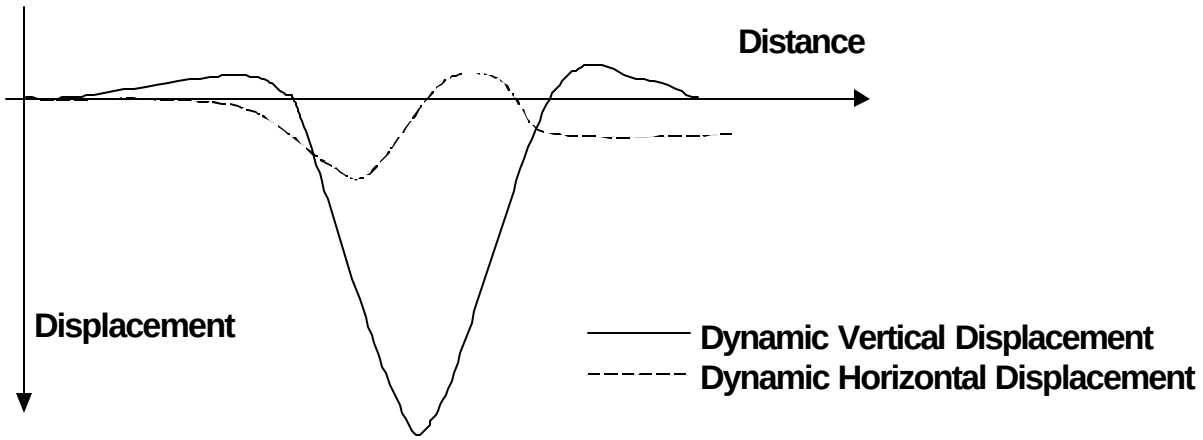

Figure 4.16. Surface Vertical and Horizontal Displacements

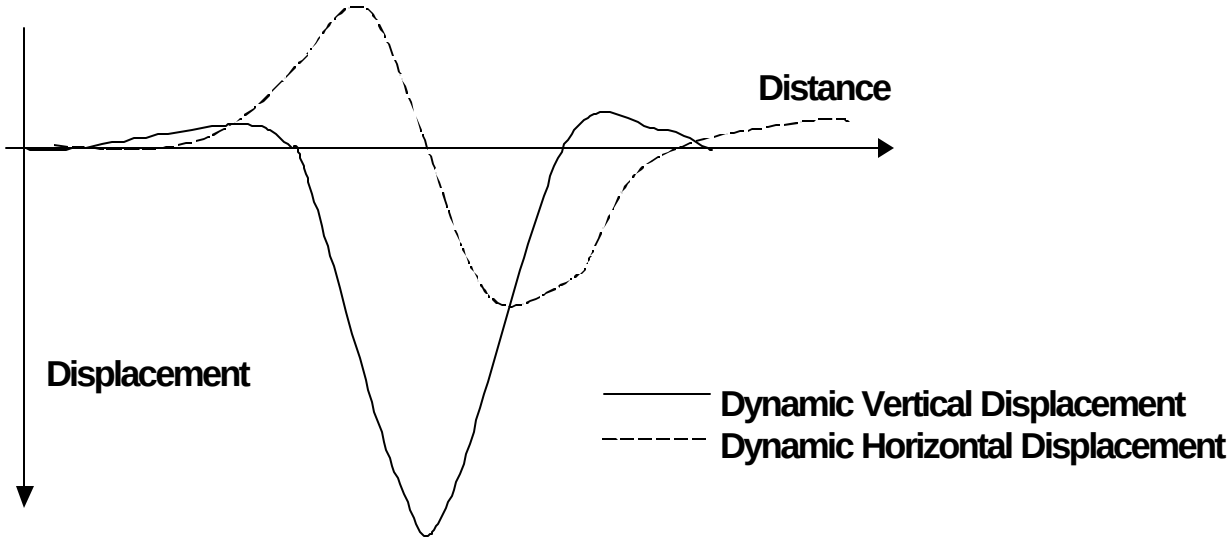

Figure 4.17. Base/Subgrade Vertical and Horizontal Displacements

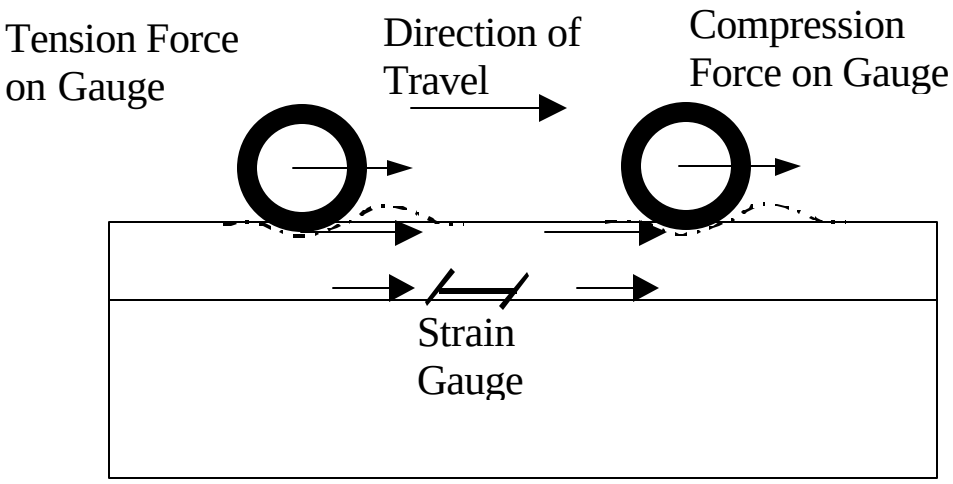

Figure 4.18. Explanation of Case II: Vertical deformation

Due to the difference in transverse and longitudinal strains, a comparison between the two is necessary to determine which direction is more critical for fatigue analysis. Fatigue equations are based on one value for the strain, however, the response in the field is a time signal that has both tensile and compressive strains. Accordingly, equivalent strains have to be calculated. Traditional methods for evaluating equivalent strain, such as the Goodman approach (Fuchs and Stephens, 1980), require parameters that relate to the static strength and the strength under repeated loading. Unfortunately, these parameters are not commonly found in the literature, and to evaluate them requires years of research, if feasible. Accordingly, the four methods described in section 3.3.1 were used on the data collected from the Virginia Smart Road. The data were first reduced to include those strain responses that were measured at 25^0C only, then further reduced to include only the data from the heaviest truck loading.

The specifications for the truck and tire types used in this study are shown in Appendix B. Table 4.2 shows the loads used for the data analysis. The cells D1 through D6 represent the tire weight on the driver's side. The cells P1 through P6 represent the tire weight on the passenger's side. The weights were measured using an electronic scale placed directly under each tire. The columns labeled L1, L2, and L3 show three different replicates of the weight measurements at different locations at the Virginia Smart Road to

account for any variability in the road surface slope. This was done to take into account the effects shown in Figure 4.19.

Table 4.2. Truck Weights

	Load (lbs)				**Load (lbs)**				**Load (lbs)**		
	L1	L2	L3		L1	L2	L3		L1	L2	L3
D1	5160	5160	5840	P1	5360	5340	5320	Axle1	10520	10500	11160
D2	9480	8920	9460	P2	9900	10360	9740	Axle2	19380	19280	19200
D3	8960	8440	8980	P3	9460	9780	9140	Axle3	18420	18220	18120
D4	8480	9420	8480	P4	9320	10460	9280	Axle4	17800	19880	17760
D5	8180	7400	8120	P5	8120	7100	8120	Axle5	16300	14500	16240
D6	7780	7340	8200	P6	8340	7900	8620	Axle6	16120	15240	16820
								TOTAL	98540	97620	99300

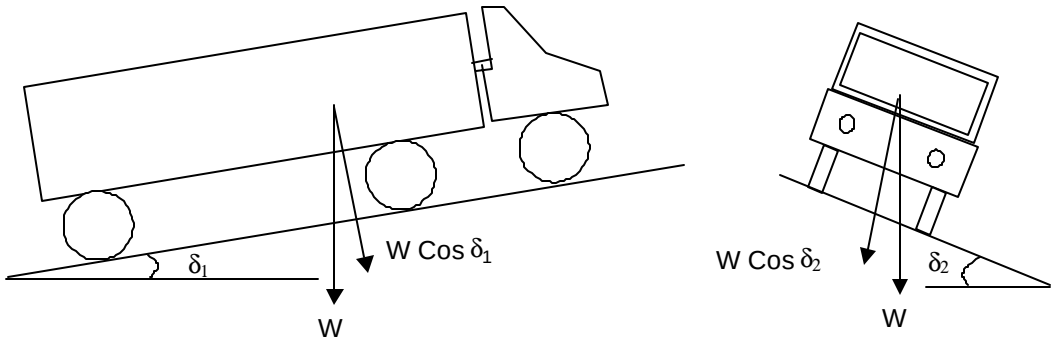

Figure 4.19. Incorrect Truck Loading Locations

Table 4.3 shows a summary of the results using the four calculation procedures. It can be seen that for all four criteria, the longitudinal strain is greater than the transverse strain with the exception of the average strain method, which results in very close strain values for the two directions. The total strain magnitude was selected to be used in the calculation. One may note that strain gauges in different directions (longitudinal vs. transverse) are exposed to different loading times when subjected to the same tire loading at a specific direction of travel.

Table 4.3. Comparisons of Longitudinal and Transverse Strain Response

Criterion		Strain (microstrain)
Max Tensile Strain	Longitudinal Strain	349.00
	Transverse Strain	271.00
Max Compressive Strain	Longitudinal Strain	229.00
	Transverse Strain	0.00
Area under Curve	Longitudinal Strain	147.32
	Transverse Strain	164.45
Total Strain	Longitudinal Strain	578.00
	Transverse Strain	271.00
Strain Rate	Longitudinal Strain	1125.76
	Transverse Strain	428.43

Based on the calculations shown above for this specific case, it can be concluded that the strains at the bottom of the 38-mm wearing surface found at the Virginia Smart Road are more damaging in the longitudinal direction than in the transverse direction. The above conclusion does not necessarily mean that the principal directions are longitudinal and transverse. In fact, the presence of the compressive strain registered in the longitudinal strain measurements provides indication that the principal directions may be at an angle.

To investigate the principal strain direction, it is first assumed that the pavement is a transverse isotropic material. This means that the HMA material properties are the same in all directions in the horizontal plane. Second, it is assumed that the out-of-plane forces (vertical forces) have little to no effect on the principal strain direction in the horizontal plane. Data from three strain gauges placed in section B at the Virginia Smart Road are then analyzed to calculate the principal strain direction. The three strain gauges were placed at three directions, longitudinal, transverse and at a 45^0 angle, to the pavement centerline, Figure 4.20. The strain gauges were not placed at the same location; accordingly, the strain response from the three gauges had to be time shifted to capture the maximum response. After aligning the strain response from all three gauges, the longitudinal compressive strain value and the corresponding strain values for the

transverse and the 45^0 gauges were noted, Figure 4.21. These three values were then used to draw Mohr's circle using the following steps:

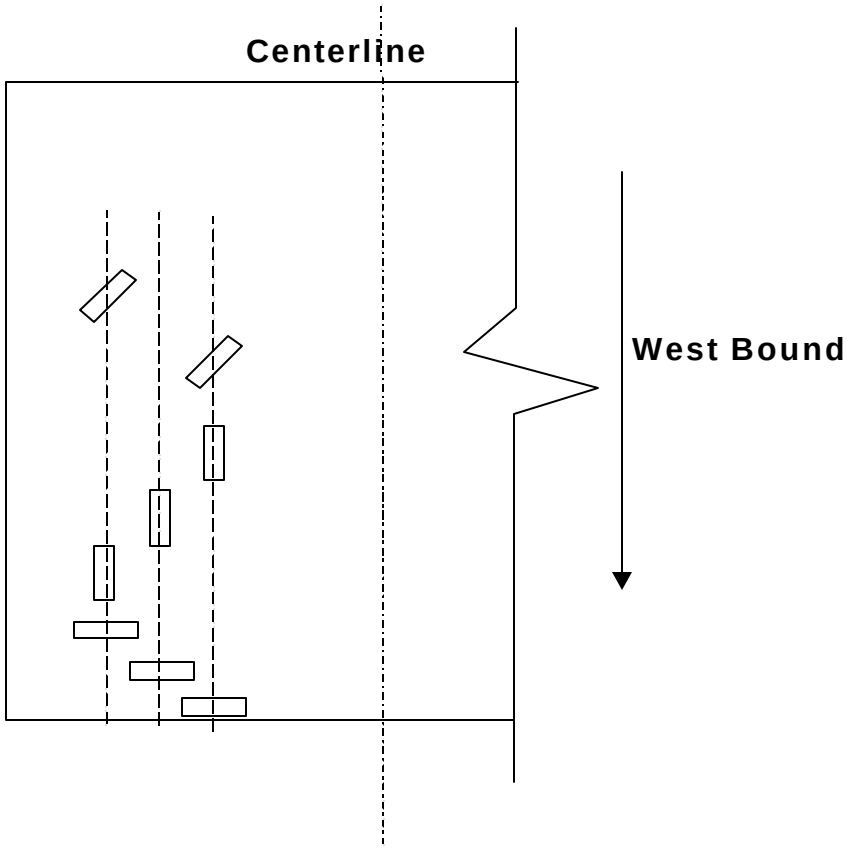

Figure 4.20 Schematic of the Instrument Locations for the Strain Rosette

1. Construct a temporary horizontal ε axis from any origin O', and measure the three measured strains, ε_ϕ, $\varepsilon_{\phi+\alpha}$, and $\varepsilon_{\phi+\alpha+\beta}$, Figure 4.22.
2. Select any point, D, on the vertical through $\varepsilon_{\phi+\alpha}$, then draw lines DA and DC at angles α and β to the vertical at D as shown, to meet the other two verticals at A and C. The circle drawn through D, A, and C is the required circle.

3. Its center, F, is determined by the intersection of the perpendicular bisectors of CD, DA. The points representing the three gauge directions are A, B, and C.

4. The ε_θ axis can now be drawn as OF, and the distances from O to the intersections with the circle give the principal strains.

Different speeds and different loads were evaluated, and the results are shown in Appendix C. Table 4.4 summaries the results obtained from this analysis.

Table 4.4 Summary of the Results from the Mohr's Circle Analysis

Speed	Trans	Long	45degrees	Tire	Shear Strain	Principal Direction Angle from Centerline	Load (N)
25	-7.98	21.80	35.09	D1	31.87	62.1	5860
45	-70.18	115.90	70.18	D1	104.30	26.9	5860
45	0.00	137.70	70.18	D1	68.86	1.1	5860
25	-38.81	21.80	17.54	D2	39.96	40.7	8880
25	-62.20	21.80	40.94	D2	73.58	55.6	8880
45	-62.20	79.75	64.33	D2	90.14	38.1	8880
45	-30.84	115.90	64.33	D2	76.54	16.5	8880
25	-62.20	28.71	5.85	D3	50.76	26.4	8140
45	-62.20	64.86	46.79	D3	78.12	35.6	8140
45	-38.81	94.10	46.79	D3	69.16	16.1	8140
5	7.44	65.39	-5.85	D4	50.75	54.7	8560
45	-31.37	57.95	-23.39	D4	57.79	39.4	8560
45	-15.42	87.19	-29.24	D4	82.91	51.8	8560
5	22.86	57.95	5.85	D5	38.22	62.0	8160
45	-77.62	72.31	-46.79	D5	86.99	30.5	8160
45	-30.84	108.99	-29.24	D5	97.33	45.0	8160
45	-62.20	64.86	-35.09	D6	73.23	29.8	8420
45	-38.81	65.39	-76.03	D6	102.88	59.8	8420

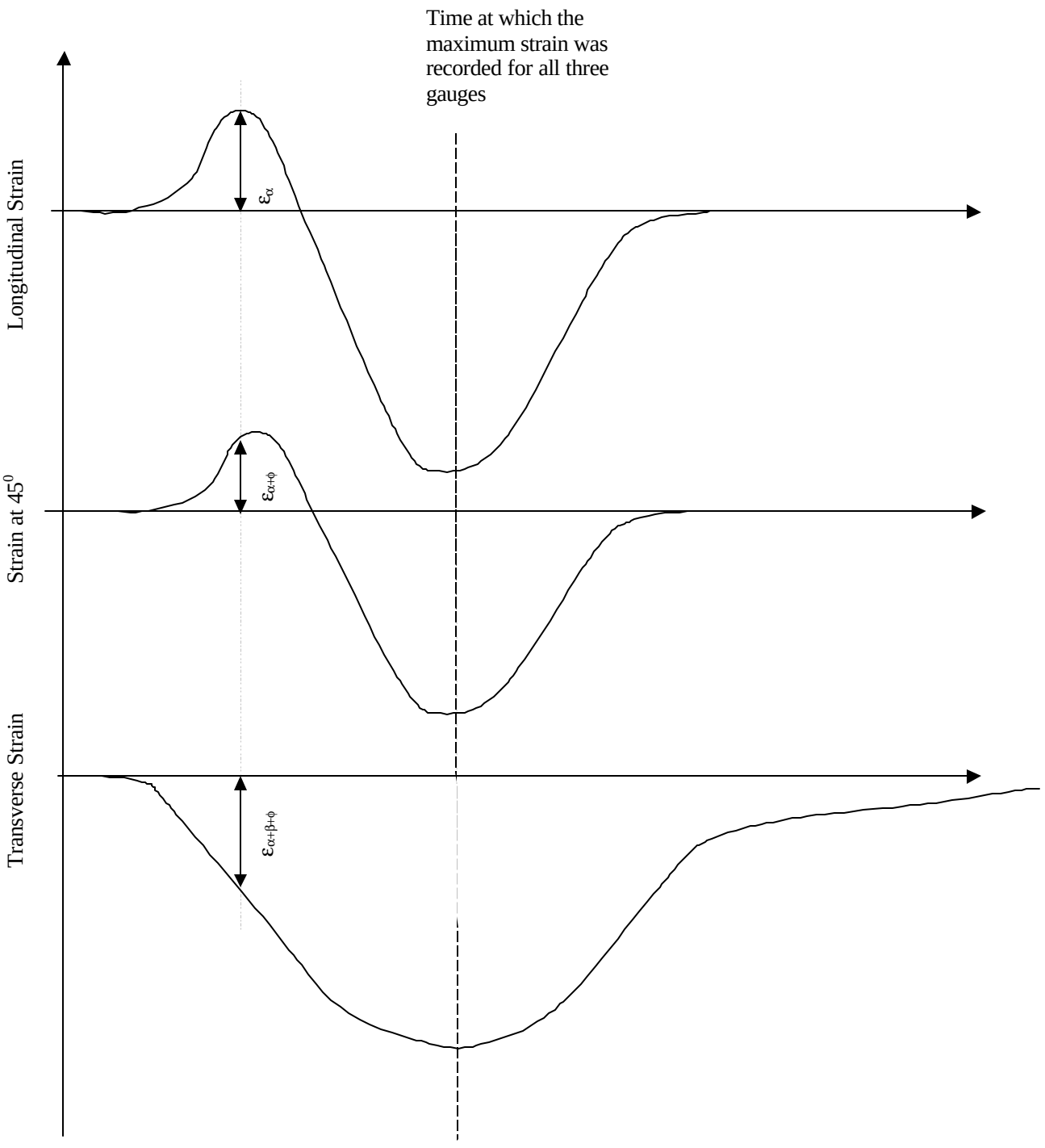

Figure 4.21 Time Shifting of Strain Signals

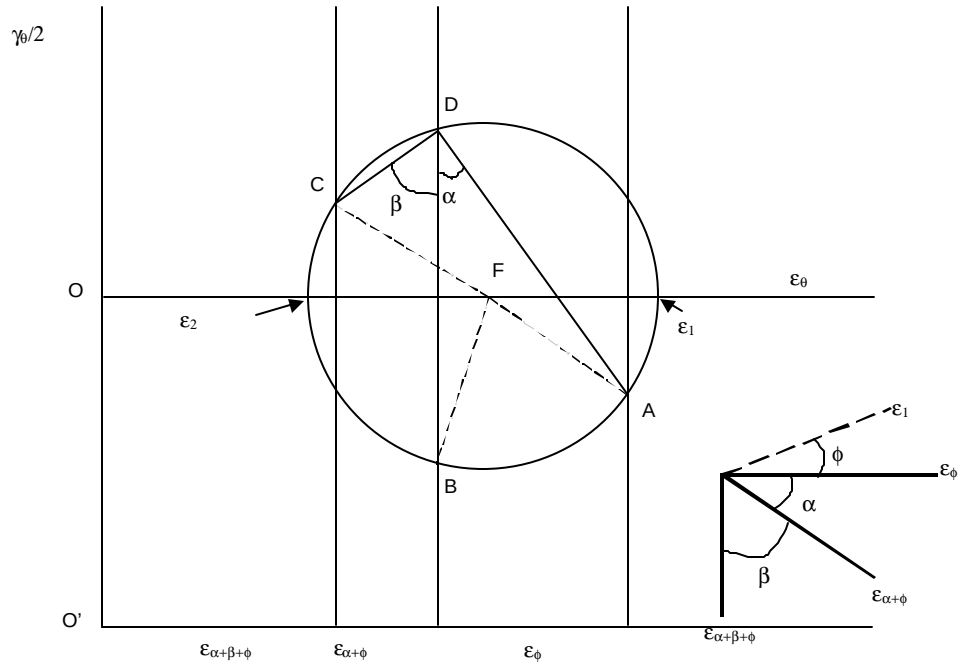

Figure 4.22. Construction of Mohr' Circle

Figure 4.22 shows the relationship between principal strain direction and load at a distance away from the gauge that has maximum compressive longitudinal strain.

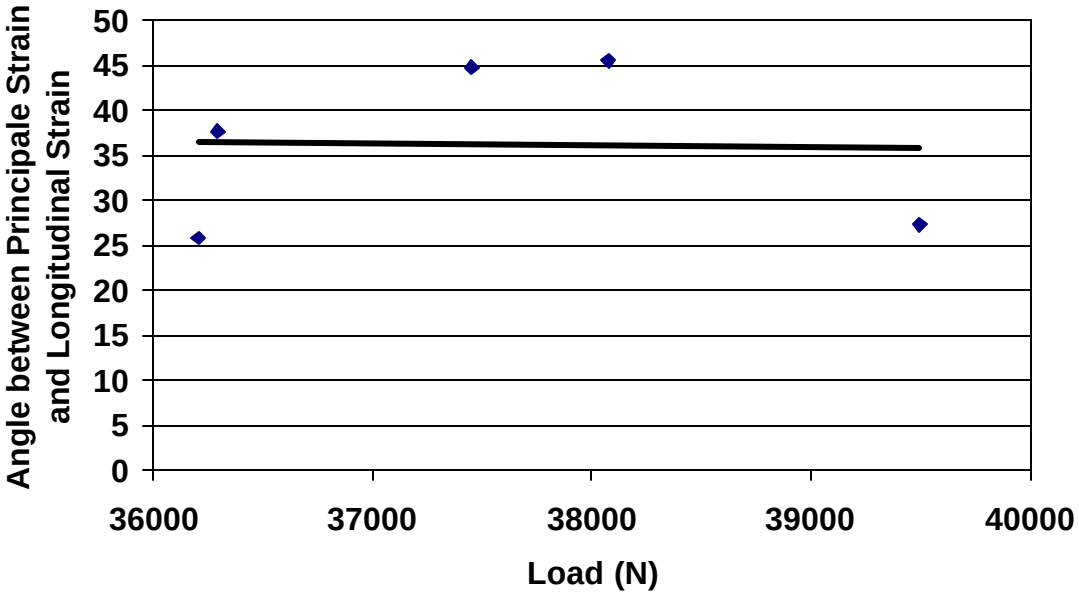

Figure 4.23. Angle between Principal Direction and Longitudinal Strain

Although there is insufficient data to deduce any relationship between the load and the principal strain directions or between speed and the principal direction, it appears that the principal direction changes as the vehicle passes over the pavement. However, further data is needed to quantify those effects that could not be achieved in this project. Therefore, for the remaining part of this dissertation, it is assumed that the strain principal directions do not change and that the principal strains are those measured by the longitudinal and transverse strain gauges.

It was shown that the response in the longitudinal direction is different from that in the transverse direction. This difference may be attributed to the loading anisotropy or material anisotropy or both. Since truck traffic travels only in the longitudinal direction, it goes without further explanation that the loading is anisotropic. The following sections present the data collected for the purpose of evaluating HMA material anisotropy.

4.3.2 Anisotropy from Compaction Data

Roller compaction is by far the most used method of compaction in the US, although Canadian and Australian experiences show that most of the pavement problems arise from initial HMA cracks caused by the steel drum roller (Richards; 1999). For a typical steel roller, the contact area between the asphalt mix and the drum is between 70 and 150mm (3 to 6in) in length, times the width of the drum, and takes the shape of the cylindrical drum. Due to this small curved contact area, the applied force has both radial and tangential components as shown in Figure 4.24. At a normal rolling speed of 10 km/hr (6 mph), the contact between the roller and the mix is about 0.036 seconds. The small contact area and load time combine to apply an intense pressure impulse (typically 1.38 MPa [200 psi]) to the HMA surface. Hence, conventional equipment presents forces that are both rapidly applied and held for merely a fraction of a second. These characteristics present two major negative effects on HMA compaction. First, loads applied rapidly for a short duration cause the HMA to respond with a high elastic

stiffness with no viscous or plastic flow, similar to the excess pore pressure effect in fine-grained soils. To overcome the increased asphalt stiffness, conventional equipment seeks to increase the applied load or to use vibration, which may cause breakage of the aggregate particles. The mix may not be efficiently compacted under these conditions. Secondly, the small contact area causes the application of horizontal (shoving) forces to the HMA layer. As shown in Figure 4.24, the radial and tangential forces applied by the steel roller both contain horizontal components. As the roller travels, the horizontal forces push and pull the HMA fore and aft of the drum, respectively, causing surface cracking with an interrelated dissipation of a significant portion of the applied compaction energy. The HMA mix is not efficiently compacted under these conditions. Furthermore, the induction of surface cracking reduces the strength and fatigue resistance of the HMA layer.

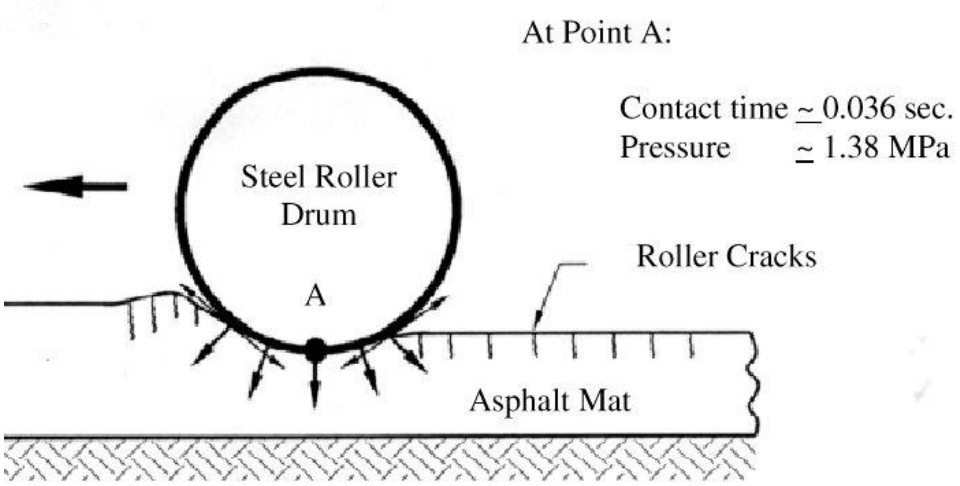

Figure 4.24. Steel Roller Compaction (Richards *et al.*, 1999).

In addition to the above-mentioned problems, data collected from the Virginia Smart Road show that the assumption that the pavement is a transverse isotropic material may not be true. A material is called transverse isotropic when the properties in the transverse direction (horizontal plane) are the same in all directions. This was observed in the measured strain both in the direction of traffic and perpendicular to traffic. Figure

4.25 shows a typical response from strain gauges placed in the direction of traffic. Figure 4.26 shows a typical response from strain gauges placed in the direction perpendicular to traffic. These two figures show that not only are the strain values different, but the shape of the response is also different. Thus, either the material property is different in both directions, or the applied loads are different, or both. The HMA, when first placed, is a loose mix that gains its strength with compaction; accordingly, the applied forces will govern how the properties change. Also, from the cylindrical shape of the roller, it is obvious that the applied forces are not the same in both directions. Furthermore, due to the compaction being done in one direction, an argument can be made that the aggregates will reorient themselves and will roll over each other in one direction only, as shown in Figure 4.27.

The SuperPave^{TM} volumetric mixture design procedure, developed by the Strategic Highway Research Program (SHRP), focuses on average percent air voids for specifying and designing HMA. However, two specimens with the same average percent voids may have a different distribution of air voids. Intuitively, these two specimens would be expected to respond differently under loading and yield distinct mechanical properties in laboratory testing. Furthermore, voids are not spherical within the same sample; therefore, a cross-section in one direction will show a different air void distribution than in another direction. Another characteristic of the HMA is aggregate distribution, orientation, and contacts (Oda; 1972a). Again, due to aggregates rolling over each other during compaction, if two perpendicular cross-sections are taken in an HMA core, it may be observed that the aggregate orientation and the number of contact points will be different.

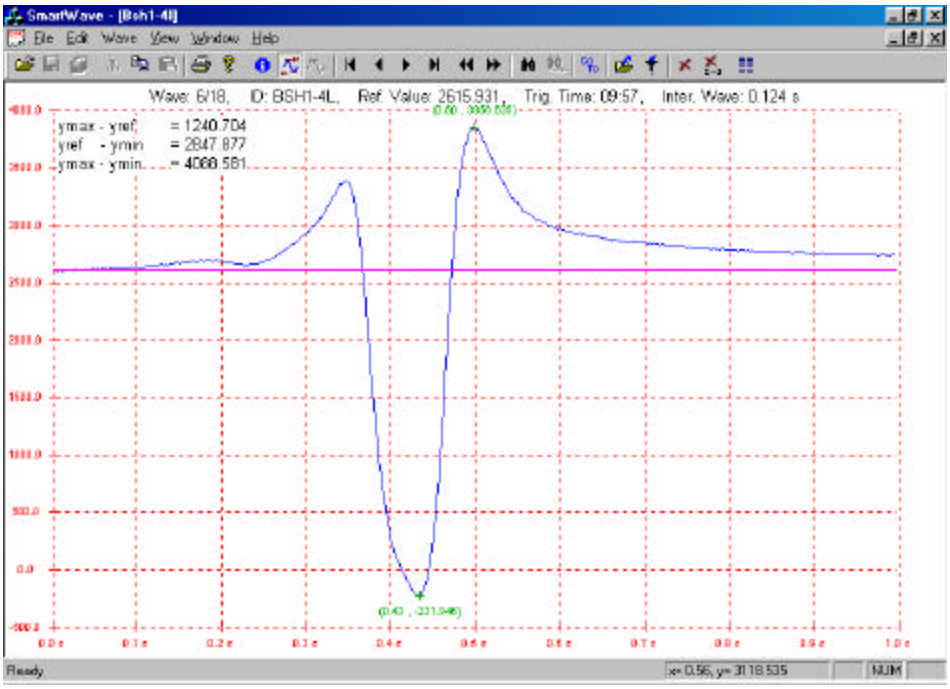

Figure 4.25. Strain Response in the Direction of Traffic

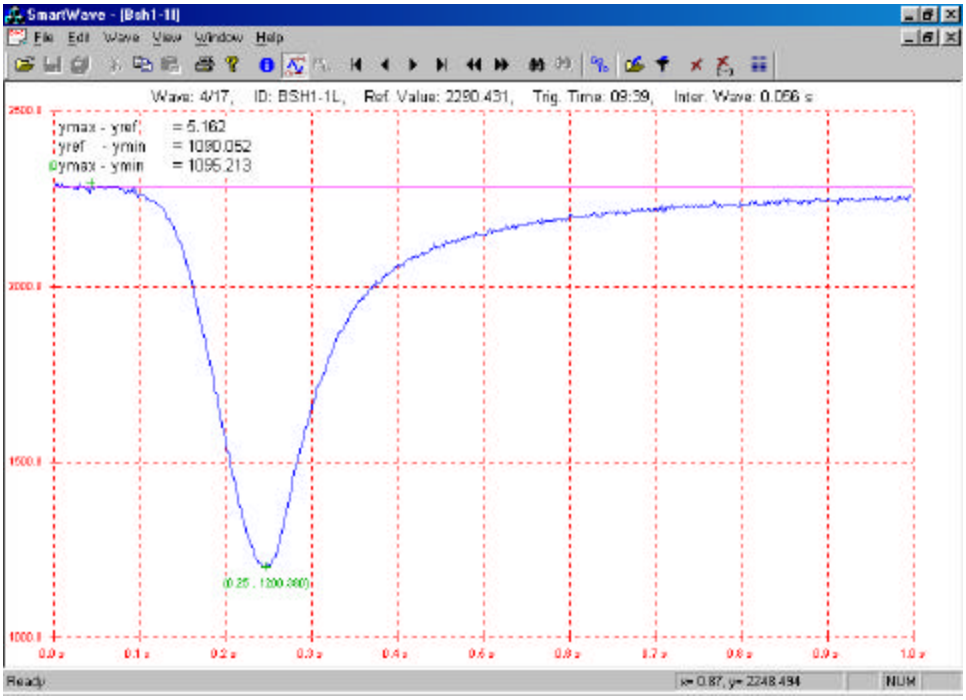

Figure 4.26. Strain Response in the Direction Perpendicular to Traffic

It was found that the difference in measured strains in both directions was very significant, as seen from Table 4.5 (where BSH1-4L is the strain in the direction of traffic and BSH1-1L is the strain perpendicular to traffic).

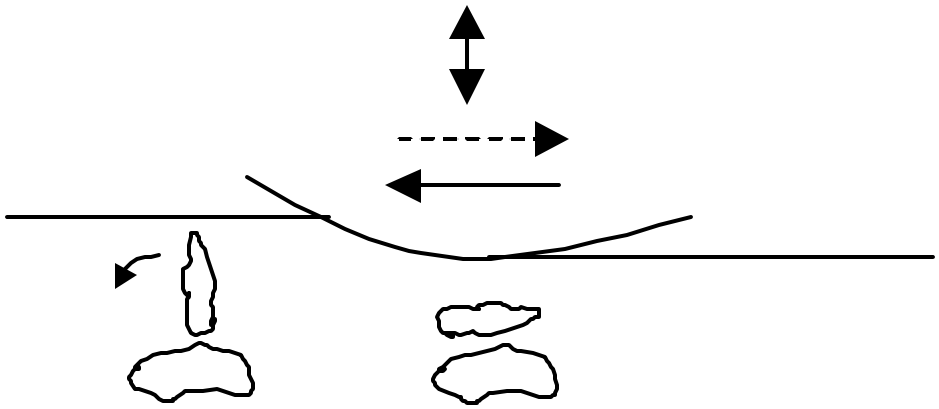

Figure 4.27.. Possible Effect of Roller Compaction on Aggregate Orientation

Table 4.5. Example of Strain Measurements in Transverse and Longitudinal Directions

Time	BSH1-	Time	BSH1-
9:39:0	828	9:39:0	5669
9:39:0	1457	9:39:0	9460
9:39:0	1661	9:39:0	8062
9:39:0	1095	9:39:0	4497
9:57:0	692	9:57:0	4089
9:57:0	990	9:57:0	4387
9:57:0	1095	9:57:0	4575
9:57:0	1101	9:57:0	4921
10:03:0	854	10:03:0	4717
10:03:0	1394	10:03:0	5131
10:05:0	246	10:05:0	3837
11:18:0	194	11:18:0	63

Figures 4.28 and 4.29 show how the strain changes with time for other strain gauges used at the Virginia Smart Road (BSH1-5L and BSH1-2L). As the HMA is compacted, it gains strength and its modulus increases accordingly; more of the measured

strain is converted into internal stresses. This shows that at the end of compaction, the modulus in one direction may be greater than the other.

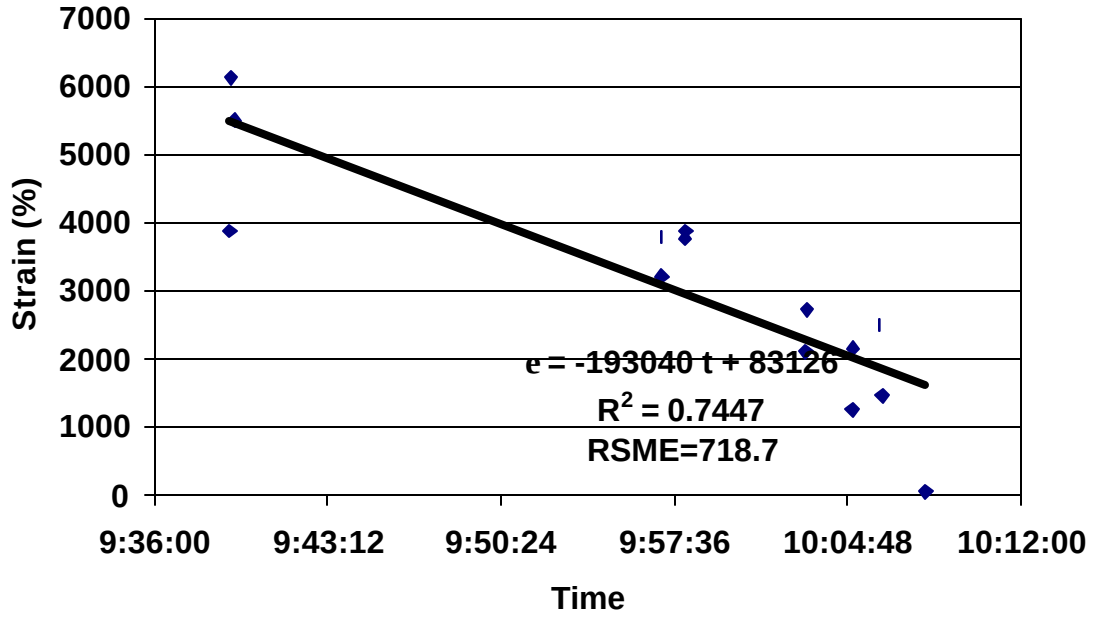

Figure 4.28. Strain Response in the Direction of Traffic During Compaction Operations

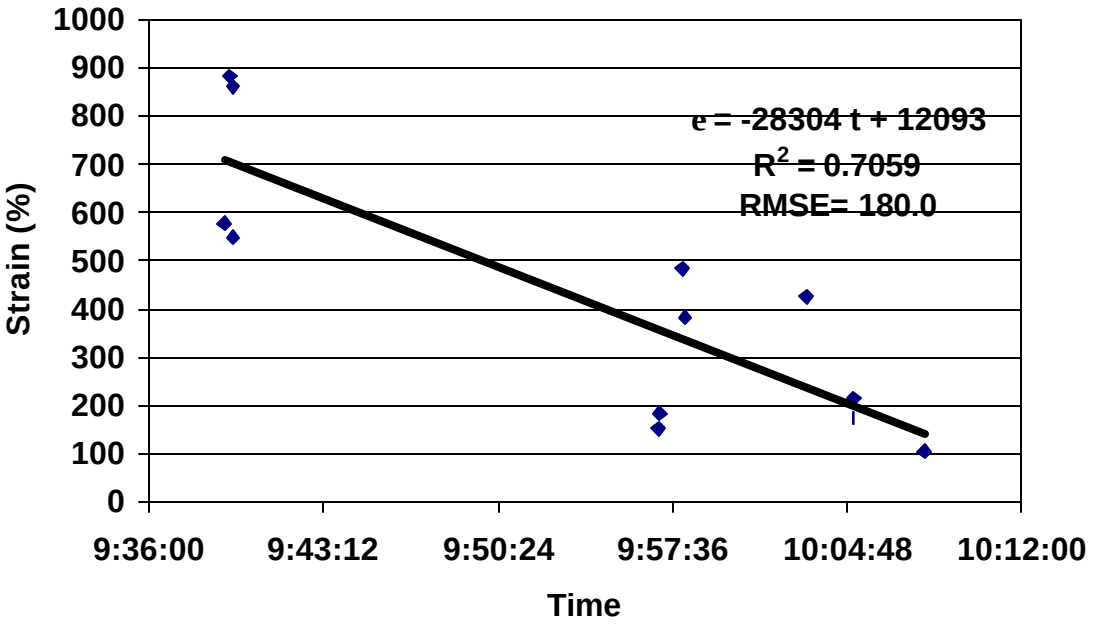

Figure 4.29. Strain Response in the Direction Perpendicular to Traffic During Compaction Operations

The more compaction effort is placed on the HMA, the more the aggregates interlock with each other to provide strength for the HMA. This, along with the binder stiffness, provides the two primary reasons for HMA stability. As the aggregate orientation evolves, so does the anisotropic variation in the HMA continuum properties such as stiffness and strength. From the above discussion, there is a need to evaluate the properties in both directions, with emphasis on strength. The next section discusses the laboratory test performed to evaluate the strength of pavement cores.

4.4 Laboratory Testing Results and Analysis

Pavement modeling is typically done by assuming the pavement to be a multi-layered elastic system or by using the finite element method to more accurately model the compatibility between the layers. Multi-layered elastic approach utilizes Burmsiter's layered theory solution, which assumes that each layer is homogenous, isotropic and linearly elastic (Huang, 1993). Finite element models such as ILLI-PAVE and MICH-PAVE use the 2-D axi-symmetric solutions to solve the pavement 3-D problem. This solution is based on cylindrical coordinates and cannot account for plane isotropy if present.

The understanding of the pavement behavior in the three principal directions is essential in pavement distress identification and accordingly, performance prediction. The three major pavement distresses, fatigue cracking, low temperature cracking and rutting, are directly influenced by the pavement properties in the three directions. For example, fatigue cracking starts as micro cracks that further grow to form alligator cracks seen on the surface. The direction of the initial cracks has to be accurately determined. Such information may assist in understanding the crack initiation and crack growth stages and thus the development of accurate performance prediction models. Low temperature cracking, on the other hand, has been identified as equally spaced transverse cracks. Appropriate testing on cored samples for this distress mode should incorporate HMA

properties in the direction of traffic where the thermal strains are largest (longitudinal direction).

In summary, when analyzing the field data collected during compaction, there is reason to believe that the HMA cannot be assumed as a transverse isotropic material. The following section presents the laboratory test results that were performed to further investigate the material anisotropy.

4.4.1 Resilient Modulus

Six cores were taken from every mix used at the Virginia Smart Road, namely SM9.5D, SM9.5A in section H, SM9.5A in section D, SM9.5E, BM25.0, OGFC, and SMA12.5. During construction, the contractor was asked to place a 10-m-long HMA strip from each mix along the side of the main pavement of the Virginia Smart Road, and the cores were taken from those strips. The direction parallel to traffic was marked before coring. To avoid any interaction due to internal damage, separate cores should be used for testing in the two directions. Accordingly, three cores were tested in the direction parallel to traffic, and three in the direction perpendicular to traffic. The data from these tests are shown in Appendix D.

A summary of the data is shown in Figure 4.30. The statistical model explained in Chapter 3 was used, and the results from running the SAS software are shown in Table 4.6.

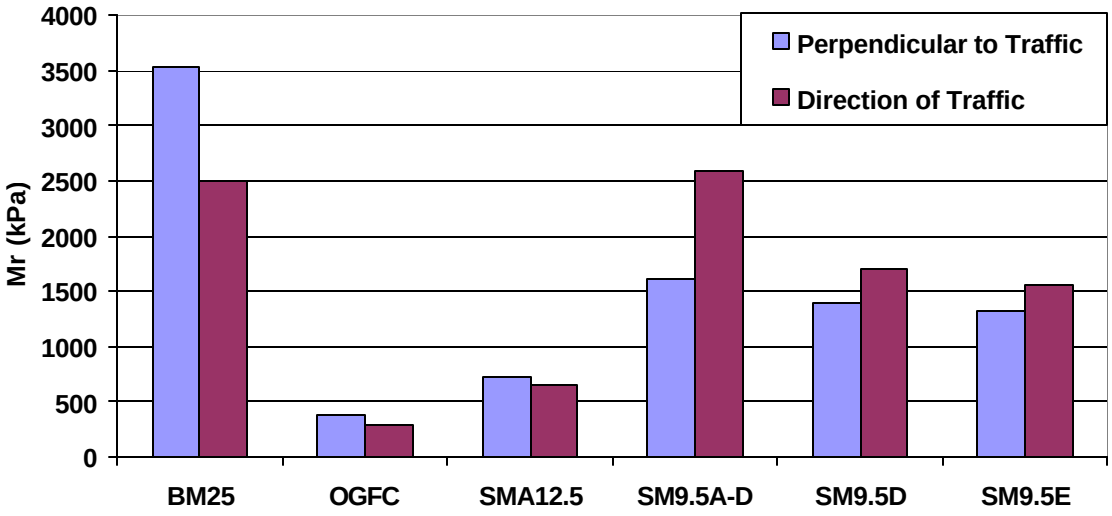

Figure 4.30 Resilient Moduli in the Direction of and Perpendicular to Traffic

A confidence level of 95% was chosen, and the results are shown in Table 4.6. Two levels were tested; first, the effect of the mix type on the overall modulus (p-value of 0.001). As expected, this explains most of the variability in the resilient modulus values since the p-value is less than 0.05. The second level is the effect of test direction on the overall variability. The p-value was found to be 0.8639, which is larger than the confidence level of 0.05; it is concluded that there is not enough evidence to accept the hypothesis and accordingly, there is not enough evidence at this time to prove that the moduli in the two directions are different. It appears that there is either no difference between the moduli in the two directions, or the Resilient Modulus test is not sensitive enough to detect the difference. It appeared from the results that the total recoverable vertical deformation and the total horizontal deformation was not a constant for all the tests. Furthermore, it was found that the higher the measured recoverable strain, the higher the modulus. Accordingly, a parameter that is independent of the amount of strain and of the amount of damage induced in the sample was needed to further investigate the isotropy hypothesis. Perhaps the only parameter that is independent of the amount of damage is the number of cycles to failure, and accordingly, the results from the fatigue tests are analyzed in the next section to further examine this supposition.

Table 4.6 ANOVA Results for Resilient Modulus Tests

Source	DF	Sums of Squares	Mean Square	F value	P-value
MIX	5	405059	810112	5.9	0.001
DTPT	1	411	411	0.03	0.8639
MIX*DTPT	5	73113	14622	1.06	0.4032

4.4.2 Fatigue S-N Curves (ITFT)

Fatigue tests were performed on two mixes, SM9.5A and SM9.5E. The two mixes have the same aggregate gradation, but different binders. The binder for the SM9.5A is PG64-22, which is just a straight binder, while the binder for the SM9.5E is PG76-22, which is a modified binder. It is well known that the asphalt binder is a viscoelastic material, i.e. its behavior depends on time and temperature. The time-dependent behavior is evaluated using the number of cycles to failure in the fatigue tests, during which the temperature is kept constant.

Typically in any fatigue test, the number of cycles to failure can be divided into two groups: the number of cycles to initial crack, and the number of cycles during crack propagation to failure. Stress fields around the crack tip control the propagation rate and the energy dissipated to form the crack surfaces. In metals, it is well known that some energy is lost through heat loss. In HMA, heat dissipation must be taken into consideration as the asphalt binder properties may vary during fatigue testing depending on the load and rate of loading. To evaluate temperature variation during the cyclic diametrical fatigue test two samples were prepared and an infrared camera was used to monitor temperature changes during the test, Figure 4.31. The crosshair on the camera was set to measure the temperature at the center of the samples, where cracks are expected to start.

The first sample was fatigued under a 5kN load, and the second was fatigued under 7kN, which is higher than the maximum load that would be used in the regular fatigue tests. A video was recorded of the sample during the test showing the

temperature changes. The results from both tests show that the temperature from the beginning of the test until failure increased by 1 ^{0}C during the 5kN load, and by 2 ^{0}C during the 7kN load test. It can, therefore, be reasonably assumed that temperature effects due to heat loss during fatigue tests can be neglected.

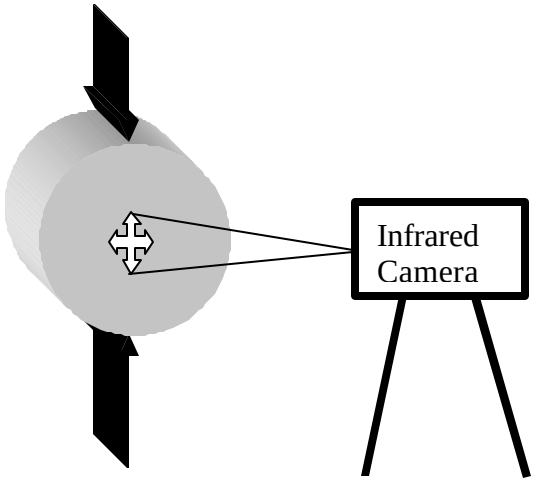

Figure 4.31 Infrared Test Camera Setup

Samples discussed in the testing plan (Chapter 3), were loaded until failure. Two mixes were tested at three different load levels, namely, 6kN, 3kN and 2kN. Two sample types were tested for each mix: mixed in the field and compacted in the field, and mixed in the field and compacted in the lab. Results from the field-mixed, field-compacted samples are shown in Table 4.7.

Table 4.7 Numbers of Cycles to Failure for Field-Mixed Field-Compacted Samples

SM9.5A Core			SM9.5E Core				
	Direction			Direction		Percent Increse (PT>DT)	
Load (kN)	DT	PT	Load (kN)	DT	PT	SM9.5A	SM9.5E
6	1209	2268.5	6	4004	10538	188%	263%
3	3737	6138	3	23876	93759	164%	393%
2	13606	21341	2	134303	698499	157%	520%

DT: specimens tested in the direction of traffic (vertical axis lined with the longitudinal direction)
PT: specimens tested in the direction perpendicular to traffic (vertical axis lined with the transverse direction)

It can be clearly seen from these results that the number of cycles to failure for the specimens tested in the direction of traffic are much lower than the number of cycles for the specimens tested in the direction perpendicular to traffic. Tests performed in the direction perpendicular to traffic are equivalent to straining the longitudinal direction, and tests performed in the direction of traffic are equivalent to straining the transverse direction, Figure 4.32. This supports the assumption previously made from the compaction strain data analysis that the transverse direction is weaker than the longitudinal direction.

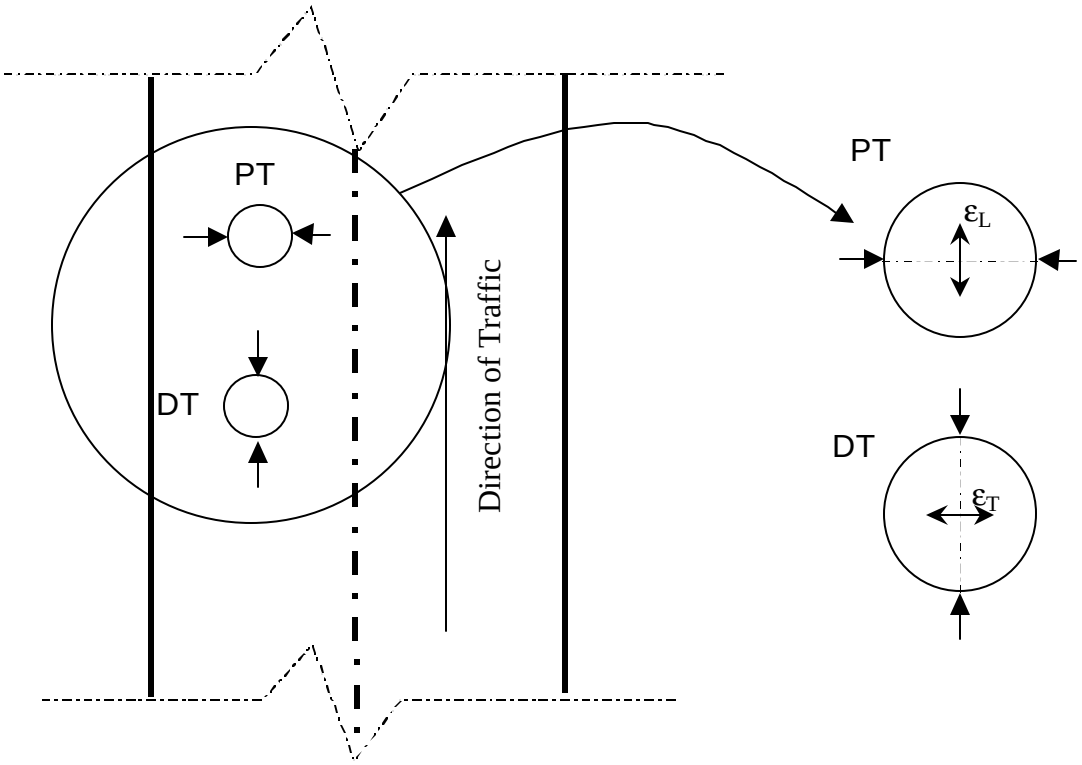

Figure 4.32. Fatigue Test Direction and its Relation to Field Measured Strain

During all the fatigue tests, the vertical elastic deformation and the vertical plastic deformation were recorded. Examples of these results are shown in Figures 4.33 and Figure 4.34. The elastic deformation is to further be used in calculating the resilient modulus, Figure 4.35. It can be seen that the elastic recoverable deformation does not change through the lifetime of the sample. Similar trends were obtained with all other tested specimens. Hence, the resilient modulus did not change from the beginning of the test until the end and internal damage based on resilient modulus could not be calculated. This behavior may be explained by one of two rationales; first, the only reason behind modulus degradation in HMA is the aging of the binder, which is not present in this research, and second, the indirect tensile mode of loading is not appropriate for use with fatigue tests due to the absence of lateral confinement.

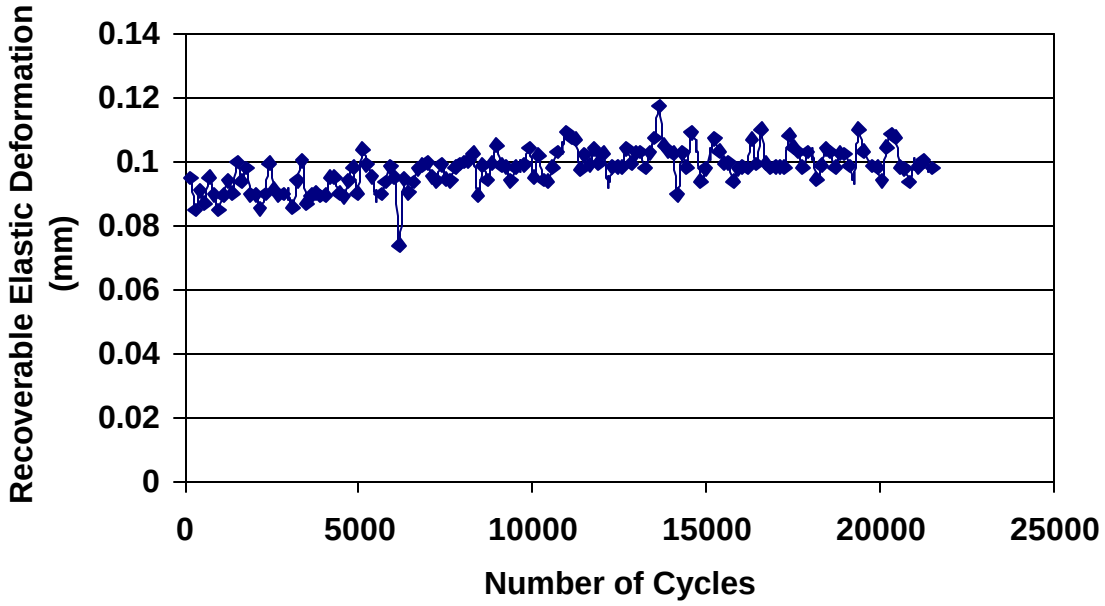

Figure 4.33. Elastic Deformation During Fatigue Testing

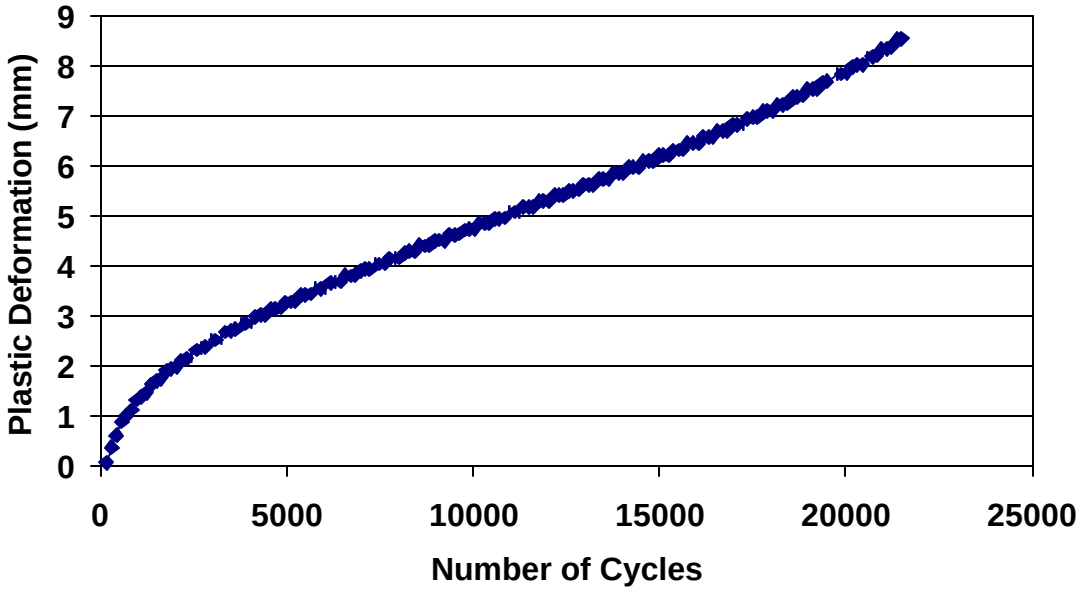

Figure 4.34. Plastic Deformation During Fatigue Testing

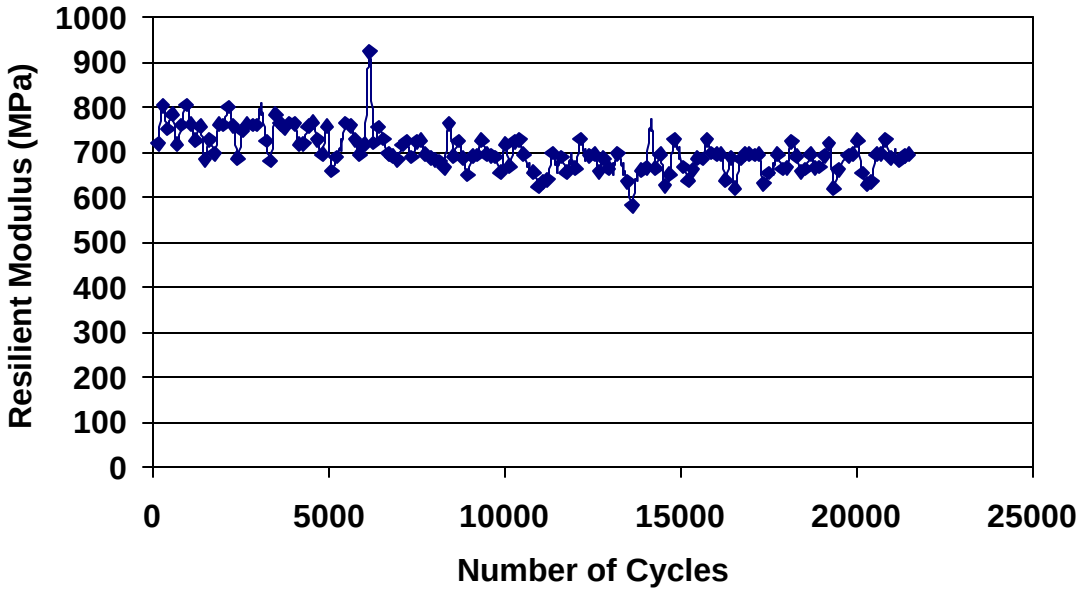

Figure 4.35. Resilient Modulus During Fatigue Tests

Further analysis of the collected data shows that the value for the elastic deformation is the same for both the DT and the PT samples tested under the same load.

Accordingly, it is concluded that the resilient modulus test setup is not suitable for inducing damage to the specimen similar to the damage induced by truck loading in the field. This is mainly due to lack of lateral confinement in the test. Furthermore, the following beam fatigue tests show that there is modulus degradation under the beam flexure mode of loading.

4.4.3 Fatigue S-N Curves (TPBT)

To determine the fatigue life and stiffness characteristics of the two mixes tested in the ITFT, a controlled-strain flexural beam test with a third-point loading system was used. All tests were performed at room temperature using 5Hz frequency sine wave. During the test, stiffness was recorded at various time intervals. Initial stiffness was defined as that occurring at the fiftieth load repetition. Fatigue failure was defined according to the AASHTO TP8 provisional standards, as a 50 percent reduction in stiffness.

A saw-cut was used to cut the samples from the test track at the Virginia Smart Road. The contractor was asked to place 100mm of each of the mixes used at the Virginia Smart Road in two equal lifts. This allowed for the acquisition of samples that are (75x50x400 mm). These were later trimmed using a dry saw to fit the fatigue fixture. The results are shown in Appendix E, and the relationships of the controlled strain fatigue versus strain are as follows:

for SM9.5E:

$$N = 2 \times 10^{11} \varepsilon^{-1.9081} \quad R^2 = 0.63 \text{ and RMSE} = 3.96 \times 10^5 \qquad (4.1)$$

for SM9.5A

$$N = 1 \times 10^{25} \varepsilon^{-7.2921} \quad R^2 = 0.96 \text{ and RMSE} = 4.90 \times 10^4 \qquad (4.2)$$

A typical modulus degradation curve and the dissipated energy curve for the SM9.5A mix are shown in Figure 4.36 and Figure 4.37, respectively. Similarly, the modulus degradation and the dissipated energy curves for the SM9.5E mix are shown in Figures 4.38 and 4.39.

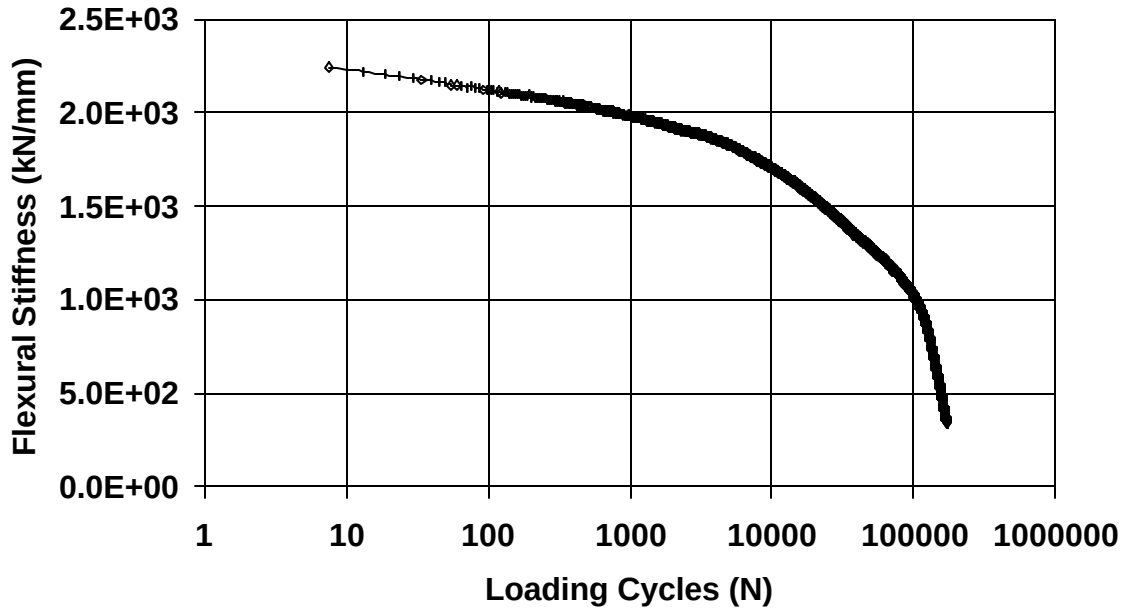

Figure 4.36. Stiffness Degradation Curve for SM9.5A

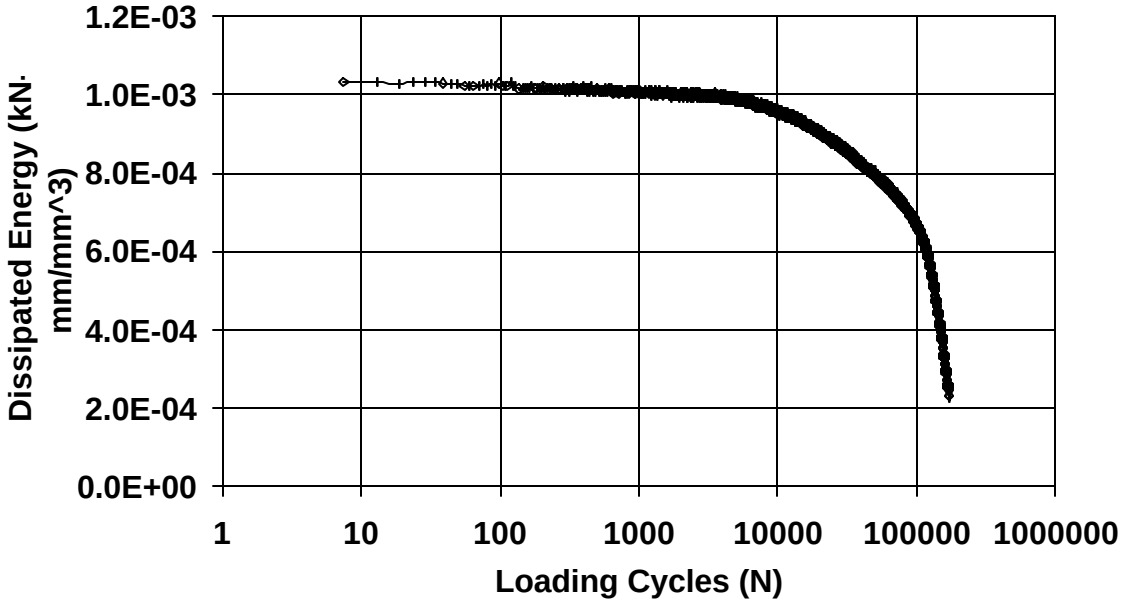

Figure 4.37. Dissipated Energy Curve for SM9.5A

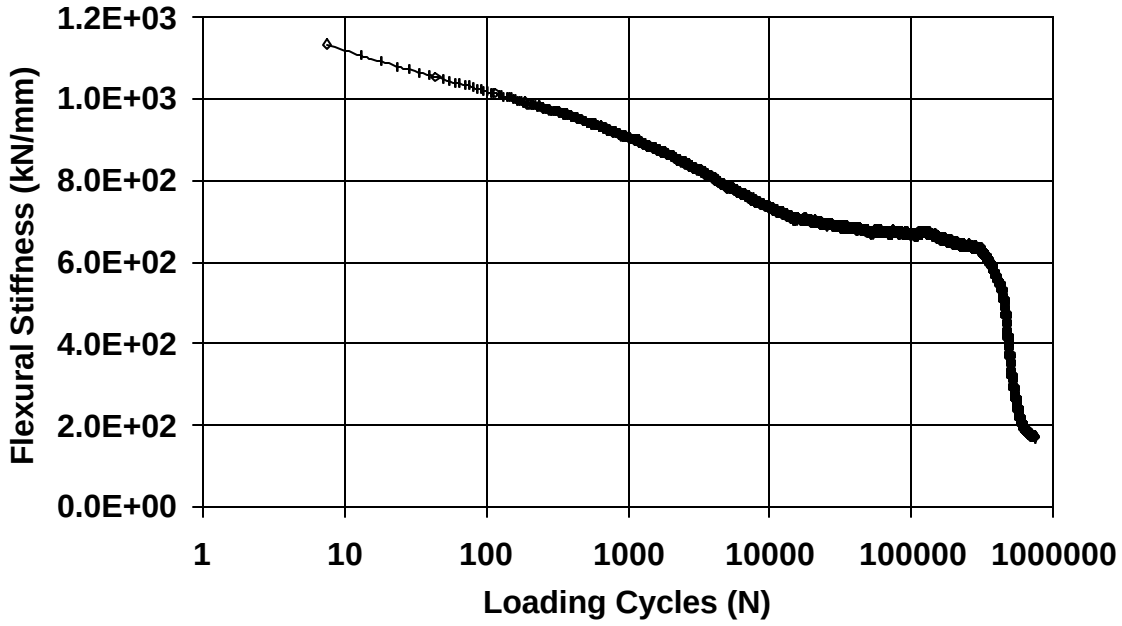

Figure 4.38. Stiffness Degradation Curve for SM9.5E

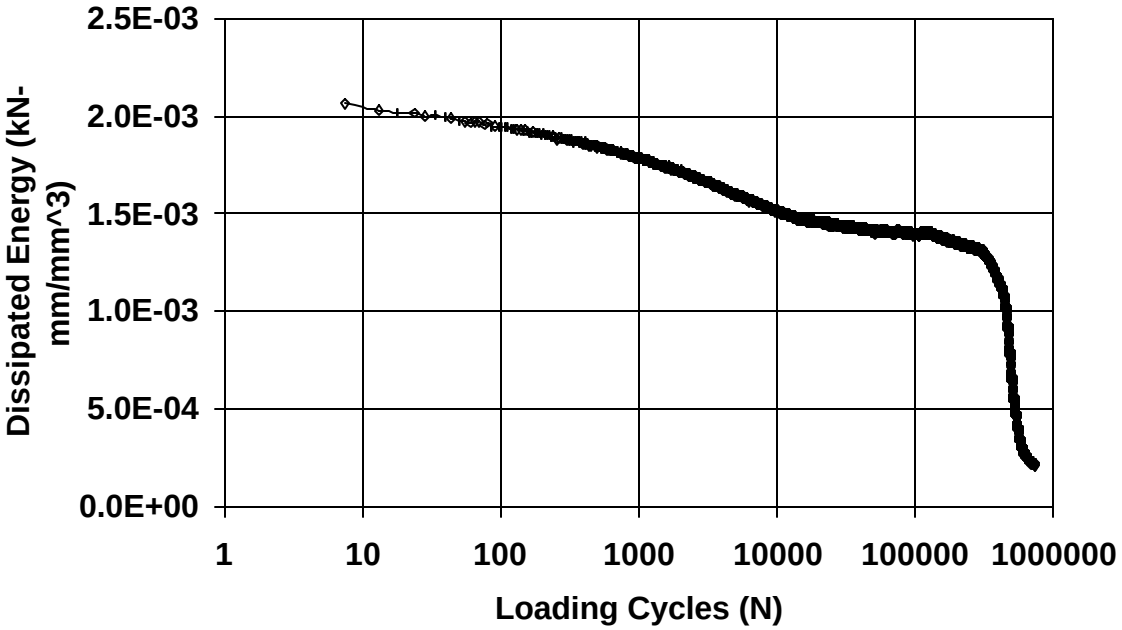

Figure 4.39. Dissipated Energy Curve for SM9.5E

It can be seen from the presented data that the SM9.5E flexural stiffness degradation curve has a plateau region, which is indicative of the presence of the polymer in the PG 76-22 binder. This behavior was not observed in the SM9.5A samples.

4.5 Shift Factors

The fatigue life of pavements determined from laboratory fatigue tests is generally lower than that observed in the field. Accordingly, the number of cycles to failure found in the lab needs to be shifted to the number of cycles to failure in the field to account for the differences in both environments. This is achieved through the calculation of the different shift factors discussed in Chapter 3.

4.5.1 Stress State Shift Factor

For the purpose of the discussion in this section, the HMA is assumed to be a transversely isotropic material, where the properties in the horizontal plane are equal, and the properties in the out-of-plane may be different. Thus, E_x may be assumed equal to E_y. Table 4.8 summarizes the calculated stress state shift factors, where $SHF_s^{Biaxial(x)}$ is the shift factor calculated using the longitudinal strain that may be used with the indirect tensile fatigue test results. Similarly, $SHF_s^{Biaxial(y)}$ is the shift factor calculated using the transverse strain and may be used with the indirect tensile fatigue test results. $SH_s^{Uniaxial(x)}$ is the shift factor calculated using the longitudinal strain and is to be used with the third point bending fatigue test results, and $SH_s^{Uniaxial(y)}$ is the shift factor calculated using the transverse strain and may be used with the third point bending fatigue test results.

Table 4.8. Stress State Shift Factor

	Shift Factor
$SHF_s^{Biaxial(x)}$	**4.5**
$SHF_s^{Biaxial(y)}$	**1.2**
$SHF_s^{Uniaxial(x)}$	**5.8**
$SHF_s^{Uniaxial(y)}$	**1.3**

Ten truck-passes for three different tire pressures and five speeds were on four separate days. The data was reduced for the response measured at $25^0C \pm 3^0C$. The reduced data was used to calculate the stress state shift factor and are shown in Table 4.8. It can be seen that the shift factor to be used with the biaxial test setup is generally lower than that to be used with the uniaxial test setup. This is due to the fact that the biaxial state of stress better resembles the triaxial state in the field than the uniaxial state. It must also be noted here that if a laboratory test setup is found that duplicates the triaxial state of stress found in pavement stress state shift factor will be equal to unity.

The values shown in Table 4.8 are to be used in predicting fatigue failure for the Virginia Smart Road pavement. However, for a different pavement configuration the method still applies with the aid of an accurate pavement response model. In addition, a shift factor to account for rutting failure can be calculated by using only the vertical component in (σ_z^2 / E_z) in Equation 3.35.

4.5.2 Traffic Wander Shift Factor

Table 4.9 shows the results for the shift factor for different values of the traffic standard deviation. It should be noted that any distribution (not necessarily normal) could be used with this analysis method. Different highways have different traffic

distributions that depend on the geometric characteristics and classification of the road. It can be seen from Table 4.9 that the smaller the standard deviation, the smaller the shift factor. As the distribution gets narrower, the strain response approaches the maximum value and the effect of traffic wander vanishes.

Table 4.9. Wander Shift Factor

Standard deviation	**$SHF_{traffic\text{-}wander}$**
1	2.7
0.75	2.1
0.5	1.6

The values shown in Table 4.9 were calculated using a normal distribution. For specific condition were traffic tends to be skewed to one side, on curved highways or under bridges, any distribution that better resembles the traffic wander may be used may be used.

4.5.3 Material Shift Factor

The material shift factor takes into account the difference in compaction procedures in the field and under laboratory environments. The equation relating the load to the number of cycles to failure obtained from the fatigue testing for SM9.5A and SM9.5E, both laboratory- and field-compacted samples, are shown in the following equations:

$$
\begin{aligned}
&\text{SM9.5E Laboratory Sample} \\
&S = 66708N^{-0.2323} \\
&\text{SM9.5A Laboratory Sample} \\
&S = 300{,}000{,}000N^{-0.8608} \\
&\text{SM9.5E Core Sample} \\
&S = 64755N^{-0.2721} \\
&\text{SM9.5A Core Sample} \\
&S = 187212N^{-0.4707}
\end{aligned}
\tag{4.3}
$$

Rewriting these equations in terms of applied load.

$$
\begin{aligned}
&\text{SM9.5E Laboratory Sample} \\
&N = 5.85\times10^{20}\times S^{-4.30} \\
&\text{SM9.5A Laboratory Sample} \\
&N = 7.05\times10^{9}\times S^{-1.16} \\
&\text{SM9.5E Core Sample} \\
&N = 4.81\times10^{17}\times S^{-3.68} \\
&\text{SM9.5A Core Sample} \\
&N = 1.59\times10^{11}\times S^{-2.12}
\end{aligned}
\tag{4.4}
$$

Therefore, a shift factor to account for the difference in compaction methods in the field and in the lab may be found as follows:

$$
SHF_{\text{material difference}} = N_{field}^{SM9.5E} / N_{lab}^{SM9.5E} \tag{4.5}
$$

$$= 0.000822\ S^{0.62} \qquad \text{for SM9.5E}$$

$$= 0.000225\ S^{0.96} \qquad \text{for SM9.5A}$$

This shows that the shift factor to account for material difference is a function of the applied stress. The HMA material was found earlier, from resilient modulus tests, to be stress dependent and accordingly, it follows that the shift factor to account for the difference in material is also stress dependent.

CHAPTER 5: Conclusions, Findings and Recommendations

Construction of the first 1.9 km of the Virginia Smart Road began in March 1999. Sensors were installed as the pavement was built. The pavement sections were divided into 12 different designs, and each layer was instrumented with load and environmental sensors.

The work in this research has been focused on developing better understanding of the pavement behavior and the assessment of the fatigue performance of two SuperPave^{TM} mixes. Part of the continuously collected data was analyzed and the measured response was explained. Finally, laboratory testing was performed to evaluate pavement performance and the associated assumptions.

5.1 Findings

The following were found during this study:

1. From the strain data collected in three directions at the bottom of the wearing surface, there is evidence that the principal strain direction changes as the vehicle passes over the pavement.
2. Strain data collected during pavement construction indicate that as the HMA is compacted using roller compactors, it gains strength faster in the longitudinal direction than in the transverse direction. Accordingly, the assumption that the pavement is a cross-isotropic material is questionable.
3. While laboratory resilient modulus testing does not support the above assumption, the number of cycles to failure clearly indicates the difference in strength between the two directions.
4. Although the indirect tensile fatigue test (ITFT) is highly repeatable, simple and relatively quick, it cannot be used to induce damage in HMA similar to that found in the field.
5. There is no significant difference in the recoverable elastic deformation recorded during the ITFT test between SM9.5A and SM9.5E. This indicates that the elastic

behavior of the mixtures is not affected by the addition of the polymer-modified binders or the test is not sensitive enough to detect the effect of polymer.

6. The addition of polymer increases the laboratory fatigue life of asphalt mixtures.
7. Visual assessment of the samples after test completion for both ITFT and third-point bending test (TPBT) show that the cracks attempt to follow the shortest route, around the interface between the coarse aggregate and the binder.
8. Sensor calibration is essential to pavement instrumentation projects. However, simulating field conditions is difficult if not impossible, and field calibration is sometimes needed. A method for calibrating pressure cells in the field is developed and used for the pressure cells at the Virginia Smart Road.
9. For the pavement designs used at the Virginia Smart Road, the response at the bottom of the wearing surface is a function of a combination of bending and shearing forces that are imposed on the pavement by moving truck load.

5.2 Conclusions

The following conclusions may be drawn from this study:

1. Fatigue equations were developed using both the ITFT and TPBT for field cores and laboratory compacted specimens. The specimen preparation effects were accounted for in the material difference shift factor. Based on the resilient modulus and fatigue testing performed, it can be concluded that the resilient modulus cannot be used to model fatigue damage in hot-mix asphalt (HMA). This is due to the fact that laboratory damage similar to the damage occurring in the field cannot be induced using the resilient modulus testing
2. Pavement instrumentation was successfully used to develop a methodology to evaluate the difference between field and laboratory environments. Data collected at the Virginia Smart Road were used to calculate shift factors to relate laboratory to field performance.

5.3 Recommendations

The following recommendations are made for future research:

1. The effect of binder type on the measured beam fatigue stiffness throughout the test is significant. Further research in the modeling of the stiffness reduction is needed. In addition, the correlation between binder stiffness and mix stiffness is needed.
2. Further research is needed to evaluate the principal strain direction in HMA pavements. To facilitate this research, instrumentation is needed to measure three in-plane strains (H-type strain gauges) and one out of plane strain (LVDT).
3. Aggregate orientation in HMA need to be quantitatively determined, possibly using image analysis on field cores. Vertical and horizontal sections within the same core may provide useful information on the compaction induced aggregate orientation. This may also be compared with vertical and horizontal sections made in laboratory prepared samples, to evaluate the validity of the SuperPave™ Gyratory compactor.
4. Research is needed to quantify the three shift factors for different types of HMA used at the Virginia Smart Road namely: SM9.5D, SM12.5D, and SMA12.5. Furthermore, conducting the tests at different temperatures and studying the effects of the different mixture components on the developed shift factors may yield very useful information for HMA design.

References

Aglan, H., Othman, A., Figueroa, L., and Rollings, R. (1993) "Effect of Styrene-Butadiene-Styrene Block Copolymer on Fatigue Crack Propagation Behavior of Asphalt Concrete Mixtures," Transportation Research Record, No. 1417, Transportation Research Board, Washington, DC, pp. 178-186.

Ali, H. A., and Tayabji, S. D. (1998) "Evaluation of Mechanistic-Empirical Performance Prediction Models for Flexible Pavements," Transportation Research Record, No. 1629, Transportation Research Record, Washington, DC, pp. 169-180.

Al-Qadi, I. L., Brandon, T. L., Smith, T., and Lacina, B. A. (1996) "How Do Geosynthetics Improve Pavement's Performance," Proceedings of Material Engineering Conference 804, ASCE, New York, NY, pp. 606-616.

Al-Qadi, I. L., Brandon, T. L., Valentine, R. J., and Smith, T. E. (1994) "Laboratory Evaluation of Geosynthetic Reinforced Pavement Sections," Transportation Research Record, No. 1439, Transportation Research Board, Washington DC, pp. 25-31.

Al-Qadi, I. L. and Bhutta, S. A. (1999) "In Situ Measurements of Secondary Road Flexible Pavement Response to Vehicular Loading," Transportation Research Record No. 1652, Transportation Research Board, Washington, DC, pp. 206-216.

Al-Suhaibani, A. R., Al-Mudaiheem, J., and Al-Fozan, F. (1992) "Effect of Filler Type and Content on Properties of Asphalt Concrete Mixes, ASTM STP 1147," American Society for Testing and Materials, Philadelphia, PA.

Ameri-gaznon, M., and Little, D. N. (1990) “Octahedral Shear Stress Analysis of an ACP Overlay on a Rigid Base,” Journal of the Association of Asphalt Paving Technologists, Vol. 59, pp. 443-480.

Asphalt Institute (1988) “Research and Development of the Asphalt Institute Thickness Design Manual (MS-1),” 9th ed., Research Report 82-2, Asphalt Institute, Lexington, KY.

Austin, D. N. and Coleman, D. M. (1993) "A Field Evaluation of Geosynthetic-Reinforced Haul Roads over Soft Foundation Soils," Proceedings of Geosynthetic Conference, Vancouver, BC, Canada, pp. 65-80.

Bahia, H., Timothy, F., Pehr, P., and Jeffrey, R. (1998) “Optimization of Constructibility and Resistance to Traffic: A New Design Approach for HMA Using the Superpave Compactor,” Journal of the Association of Asphalt Paving Technologists, Vol. 67, pp.189-232.

Baker, H. B., Buth, M. R., and Van Deusen, D. A., (1994) “Minnesota Road Research Project: Load Response Instrumentation Installation and Testing Procedures,” Final Report, 1992-94, Report No. MN/PR-94/01, Minnesota Dept. of Transportation, Maplewood.

Bayomy, F., Nassar, W. and Al-Kandari, F. (1995) “Development of Mechanistic Based Overlay Design Systems for Idaho,” Final Report, Volumes I and II, Research Project No. 95-60-121, National Center of Advanced Transportation Technology, University of Idaho, ID.

Beer, M., Johnson, G., Van Deusen, D. (1997) "Performance of MnRoad Load Response and Environmental Instrumentation," Transportation Research Board, Preprint in 76th Annual Meeting, January 12-16, Washington, DC.

Bonnaure, F., Gravois, A., and Udron, J. (1980) "A New Method for Predicting the Fatigue Life of Bituminous Mixes," Journal of the Association of Asphalt Paving Technologists, Vol. 49, pp. 499-529.

Brandon, T. L., Al-Qadi, I. L., Lacina, B. A., and Bhutta, S. A. (1996) "Construction and Instrumentation of Geosynthetically Stabilized Secondary Road Test Sections," Transportation Research Record, No. 1534, Transportation Research Board, Washington, DC, pp 50-57.

Brennan, M. J., Meade, J., Hynes, M., Murphy, D. J., and Lycett, C. (1996) "A Pilot Study of the Performance of Porous Asphalt in Static Creep and Repeated Loading," Eurasphalt & Eurobitume Congress, Strasbourg, France.

Brown, E. R., and Cross, S. A. (1989) "A Study of In-Place Rutting of Asphalt Pavements," Journal of the Association of Asphalt Paving Technologists, Vol. 59, pp. 1-39.

Brunton, J. M. (1989) "Development in the Analytical Design of Asphalt Pavements Using Computers," Ph.D. Thesis, Department of Civil Engineering, University of Nottingham, Nottingham, UK.

Burmister, D. M. (1958) "Evaluation of Pavement Systems of the WASHO Road Test by Layered Systems Method," Highway Research Board, Bulletin 177, pp. 26-54.

Busch, C., and Ullidtz, P. (1978) " Laboratory Testing of a Full Scale Pavement," Report No.19, The Institute of Roads, Transport and Town Planning, The Technical University of Denmark, Lyngby.

Busching, H. W., Goetz W. H., and Harr, M. E. (1967) "Stress-Deformation Behavior of Anisotopic Bituminous Mixtures," Journal of the Association of Asphalt Paving Technologists, Vol. 36, pp. 632-672.

Buttlar, W. G., and Roque, R. (1994) "Development and Evaluation of the Strategic Highway Research Program Measurement and Analysis System for Indirect Tensile Testing at Low Temperature," Transportation Research Record, No. 1454, Transportation Research Board, Washington, DC, pp. 163-171.

Button, J. W., Little, D., Jagadam, N., V., and Pendleton, O. J. (1994) "Correlation of Selected Laboratory Compaction Methods with Field Compaction," Transportation Research Record, No. 1454, Transportation Research Board, Washington, DC, pp. 193-201.

Case, S. W and Reifsnider, K. L. (1998) "MRLife 11: A Strength and Life Prediction Code for Laminated Composite Materials," Materials Response Group, Virginia Polytechnic Institute and State University, Blacksburg, VA.

Cavliere, M. G., Via, M. D., and Diani, E. (1996) "Dynamic Mechanical Characterization of Binder and Asphalt," Eurasphalt & Eurobitume Congress, Strasbourg, France.

Chang, K. G. and Meegoda, J. (1997) "Micromechanical Simulation of Hot Mix Asphalt," Journal of Engineering Mechanics, American Society of Civil Engineers, pp. 495-503.

Chatti, K., Mahoney, J. P., Monismith, C. L., and Tom, M. (1995) "Field Response and Dynamic Modeling of an Asphalt Concrete Pavement Section Under Moving Heavy Trucks," Road Transportation Technology-4, University of Michigan Transportation Research Institute, Ann Arbor, MI.

Chatti, K., Yun, K. K., Kim, H. B., and Utamsingh, R. (1995) "PACCAR Full-Scale Pavement Tests," University of California Berkeley, and the California Department of Transportation, Berkeley, CA.

Christensen, D. W., and Anderson, D. A., (1992) "Interpretation of Dynamic Mechanical Test Data for Paving Grade Asphalt Cements," Journal of the Association of Asphalt Paving Technologists, Vol. 61, pp. 67-116.

Collop, A. C. and Cebon, D. (1996) "Stiffness Reduction of Flexible Pavement Due to Cumulative Fatigue Damage," Journal of Transportation Engineering, Vol. 122 (2), pp. 131-139.

Consuegra, A., Little, D. N., Quintus, H. V., and Burati, J. (1989) "Comparative Evaluation of Laboratory Compaction Devices Based on Their Ability to Produce Mixtures with Engineering Properties Similar to Those Produced in the Field," Transportation Research Record No. 1228, National Research Council, Washington, DC, pp. 80-87.

Dai, S. and Van Deusen, D. (1998) "Field Study of In-situ Subgrade Soil Response under Flexible Pavements," Transportation Research Record, No. 1639, Transportation Research Board, Washington, DC, pp. 23-35.

Des Croix, P., and Di Benedetto, H. (1996) "Binder-Mix Rheology: Limits of Linear Domain, Non-linear Behavior," Eurasphalt & Eurobitume Congress, Strasbourg, France.

Djakfar, L., and Roberts, F. (2000) "Performance Prediction of Louisiana ALF Test Sections," Prepared for Presentation and Publication in the 79th Annual Meeting of The Transportation Research Board, Washington, DC.

Dongre, R., and Anderson, D. A. (1996) "Determination of Uniaxial Stress-Strain Curves Using Shear Complex Modulus Obtained from Dynamic Shear Rheometer," Eurasphalt & Eurobitume Congress, Strasbourg, France.

Douglas, A., and Tons, E. (1961) " Strength Analysis of Bituminous Mastic Concrete," Journal of the Association of Asphalt Paving Technologists, Vol. 30, pp. 238-269.

Eduardo, K., and Manuel, R. J. (1981) "Stiffness Matrices for Layered Soils," Bulletin of The Seismological Society of America, Vol. 71, No. 6, pp. 1743-1761.

Ekse, M., and LaCross, L. M. (1957) "Model Analysis of Flexible Pavement and Subgrade Stresses," Journal of the Association of Asphalt Paving Technologists, Vol. 26, pp. 312-320.

Epps, J. and Monismith, C. L. (1970) ”Influence of Mixture Variables on the Direct Tensile Properties of Asphalt Concrete,” Journal of the Association of Asphalt Paving Technologists, Vol. 39, pp. 207-241.

Epps, J. and Monismith, C. L. (1998) ” Symposium: Westrack Performance Interim Findings,” Journal of the Association of Asphalt Paving Technologists, Vol. 68, pp. 738-782.

Finn, F., Sarsf, C. L., Kulharni, R., Nair, K., Smith, W., and Abdullah, A. (1987) “Development of Pavement Structural Subsystems,” National Cooperative Highway Research Program (NCHRP) No. 291, National Research Council, Washington DC.

Ford, M. C., (1988) “Pavement Densification Related to Asphalt Mix Characteristics,” Transportation Research Record, No. 958, Transportation Research Board, Washington, DC, pp. 9-15.

Francken, L., and Vanelstraete, A. (1996) “Complex Moduli of Bituminous Binders and Mixes,” Eurasphalt & Eurobitume Congress, Strasbourg, France.

Fredlund, D. G., Gan, J. K., Guan, Y., and Richardson, N., (1995) “Suction Measurements on a Saskatchewan Soil Using a Direct-Measurement, High Range Suction Sensor,” Transportation Research Board 1596, pp. 84-92.

Fuchs, H. O., and Stephens, R., I. (1980) Metal Fatigue in Engineering, John Wiley.

Geller, M. (1984) "Compaction Equipment for Asphalt Mixes. Placement and Compaction of Asphalt Mixtures, ASTM STP 829," American Society for Testing and Materials, Philadelphia.

Ghuzlan, K., and Carpenter, S. H. (2000) "An Energy-Derived/Damage-Based Failure Criteria for Fatigue Testing," Transportation Research Record, No. 1723, Transportation Research Board, Washington, DC, pp. 141-149.

Gunaratne, M, and Sanders, O. (1996) "Response of a Layered Elastic Medium to a Moving Strip Load," International Journal for Numerical and Analytical Methods in Geomechanics, Vol 20, pp. 191-208.

Haddad, Y. M. (1995) Viscoelasticity of Engineering Materials. Chapman and Hall, New York, NY.

Harvey, J., and Monismith, C. L. (1993) "Effects of Laboratory Asphalt Concrete Specimen Preparation Variables on Fatigue and Permanent Deformation Test Results Using Strategic Highway Research Program A-003A Proposed Testing Equipment," Transportation Research Record 1417, Transportation Research Board, National Research Council, Washington, D C.

Harvey, J., Lee, T., Sousa, J., Pak, J., and Monismith, C. L. (1993) "Evaluation of Fatigue and Permanent Deformation Properties of Several Asphalt-Aggregate Field Mixes Using Strategic Highway Research Program A-003A Equipment," Transportation Research Record, No. 1454, Transportation Research Board, Washington, DC, pp. 123-133.

Herve, D. B., Ali, A. S., and Pierre, C. (1996) "The Fatigue of the Bituminous Mixes: a Pertinent Approach of its Measurement and of its Characterization," Eurasphalt & Eurobitume Congress, Strasbourg, France.

Heukelom, W. (1966) " Observations on the Rheology and Fracture of Bitumens and Asphalt Mixes," Journal of the Association of Asphalt Paving Technologists, Vol. 35, pp. 358-399.

Hicks, R. G., and Finn, F. N. (1970) "Analysis of Results from the Dynamic Measurements Program on the San Diego Test Road," Journal of the Association of Asphalt Paving Technologists, Vol. 39, pp. 153-185.

Hines, M. L., La roche, D., and Chaverot, P. (1998) "Symposium: Evaluation of Fatigue Behavior of Hot Mix Asphalt with the LCPC Nantes Test Track and SHRP Testing Tools," Journal of the Association of Asphalt Paving Technologists, Vol. 68, pp. 717-737.

Hopman, P. C. (1996) "A Visco-Elastic Analysis of Asphalt Pavements Using VEROAD," Eurasphalt & Eurobitume Congress, Strasbourg, France.

Huang, E. Y., and Grisham, D. A. (1967) "Effect of Geometric Characteristics of Aggregates on the Fatigue Response of Bituminous Mixtures," American Society of Testing Standards, Special Technical Publication, STP 508: Fatigue of Compacted Bituminous Aggregate Mixtures, ASTM, Philadelphia, pp. 141-160.

Huang, H., and White, T. D. (1998) "Modeling and Analysis of Accelerated Pavement Tests," Presented at the 77th Annual Meeting, Transportation Research Board, Washington, DC.

Huang, Y. H. (1993) Pavement Analysis and Design. Prentice Hall, Englewood Cliffs, New Jersey, NJ.

Huber, G. A., and Heiman, G. H. (1987) "Effects of Asphalt Concrete Parameter on Rutting Performance: A Field Investigation," Journal of the Association of Asphalt Paving Technologists, Vol. 56.

Huhtala, M., Alkio, R., Pihljamaki, J., Pienmaki, M., and Halonan, P. (1990) "Behavior of Bituminous Materials Under Moving Wheel Loads," Journal of the Association of Asphalt Paving Technologists, Vol. 59, pp. 422-442.

Huhtala, M., and Pihlajamaki, J. (1991) "Strain Response and Stress Measurements in Pavements," Proceedings of the Conference on Road and Airport Pavement Response Monitoring Systems, West Lebanon, New Hampshire.

Huhtala, M., Pihlajamaki, J. and Pienimaki, M. (1989) "Effects of Tires and Tire Pressures on Road Pavements," Transportation Research Record, No. 1227, Transportation Research Board, Washington DC, pp. 107-114.

Jackson, N. M., and Vinson, T. S. (1995) "Analysis of Thermal Fatigue Distress of Asphalt Concrete Pavements," Transportation Research Record, No. 1545, Transportation Research Board, Washington DC, pp. 43-49.

Jackson, T. J. (1990) "Laboratory Evaluation of a Field-Portable Dielectric/Soil-Moisture Probe." IEEE Transactions on Geoscience and Remote Sensing, Vol. 28, No. 2, pp.241-245.

Jacobs, M. J., Hopman, P. C., and Molenaar, A. A. (1996) "The Crack Growth Mechanism in Asphalt Mixes," Eurasphalt & Eurobitume Congress, Strasbourg, France.

Janoo, V. C., and Eaton, R. A., "Road and Airport Pavement Response Monitoring Systems," American Society of Civil Engineers, Proceedings of the Conference Sponsored by the US Army Regions Research & Engineering Laboratory, Federal Aviation Administration, pp. 244-260.

Jeng, Y., and Perng, J. (1991) "Analysis of Crack Propagation in Asphalt Concrete Using a Cohesive Crack Model," Presented at 70th Annual Transportation Research Board Meeting, Washington, DC.

Jimenez, R. A. (1967) "Fatigue Testing of Asphaltic Concrete Slabs," American Society of Testing Standards, Special Technical Publication, STP 508: Fatigue of Compacted Bituminous Aggregate Mixtures, ASTM, Philadelphia, pp. 3-18.

Jimenez, R. A. (1967) "Aspects on the Bending Strength of Asphaltic Concrete," Journal of the Association of Asphalt Paving Technologists, Vol. 36, pp. 703-730.

Jones, S. D., Mahboub, K. C., Anderson, R. M., and Bahia, H. (1998) "Applicability of SuperPave to Modified Asphalts – A Mixture Study," Transportation Research Record, No. 1620, Transportation Research Board, Washington DC, pp. 42-50.

Judycki, J. (1996) "Non-Linear Effects in Rheological Properties of Asphalt Concrete," Eurasphalt & Eurobitume Congress, Strasbourg, France.

Kallas, B. F. (1970) "Dynamic Modulus of AC in Tension and Tension-Compression," Journal of the Association of Asphalt Paving Technologists, Vol. 39, pp. 1-23.

Kallas, B. F., and Puzinauskas, V. P. (1967) "Flexure Fatigue Tests on Asphalt Paving Mixtures," American Society of Testing Standards, Special Technical Publication, STP 508: Fatigue of Compacted Bituminous Aggregate Mixtures, ASTM, Philadelphia, pp. 47-65.

Kandhal, P. S., Foo, K. Y., and D'Angelo, J. A. (1996) "Field Management of Hot Mix Asphalt Volumetric Properties," ASTM STP 1299, American Society for Testing and Materials, Philadelphia.

Kennedy, J. C., and Everhart, R. D. (1998) "Modeling Pavement Response to Vehicular Traffic on the Ohio Test Road," Transportation Research Record, No. 1629, Transportation Research Board, Washington DC, pp. 24-31.

Khanal, P. P., and Mamlouk, M. (1995) "Tensile Versus Compressive Moduli of Asphalt Concrete," Transportation Research Record, No. 1482, Transportation Research Board, Washington, pp. 22-28.

Kim, Y. R., Lee, H. J., and Little, D. N. (1998) "Fatigue Characterization of Asphalt Concrete Using Viscoelasticity and Continuum Damage Theory," Journal of the Association of Asphalt Paving Technologists, Vol. 67, pp. 520-569.

Klemunes, Jr., J. A. (1995) "Determining Soil Volumetric Moisture Content Using Time Domain Reflectometry." Master of Science Thesis, University of Maryland at College Park.

Knight, J. H., White, I., and Zegelin, S.J. (1994) "Sampling Volume of TDR Probes Used for Water Content Monitoring," Symposium and Workshop on: Time Domain Reflectometry in Environmental, Infrastructure and Mining Applications, United States Department of Interior Bureau of Mines at Northwestern, SP-19-94, pp. 93-97.

Kong, K. W., Theyse, H. L., Verhaeghe, B. M. J. A., and Knottenbelt, E. C., (1997) "Stiffness and Fatigue Characteristics of Asphalt Wearing Courses Used In South Africa," 8th International Conference Asphalt Pavements, Vol. II, Washington, WA, pp. 951-968.

Krarup, J. (1991) "Instrumentation for a Full-Scale Pavement Test in the Danish Road Testing Machine," Proceedings of the Conference on Road and Airport Pavement Response Monitoring Systems, West Lebanon, New Hampshire.

La Roche, C., and Riviere, N. (1997) "Fatigue Behavior of Asphalt Mixes: Influence of Laboratory Test Procedures on Fatigue Performance," 8th International Conference on Asphalt Pavements, Vol. II, Washington, WA, pp. 899-917.

La Roche, C., Odeon, H., Simoncelli, J., and Spernol, A., (1994) "Study of Fatigue In Asphalt Pavements Using the LCPC's Test Track in Nantes-France," Prepared for Presentation at the 73rd Annual Meeting, Transportation Research Board, Washington, DC.

Li, G., Metcalf, J. B., and Pang, S. (1999) "Elastic Modulus Prediction of Asphalt Concrete," Journal of Materials in Civil Engineering, American Society of Civil Engineers, pp. 236-241.

Little, D. N., Button, J. W. et al. (1989) “Investigation of Asphalt Additives.” Report FHWA-R-D87/001. FHWA, U.S. Department of Transportation.

MacDonald, R. and Zhang, W. (1997) “Construction, Instrumentation and Load Testing of the Danish Road Testing Machine for the International Pavement Subgrade Performance Study,” Transportation Research Record, No. 1596, Transportation Research Board, Washington, DC, pp. 7-14.

Majidzadeh, K., and Schweyer, H. E. (1967) “Viscoelastic Response of Asphalt in the Vicinity of the Glass Transition Point,” Journal of the Association of Asphalt Paving Technologists, Vol. 36, pp. 80-105.

Majidzadeh, K., Ilves, G. J., and May, R. W. (1986) “Overlay Design of Flexible Pavements: OAF Program,” Transportation Research Record, No. 930, Transportation Researh Board, Washington, DC, pp. 18-25.

Majidzadeh, K., Kauffmann, E. M., and Saraf, C. L. (1967) “Analysis of Fatigue of Paving Mixtures from the Fracture Mechanics View-Point,” American Society of Testing Standards, Special Technical Publication, STP 508: Fatigue of Compacted Bituminous Aggregate Mixtures, ASTM, Philadelphia, pp. 67-84.

Majidzadeh, K., Ramsamooj, D. V., and Fletcher, T. A. (1969) ”Analysis of Fatigue of Sand-Asphalt Mixture,” Journal of the Association of Asphalt Paving Technologists, Vol. 38, pp. 495-518.

Mamlouk, S. M., Zaniewski, J. P., and Houston, S. L. (1991) “Overlay Design Method for Flexible Pavements in Arizona,” Transportation Research Record, No. 1286, Transportation Research Board, Washington DC, pp.112-122.

Masad, E., Muhunthan, B., ShaShidahar, N., and Harman, T. (1998) “Quantifying Laboratory Compaction Effects on the Internal Structure of Asphalt Concrete,” In Transportation Research Record (CD-ROM), Transportation Research Board, National Research Council, Washington, DC.

McCullough, B. F., Van Til, C. J., and Hicks, R. G. (1972), “Evaluation of AASHO Interim Guides for Design of Pavement Structures," NCHRP Report 128.

Mcleod, N. W. (1954) ”An Ultimate Strength Approach to Flexible Pavement Design,” Journal of the Association of Asphalt Paving Technologists, Vol. 23, pp. 119-236.

McRae, J. B., and Sellers, J. B. (1982) Vibrating Wire Piezometer Manual, Geokon Inc., Lebanon, NH.

Metcalf, J. B. (1998) “Accelerated Pavement Testing, a Brief Review Dirwected Towards Asphalt Interests,” Journal of the Association of Asphalt Paving Technologists, Vol. 67, pp. 553-572.

Metcalf, L. (1996) “Application of Full-Scale Accelerated Pavement Testing,” NCHRP Synthesis 235, Transportation Research Board, National Research Council, Washington, DC.

Metcalf, L., Romanschi J. B., and Rasoulian S. A. (1999) “Development of The Louisiana ALF Program, the First Experiment,” Transportation Research Record, No. 1655, Transportation Research Board, Washington DC, pp. 219-226.

Michele, A., Roberto, B., and Maurizio, D. (1996) “Experimental Investigation of the Behavior of Asphalt for Loading Three Orthogonal Directions,” Eurasphalt & Eurobitume Congress, Strasbourg, France.

Miner, M. A. (1945) “Cumulative Damage In Fatigue,” Journal of Applied Mechanics, Transactions of the American Society of Mechanical Eningeers, Vol. 66, pp. A150-A164.

Minnesota Road Research Project. (1994) "Load Response Instrumentation Installation and Testing Procedures," Final Report.

Moavenzadeh, F. (1967) “Asphalt Fracture,” Journal of the Association of Asphalt Paving Technologists, Vol. 36, pp. 51-79.

Moavenzadeh, F., and Carnaghi, W. A. (1966) “Viscoelastic Response of Sand-Asphalt Beams on Elastic Foundations Under Repeated Loading,” Journal of the Association of Asphalt Paving Technologists, Vol. 35, pp. 514-528.

Monismith, C. L. (1958) ”Flexibility Characteristics of Asphalt Paving Mixtures,” Journal of the Association of Asphalt Paving Technologists, Vol. 27, pp. 74-106.

Monismith, C. L., and Epps, J. A. (1966) “Asphalt Mixture Behavior in Repeated Flexure,” Institute of Transportation and Traffic Engineering, University of California, Berkeley.

Monismith, C. L., Secor, K. E., and Blackmer, E. W. (1961) "Asphalt Mixture Behavior in Repeated Flexure," Journal of the Association of Asphalt Paving Technologists, Vol. 30, pp. 188-222.

Monismith, C. L., Alexander, R. L., and Secor, K. E. (1966) "Rheologic Behavior of Asphalt Concrete," Journal of the Association of Asphalt Paving Technologists, Vol. 35, pp. 400-450.

Oda, M. (1972a) "Initial Fabric and Their Relations to Mechanical Properties of Granular Material," Soils and Foundations, Vol. 12, No. 1, pp. 17-36.

Oda, M. (1972b) "The Mechanism of Fabric Changes During Compressional Deformation of Sand," Soils and Foundations, Vol. 12, No. 2, pp. 1-8.

Oda, M. (1977) Co-Ordination Number and Its Relation to Shear Strength of Granular Material. Soils and Foundations, Vol. 17, No. 2, pp. 29-42.

Odeon, H., and Caroff, G. (1997) "Asphalt Mix Fatigue Behavior: Experimental Structures and Modeling," 8th International Conference on Asphalt Pavements, Seattle Washington, Vol. II, pp. 881-897.

Othman, A., Figueroa, L., and Aglan, H. (1995) "Fatigue Behavior of Styrene-Butadiene-Styrene Asphaltic Mixtures Exposed to Low-Temperature Cyclic Aging," Transportation Research Record, No. 1492, Transportation Research Board, Washington DC, pp. 129-134.

Parker, F., and Brown, E. R. (1992) "Effects of Aggregate Properties on Flexible Pavement Rutting in Alabama," Effects of Aggregate and Mineral Fillers on Asphalt Performance, ASTM STP 1147, American Society for Testing and Materials, Philadelphia.

Pell, P. S., and Cooper, K. E. (1975) "The Effect of Testing and Mix Variables on the Fatigue Performance of Bituminous Materials," Journal of the Association of Asphalt Paving Technologists, Vol. 44, pp. 1-37.

Pierce, L. M., and Mahoney, J. P. (1996) "An Examination of WSDOT Transfer Function for Mechanistic Empirical AC Overlay," Transportation Research Record, No. 1539, Transportation Research Board, Washington DC, pp. 25-32.

Poelorz, A., and Nadolski, W. (1989) "Longitudinal Waves In a Damped Layered System," Ingenieur-Archiv, Springer-Valag.

Prozzi, J., Harvey, J., Deaccon, J., Guada, I., and Hung, D. (1998) "Analysis of Observed and Predicted Performance for CAL/APT Flexible Pavement Structures," Prepared for Presentation at the 73rd Annual Meeting, Transportation Research Board, Washington, DC.

Raad, L., Saboundjian, S., and Corcoran, J. (1992) "Remaining Life Analysis: Comparison Between Dense-Graded Conventional Asphalt Concrete and Gap-Graded Asphalt-Rubber Hot Mix," Transportation Research Record, Vol. 1388, Transportation Research Board, Washington, DC, pp. 97-107.

Rada, G. R. (1994) "LTPP Seasonal Monitoring Program: Instrumentation Installation and Data Collection Guidelines," FHWA-LTPP Tech Rep., Beltsville, MD.

Rada, G. R., Elkins, G. E., Henerson, B., Van Sambeek, R. J., and Lopez, Jr., A. (1995) "LTPP Seasonal Monitoring Program: Instrumentation Installation and Data Collection Guidelines." Report No. FHWA-RD-94-110, Federal Highway Administration, Version 2.1.

Rada, G. R., Lopez, A., and Elkins, G. E., (1994) "Monitoring of Subsurface Moisture in Pavements Using Time-Domain Reflectometry," Symposium and Workshop on: Time Domain Reflectometry in Environmental, Infrastructure and Mining Applications, United States Department of Interior Bureau of Mines at Northwestern, SP-19-94, pp. 422-433.

Raithby, K. D., and Sterling, A. B. (1970) "The Effect of Rest Periods on the Fatigue Performance of a Hot Rolled Asphalt Under Reversed Axial Loading," Journal of the Association of Asphalt Paving Technologists, Vol. 39, pp. 134-152.

Rajapakse, R. K. N. D., and Senjuntichai, T. (1995) "Dynamic Response of a Multilayered Poroelastic Medium," Earthquake Engineering and Structural Dynamics, Vol. 24, pp. 703-722.

Read, J. M. (2000) "New Method for Measuring Crack Propagation in Asphalts," International Journal of Pavement Engineering, Vol. 1, Gordon and Breahc, Malaysia, pp. 15-34.

Read, J. M., and Brown, S. (1996) "Practical Evaluation of Fatigue Strength for Bituminous Paving Mixtures," Eurasphalt & Eurobitume Congress, Strasbourg, France.

Read, J. M., and Collop, A. (1997) "Practical Fatigue of Bituminous Paving Mixtures," Journal of the Association of Asphalt Paving Technologists, Vol. 66.

Reifsnider, K. L. (1993) "Use of Mechanistic Life Prediction Methods for the Design of Damage-Tolerant Composite Material Systems," American Society of Testing Standards, Special Technical Publication, STP 211: Advances in Fatigue Lifetime Predictive Techniques: Second Volume, ASTM, Philadelphia, PA, pp. 3-18.

Richards, I., Goodman, S., Pagani, J., Abd El Halim, A. O., and Haas, R. (1999) "Practical Realization of a New Concept for Asphalt Compaction," Paper Presented at the 1999 Annual Meeting of the Transportation Research Board, Washington, DC.

Roberts, F. L., Kandhal, P. S., Brown, E. R., Lee, D., and Kennedy, T. W. (1996) "Hot Mix Asphalt Materials, Mixture Design, and Construction," NAPA Education Foundation, Lanham, Maryland.

Roque, R., and Buttlar, W. (1992) "The Development of a Measurement and Analysis System to Accurately Determine Asphalt Concrete Properties Using the Indirect Tensile Mode," Journal of the Association of Asphalt Paving Technologists, Vol. 61, pp. 304-332.

Roque, R., and Ruth B. E. (1990) "Mechanisms and Modeling of Surface Cracking in Asphalt Pavements," Journal of the Association of Asphalt Paving Technologists, Vol. 59, pp. 396-421.

Rosen, S. L. (1993) Fundamental Principles of Polymeric Materials, Second Edition. Wiley Interscience, John Wiley & Sons, Canada.

Rowe, G. M. (1993) "Performance of Asphalt Mixtures in the Trapezoidal Fatigue Test," Journal of the Association of Asphalt Paving Technologists, Vol. 62, pp. 344-384.

Ruth, B. E., Bloy, L. A., and Avital, A. A. (1982) "Prediction of Pavement Cracking at Low Temperatures," Journal of the Association of Asphalt Paving Technologists, Vol. 52, pp. 53-103.

Safwat, S. (1996) "Fatigue and Stiffness Properties of Road-base Layer Using Indirect Tensile Test," Eurasphalt & Eurobitume Congress, Strasbourg, France.

Salam Y. M., and Monismith, C. L. (1972) "Fracture Characteristics of Asphalt Concrete," Journal of the Association of Asphalt Paving Technologists, Vol. 41, pp. 215-256.

Santucci, L. E., and Schmidt, R. J. (1969) "The Effect of Asphalt Properties on the Fatigue Resistance of Asphalt Paving Mixtures," Journal of the Association of Asphalt Paving Technologists, Vol. 38, pp. 39-64.

Sargand, S. and Hazen, G. A. (1996) "A Demonstration Project on Instrumentation of a Flexible Pavement," Final Report to Ohio Department of Transportation and the Federal Highway Administration, Report No. FHWA/OH-97/002.

Sargand, S. M., Green, R. and Khoury, I. (1997) "Instrumentation Ohio Test Pavement," Transportation Research Record, No. 1596, Transportation Research Board, Washington, DC, pp. 23-30.

Schutz, O. W. (1995) "Construction Procedures for Asphalt Concrete Pavements in Europe," Journal of the Association of Asphalt Paving Technologists, Vol. 64.

Sebaaly, P. E., and Mamlouk, M. (1987) "Prediction of Pavement Response to Actual Traffic Loading, Transportation Research Board.

Sebaaly P. E., and Tabatabaee, N. (1993) "Influence of Vehicle Speed on Dynamic Loads and Pavement Response," Transportation Research Record, No. 1410, Transportation Research Board, Washington, DC, pp. 107-114.

Sebaaly, P. E., Tabatabee, N., Kulakowski, B., and Scullion, T. (1991) "Instrumentation For Flexible Pavements – Field Performance of Selected Sensors," Report FHWA-RD-91-094, Federal Highway Administration, Washington, DC.

Sebaaly, P., Ridolfi, D., Gangavaram, R. S., and Epps, J. (1997) "Selecting Most Desirable Hot-Mix-Asphalt Mixtures." In Transportation Research Record, No. 1590, Transportation Research Board, Washington, D C., pp. 99-107.

Secor, K. E., and Monismith, C. L. (1965) "The Viscoelastic Response of Asphalt Paving Slabs Under Creep Loading," Highway Research Record, No. 67, Highway Research Board, Washington DC, pp. 84-97.

Selig, E. T., Zhang, J., and Ebersohn, W. (1997) "Evaluation of Dynamic Earth Pressure Cells for Subgrade," Transportation Research Record, No. 1596, Transportation Research Board, pp. 1-6.

Senjuntichai, T., and Rajapakse, R. K. N. D. (1995) "Exact Stiffness Method for Quasi-Statics of a Multi-layered Poroelastic Medium," International Journal of Solid Structures, Vol. 32, No. 11, Great Britain, pp. 1535-1553.

Sherard, J. L. (1981) "Piezometers in Earth Dam Impervious Section," Symposium on Instrumentation Reliability and Long Term Performance Monitoring in Embankment Dams, American Society of Civil Engineers, New York.

Shields, H. D., Zeng,. M., and Kwok, R. (1998) "Nonlinear Viscoelastic Behavior of Asphalt Concrete in Stress Relaxation," Journal of the Association of Asphalt Paving Technologists, Vol. 67, pp. 358-400.

SHRP Asphalt Research Program (1994) Fatigue Response of Asphalt-Aggregate Mixes, SHRP-A-404 Report Strategic Highway Research Program, National Research Council, Washington, DC.

SHRP P-001B Technical Assistance Staff (1991) SHRP Layer Moduli Backcalculation Procedure, PCS/LAW Engineering Beltsville, Maryland, MA.

Siddarthan, R., Zafir, Z. and Norris, G. M. (1993) "Moving Load Response of Layered Soil. I: Formulation" Journal of Engineering Mechanics, American Society of Civil Engineers 119(10), pp. 2052-2071.

Siddharthan, R., Yao, J., and Sebaaly, P. E. (1998) "Pavement Strain from Moving Dynamic 3D Load Distribution," Journal of Transportation Engineering, American Society of Civil Engineers, pp. 557-566.

Siddharthan, R. V, and Sebaaly, P. E. "Investigation of Asphalt Concrete Layer Strains from Wide-Base Tires," Transportation Research Record, No. 1655, Journal of the Transportation Research Board, Washington, DC, pp. 168-174.

Simmons, J. W., and Seaman, L. (2000) "Finite Element Analysis of Fatigue Lifetime in Pavements," Presented at the 79th Annual Meeting, Transportation Research Board, Washington, DC.

Tayebali, A., Deacon, A., John, A. J., Coplantz, S., Harvey, J. T., and Monismith, C. L. (1994) "Mix and Mode-of-Loading Effects on Fatigue Response of Asphalt-Aggregate Mixes." Journal of the Association of Asphalt Paving Technologists, Vol. 63, pp. 118-151.

Tayebali, A. A., Deacon, J. A., and Monismith, C. L. (1995) "Development and Evaluation of Dynamic Flexural Beam Fatigue Test System," Transportation Research Record, No.1545, Transportation Research Board, Washington, DC, pp. 89-97.

Tayebali, A. A., Goddrich, J. L., Sousa, J. B., and Monismith, C. L. (1991) "Relationship Between Modified Asphalt Binders Rheology and Binder-Aggregate Mixture Permanent Deformation Response," Journal of the Association of Asphalt Paving Technologists, Vol. 60, pp. 121-159.

Tayebali, A. A., Rowe, G. M., and Sousa, J. B. (1992) "Fatigue Response of Asphalt Aggregate Mixtures," Journal of the Association of Asphalt Paving Technologists, Vol. 61, pp. 333-360.

Terrel, R. L. (1967) "Fatigue Behavior: Field Observations and Analytical Predictions," American Society of Testing Standards, Special Technical Publication,

STP 508: Fatigue of Compacted Bituminous Aggregate Mixtures, ASTM, Philadelphia, pp. 117-144.

Terrel, R. L. (1971) Fatigue Behavior: Field Observations and Analytical Predictions. ASTM STP 508: Fatigue of Compacted Bituminous Aggregate Mixtures, American Society for Testing and Materials, Atlantic City, N. J.

Terrel, R. L., and Krukar, M. (1970) ”Evaluation of Test Tracking Pavements,” Journal of the Association of Asphalt Paving Technologists, Vol. 39, pp. 273-296.

Timoshenko, S. P. and Goodier, J. N. (1951) Theory of Elasticity, Third Edition, McGraw-Hill Book Company.

Topp, G. C. and J. L. Davis. (1985) "Measurement of Soil Water Content Using TDR: a Field Evaluation." Soil Science Society of America Journal, Vol. 49, pp. 19-24.

Topp, G. C., J. L. Davis, and Annan, A. P. (1980) “Electromagnetic Determination of Soil Water Content: Measurements in Coaxial Transmission Lines,” Water Resources Research, Vol. 16, No. 3, pp. 574-582.

Topp, G. C., Zegelin, S. J., and White, I. (1994) “Monitoring Soil Water Using TDR: An Overview of Progress,” Symposium and Workshop on Time Domain Reflectometry in Environmental, Infrastructure and Mining Applications, United States Department of Interior Bureau of Mines at Northwestern, SP-19-94, pp. 67-79.

Troy, C., and Sparrow, R. W. (1966) "Behavior of a Soil Mass Under Dynamic Loading," Journal of the Soil Mechanics and Foundation Division, Proceedings of the American Society of Civil Engineers.

Tseng, K. H., and Lytton, R. L. (1990) "Fatigue Damage Properties of Asphaltic Concrete Pavements," In Transportation Research Board, No. 1286, Transportation Research Record, Washington, DC, pp. 150-162.

Ullidtz, P. (1987) "Pavement Analysis," Elsevier, N.Y.

Ullidtz, P. (1993) "Mathematical Model of Pavement Performance Under Moving Wheel Load," Transportation Research Record, No. 1384, Transportation Research Board, Washington, DC, pp.94-99.

Ullidtz, P., and Busch, C. (1979) "Laboratory Testing of a Full-Scale Pavement: The Danish Road Testing Machine," Transportation Research Board, Transportation Research Record, Issue No. 715.

Uzan, J., Scullion, T., Michelek, C. H., Parades, M. and Lytton., R. L. (1988) "A microcomputer-based Procedure for Backcalculating Layer Moduli from FWD data," Research Report 1123-1. Texas Transportation Institute, Texas A&M University, College Staion.

Van Dijk, W. (1975) "Practical Fatigue Characterization of Bituminous Mixes," Journal of the Association of Asphalt Paving Technologists, Vol. 44, pp. 38-74.

Van Dijk, W., and W. Visser. (1977) "The Energy Approach to Fatigue for Pavement Design," Journal of the Association of Asphalt Paving Technologists, Vol. 46, pp. 1-40.

Van Niekerk, P. E., and Visser, A. T. (1993) "Vehicle Configuration Influences on Weight-In-Motion Response," Transportation Research Record, No. 1410, Transportation Research Board, Washington, DC, pp.100-106.

Vanelstraete, A., Francken, L., and Reyaert, R. (1996) "Influence of Binder Properties on the Performance of Asphalt Mixes," Eurasphalt & Eurobitume Congress, Strasbourg, France.

Vogelzang, C., H., and Bouman, S. R. (1991) "In-situ Stress and Strain Measurements in Dynamically Loaded Asphalt Pavement Structures," Proceedings of the Conference on Road and Airport Pavement Response Monitoring Systems, West Lebanon, New Hampshire.

Von Quintus, H. L., Rauhut, J. B., and Kennedy, T. W. (1982) "Comparisons of Asphalt Concrete Stiffness as Measured by Various Testing Techniques," Journal of the Association of Asphalt Paving Technologists, Vol. 51, pp. 35-52.

Wu, Z., Hossain, M., and Gisi, A. J. (2000) "Performance of SuperPave Mixtures Under Accelerated Load Testing," Transportation Research Record, No. 1716, Transportation Research Board, Washington, DC, pp. 126-134.

Zahavi, E. (1996) Fatigue Design: Life Expectancy of Machine Parts, CRC Press.

Zube, E. and Skog, J. (1969) “Final Report on the Zaca-Wigmore Asphalt Test Road,” Journal of the Association of Asphalt Paving Technologists, Vol.38.

Appendix A

Pressure Cell Calibration

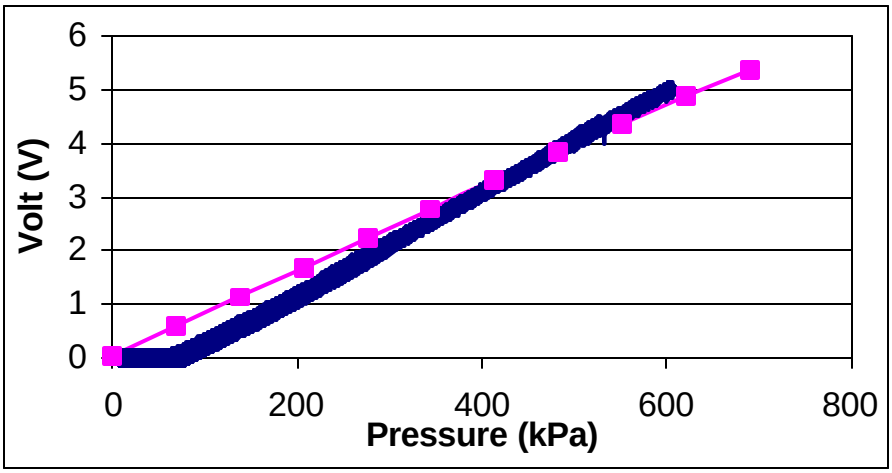

Figure 1 Calibration for Cell Labeled 1p1-3

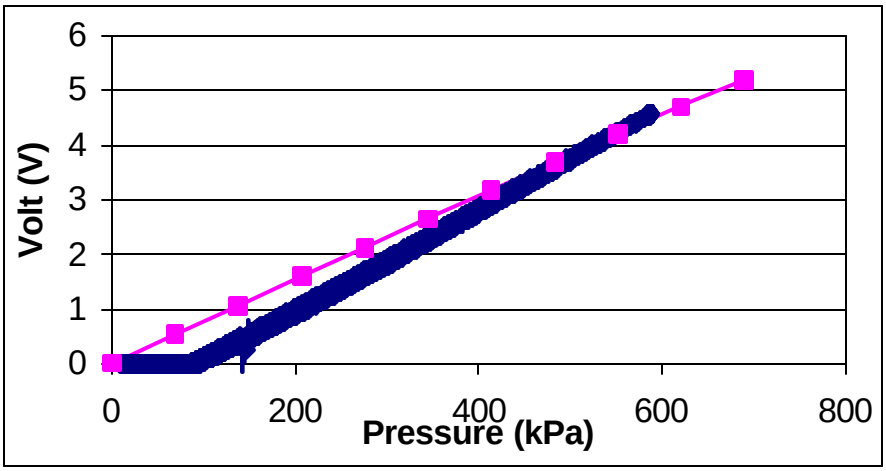

Figure Calibration for Cell Labeled 2 2p1-1

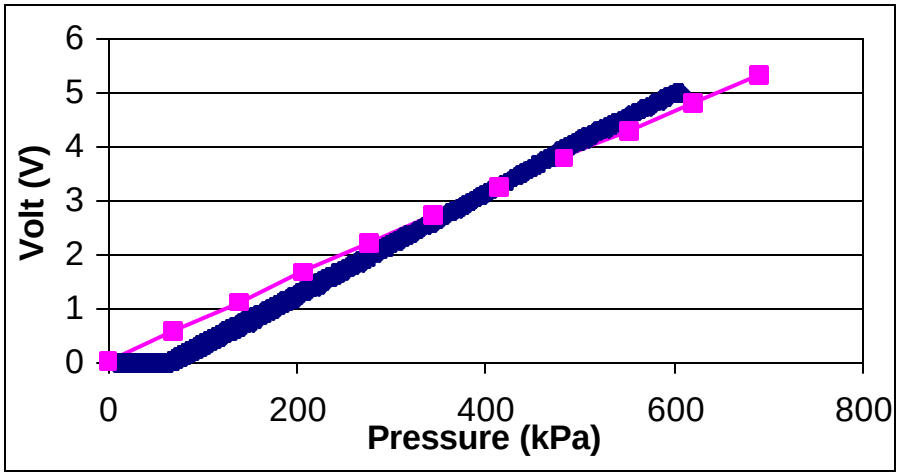

Figure 3 Calibration for Cell Labeled 3p1-2

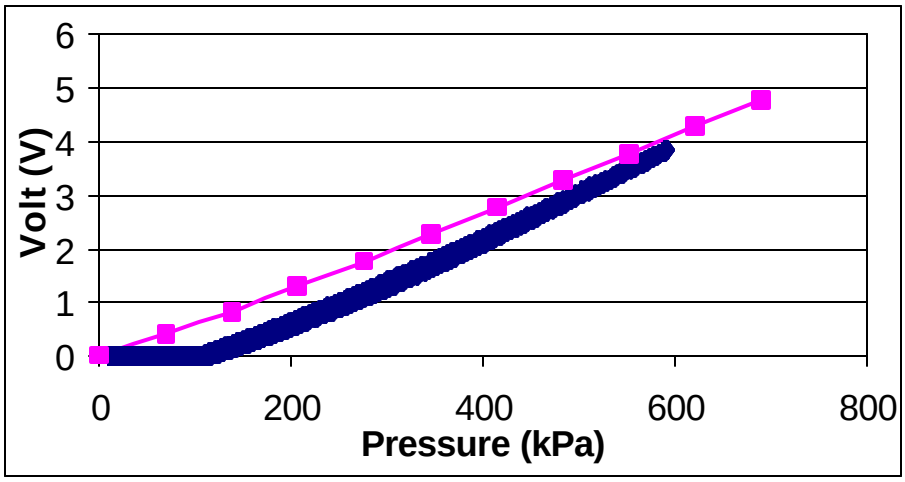

Figure 4 Calibration for Cell Labeled 8p2-1

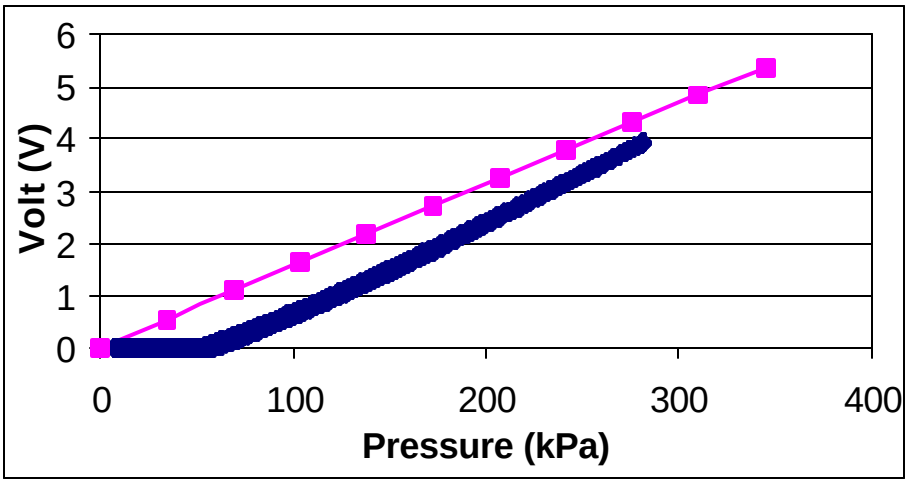

Figure 5 Calibration for Cell Labeled 10p6-2

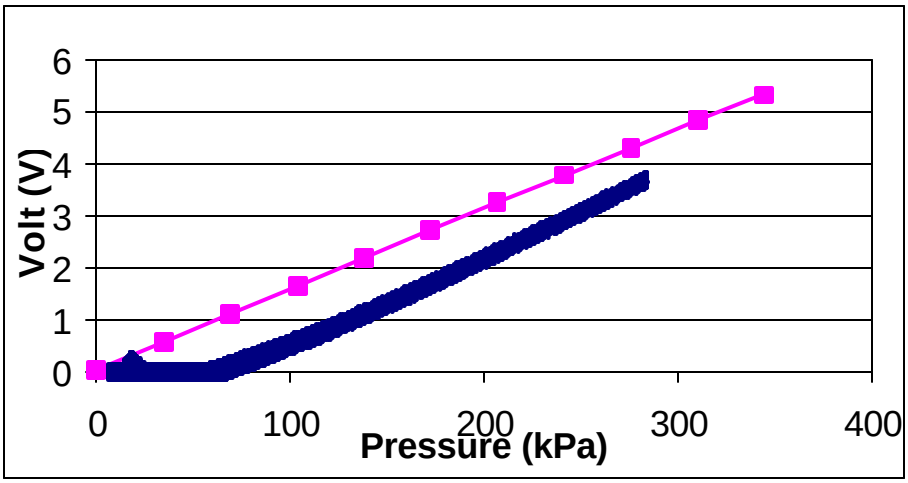

Figure 6 Calibration for Cell Labeled 10p6-3

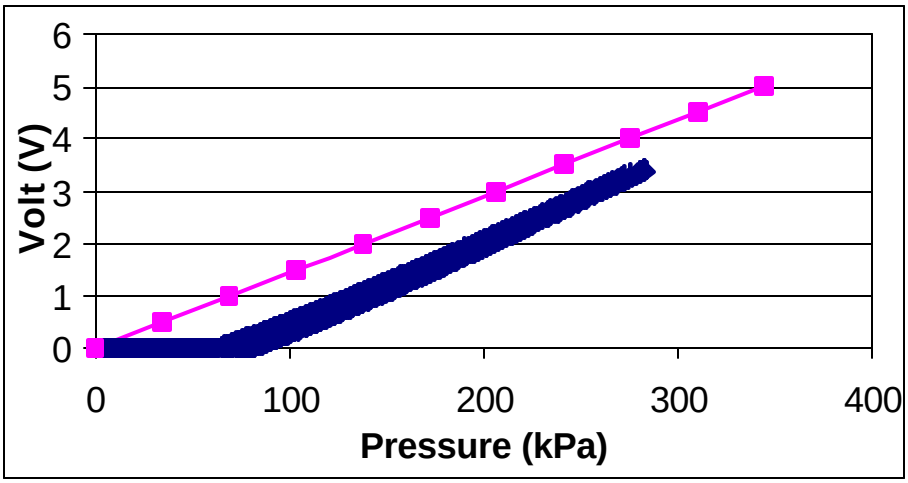

Figure 7 Calibration for Cell Labeled 12p5-2

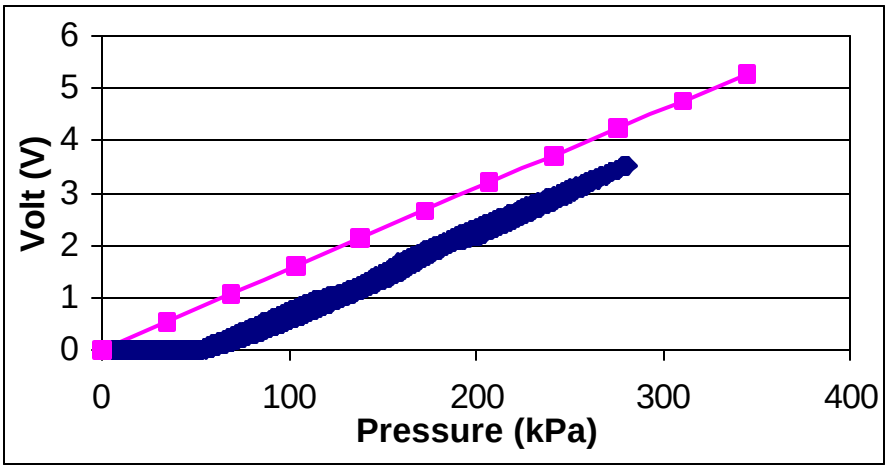

Figure 8 Calibration for Cell Labeled 1p5-1

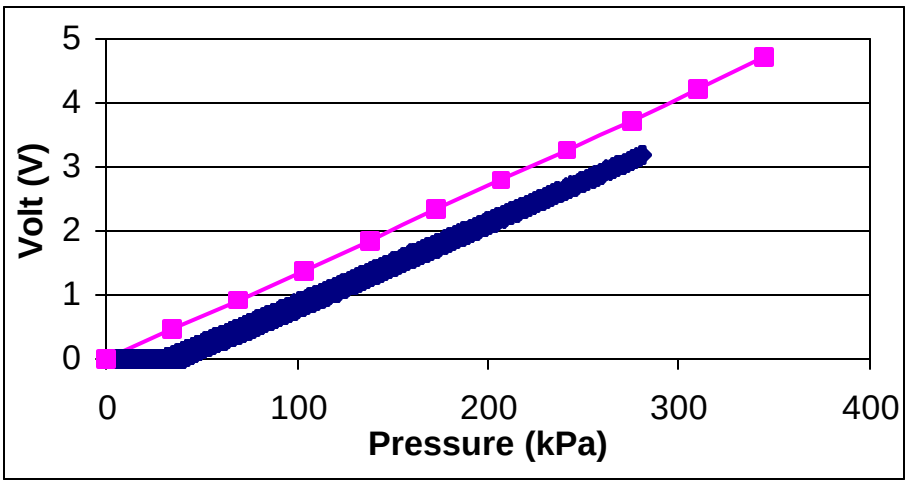

Figure 9 Calibration for Cell Labeled 1p5-2

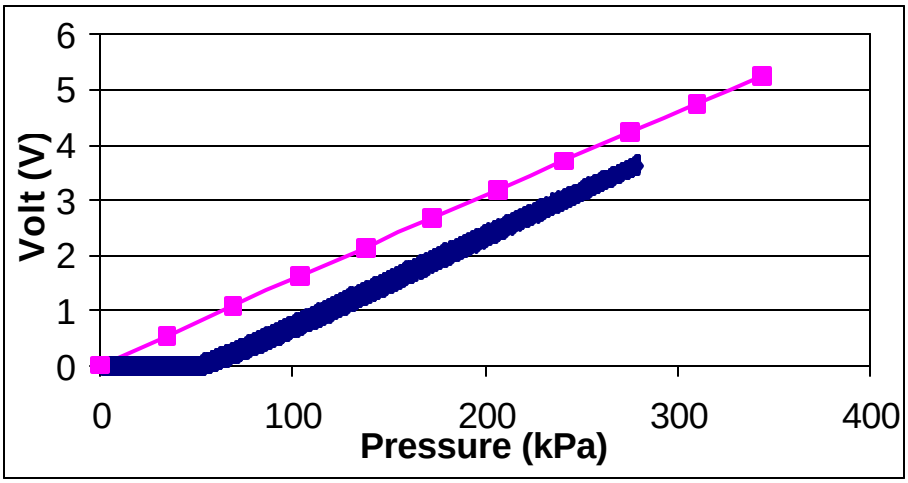

Figure 10 Calibration for Cell Labeled 1p5-3

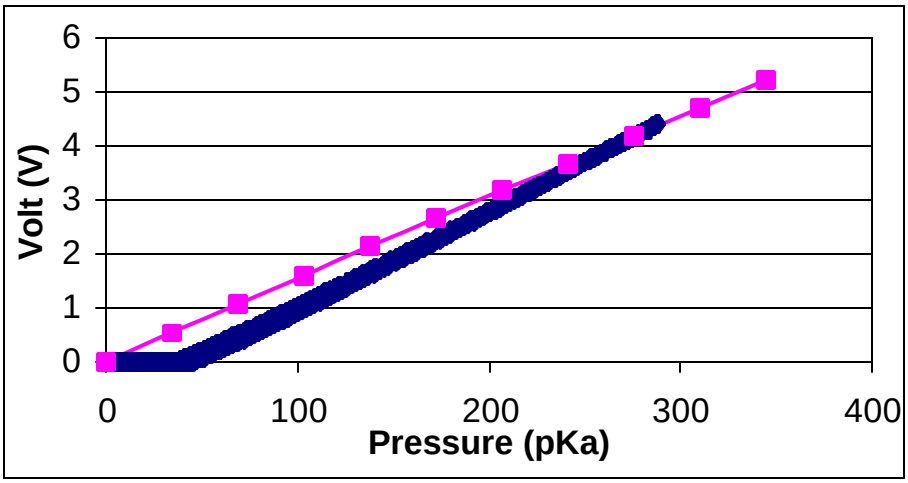

Figure 11 Calibration for Cell Labeled 1p7-1

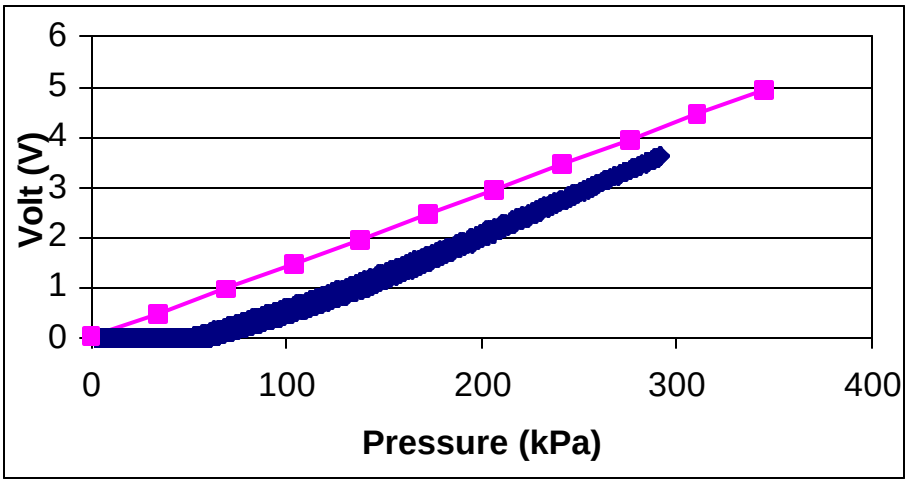

Figure 12 Calibration for Cell Labeled 1p7-2

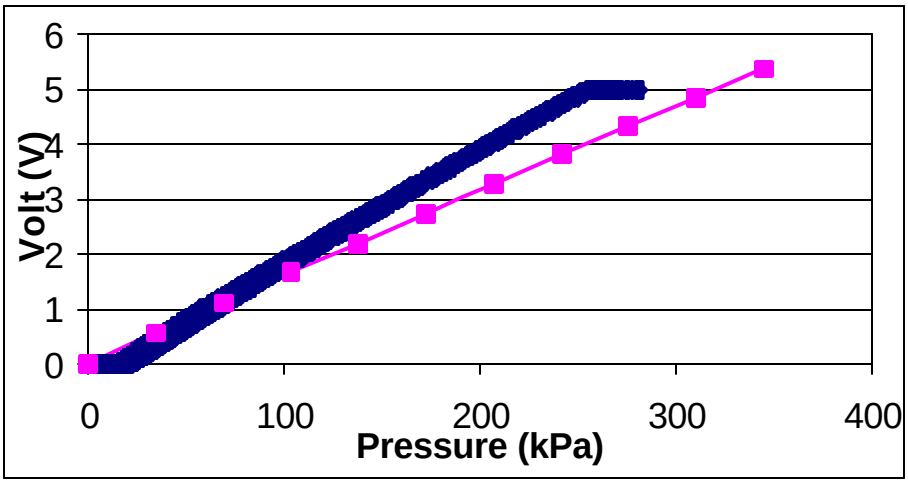

Figure 13 Calibration for Cell Labeled 1p7-3

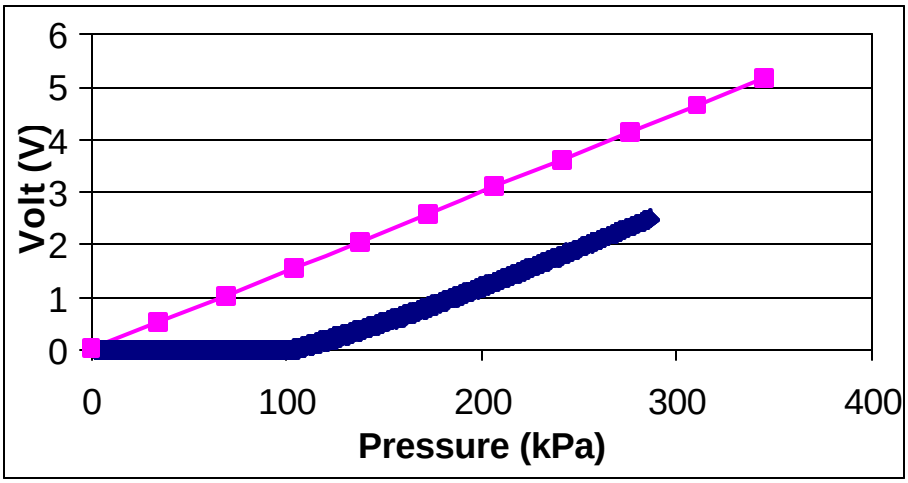

Figure 14 Calibration for Cell Labeled 2p5-2

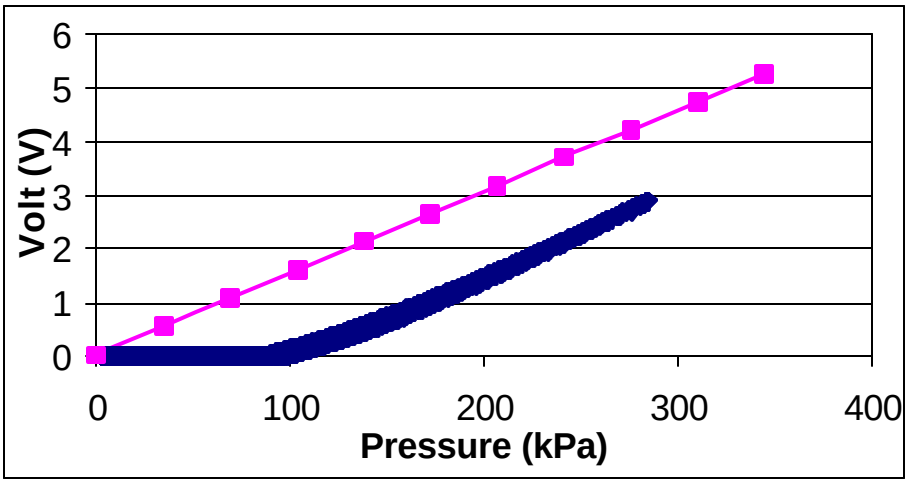

Figure 15 Calibration for Cell Labeled 2p5-3

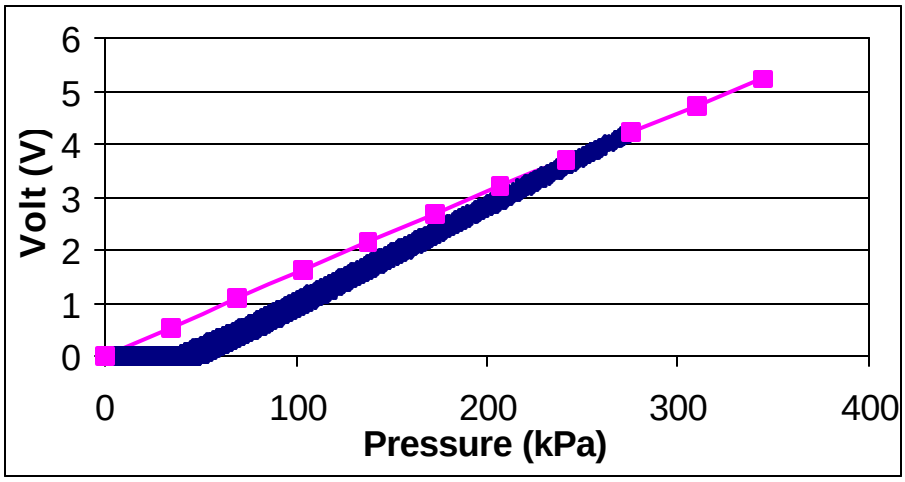

Figure 16 Calibration for Cell Labeled 3p5-1

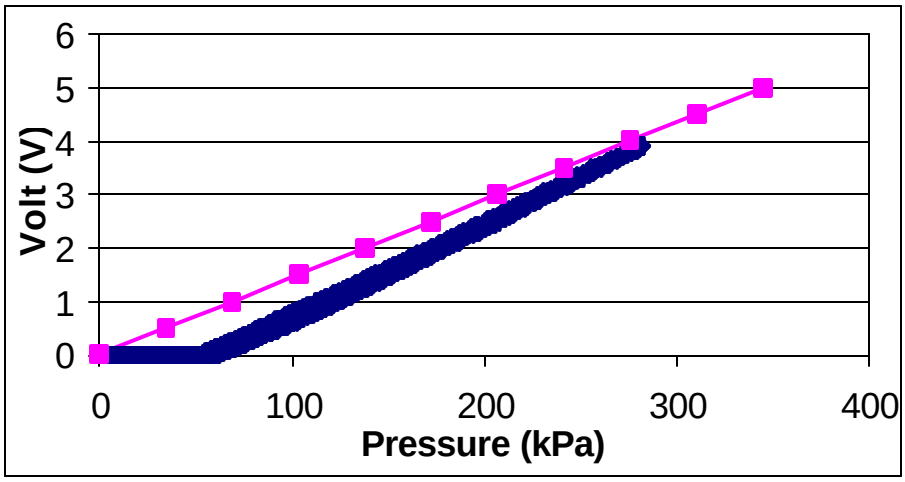

Figure 17 Calibration for Cell Labeled 3p5-2

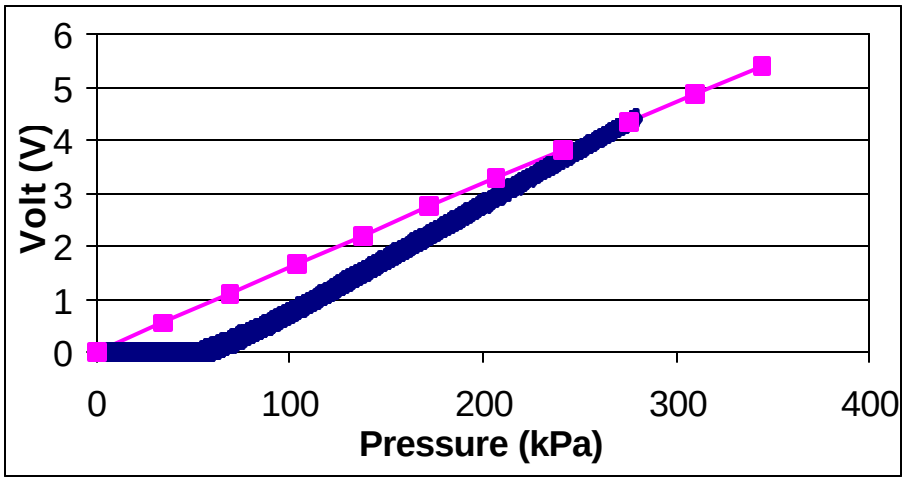

Figure 18 Calibration for Cell Labeled 3p5-3

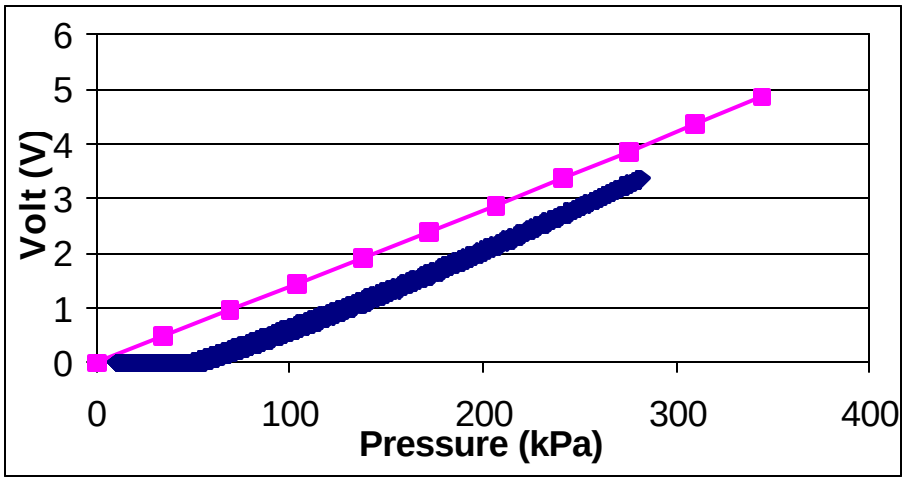

Figure 19 Calibration for Cell Labeled 3p7-1

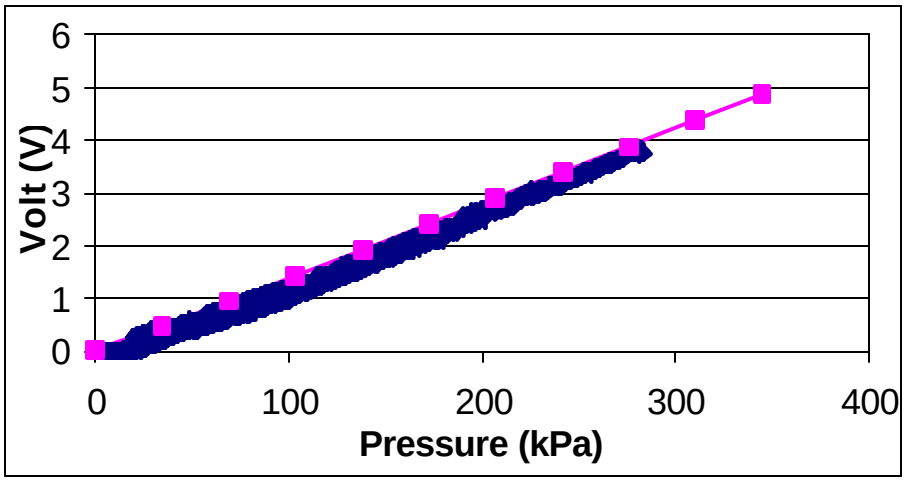

Figure 20 Calibration for Cell Labeled 3p7-2

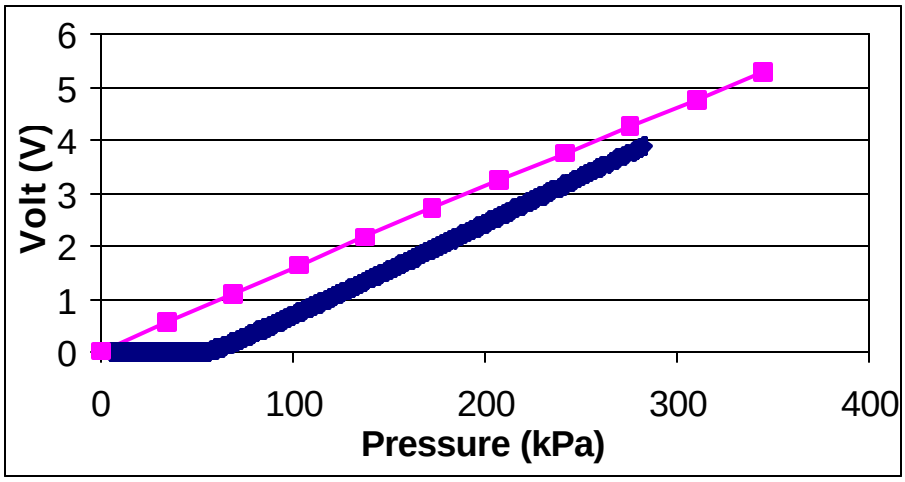

Figure 21 Calibration for Cell Labeled 4p5-1

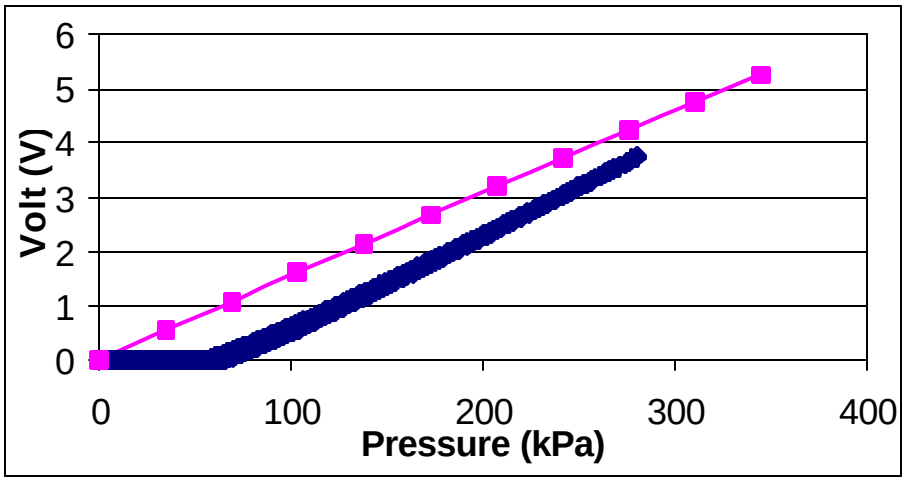

Figure 22 Calibration for Cell Labeled 4p5-2

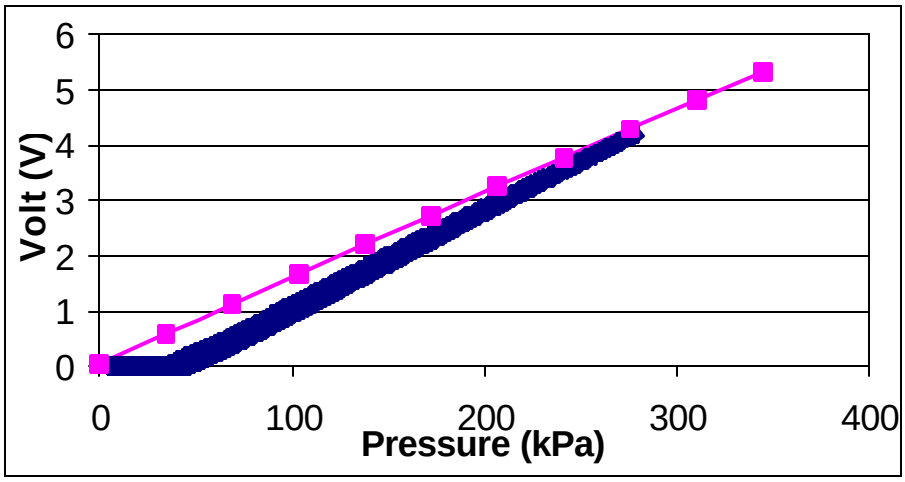

Figure 23 Calibration for Cell Labeled 4p5-3

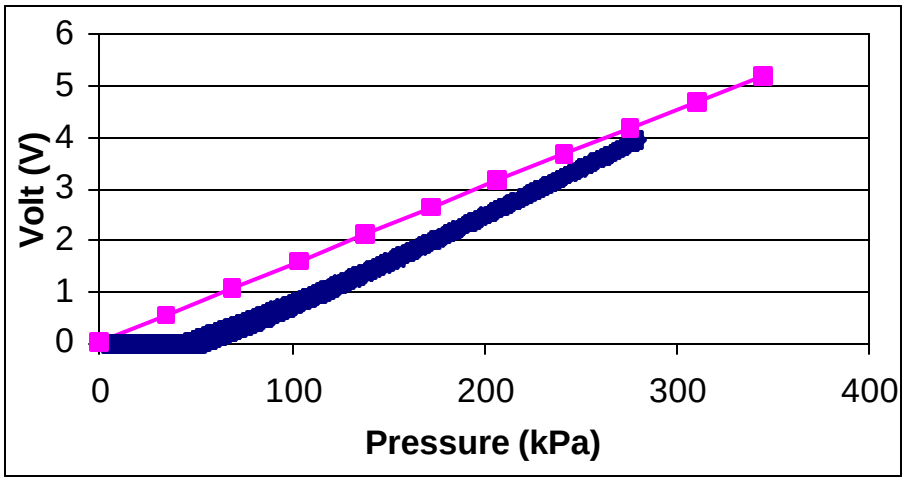

Figure 24 Calibration for Cell Labeled 7p5-2

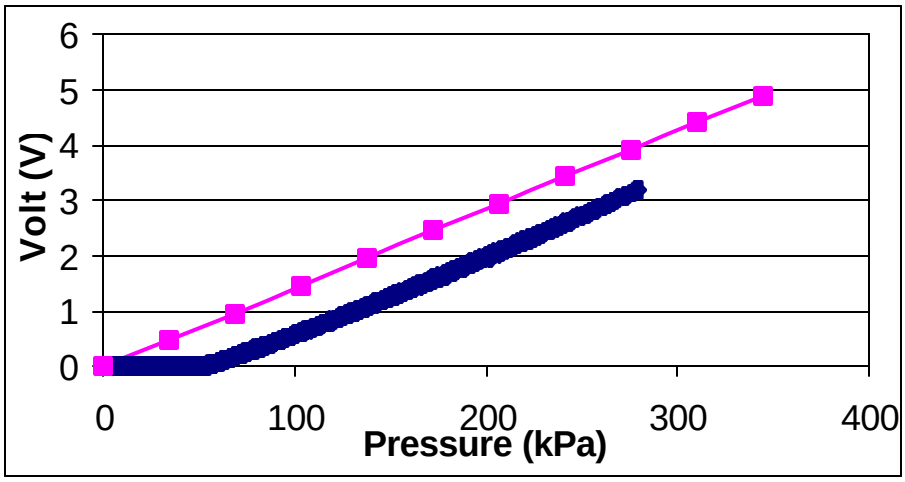

Figure 25 Calibration for Cell Labeled 3p7-3

Appendix B

Test Truck Information

Front Single Tires:

Michelin 11R22.5 XZA-1
Max Load Single 6175 @100 psi cold
Max Load Dual 5675 @ 100 psi cold

Tandem Tires:

General 11R22.5
Ameri * D440
Regroovable Radial Tubeless
Max Load Single 6040 @105 psi cold
Max Load Dual 5300 @ 95 psi cold

Tridem Tires:

Goodyear 10.00R15TR
G114 Unisteel Regroovable
Max Load Single 5050 @100 psi cold
Max Load Dual 4430 @ 100 psi cold

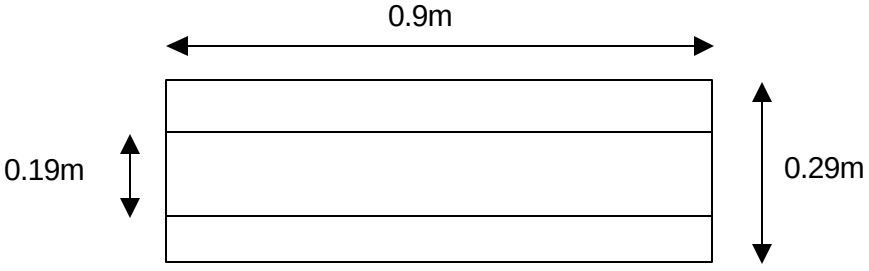

Truck

Make Model: International 8200
Engine Power: 350hp @ 2100 rpm
Class 887 Tucks-Tractor-Tandem Axle – 50000GVW
Equip ID: VDOT R62077

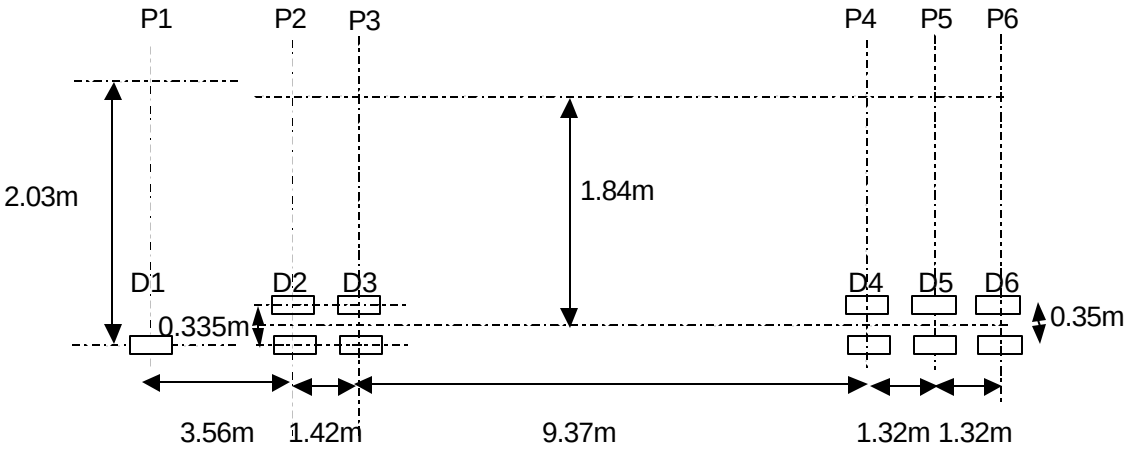

Gross Weight: 40,823 kg
Overall Length: 24.38 m
Overall Width:3.58 m
Licensed For 36,287 kg

Appednix C

Mohr’s Circle Diagrams

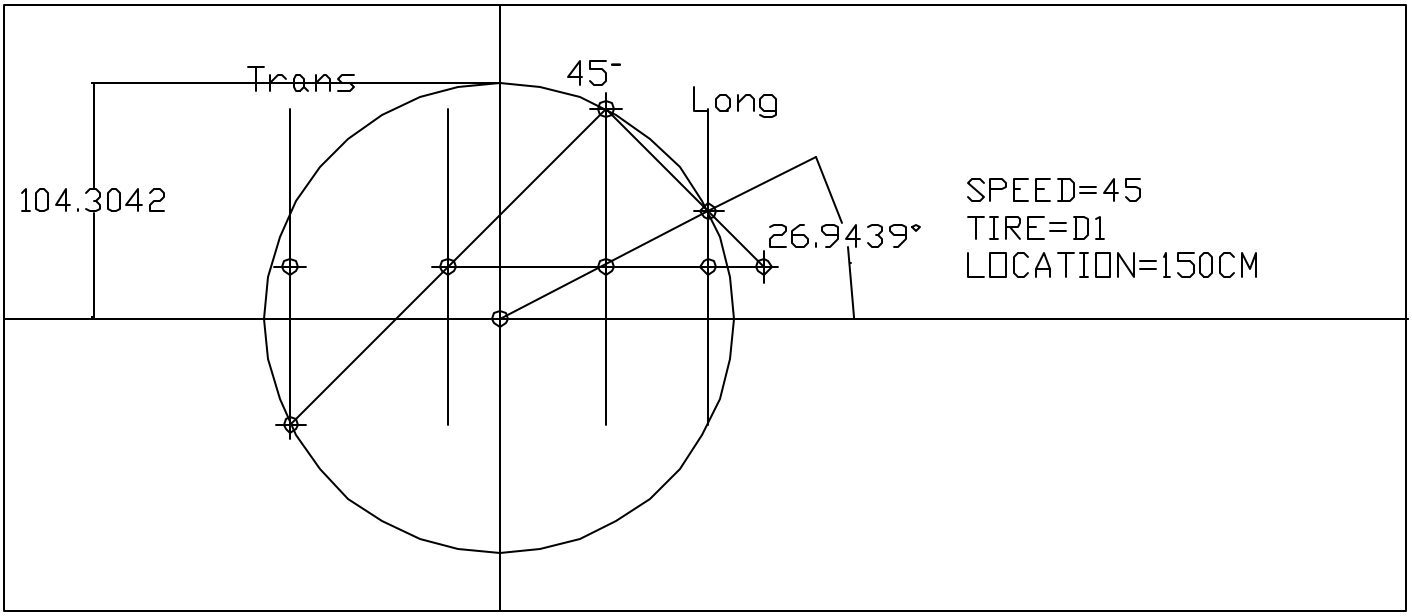

Figure 1 Mohr's Circle for the Speed of 72km/h and the Load of D1

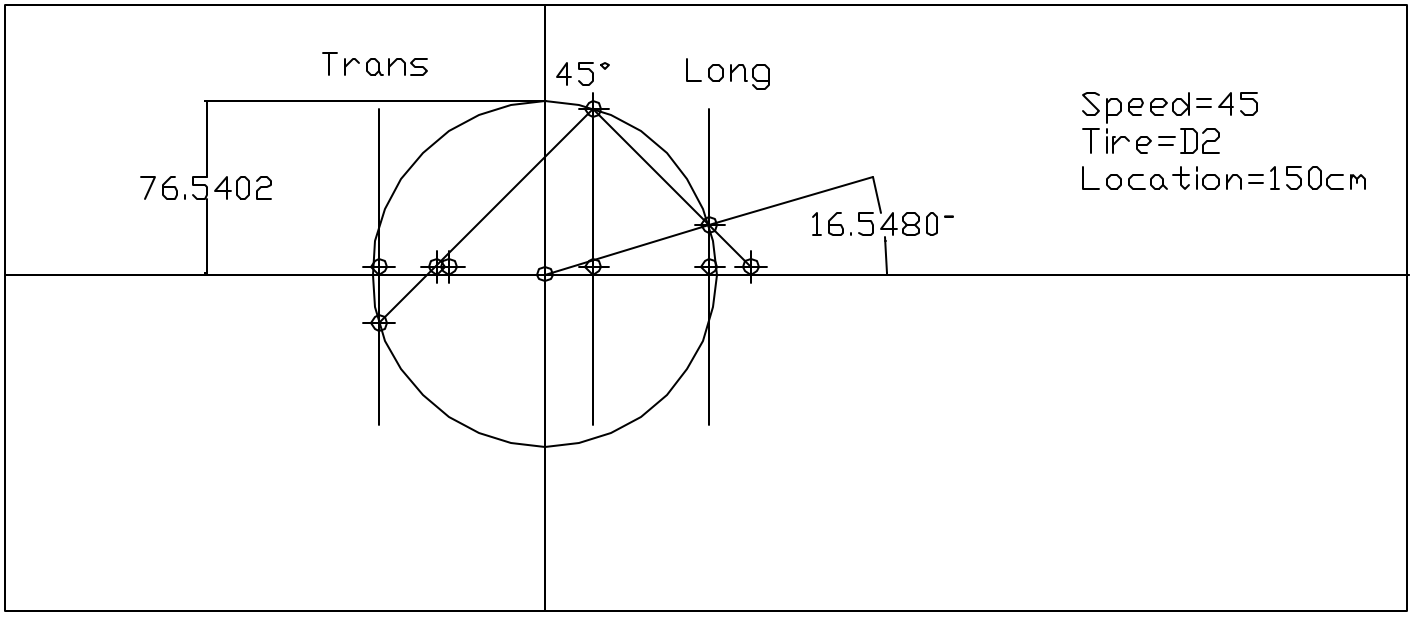

Figure 2 Mohr's Circle for the Speed of 72km/h and the Load of D2

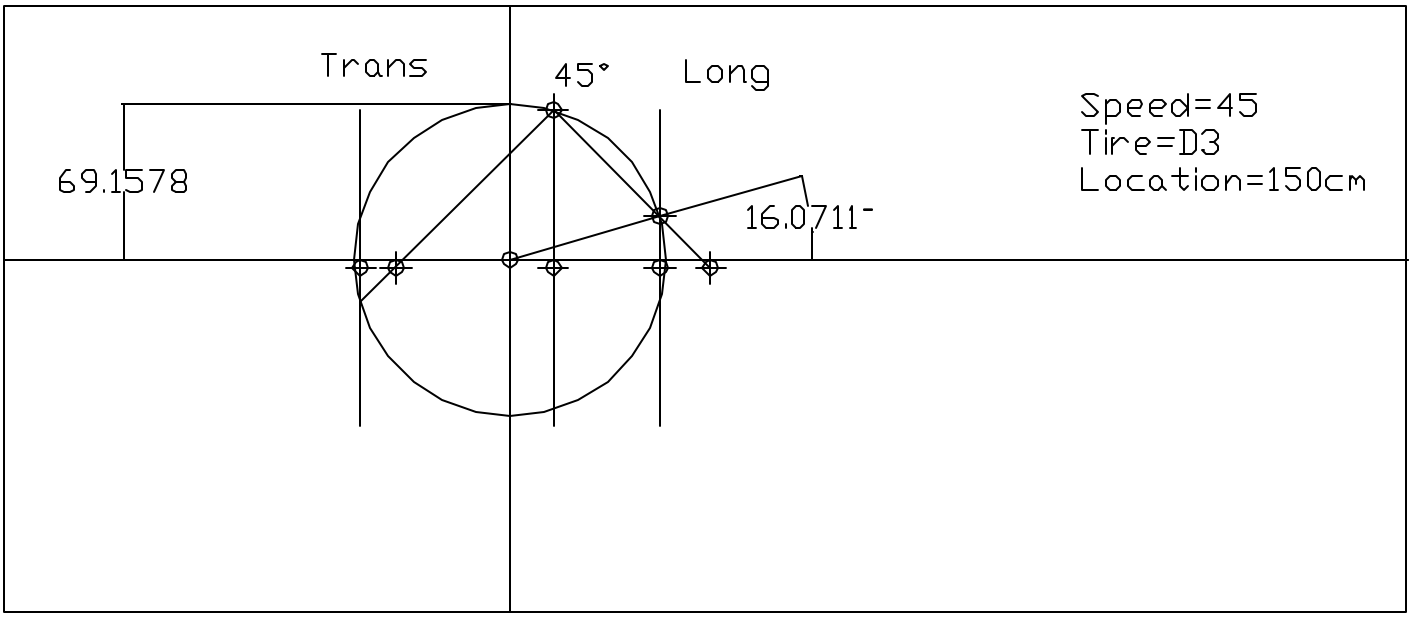

Figure 3 Mohr's Circle for the Speed of 72km/h and the Load of D3

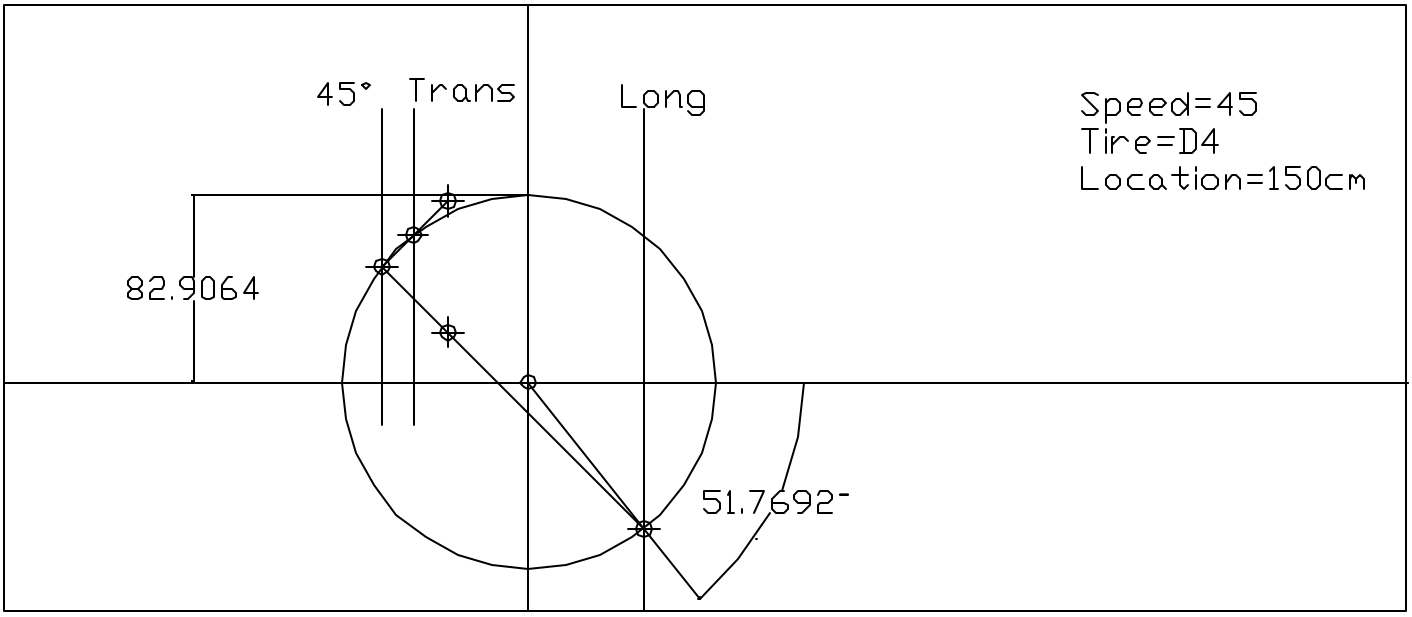

Figure 4 Mohr's Circle for the Speed of 72km/h and the Load of D4

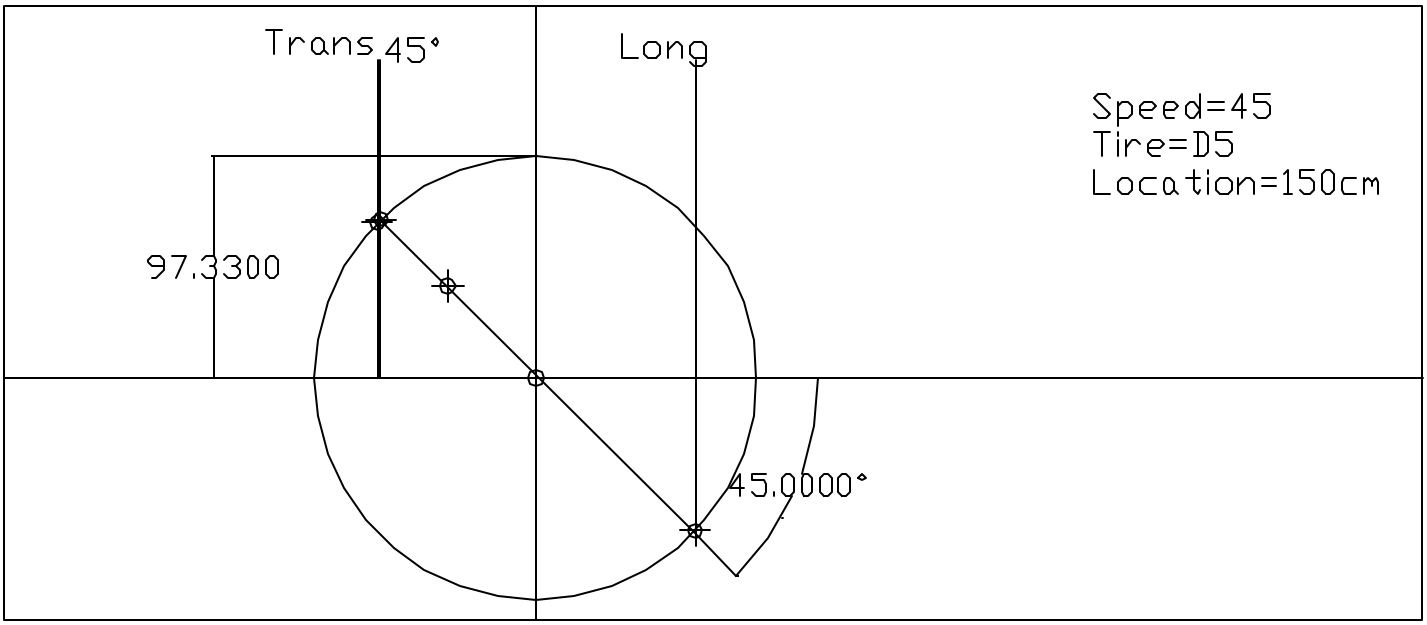

Figure 5 Mohr's Circle for the Speed of 72km/h and the Load of D5

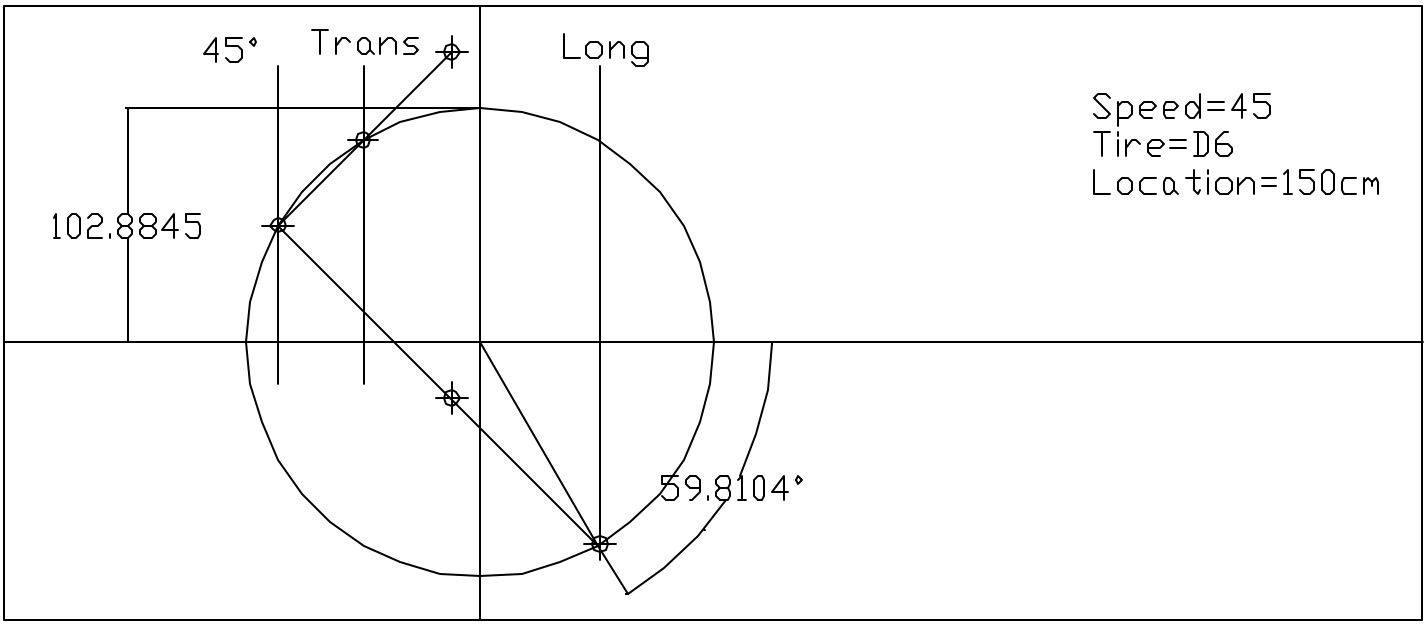

Figure 6 Mohr's Circle for the Speed of 72km/h and the Load of D6

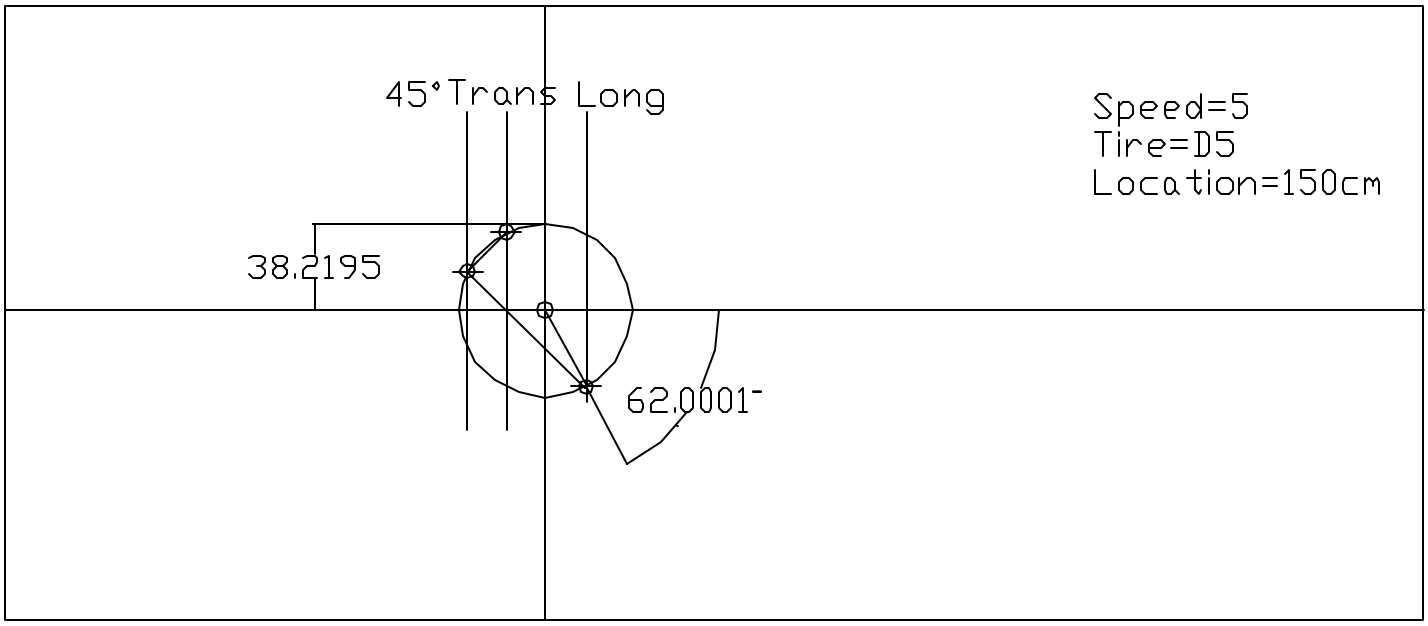

Figure 7 Mohr's Circle for the Speed of 8km/h and the Load of D5

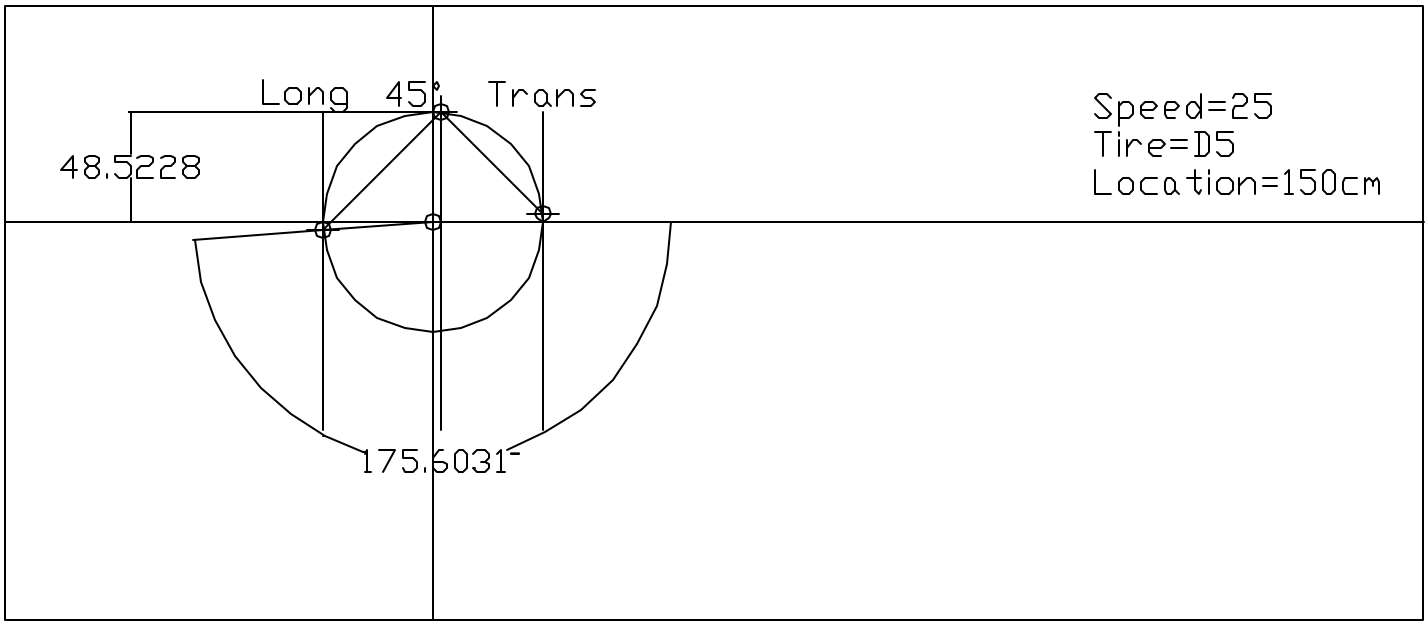

Figure 8 Mohr's Circle for the Speed of 40km/h and the Load of D5

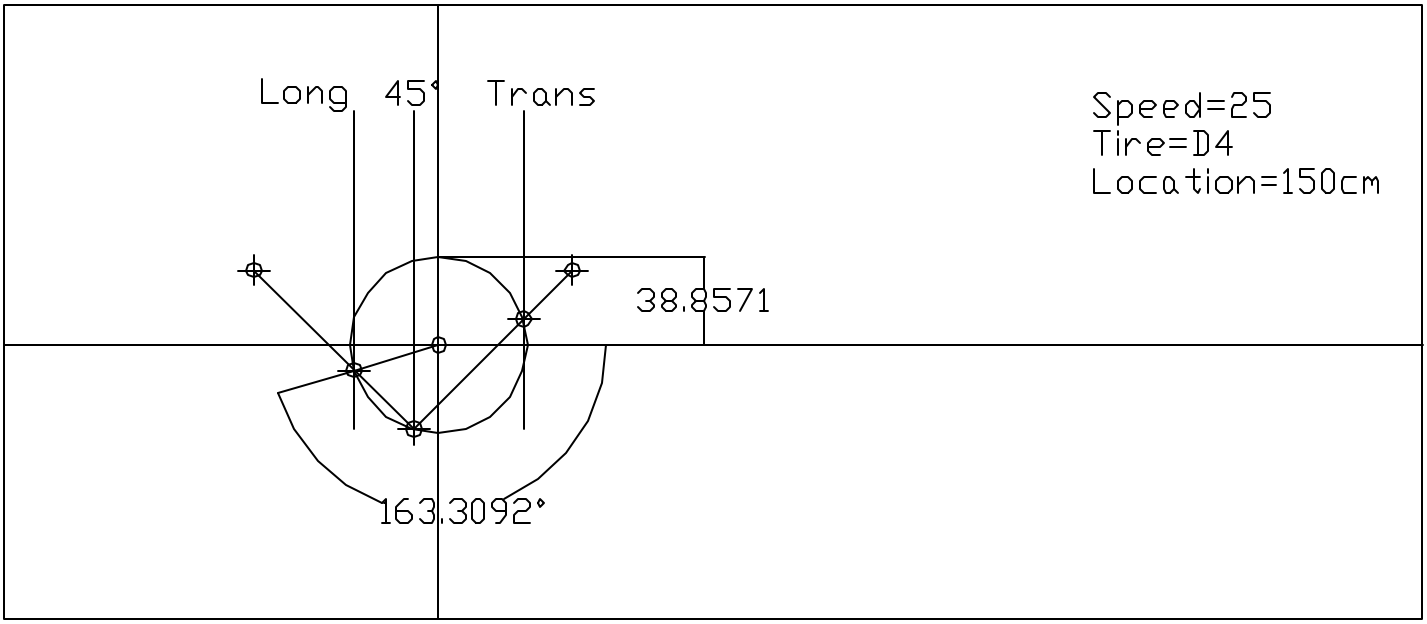

Figure 9 Mohr's Circle for the Speed of 40km/h and the Load of D4

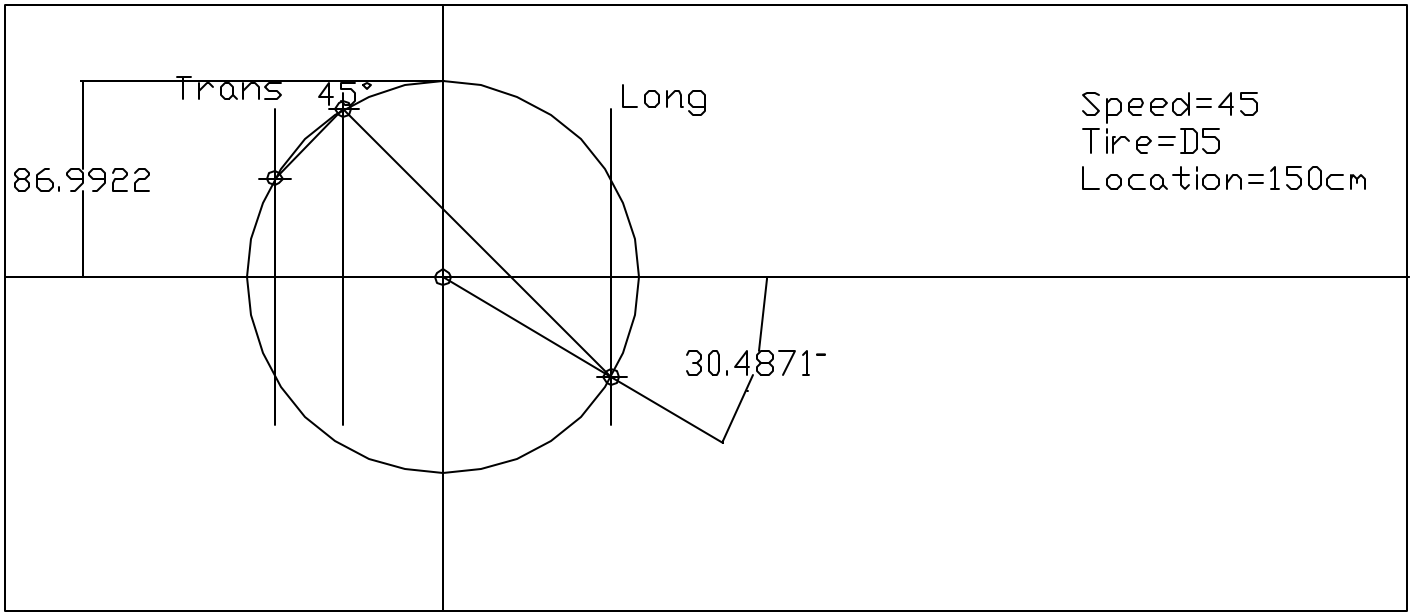

Figure 10 Mohr's Circle for the Speed of 72km/h and the Load of D5

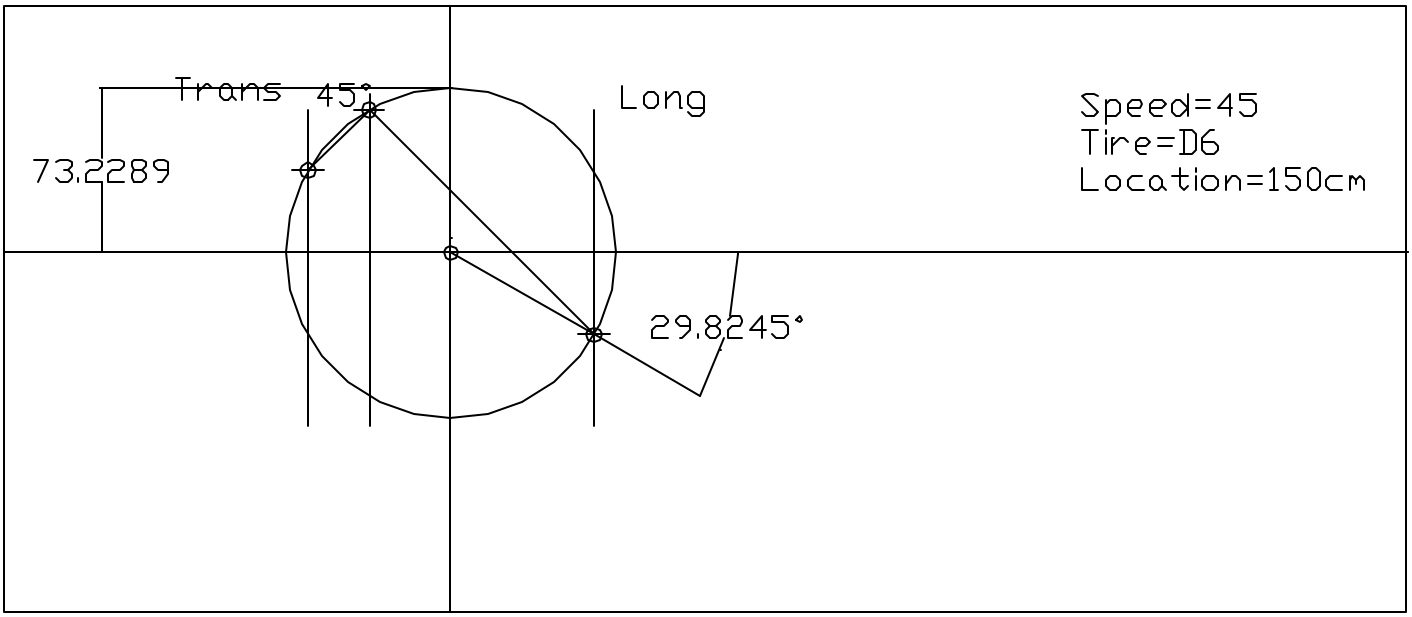

Figure 11 Mohr's Circle for the Speed of 72km/h and the Load of D6

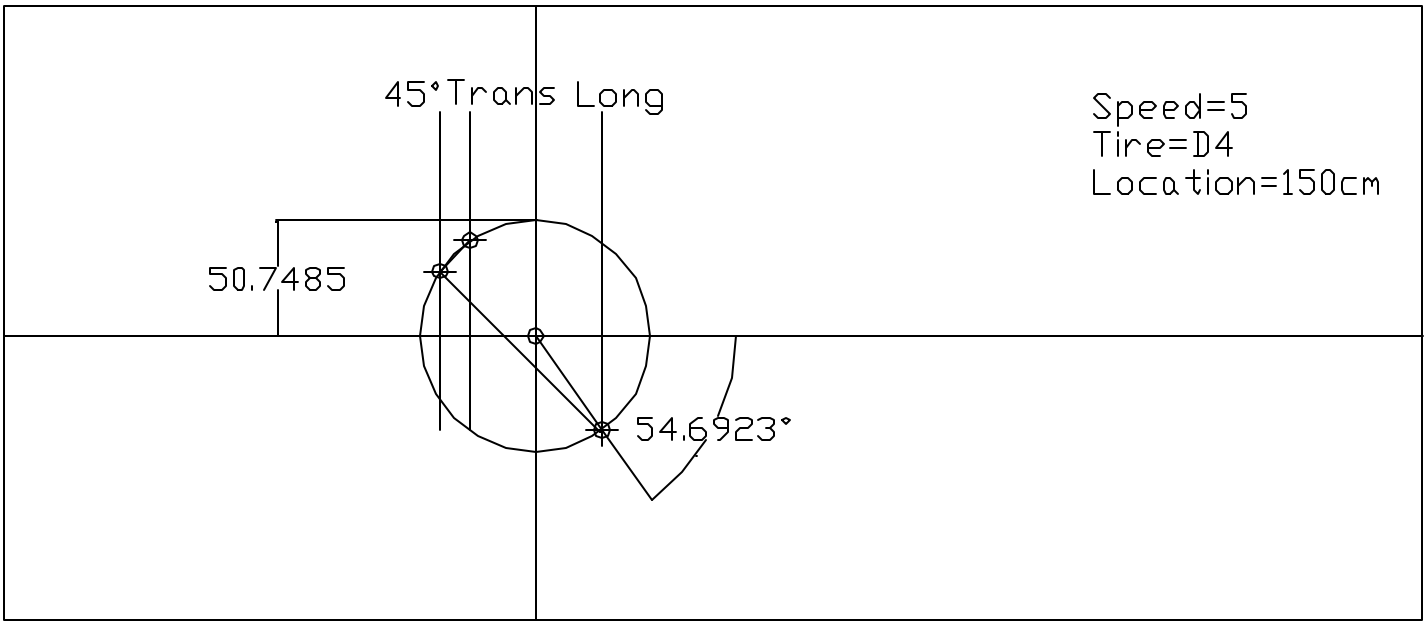

Figure 12 Mohr's Circle for the Speed of 8km/h and the Load of D4

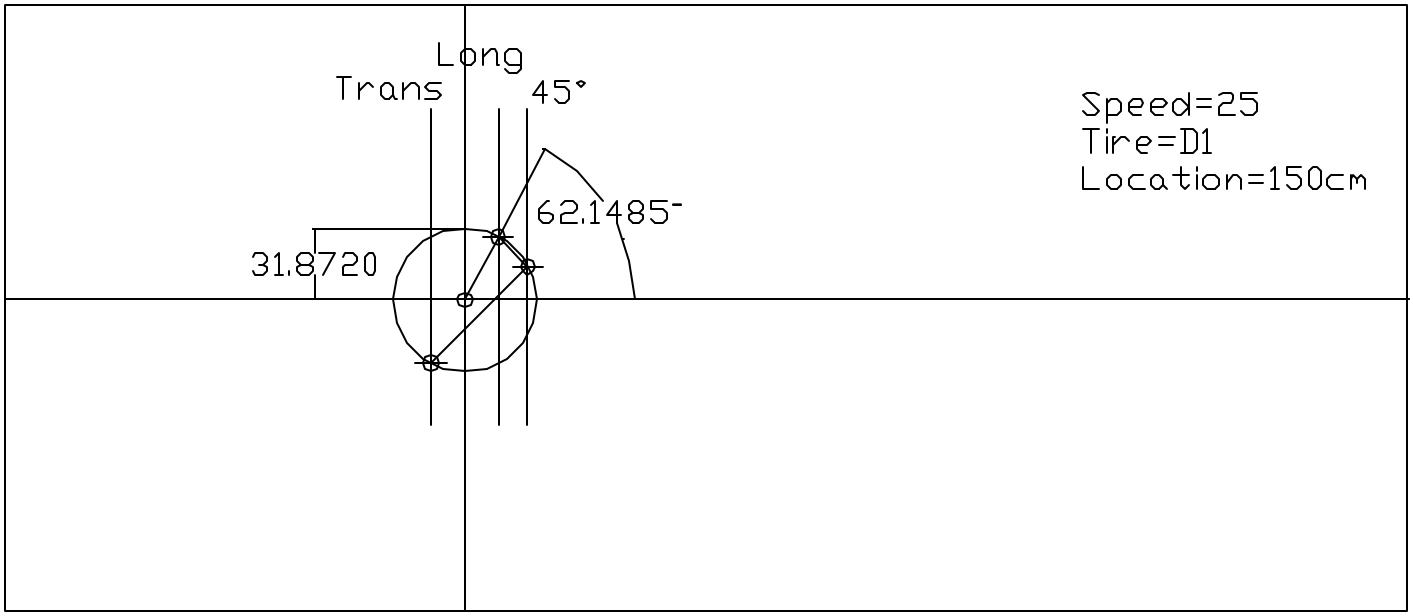

Figure 13 Mohr's Circle for the Speed of 40km/h and the Load of D1

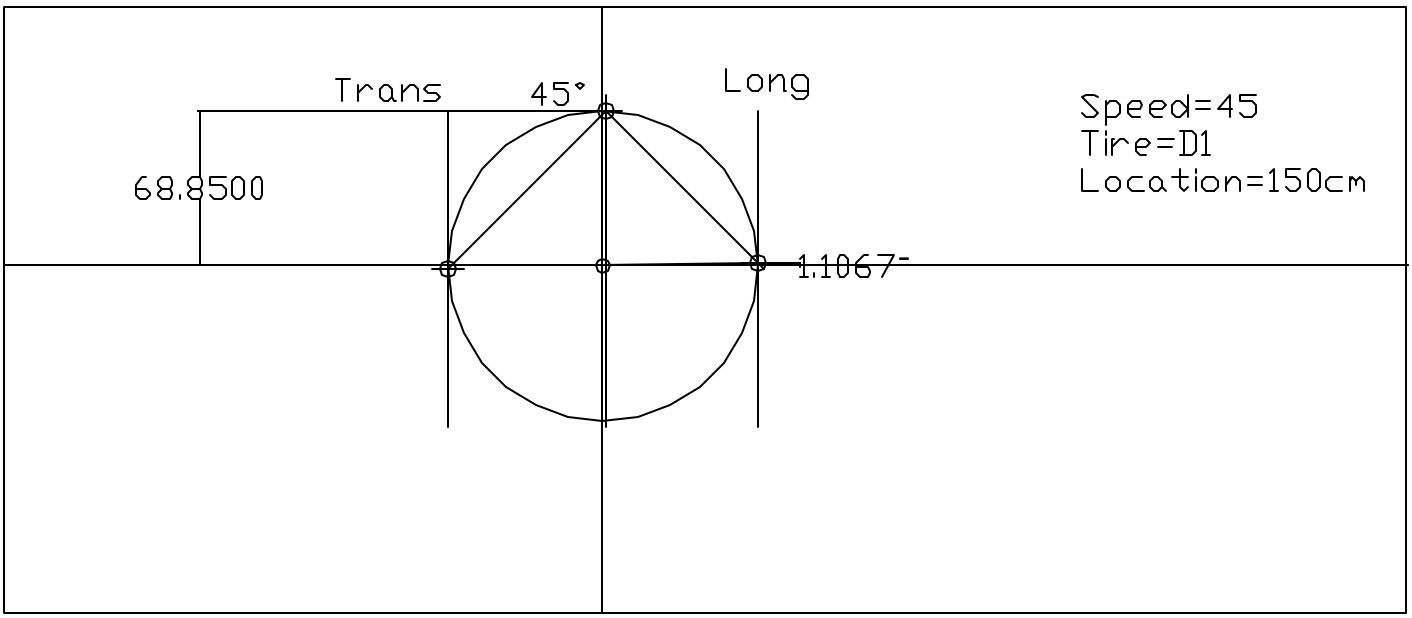

Figure 14 Mohr's Circle for the Speed of 72km/h and the Load of D1

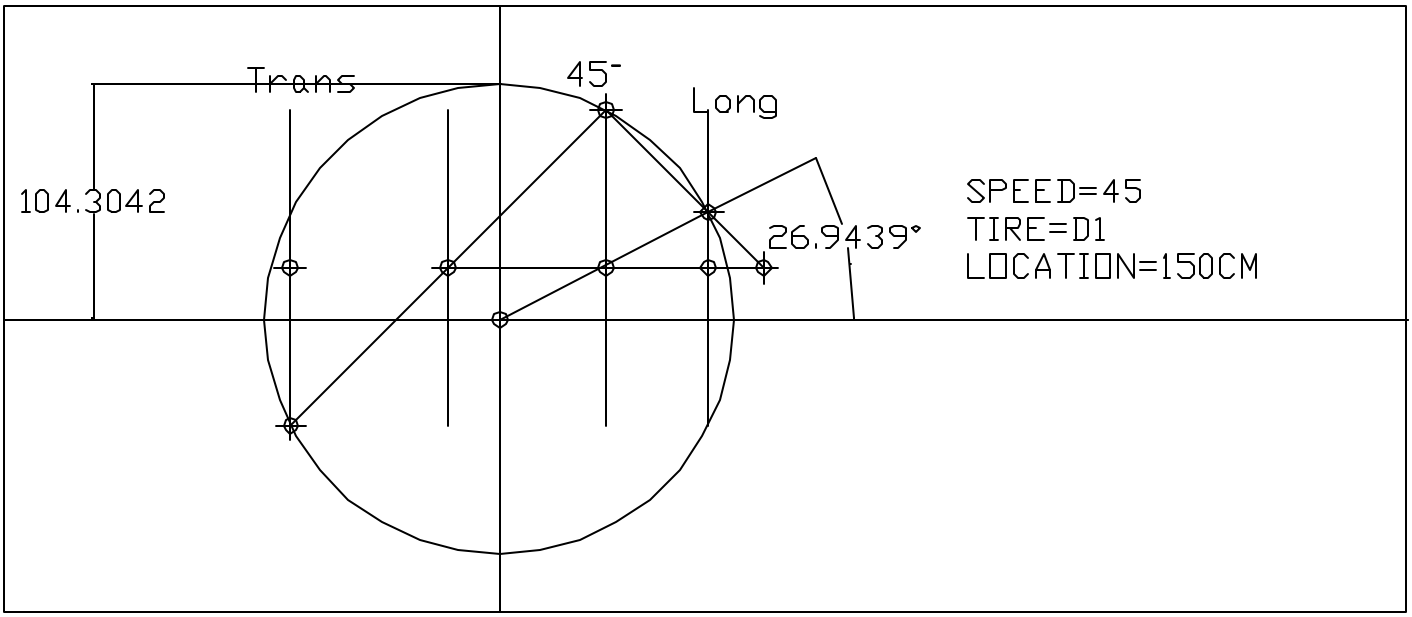

Figure 15 Mohr's Circle for the Speed of 72km/h and the Load of D1

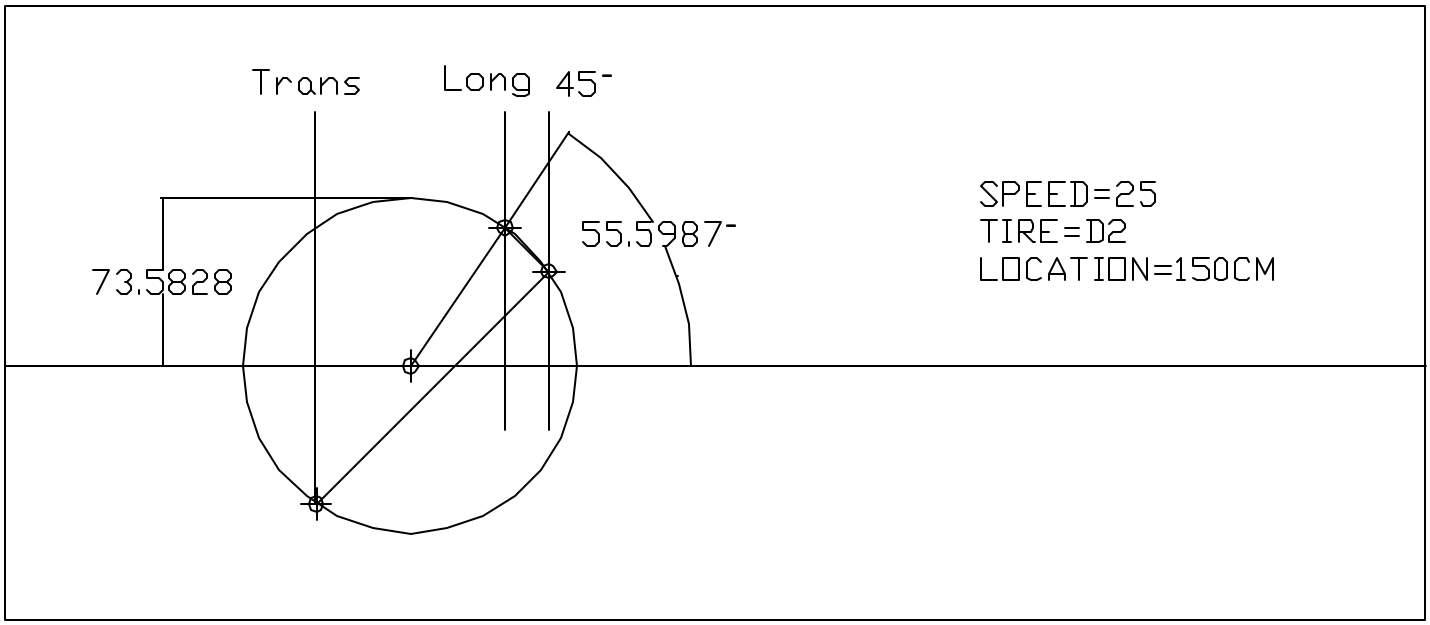

Figure 16 Mohr's Circle for the Speed of 40km/h and the Load of D2

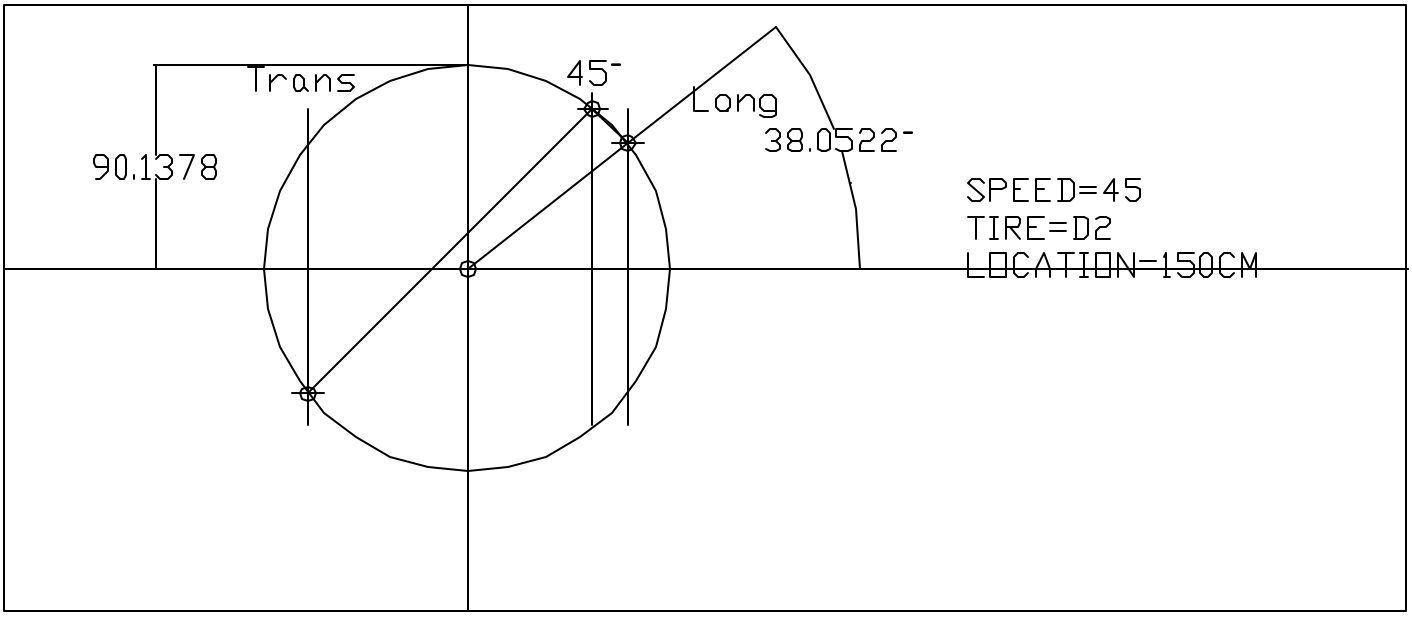

Figure 17 Mohr's Circle for the Speed of 72km/h and the Load of D2

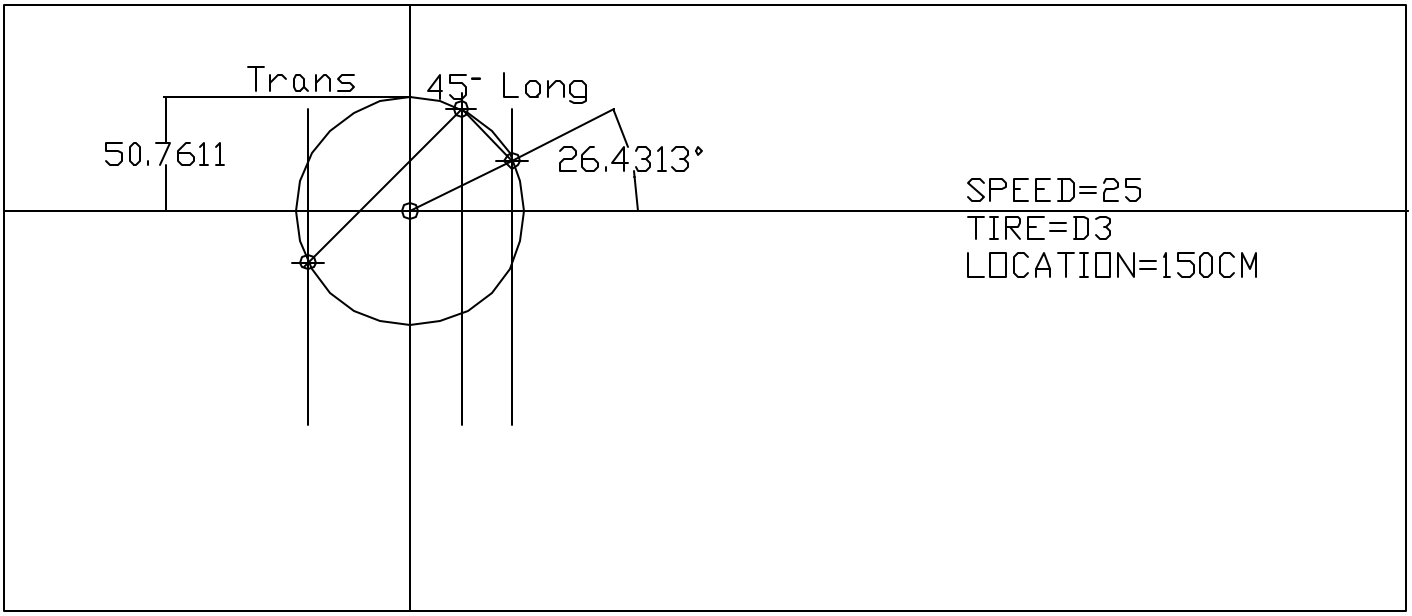

Figure 18 Mohr's Circle for the Speed of 40km/h and the Load of D3

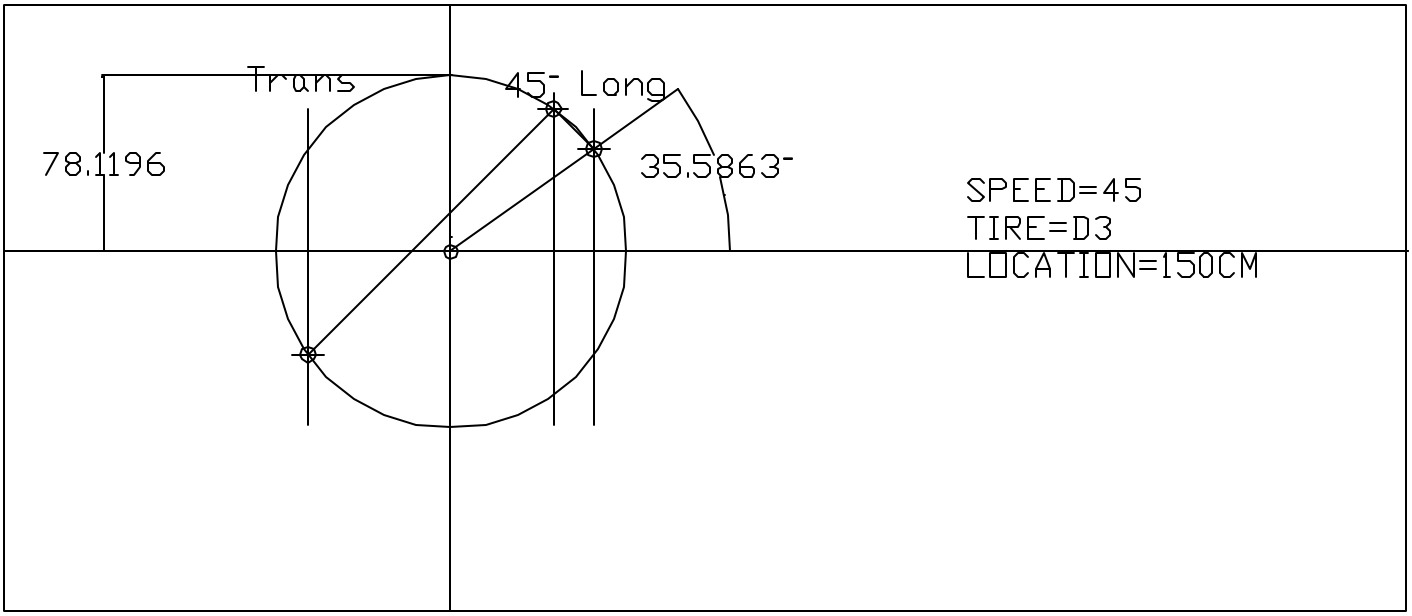

Figure 19 Mohr's Circle for the Speed of 72km/h and the Load of D3

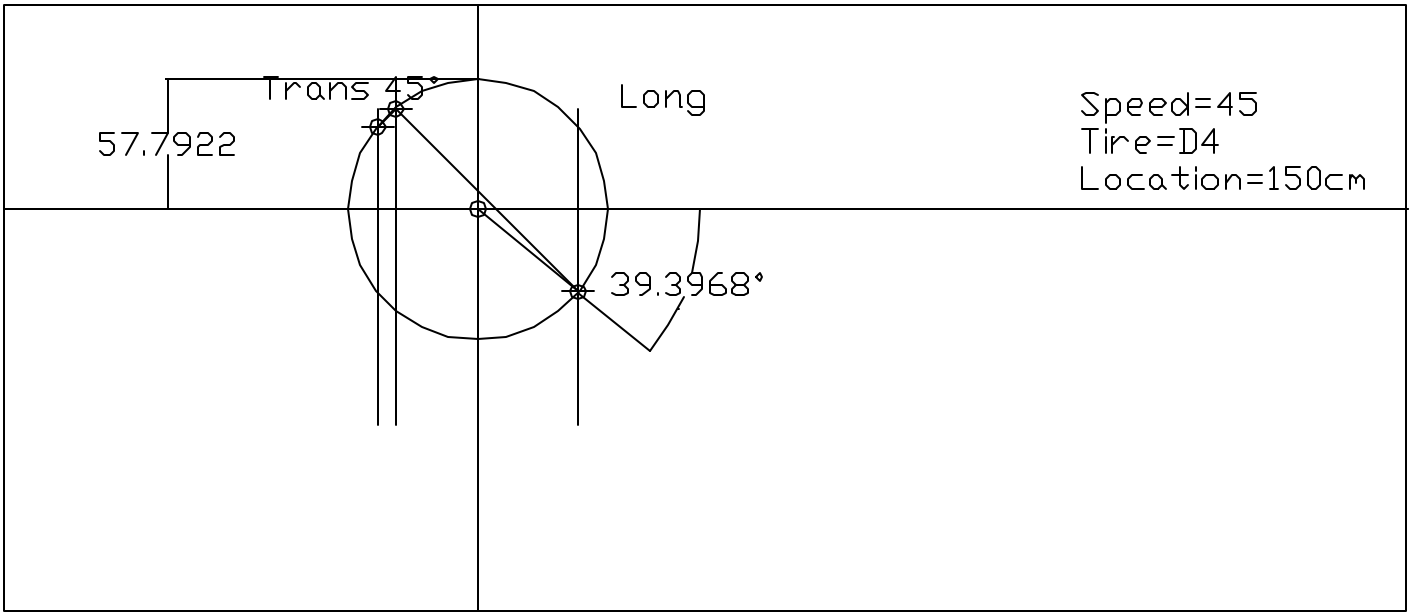

Figure 20 Mohr's Circle for the Speed of 72km/h and the Load of D4

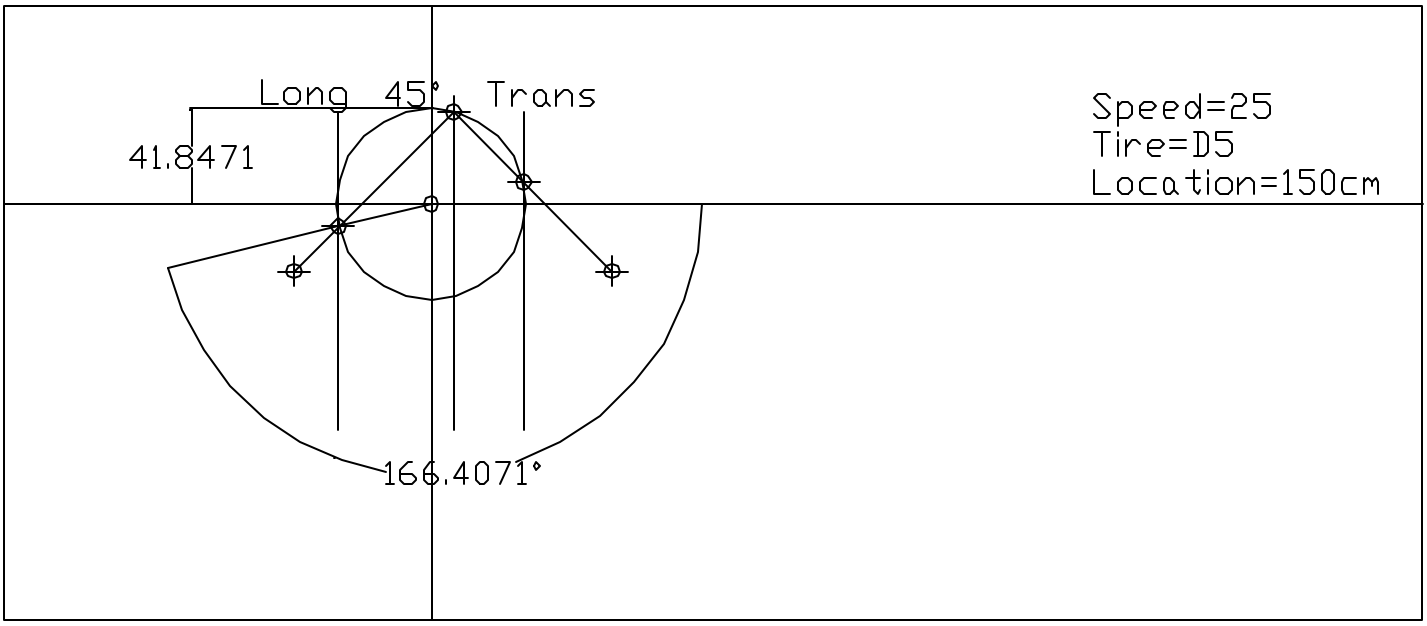

Figure 21 Mohr's Circle for the Speed of 40km/h and the Load of D5

Appendix D

Resilient Modulus Tests

ID	Sample	Position	Input P (N)	t (mm)	Mr(software)	ν (software)	Calculations $\Delta H_t / \Delta V_t$	ΔH_t
1	BM25	DT1	3000	69	19149	1.54	0.50418	0.00411
2	BM25	PT1	3000	69	17128	1.31	0.44011	0.00401
3	BM25	PT3	3700	84	18603	1.89	0.60167	0.00511
4	BM25	DT3	3700	84	41664	4.84	1.42340	0.00540
5	OGFC	DT1	1000	80	2961	1.87	0.59666	0.00904
6	OGFC	PT1	1000	85	2107	1.90	0.60306	0.01209
7	OGFC	DT2	1000	83	2660	1.89	0.60028	0.00976
8	SM12.5D	PT3	2500	82	13705	1.49	0.49025	0.00392
9	SM12.5D	DT3	2500	80	11619	1.40	0.46518	0.00449
10	SM9.5A-D	DT1	2000	90	8461	1.34	0.44847	0.00423
11	SM9.5A-D	PT1	3000	83	13147	1.15	0.39554	0.00390
12	SM9.5A-D	DT2	2000	80	9172	1.39	0.46240	0.00452
13	SM9.5A-D	PT2	2000	84	13576	2.20	0.68802	0.00433
14	SM9.5A-D	PT3	2000	85	39914	6.89	1.99443	0.00422
15	SM9.5A-D	DT3	2000	85	10226	1.55	0.50696	0.00419
16	SM9.5A-H	PT1	3000	80	12718	1.14	0.39276	0.00416
17	SM9.5A-H	DT1	3000	79	14814	1.42	0.47075	0.00433
18	SM9.5A-H	PT2	3000	75	15663	1.80	0.57660	0.00529
19	SM9.5A-H	DT2	3000	80	16194	1.59	0.51811	0.00431
20	SM9.5A-H	PT3	2000	80	11352	1.86	0.59331	0.00469
21	SM9.5A-H	DT3	2500	80	13332	1.71	0.55153	0.00464
22	SM9.5D	DT1	2000	82	9167	1.47	0.48468	0.00463
23	SM9.5D	PT1	2000	80	12690	2.00	0.63231	0.00447
24	SM9.5D	PT2	2500	86	13455	1.96	0.62117	0.00482
25	SM9.5D	DT2	2500	79	13404	1.88	0.59889	0.00508
26	SM9.5D	PT3	2500	80	10491	1.38	0.45961	0.00491
27	SM9.5D	DT3	2500	85	9055	1.60	0.52089	0.00607
28	SM9.5E	DT1	2000	78	8138	1.54	0.50418	0.00570
29	SM9.5E	PT1	2000	79	10391	2.09	0.65738	0.00575
30	SM9.5E	PT2	2000	82	10757	2.30	0.71588	0.00583
31	SM9.5E	DT2	2000	84	9962	1.82	0.58217	0.00500
32	SM9.5E	DT2	2000	84	9780	1.96	0.62117	0.00543
33	SM9.5E	DT3	2000	81	11680	1.75	0.56267	0.00427
34	SM9.5E	PT3	2000	81	12100	1.63	0.52925	0.00388
35	SMA12.5	DT1	1000	88	5105	1.62	0.52646	0.00421
36	SMA12.5	DT1	1000	88	5105	1.62	0.52646	0.00421
37	SMA12.5	DT2	2000	80	5125	1.52	0.49861	0.00873
38	SMA12.5	PT2	1000	80	3878	1.10	0.38162	0.00442
39	SMA12.5	DT3	2000	72	6255	2.05	0.64624	0.01030
40	SMA12.5	PT3	2000	85	4799	1.96	0.62117	0.01093

ID	ΔV_t	ν	$M_{r(ASTM)}$(KSI)	ε_H	ε_V	ASTM ν	ASTM $M_{r(ASTM)}$(KSI)	Elastic Analysis ν	Elastic Analysis $M_{r(Elastic)}$(KSI)
1	0.00815	0.24	780.52	0.00016	0.00032	1.54	2777	0.27	411
2	0.00911	0.16	674.17	0.00016	0.00036	1.31	2484	0.18	358
3	0.00850	0.35	778.47	0.00020	0.00033	1.89	2698	0.42	416
4	0.00380	0.50	914.11	0.00021	0.00015	4.84	6043	2.41	1453
5	0.01516	0.35	125.02	0.00036	0.00060	1.87	429	0.41	66
6	0.02005	0.35	87.97	0.00048	0.00079	1.90	306	0.42	47
7	0.01626	0.35	111.56	0.00038	0.00064	1.89	386	0.42	59
8	0.00799	0.20	535.99	0.00015	0.00031	1.49	1988	0.25	292
9	0.00966	0.17	450.94	0.00018	0.00038	1.40	1685	0.22	245
10	0.00943	0.14	317.15	0.00017	0.00037	1.34	1227	0.20	177
11	0.00987	0.10	500.87	0.00015	0.00039	1.15	1907	0.13	270
12	0.00979	0.17	355.49	0.00018	0.00039	1.39	1330	0.22	193
13	0.00630	0.49	607.22	0.00017	0.00025	2.20	1969	0.56	316
14	0.00212	0.50	624.99	0.00017	0.00008	6.89	5789	5.93	2277
15	0.00826	0.22	400.27	0.00016	0.00033	1.55	1483	0.28	220
16	0.01059	0.10	487.97	0.00016	0.00042	1.14	1845	0.12	261
17	0.00920	0.18	578.02	0.00017	0.00036	1.42	2149	0.23	314
18	0.00917	0.33	661.12	0.00021	0.00036	1.80	2272	0.38	347
19	0.00831	0.24	647.46	0.00017	0.00033	1.59	2349	0.29	350
20	0.00791	0.35	478.11	0.00018	0.00031	1.86	1646	0.41	253
21	0.00841	0.28	544.92	0.00018	0.00033	1.71	1934	0.34	292
22	0.00955	0.19	357.42	0.00018	0.00038	1.47	1330	0.25	195
23	0.00707	0.41	550.55	0.00018	0.00028	2.00	1841	0.47	288
24	0.00776	0.38	567.48	0.00019	0.00031	1.96	1951	0.45	304
25	0.00848	0.36	568.62	0.00020	0.00033	1.88	1944	0.41	300
26	0.01069	0.17	406.08	0.00019	0.00042	1.38	1522	0.21	221
27	0.01166	0.24	357.40	0.00024	0.00046	1.60	1313	0.30	196
28	0.01131	0.22	324.36	0.00022	0.00045	1.54	1180	0.27	175
29	0.00875	0.45	461.22	0.00023	0.00034	2.09	1507	0.51	238
30	0.00814	0.50	469.27	0.00023	0.00032	2.30	1560	0.61	253
31	0.00858	0.32	410.99	0.00020	0.00034	1.82	1445	0.39	221
32	0.00874	0.38	415.28	0.00021	0.00034	1.96	1418	0.45	221
33	0.00759	0.30	479.69	0.00017	0.00030	1.75	1694	0.36	257
34	0.00733	0.25	485.84	0.00015	0.00029	1.63	1755	0.31	262
35	0.00799	0.24	200.31	0.00017	0.00031	1.62	740	0.31	111
36	0.00799	0.24	200.31	0.00017	0.00031	1.62	740	0.31	111
37	0.01751	0.21	202.50	0.00034	0.00069	1.52	743	0.27	110
38	0.01157	0.10	153.14	0.00017	0.00046	1.10	562	0.11	79
39	0.01594	0.45	280.99	0.00041	0.00063	2.05	907	0.49	143
40	0.01760	0.38	203.09	0.00043	0.00069	1.96	696	0.45	108

ID	SHRP(P07) ν	SHRP(P07) $M_{r(SHRP)}$(KSI)	Roque & Buttlar ν	Roque & Buttlar $M_{r(R\&B)}$(KSI)	Ass ν	H	Y	ε_{CTRx}	ε_{CTRy}	σX_{CORR}	σY_{CORR}
1	1.16	116	0.107	357	0.11	0.004	-0.008	0.000	0.000	46.153	-115.096
2	0.98	102	0.100	357	0.03	0.004	-0.009	0.000	0.000	46.153	-115.096
3	1.41	115	0.236	370	0.24	0.005	-0.008	0.000	0.000	46.757	-116.603
4	3.34	288	0.500	667	2.24	0.004	-0.003	0.000	0.000	46.757	-116.603
5	1.40	18	0.229	59	0.23	0.008	-0.015	0.000	-0.001	13.269	-33.090
6	1.42	13	0.238	42	0.24	0.011	-0.019	0.000	-0.001	12.488	-31.144
7	1.41	16	0.234	53	0.23	0.009	-0.016	0.000	-0.001	12.789	-31.894
8	1.12	83	0.100	258	0.09	0.004	-0.008	0.000	0.000	32.363	-80.708
9	1.05	70	0.100	230	0.06	0.004	-0.010	0.000	0.000	33.172	-82.725
10	1.01	51	0.100	173	0.04	0.004	-0.009	0.000	0.000	23.589	-58.827
11	0.86	78	0.100	303	-0.02	0.004	-0.010	0.000	0.000	38.368	-95.682
12	1.05	55	0.100	182	0.06	0.004	-0.010	0.000	0.000	26.538	-66.180
13	1.64	85	0.361	287	0.36	0.004	-0.006	0.000	0.000	25.274	-63.029
14	4.48	288	0.500	-2630	9.00	-0.001	0.000	0.000	0.000	24.977	-62.287
15	1.16	62	0.111	191	0.11	0.004	-0.008	0.000	0.000	24.977	-62.287
16	0.86	75	0.100	295	-0.03	0.004	-0.011	0.000	0.000	39.807	-99.270
17	1.07	89	0.100	290	0.07	0.004	-0.009	0.000	0.000	40.311	-100.527
18	1.35	96	0.201	306	0.20	0.005	-0.009	0.000	0.000	42.460	-105.889
19	1.19	98	0.125	304	0.12	0.004	-0.008	0.000	0.000	39.807	-99.270
20	1.39	70	0.224	224	0.22	0.004	-0.008	0.000	0.000	26.538	-66.180
21	1.28	82	0.168	256	0.17	0.004	-0.008	0.000	0.000	33.172	-82.725
22	1.10	55	0.100	175	0.08	0.004	-0.009	0.000	0.000	25.891	-64.566
23	1.49	79	0.279	258	0.28	0.004	-0.007	0.000	0.000	26.538	-66.180
24	1.46	83	0.263	271	0.26	0.004	-0.007	0.000	0.000	30.858	-76.954
25	1.41	83	0.232	266	0.23	0.005	-0.008	0.000	0.000	33.592	-83.773
26	1.04	63	0.100	210	0.05	0.005	-0.011	0.000	0.000	33.172	-82.725
27	1.20	55	0.128	170	0.13	0.006	-0.011	0.000	0.000	31.221	-77.859
28	1.16	49	0.107	152	0.11	0.005	-0.011	0.000	0.000	27.218	-67.877
29	1.56	65	0.315	215	0.31	0.005	-0.008	0.000	0.000	26.874	-67.018
30	1.71	68	0.404	232	0.40	0.005	-0.008	0.000	0.000	25.891	-64.566
31	1.36	61	0.209	195	0.21	0.005	-0.008	0.000	0.000	25.274	-63.029
32	1.46	61	0.263	197	0.26	0.005	-0.008	0.000	0.000	25.274	-63.029
33	1.31	72	0.183	226	0.18	0.004	-0.007	0.000	0.000	26.210	-65.363
34	1.22	74	0.139	229	0.14	0.004	-0.007	0.000	0.000	26.210	-65.363
35	1.22	31	0.135	96	0.14	0.004	-0.008	0.000	0.000	12.063	-30.082
36	1.22	31	0.135	96	0.14	0.004	-0.008	0.000	0.000	12.063	-30.082
37	1.14	31	0.100	95	0.10	0.008	-0.017	0.000	-0.001	26.538	-66.180
38	0.83	23	0.100	92	-0.04	0.004	-0.012	0.000	0.000	13.269	-33.090
39	1.53	39	0.299	128	0.30	0.010	-0.015	0.000	-0.001	29.486	-73.534
40	1.46	30	0.263	97	0.26	0.010	-0.017	0.000	-0.001	24.977	-62.287

Appendix E

Beam Fatigue Test Results

Asphalt Flexural Fatigue Test
Batch Results

Specimen Identifier	Loading Frequency (Hz)	Loading Cycles Applied	Average Applied Tensile Strain (microStrain)	Cumulative Dissipated Energy (kN-mm/mm^3)
SM9.5A-Beam Fatigue	5.0	425,612	368	9.8719E+01

Number of Tests	1

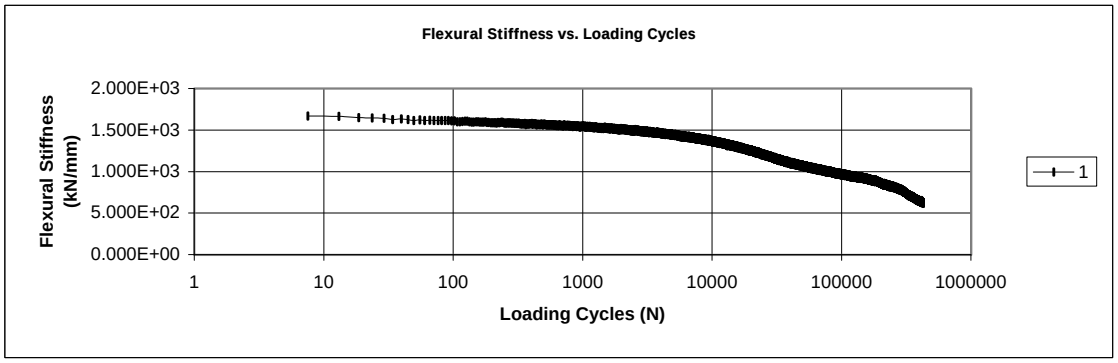

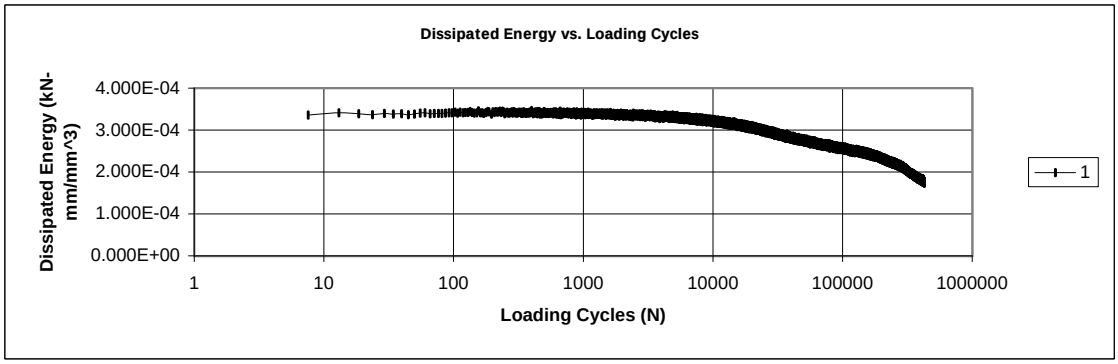

Asphalt Flexural Fatigue Test
Batch Results

Specimen Identifier	Loading Frequency (Hz)	Loading Cycles Applied	Average Applied Tensile Strain (microStrain)	Cumulative Dissipated Energy (kN-mm/mm^3)
2	5.0	2,278,933	368	8.5961E+02

Number of Tests	1

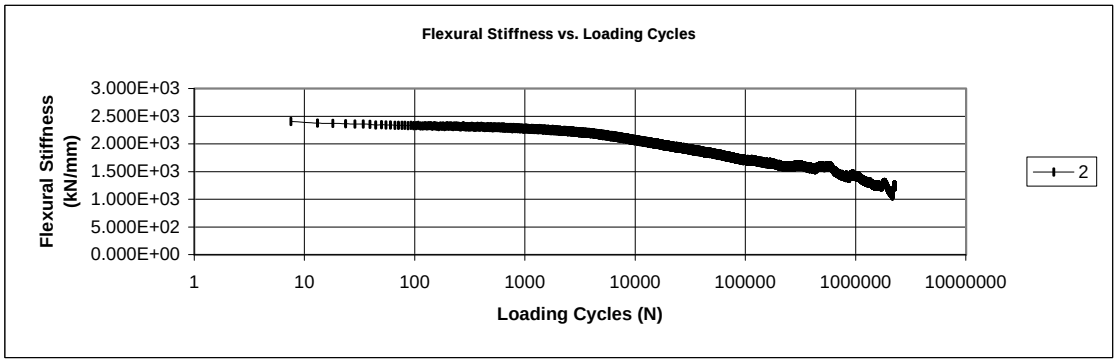

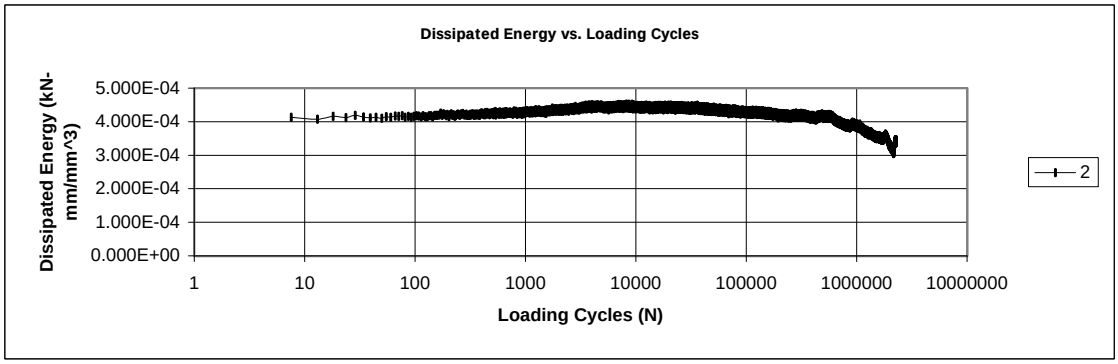

Asphalt Flexural Fatigue Test
Batch Results

Specimen Identifier	Loading Frequency (Hz)	Loading Cycles Applied	Average Applied Tensile Strain (microStrain)	Cumulative Dissipated Energy (kN-mm/mm^3)
3	5.0	171,901	551	1.1556E+02

Number of Tests	1

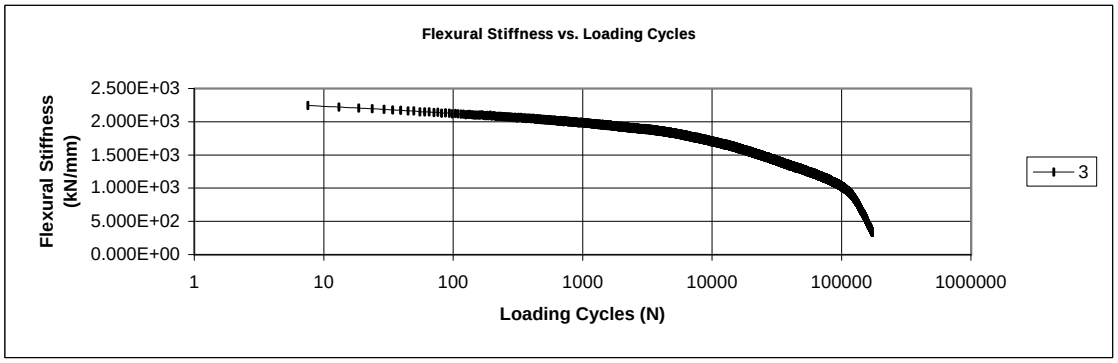

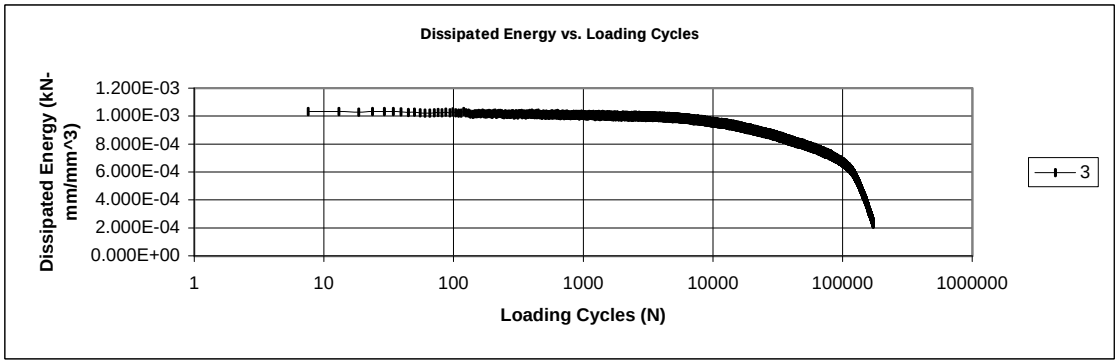

Asphalt Flexural Fatigue Test
Batch Results

Specimen Identifier	Loading Frequency (Hz)	Loading Cycles Applied	Average Applied Tensile Strain (microStrain)	Cumulative Dissipated Energy (kN-mm/mm^3)
4	5.0	388,123	551	2.5291E+02

Number of Tests	1

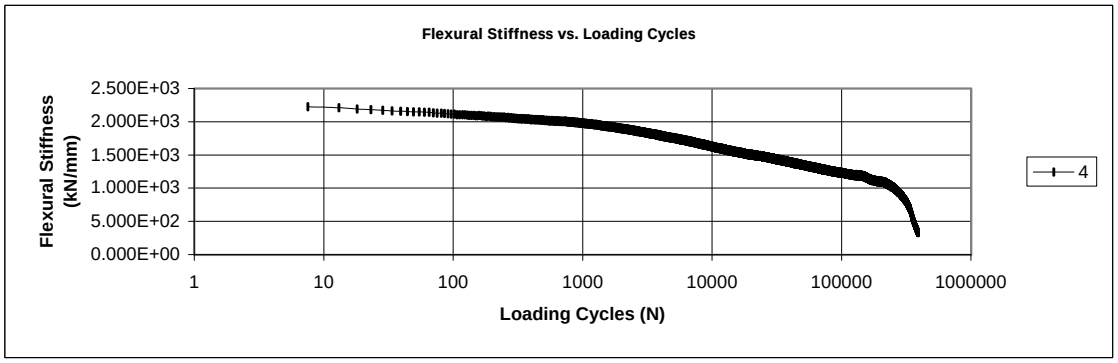

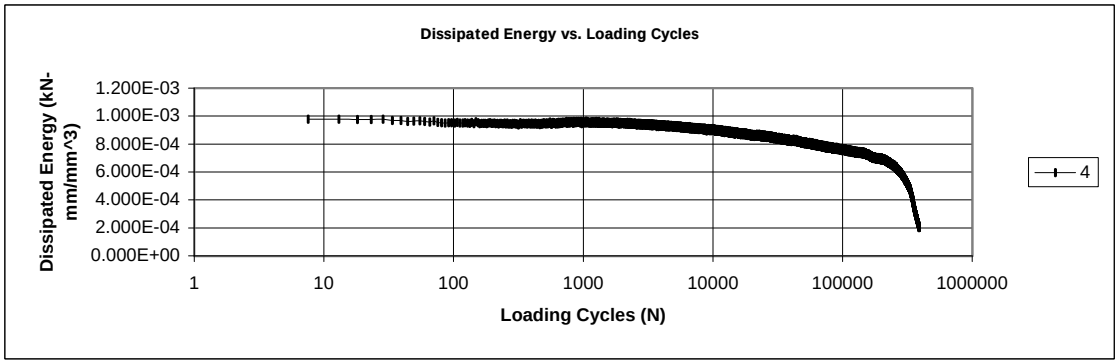

Asphalt Flexural Fatigue Test
Batch Results

Specimen Identifier	Loading Frequency (Hz)	Loading Cycles Applied	Average Applied Tensile Strain (microStrain)	Cumulative Dissipated Energy (kN-mm/mm^3)
5	5.0	1,383,531	578	9.0731E+02

Number of Tests	1

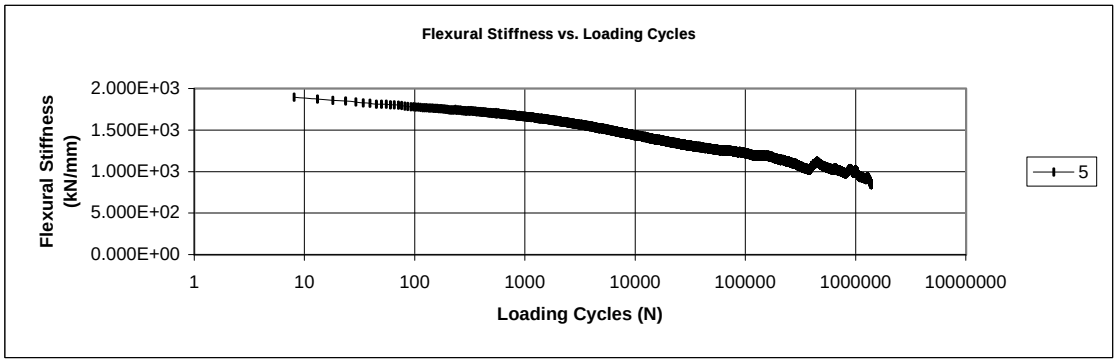

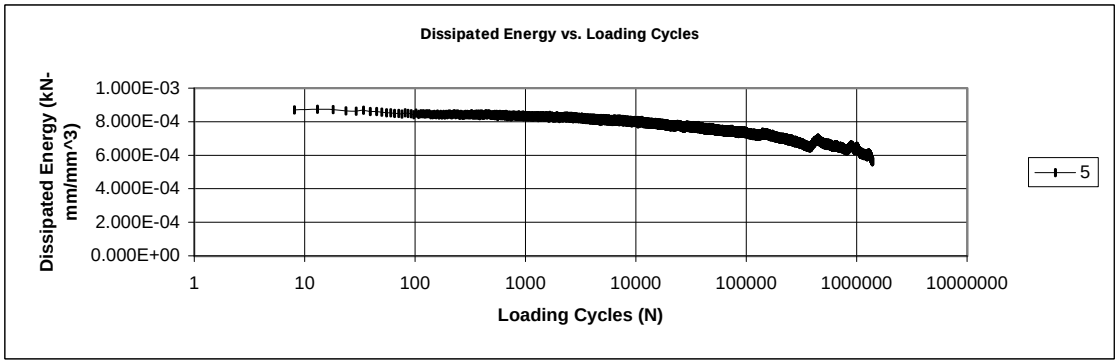

Asphalt Flexural Fatigue Test
Batch Results

Specimen Identifier	Loading Frequency (Hz)	Loading Cycles Applied	Average Applied Tensile Strain (microStrain)	Cumulative Dissipated Energy (kN-mm/mm^3)
6	5.0	1,580,947	746	1.5895E+03

Number of Tests	1

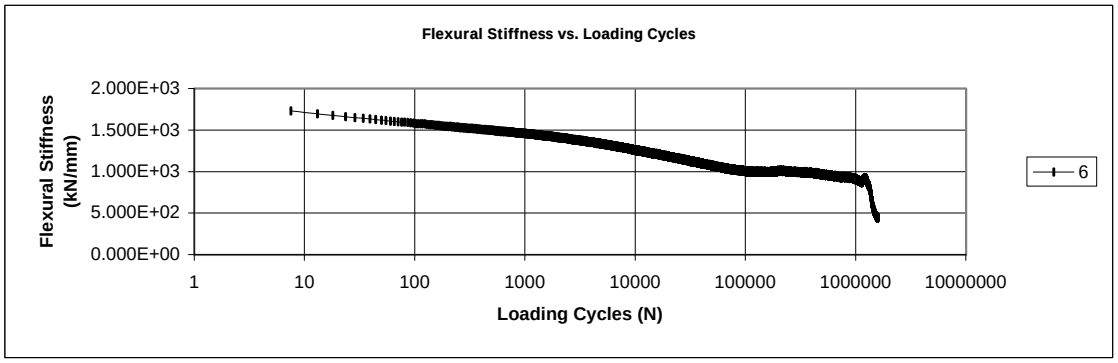

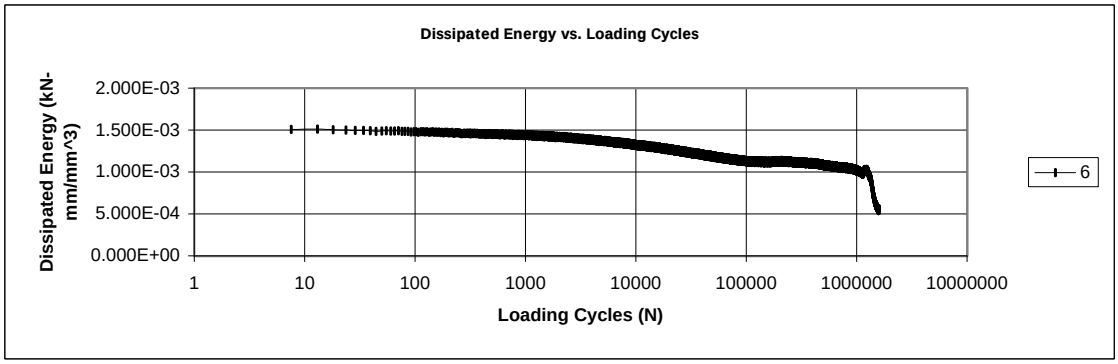

Asphalt Flexural Fatigue Test
Batch Results

Specimen Identifier	Loading Frequency (Hz)	Loading Cycles Applied	Average Applied Tensile Strain (microStrain)	Cumulative Dissipated Energy (kN-mm/mm^3)
7	5.0	736,674	983	7.1465E+02

Number of Tests	1

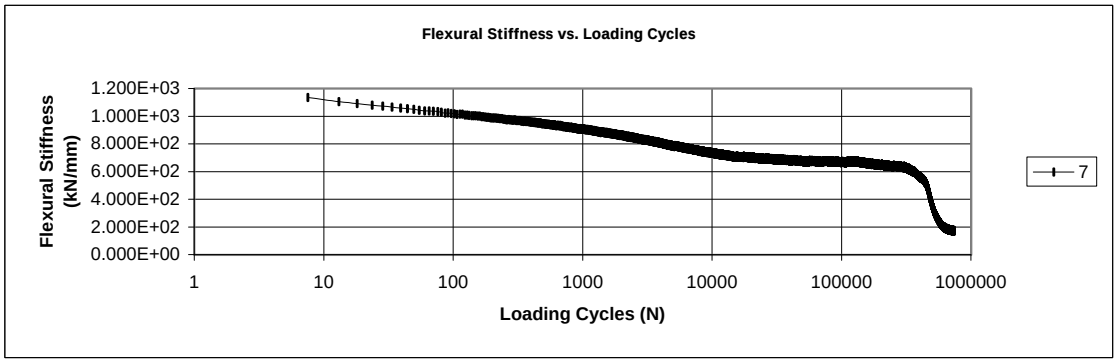

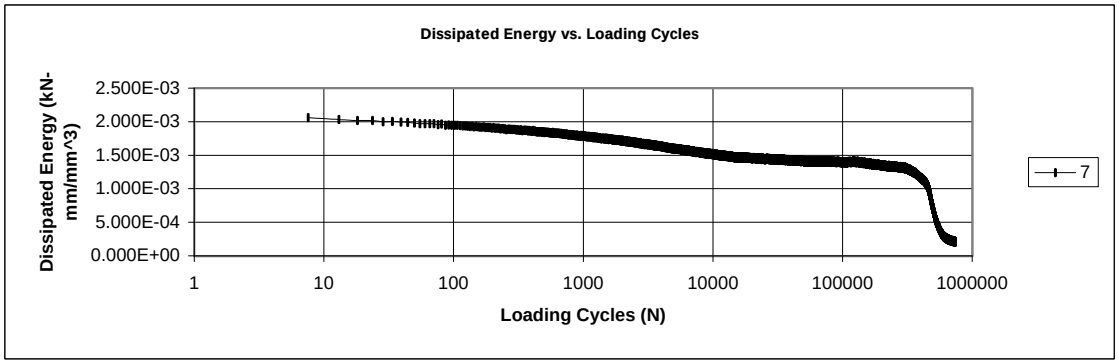

Asphalt Flexural Fatigue Test
Batch Results

Specimen Identifier	Loading Frequency (Hz)	Loading Cycles Applied	Average Applied Tensile Strain (microStrain)	Cumulative Dissipated Energy (kN-mm/mm^3)
8	5.0	59,453	983	1.0295E+02

Number of Tests	1

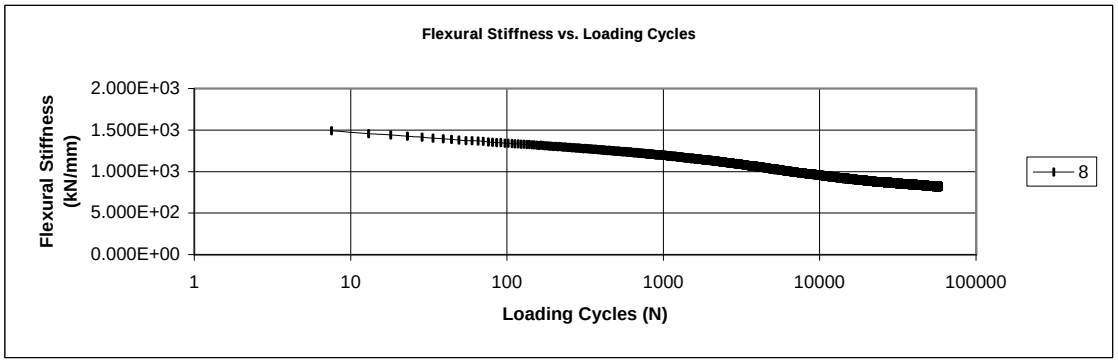

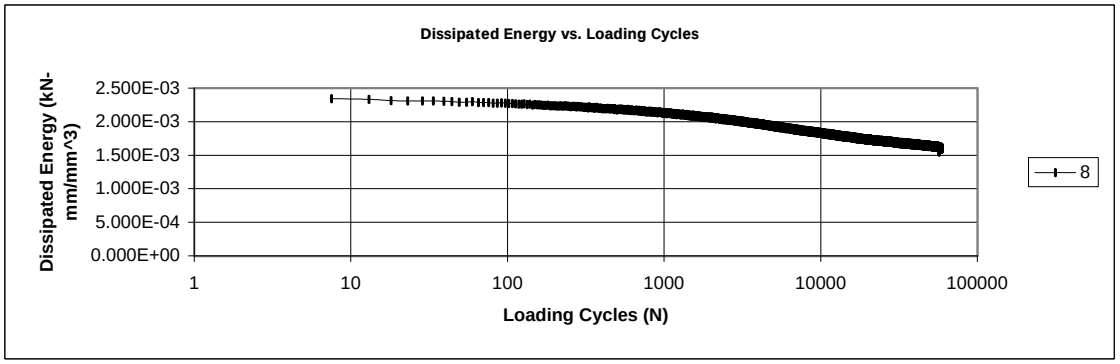

VITA

Walid M. Nassar was born in Cairo, Egypt, on September 12th, 1972. He attended Cairo University where he got his Bachelors Degree in Civil Engineering. He worked as a lecturer in Kuwait University, Kuwait. He then moved to the Idaho University where he got his Masters of Science degree in Civil Engineering in 1997. He enrolled at Virginia Polytechnic Institute and State University, Blacksburg, Virginia in August, 1997. He has served at Virginia Polytechnic Institute and State University since 1997 as a Research Assistant and Research Associate.